INDOOR WIDE BAND RADIO WAVE PROPAGATION MEASUREMENTS AND MODELS AT 1.3 GHz AND 4.0 GHz

by

Dwayne Allen Hawbaker

Thesis submitted to the faculty of the

Virginia Polytechnic Institute and State University

in partial fulfillment of the requirements for the degree of

MASTER OF SCIENCE

in

Electrical Engineering

APPROVED:

Theodore S. Rappaport, Chairman

Charles W. Bostian

Gary S. Brown

Indoor Wide Band Radio Wave Propagation Measurements and Models at 1.3 GHz and 4.0 GHz

by

Dwayne Allen Hawbaker

Theodore S. Rappaport, Chairman

Electrical Engineering

(ABSTRACT)

An extensive radio wave propagation measurement campaign was conducted at 1.3 GHz and 4.0 GHz inside four buildings, including a sports arena, a modern closed-plan office building, and two dissimilar, open-plan factories. Measurements were recorded at 57 locations using base station antenna heights of 1.7 meters and 4.0 meters. Results were obtained for mean and maximum excess delay, rms delay spread, time delay jitter, differential delay jitter, and path loss through analyses of impulse response estimates, which were obtained via repetitive 5 ns probing pulses. The effects of frequency, antenna height, topography (line-of-sight or obstructed direct path), and building environment on delay spread and path loss are quantified. Results indicate that, on average, the frequencies and antenna heights used in this study have minimal impact on rms delay spread and path loss. However, topography and building environment significantly affect these parameters. RMS delay spread values as high as 230 ns were observed in open-plan factories. Computed path loss power law exponents are 1.84 and 2.35 for line-of-sight and obstructed topographies, respectively. A second campaign was conducted to determine the effects of antenna directivity and polarization on propagation parameters. On average, line-of-sight indoor channels offer 8 dB of cross-polarization discrimination, whereas obstructed environments offer less than 3 dB. Directional antennas provide a significant reduction in rms delay spread over omni-directional antennas. In line-of-sight environments, circular polarization provides an additional delay spread reduction.

Acknowledgments

I wish to express a sincere appreciation to my academic advisor and friend, Dr. Ted Rappaport, for his guidance, patience, and support during my graduate career. Many thanks are also due to my committee members, Dr. Charles Bostian and Dr. Gary Brown, for their helpful suggestions.

I am especially grateful for the tremendous support that was offered during the difficult and exhausting process of data collection. Much appreciation is extended to Joey Lui for collecting the narrow band data and to Ken Blackard for the seemingly endless hours of navigating the autonomous guided vehicle in the factories. Thanks also to Scott McCulley, Sal Yusef, Thomas Gee and Kurt Schaubach for their assistance at various times throughout the campaign. A very special thanks goes to Scott Seidel for not only his specific contributions of on-sight assistance and narrow band data processing, but for his immeasurable and sincere support throughout the entire campaign.

The efforts of Mike Keitz, Scott McCulley, and Lynn Ailes in developing the autonomous guided vehicle, and Alan Fox in providing the RF bandpass filters, are greatly appreciated.

Thanks to the personnel at the buildings in which measurements were taken. Without their cooperation, the compilation of the extensive propagation database would have been impossible.

This research has been sponsored, in part, by AICOMM, Inc., Virginia's Center for Innovative Technology, a Bradley Fellowship award, and affiliates of the Mobile and Portable Radio Research Group; I gratefully acknowledge this support.

During the seven years of my college career, my parents, grandparents, and fiancée, Kimberly, have lived through the highs and lows nearly as much as I have. Their unreserved love and encouragement have helped me tremendously. It is to them I owe all the thanks in the world.

Table of Contents

List of Figures

List of Tables

1 Introduction

A recent interest in the field of radio communication has been to develop mobile systems for indoor environments. The development of such systems has immediate potential for improvement in point-to-point communication between co-workers in manufacturing and office environments. With such systems, employees would no longer be restricted to and inconvenienced by the stationary telephone in an office or on a factory floor. These systems may also play an important role in a long-term objective to develop worldwide personal communications, in which telephones would no longer be associated with locations, but with individual persons. Modern cellular telephone systems are merely a first step in the development of personal communication systems of the future [1].

Besides communication, radio has other potential applications as an integrated part of factories and office buildings of the future. Along with continuous efforts to improve the efficiency of manufacturing techniques is the need for reliable and efficient stationary and portable data transmission systems for diverse applications. A major part of the development of intelligent manufacturing centers is the installation of computer-controlled automated machinery [2]. Currently, coaxial and fiber optic cable serve as the transmission media in nearly all computer/machine data links. As the number of computer-controlled machines and hard-wired telephone systems and local area networks increase within a factory, so does the amount of coaxial cable. Factory engineers will look towards radio as a suitable alternative for both data and voice transmission systems. The concept of radio based local area networks (RLANs) has merit. Network installation, reconfiguration, and upkeep would be considerably less expensive and time-consuming with radio as a primary means of data transmission. Factories and office buildings will most likely employ mobile robots, or autonomous guided vehicles (AGVs) to transport work-in-progress from one area to another. The mobility of radio makes it an attractive means for

controlling future AGVs.

In order to develop reliable indoor radio systems, a solid understanding of the dynamic channels in which these systems will operate is necessary. Analysis of extensive propagation data is one method for developing an understanding of such complicated channels. As an understanding of the vagaries of indoor radio channels evolves, so too will tools that predict radio coverage without the need for measured data. This research project involved the collection and analysis of extensive propagation data in diverse indoor environments. The material presented in this thesis lays a foundation from which propagation prediction tools can be developed.

This thesis is arranged in 8 chapters. Chapter 1 discusses the concept of multipath propagation and how it affects indoor wireless communications, discusses previous studies in the field of indoor propagation and modeling, and briefly states the objectives and unique features of this work. Chapter 2 details the experiment design used in the data collection phase of the project. Chapter 3 describes the data reduction and processing techniques, and the major parameters for wide band propagation data. Chapter 4 details all results obtained from the data. Chapter 5 describes results from a secondary, less extensive campaign, which was initiated to determine the effects of antenna directivity and polarization on multipath propagation. The next two chapters each introduce an important research area in which the data and results can be further used. Chapter 6 introduces site-specific propagation modeling and prediction. Chapter 7 provides a brief presentation of system design parameters and their relationships to propagation results. Chapter 8 summarizes this work and concludes the thesis.

1.1 Multipath Propagation

Multipath propagation is caused by the reflection, refraction, diffraction, and scattering of radio waves as they travel from the transmitter to the receiver. Multipath degrades radio signals differently for different types of transmission. For a continuous wave (CW) radio signal (i.e. a sinusoidal signal with a constant frequency), multipath induces fades (reduced power levels) at times and locations in which two or more multipath signal electric field vectors add vectorially such that the resultant amplitude is very small. The amplitudes and, more

the phases of the electric field of the received signal are a function of the path lengths of the direct and multipath components, and thus the exact location of the transmitter and receiver. Therefore, in a highly dynamic environment such as a factory floor, the resultant amplitude of the electric field changes significantly as one or both terminals is moved. This is known as CW fading.

Multipath also induces what is known as frequency-selective fading in a radio channel. A signal received from a frequency-selective channel will exhibit fades throughout the radio frequency (RF) pass band. That is, different frequency components within the RF bandwidth of interest arrive with different amplitudes in frequency-selective fading channels, whereas in flat fading channels, all frequencies within the RF bandwidth of interest arrive at the receiver with approximately the same amplitudes. The smallest average RF bandwidth in which frequency-selective fading is observed in a radio channel is sometimes referred to as the coherence bandwidth of the channel [3]. For signals in which the RF bandwidth exceeds the coherence bandwidth, frequency-selective fading will be possible, and it is likely that adaptive equalization techniques will be needed in the receiver to combat this fading.

The multipath characteristics of a radio channel can be thoroughly examined from the time domain impulse response, or power delay profile, of a received signal [3]. The true impulse response of a channel is impossible to attain since, from Fourier transform theory, the transmission of an impulse requires equal amplitude transmission of all frequencies, which is physically impossible to achieve. The accuracy of the impulse response estimate is thus dependent on the time extent of the transmitted finite duration pulse. Information about the causes of multipath can be attained from the time delays and amplitudes of multipath components in a power delay profile. This information can not be attained from CW fading data. Power delay profiles allows the computation of important time dispersed parameters such as root mean square (rms) delay spread, a parameter which can be computed directly from a profile delay profile. RMS delay spread quantifies the severity of multipath propagation in a channel, which is important since multipath leads to intersymbol interference, and thus bit errors in a digital signal [4-6]. Chapter 3 of this thesis formally defines and further describes rms delay spread and other time dispersed parameters.

The data collected during this campaign were time-domain responses of pulse transmissions with 4 ns root mean square (rms) pulse widths. At 1.3 GHz, narrow band fading measurements were recorded simultaneously with the impulse response estimates. The narrow band measurements were taken by a commercial receiver, which filtered the 1.3 GHz component of the wide band transmitted signal. Throughout the thesis, the narrow band results will commonly be referred to as CW fading results, although it must be made clear that the transmitted signal was always wide band, and the "CW" data was obtained by filtering the carrier component. Figure 1.1-1 illustrates a 2-dimensional representation of a single impulse response estimate (a) and 3-dimensional representation of a sequence of impulse response estimates (b). The depth axis (into the page) on Figure 1.1-1(b) represents 20 impulse responses uniformly recorded over a 5 wavelength (5λ) measurement track, in which the transmitter was moving along the line-of-sight path directly away from the receiver. The narrow band data which corresponds to the 5λ segment is shown in the upper right corner of Figure 1.1-1(b).

1.2 Previous Work

Much of the pioneering work in the study of the characteristics of indoor radio propagation was performed by Cox at Bell Laboratories [7-10]. In these early propagation experiments, a CW signal was transmitted in the 800-900 MHz band and the received power was recorded as a function of receiver location within or around buildings. In [10], it is shown that 900 MHz propagation experiences signal fluctuations on the order of 25-35 dB as the receiver is moved 6 to 8 inches, or approximately $\lambda/2$. These measurements were made in a vacant metal building with no obstructions between the transmitter and receiver. This clearly indicates the fading effects of multipath propagation on a CW signal. Other technical literature also report CW fading measurements in buildings [11-15].

What CW measurements fail to indicate is the time dispersed characteristics of the multipath channel, which provide meaningful information about the time and amplitude of specific multipath components. Thus the need for impulse response measurements to gain a better understanding of the sources

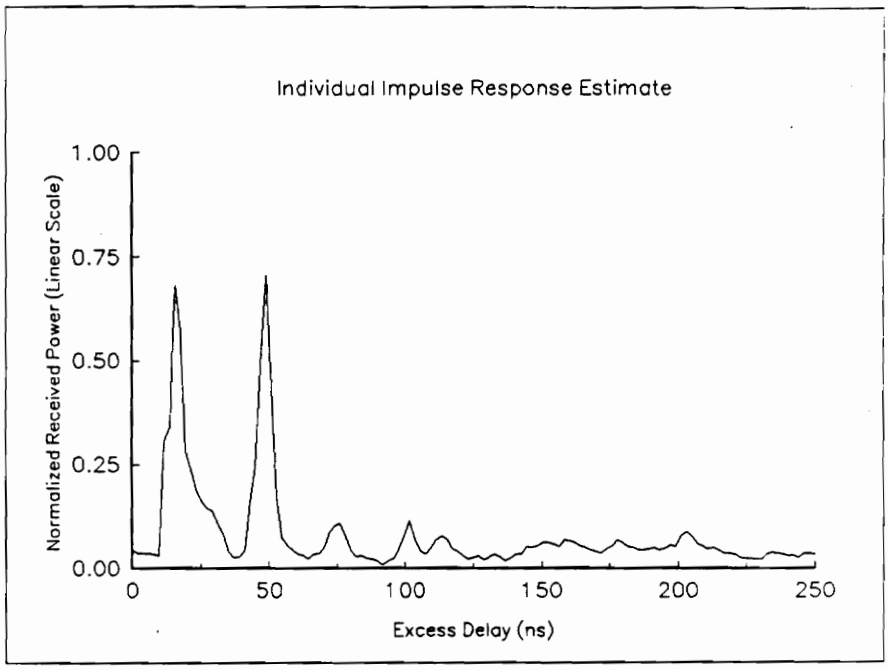

(a) Individual Impulse Response

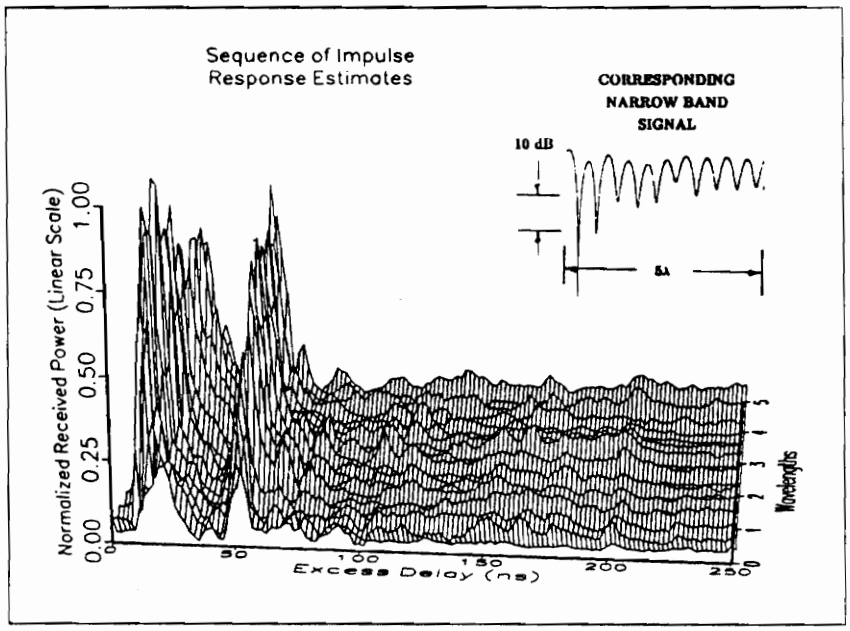

(b) Sequence of Impulse Responses

Figure 1.1-1. Examples of (a) 2-dimensional representation of an individual impulse response estimate and (b) 3-dimensional impulse response sequence over a 5λ segment at 1.3 GHz. Corresponding narrow band signal strength in upper right corner of (b).

and vagaries of multipath propagation was evident to researchers. Devasirvatham reports measurements in which a spread spectrum technique is employed to obtain time delay spread and signal strength measurements at 850 MHz in and around residential and office environments [16-19]. In [16], measurements were made over inside-to-outside radio paths at two residential locations and an office building. In the residential environments, rms delay spread values as high as 420 ns are reported. A comparison of results for measurements made in two dissimilar office buildings at 850 MHz, 1.7 GHz, and 4.0 GHz is given in [19], in which it is reported that rms delay spread statistics do not change significantly with frequency in these office environments. It is also reported that the variation of rms delay spread increases with increasing frequency, and that average path loss values were slightly less at the highest frequency. A comparison of delay spread measurements at 910 MHz and 1.75 GHz is reported in [20]. This paper indicates very similar results as reported in [19] – no significant difference in overall statistics between the two frequencies, and slightly less randomness in rms delay spread results for the lower frequency. Other wide band measurements in office environments also report similar delay spread results [21,22].

Reports of wide band measurements on factory floors have been limited. Path loss and delay spread results from an extensive campaign at 1.3 GHz is reported in [23]. Values for rms delay spread range from 30 ns to 300 ns, with a median value of 96 ns for measurements in which a line-of-sight direct path is present. Average path loss values were found to be a function of distance to the 2.2 power. Wide band measurements were also conducted on factory floors at 910 MHz [24]. Median rms delay spread values for these measurements ranged from 53 ns for one topography, and as low as 15 ns for another. One possible reason for the discrepancy between the two sets of factory rms delay spread results may be the lack of a noise thresholding procedure for the measurements in [23]. Another reason may be that the system in [24] lacked sufficient dynamic range to detect weak multipath components.

1.3 Purpose of this Research

The primary objective of this study is to develop radio channel models that aid in the design of future indoor wireless communication systems based on results

of an extensive collection of propagation data recorded in diverse indoor environments. The effects that frequency, antenna height, topography (line-of-sight (LOS) or obstructed (OBS) direct path), building environment, and antenna directivity and polarization have on various channels parameters and path loss are quantified through statistical analyses. A thorough examination of such a large propagation database has not yet been reported in the literature.

A long-term objective of this research is to develop a "hybrid" modeling technique which uses both statistical results from this and other measurement campaigns and theoretical techniques applied to site-specific geometries. This objective offers the potential for the accurate determination, *a priori*, of the propagation characteristics and appropriate system designs for given topographies, and thus the realization of high quality portable indoor radio communications.

2 Experiment Design

This chapter discusses the experiment design used for the first measurement campaign, including a complete description of the measurement apparatus, a step-by-step explanation of the measurement procedure, and physical descriptions of all measurement locations. A link budget analysis and pertinent system calculations which give insight into limiting factors of the measurement system are presented.

2.1 Measurement Apparatus

The measurement system is a time-domain dual-channel radar with a portable transmitter and receiver. The system generates a repetitive radio frequency (RF) probing pulse with a 5 ns pulse width (4 ns rms) and a 10 μs pulse repetition period. The system operates at two carrier frequencies, 1.3 GHz and 4.0 GHz. The pulse is detected by a tuned RF receiver using non-coherent detection, in which the detector is able to receive the amplitude, or envelope of the signal, without knowledge of the signal's phase. Coherent detection receivers, although more desirable in terms of receiver sensitivity (ability to detect low-level signals), are more complex in that phase detection circuitry is required.

Figure 2.1-1(a) is a block diagram of the transmitter. To transmit pulsed RF signals, 5 ns baseband pulses are generated by an HP-8082A pulse generator and individually mixed with 1.3 GHz and 4.0 GHz carrier frequencies, which are generated by Fluke 6062A and General Electric 1107A signal generators, respectively. A Mini-Circuits ZEM-4300 double sideband level-7 (+7 dBm local oscillator power required) is used to mix the pulse train and the carrier. The 1.3 GHz RF pulse train is amplified by a Mini-Circuits ZHL-4240 wide band 1 watt power amplifier, and the 4.0 GHz RF pulse train is amplified by an Avantek AWP-42100 wide band 10 watt power amplifier. An RF coaxial cable connects the power amplifier to the transmitting antenna, which remained at a height of

1.7 meters (a typical height for a handheld portable telephone) throughout the measurement campaign.

All transmitting equipment was mounted on an autonomous guided vehicle (AGV) developed by Virginia Tech [25]. The AGV is capable of traversing a linear path of desired length at a user-specified constant velocity. This feature greatly streamlined the measurement process (details are given in Section 2.3) and aided in transporting the heavy transmitting equipment throughout the buildings.

It may seem that the measurement range of the system is limited by the 1 watt transmitter power at 1.3 GHz. However, it is easy to show that for a particular transmitter-receiver (T-R) separation, the free space loss at 1.3 GHz is a factor of 9 (nearly 10 dB) lower than the free space loss at 4.0 GHz over an identical path. The received power at a given T-R separation d in free space is given by Friis transmission formula

$$P_R = \frac{P_T G_T G_R \lambda^2}{(4\pi d)^2} \tag{2.1.1}$$

For constant transmitting and receiving antenna gains (G_T and G_R respectively), transmitting power P_T, and T-R separation d, the power received from a 1.3 GHz signal is a factor of 9 stronger than that received from a 4.0 GHz signal, due to the factor of 3 difference in wavelength. In this measurement system, P_T at 1.3 GHz (1 Watt) is a factor of 10 weaker than P_T at 4.0 GHz (10 Watts). This factor of 10 loosely compensates for the factor of 9 difference in free space path loss between the two frequencies.

Figure 2.1-1(b) is a block diagram of the tuned RF receiver. The receiver consists of an antenna followed by an RF bandpass filter chain, which consists of 2 filters cascaded to improve signal attenuation in the stop band. The filter cascades were manually interchanged depending on the frequency of operation. After the bandpass filter is a Mini-Circuits ZHL-4240 40 dB gain amplifier. Although this type of amplifier has a 1 watt rated output power (recall that an identical amplifier was used as the 1.3 GHz power amplifier at the transmitter), the wide bandwidth (0.7 – 4.2 GHz), low cost, and acceptable 4 dB noise figure make it the most logical choice for the receiver "low noise" amplifier. After the

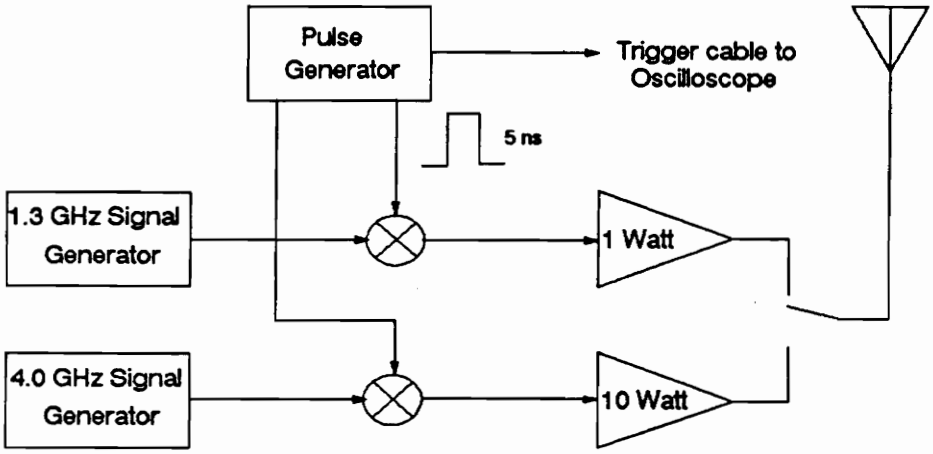

(a) Transmitter

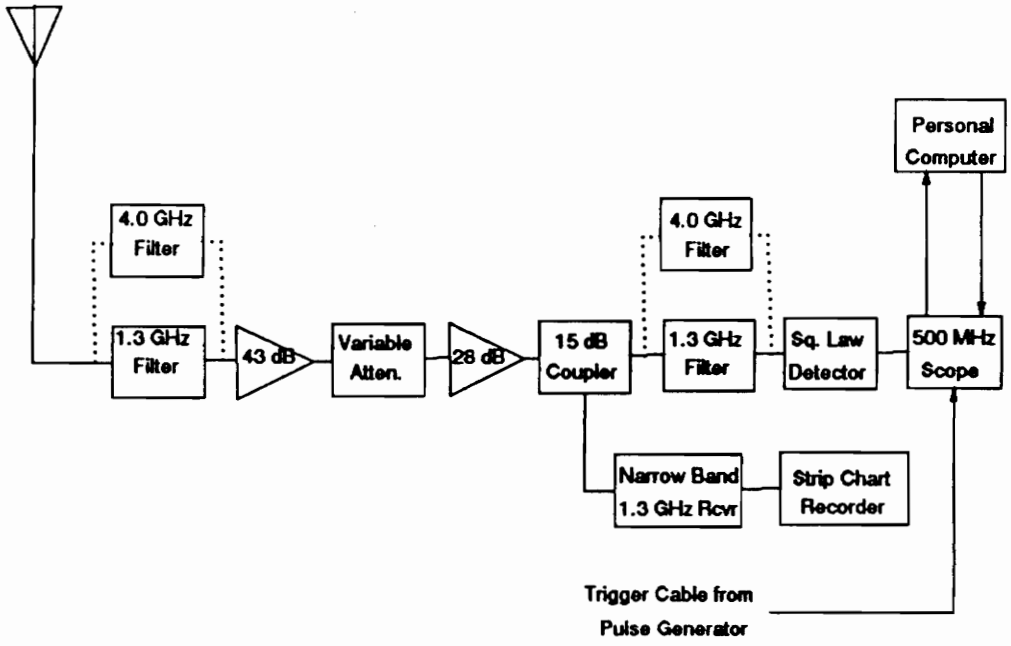

(b) Receiver

Figure 2.1-1. Block diagram of (a) transmitter and (b) receiver.

amplifier are two variable attenuators, an HP–8495A 0–70 dB attenuator and an HP–8494A 0–11 dB attenuator. Secondary amplification is then provided by a Mini-Circuits ZHL-1042J 30 dB gain amplifier. After the amplifier is a Mini-Circuits 15 dB coaxial coupler, which directs –15 dB (3.2%) of the power into a calibrated 1.30 GHz ICOM IC-R7000 narrow band commercial receiver, and the remainder through a second interchangeable bandpass filter cascade to a KDI – Triangle PT – 36A square law detector. The narrow band receiver allows for continuous wave (CW) data acquisition at 1.3 GHz. Proper detection is guaranteed through adjustment of the attenuators such that the detector operates in the square law region. The output voltage of the square law detector is proportional to the square of the input voltage and thus the power in the signal ($V_{IN}^2 \propto V_{OUT} \propto P$). The square law region was determined by a controlled characterization of the detector. Figure 2.1-2 shows the results of this characterization for both frequencies. These curves illustrate the detector output voltage in –mV versus the detector input power in dBm. The input power refers to the peak power in a repetitive pulse train, and thus is independent of the repetition period [26]. Figure 2.1-2 indicates that for detector input powers from –33 dBm to –9 dBm, the detector output voltage approximately follows the square law. The 4 dB differential from true square law over this range of input powers actually enhances the limited display dynamic range to about 24 dB. After the detector, an HP 54503A oscilloscope digitizes each power delay profile and stores the data on the 40 Megabyte hard disk drive of a Micro Express Regal 286 portable personal computer. All receiver equipment was secured on an industrial strength push cart with pneumatic tires throughout the measurement campaign.

Discone antennas were used at the transmitter and receiver. The discone antenna is omni-directional, broadband, and, when designed and fabricated properly, has a gain of $\sim$1.5 dBi. A detailed description of the discone can be found in [27].

The measurement system is an improved version of the one reported in [23], with the following notable differences. The measurement system for our campaign has a dual frequency capability, while [23] reports measurements at only 1.3 GHz. Although narrow band measurements are reported in [23], the narrow

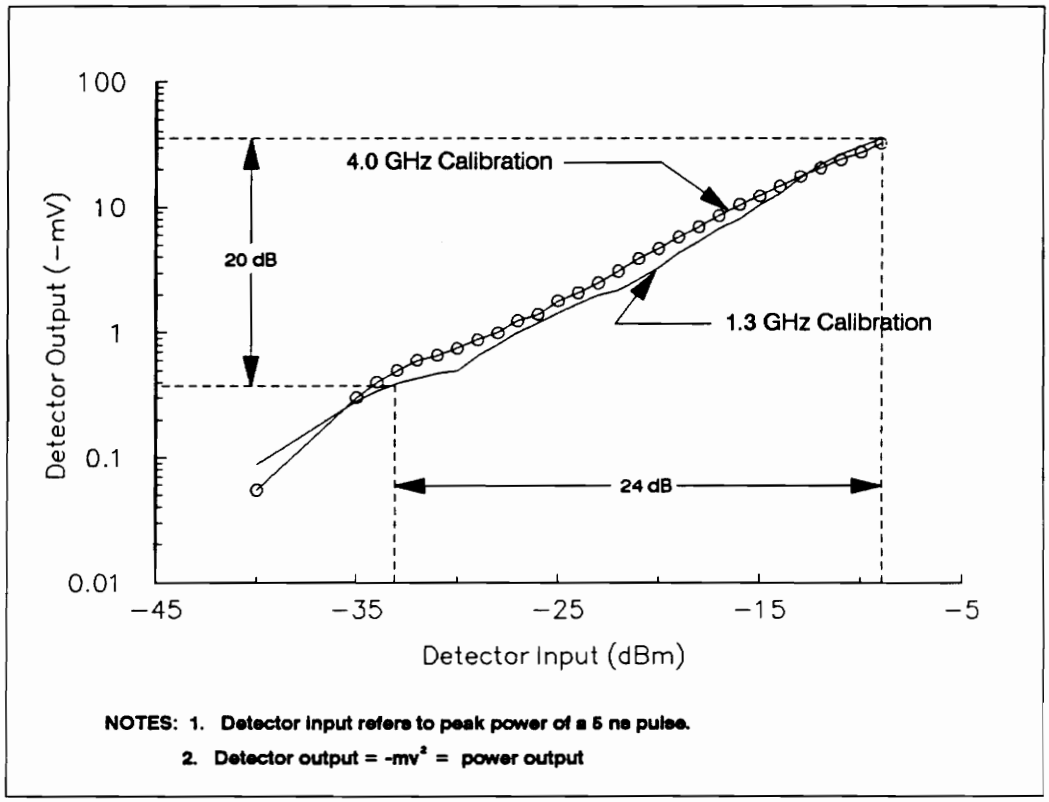

Figure 2.1-2. Calibration curves of the receiver square law detector for 1.3 GHz and 4.0 GHz.

and wide band measurements were not taken simultaneously. Our measurement apparatus uses a triggering cable to connect the transmitter and receiver, which permits exact time delay measurements in that it allows synchronization between the oscilloscope triggering mechanism and the trigger output of the pulse generator. A triggering cable was not used in [23]. The system reported in [23] had a variable attenuator at the transmitter to control detector linearity, but adjusting the transmitter power while monitoring the signal level at the receiver was difficult and time-consuming. As stated above, this measurement system has 2 variable attenuators at the receiver, which is a convenient and simple method to control the detector input power.

Although the measurement system has many positive features that allow for accurate, diverse propagation measurements, the apparatus also has several disadvantages, most of which were only inconveniences to the system operators and did not limit system performance. These limitations, regardless of their severity, should be mentioned as casual warnings to researchers who wish to develop similar systems. When a measurement was completed at one carrier frequency, the power amplifiers at the transmitter and the bandpass filters at the receiver were switched manually before measurements were made at the other frequency. This transition took 5–10 minutes for each frequency change. Switching the components several times a day became monotonous and tiresome. Automatic computer-driven switching between the frequency-dependent hardware, or more ideally, simultaneous transmission and reception of the two frequencies would have made the measurement process easier and less time-consuming. The CW measurements were received by a narrow band receiver and recorded on a strip chart recorder. A system in which the output of the narrow band receiver is immediately digitized and stored in a computer would have made CW data processing easier. Since the time of the measurement campaign (March, 1990), such a system has been developed, and will be utilized during future narrow band measurements. Although the triggering cable provided stable, accurate time delay measurements, the researchers found the process of carefully routing the cable from the transmitter to the receiver for every measurement location to be very time-consuming. A more viable, albeit expensive, alternative would have been to employ ultra-stable time standards at each terminal.

2.2 System Calculations

The following calculations reveal the limiting factors in the system performance. It is shown in [28], that in typical manufacturing environments, it is reasonable to assume that a man-made noise factor of approximately 10 dB is present at the receiver. In the system calculations, this noise factor is additive with the calculated thermal noise power. The thermal noise floor calculation is based on several crude estimations. First, an effective receiver antenna noise temperature of ~ 400 K is assumed. An effective receiver bandwidth of 400 MHz, the bandwidth of the bandpass filters, is used in the calculation. The receiver consists of 3 "components" before the low noise amplifier (LNA) – a discone antenna, an RG-142 coaxial cable, and a bandpass filter chain. In order to estimate the system noise figure, insertion losses of these "pre-LNA" components are found. For each bandpass filter cascade, an insertion loss of 5.0 ± 1 dB was measured, and is used in the system calculation. Two meters of RG-142 cable has about 2.5 dB of attenuation at 1.3 GHz, and about 3.5 dB of attenuation at 4.0 GHz. Thus the total "pre-LNA" system losses are roughly estimated to be 8.5 dB at 1.3 GHz, and 10 dB at 4.0 GHz.

The LNA has a rated noise figure of 4 dB, which corresponds to a noise temperature of 440 K. The system losses estimated above correspond to effective noise temperatures of 1760 K and 2610 K for 1.3 GHz and 4.0 GHz, respectively. Due to the high gain of the LNA (40 dB), it is valid to assume that noise contributions of components after the LNA to the system noise temperature are negligible. Subsequently, the system noise temperature referred to the receiver antenna terminals is given by the following equation

$$T_{SYS}(\text{dBK}) = 10 \log \left(T_{ANT} + T_{PRE} + \frac{T_{LNA}}{G_{PRE}} \right) \tag{2.2.1}$$

In (2.2.1), G_{PRE} and T_{PRE} are the gain ($G_{PRE} < 1$) and effective noise temperature of the pre-LNA losses. The system noise temperature was found to be 37.2 dBK at 1.3 GHz, and 38.7 dBK at 4.0 GHz.

The thermal noise power (in dBm) referred to the antenna terminals in an

effective receiver bandwidth B (400 MHz) is given by

$$P_N \text{ (dBm)} = 10 \log B \text{ (MHz)} + T_{SYS} \text{ (dBK)} - 138.6 \qquad (2.2.2)$$

This is the logarithmic form of the classical thermal noise power equation, $P_N = kTB$. A complete discussion of noise figure topics is in [29]. From (2.2.2) and the 10 dB man-made noise factor assumption, the total noise into the receiver is estimated to be –65.4 dBm at 1.3 GHz, and –63.9 dBm at 4.0 GHz.

One advantage of a time averaging oscilloscope is that it provides post-detection integration gain when compared with a single sweep receiver. As shown in [26], a post-detection integration SNR improvement of 9 dB can be achieved when 16 consecutive profiles are time averaged at the oscilloscope. However, for square law detection, there exists a 3 dB SNR conversion loss between RF and baseband for an input SNR greater than about 8 dB [26]. Thus 3 dB of the 9 dB post-detection advantage is lost in the detector RF-to-baseband conversion. Setting a 7 dB SNR threshold required to detect a multipath component, a minimum detectable signal level due to **thermal and man-made noise** is determined to be –64.4 dBm at 1.3 GHz and –62.9 dBm at 4.0 GHz.

The square law detector has a minimum sensitivity of –36 dBm for a 200 MHz baseband bandwidth (See Figure 2.1-2). From the fixed values of gain and attenuation in the receiver (assume the variable attenuators are set to 0), a minimum detectable signal level due to **detector sensitivity** is found to be approximately –85 dBm at 1.3 GHz and –82 dBm at 4.0 GHz. Table 2.2-1 summarizes the link budget analysis, and illustrates that thermal noise, and not detector sensitivity, is the limiting factor in weak signal reception.

2.3 Measurement Procedure

Multipath and CW measurements were recorded in four buildings during the first campaign, including one 10,000 person capacity sports arena, one multi-floor, closed-plan office building, and two typical factory buildings. Specific details of the four measurement locations, which have been designated Sites A-D, are presented in Section 2.5. In order to most accurately simulate possible future wireless indoor systems, 4 ***base station locations*** were selected at each site, with

Table 2.2-1. Measurement system link budget parameters.

	1.3 GHz	4.0 GHz
System Noise Temp.	37.2 dBK	38.7 dBK
Effective Bandwidth	400 MHz	400 MHz
Thermal Noise Floor @ 400 MHz	-75.4 dBm	-73.9 dBm
Man-Made Noise Fact.	10 dB	10 dB
Total Receiver Noise @ 400 MHz	-65.4 dBm	-63.9 dBm
Integration Gain	9 dB	9 dB
SNR Threshold	7 dB	7 dB
Det. SNR Conv. Loss	3 dB	3 dB
Minimum Detectable Signal due to Receiver Noise @ 200 MHz Baseband	-64 dBm	-63 dBm
Detector Sensitivity @ 200 MHz Baseband	-36 dBm	-36 dBm
Receiver Gain	70 dB	70 dB
Fixed Attenuation	21 dB	24 dB
Minimum Detectable Signal due to Detector Sensitivity @ 200 MHz Baseband	-85 dBm	-82 dBm

the exception of Site D (the closed-plan office building), where a limited amount of data was recorded using only 1 base station location. While the receiver remained at a base station, the transmitter was transported to 4-6 ***measurement locations***, located from 10 to 100 meters away from the receiver. This represents the portable terminal in a typical mobile link. A total of 57 measurement locations using 13 base station locations were used during the campaign. The number of base station and measurement locations for each site are given in Section 2.5.

At each measurement location, the transmitter traversed a 32 wavelength path at a uniform speed via the AGV, while the receiver simultaneously recorded 128 power delay profiles at $\lambda/4$ intervals. This process, designated as a ***measurement run***, was repeated 4 times at each measurement location, at 1.3 GHz and 4.0 GHz with high (4.0 meters) and low (1.7 meters) receiver antenna heights. The transmitter and receiver locations, and the direction in which the transmitter moved during each measurement run were carefully documented on building blueprints. The transmitter moved perpendicular to the line-of-sight path (transverse with respect to the receiver) for approximately 50% of the measurement runs and parallel to the line-of-sight path for approximately 50% of the measurement runs.

2.4 System Calibration

The entire measurement system was periodically calibrated throughout the measurement campaign to normalize any fluctuations in the system such as amplifier gain or generator power output. To calibrate the system, the transmitter and receiver were connected back-to-back with only a variable attenuator (0-70 dB) between the cables that led to the antennas, which were eliminated from the back-to-back calibration. The received pulse was observed on the oscilloscope screen, and recorded on the computer's hard drive. These "closed-loop" calibration runs were nominally made before and after measurements at each base station location. In order to account for the antenna gains in the calibration procedure, a controlled, over-the-air measurement in a multipath-free environment was necessary. To achieve this, the entire system was taken outdoors. A typical closed-loop back-to-back calibration was first

performed. Then the terminals were separated exactly 10 wavelengths, and a free space or "open-loop" calibration was recorded at each frequency. Figure 2.4-1 illustrates the closed-loop(a) and open-loop(b) calibration profiles at 1.3 GHz. For each of these measurements, the time delay of the oscilloscope was adjusted such that the profile appeared in the center of the time axis on the screen. Therefore, the time displayed on the graphs is not significant.

2.5 Measurement Locations

This section describes the four buildings at which propagation data were collected. In addition to physical descriptions of each building, the outstanding characteristics of typical measurements are presented. For example, the causes of obstructions between transmitter and receiver generally differ from one building topography to another.

Site A was Cassell Coliseum, an indoor sports arena located on the campus of Virginia Tech. The outside dimensions of the four story coliseum are 78 meters long by 68 meters wide; the outside walls are constructed of concrete reinforced with steel. The inside of the coliseum consists mostly of the "arena", an open area that is 40 meters by 23 meters at the lowest level, and tapers outward to nearly the outside dimensions of the coliseum, at the highest level, approximately 16 meters higher than the lowest level. This forms a bowl-like structure made of wooden seats and reinforced concrete steps. The base of the arena is a hardwood floor (typical basketball playing surface) over a concrete base. A total of 18 portals are located approximately 10 meters above the playing surface. The portals open into a 6 meter wide oval concourse which surrounds the arena.

Typical measurements recorded at the coliseum are characterized by either clearly visible line-of-sight (LOS) paths or completely obstructed (OBS) paths. Representative LOS paths were with the base station and mobile located on the playing surface, the mobile located on the playing surface and the base station located at a portal entrance, or both terminals located at different portal entrances, with one portal clearly visible from the other. Representative OBS paths were typically with the transmitter and receiver located at two different areas in the concourse, or with the transmitter located on the playing surface and the receiver located in the concourse. These topographies differ from those taken

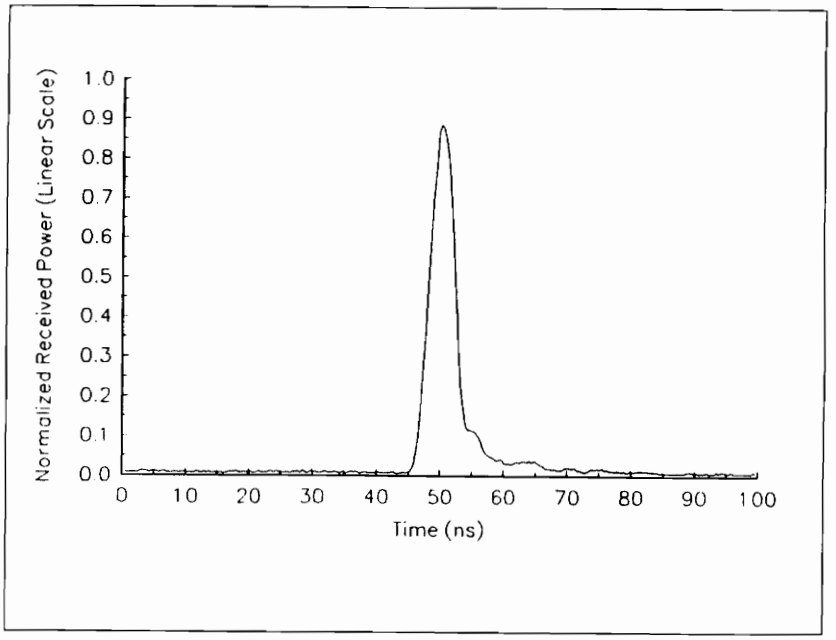

(a) Back-to-Back Calibration

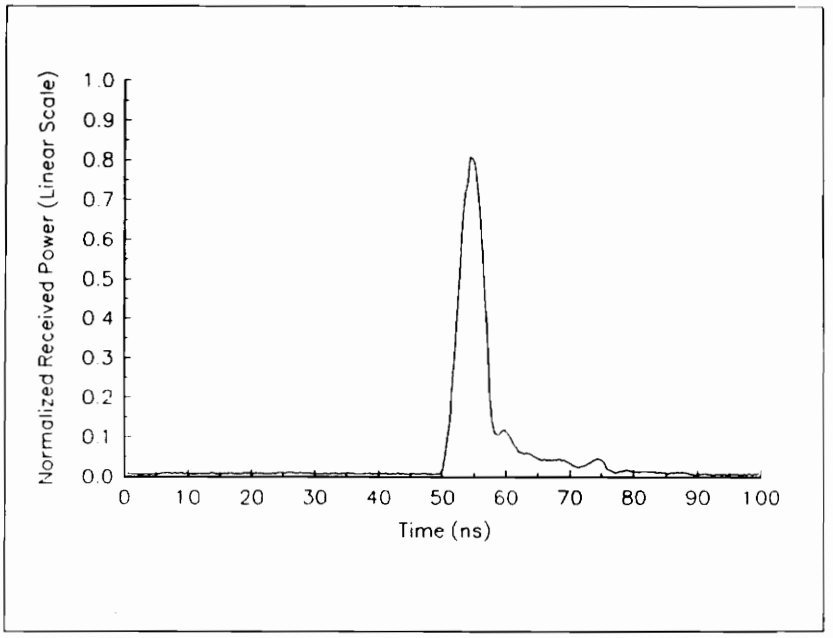

(b) Over-the-Air 10λ Calibration

Figure 2.4-1. Impulse responses of (a) back-to-back (closed-loop) and (b) over-the-air 10λ (open-loop) system calibration measurements at 1.3 GHz.

in the open-plan factories in that the LOS paths are more clearly defined due to the absence of machinery and inventory which typically surround the base station and mobile in most open-plan factory topographies. The OBS paths at Site A are determined by measurements between two completely different areas separated by walls, whereas in typical open-plan factories, OBS paths are determined by machinery and inventory between the two terminals. A total of 16 measurement locations using 4 base station locations were used at Site A.

Site B was an open-plan engine bearing manufacturing plant. It is a single story factory which has approximate outside dimensions of 146 meters long by 110 meters wide. There is a small partitioned extension to the factory that is composed of offices and an employee cafeteria. However, no measurements were recorded in this area; all Site B measurements were restricted to the large open area with the given dimensions. This area has a concrete floor and a metallic grid-like roof design located about 8 meters above the floor. The grid-like roof design refers to high conveyor belts, hanging lights, metal conduit, etc., and is consistent throughout the factory. With the exception of one 25 meter section of one wall constructed of sheet metal, all exterior walls are constructed of preformed concrete.

The plant layout, although simple in terms of overall size and general structure, is very complex when the details of each potential radio wave scatterer are considered due to the large amount of machinery and inventory within the building. An attempt to describe each of them would be futile. However, a general large-scale environment of various machinery and inventory is consistent throughout the factory.

Representative channels at Site B are from the base station through a environment of machines, inventory, and factory personnel to the mobile terminal. OBS topographies for Site B are determined when one antenna is shadowed from the other by machines or inventory, which differs from Site A, in which OBS paths are typically determined when one terminal is in a completely different part of the building, or "room", than the other. For most measurements at Site B, little physical differences exist between the high and low antenna configurations; only in rare cases when the mobile antenna is completely obstructed from the low base station antenna but is clearly unobstructed from the high base station

antenna does a significant difference exist. However, this difference does not occur very often in any building. Measured propagation results presented in Chapter 4 indicate this. Generally, the large-scale geometric characteristics of all Site B measurement locations are similar. Propagation results which indicate the randomness of measured path loss values recorded at Site B support this statement. A total of 19 measurement locations using 4 base station locations were used at Site B.

Site C was a 6 floor textile manufacturing plant. The factory has areas that are similar to the open areas at Site B, as well as areas which are smaller and more congested with dense machinery that spans floor-to-ceiling, which are denoted as the confined areas of Site C. The confined areas have an "effective" ceiling height of about 3 meters, as opposed to about 7 meters in the open-plan areas. The "effective" ceiling height again refers to the height above the floor at which a grid-like structure of pipes, conduit, and steel beams is located. Although the factory has 6 floors, only the ground floor contains the open-plan areas, while floors 2–6 are all similar in size to each other and make up the confined areas. Exactly half of the measurements recorded at Site C (base station locations A and B) were taken in confined areas of the second and third floor, and half were located in the open-plan areas of the first floor (base station locations C and D). Since the topographies of these areas are distinctly different, they will be described separately.

The general layout of the confined areas is sketched in Figure 2.5-1. The confined areas are in rooms with overall approximate dimensions of 66 meters long by 26 meters wide. The walls of the confined areas are brick but are typically shadowed by nearby metal storage bins and machinery. Rows of metal machinery that extend from floor to ceiling expand the entire length of the room and run parallel to the end walls. From the center of one row of machinery to the center of the next spans 4.5 meters, with the rows of machines approximately 2.4 meters wide and aisles between them approximately 2.1 meters wide. Each row of machines is continuous in that no physical separation exists between machines in a row. Each row is 18 meters long. Aisles that run perpendicular to the rows are between the ends of the rows and the side walls.

Measurements taken in the open-plan areas of Site C are similar to the

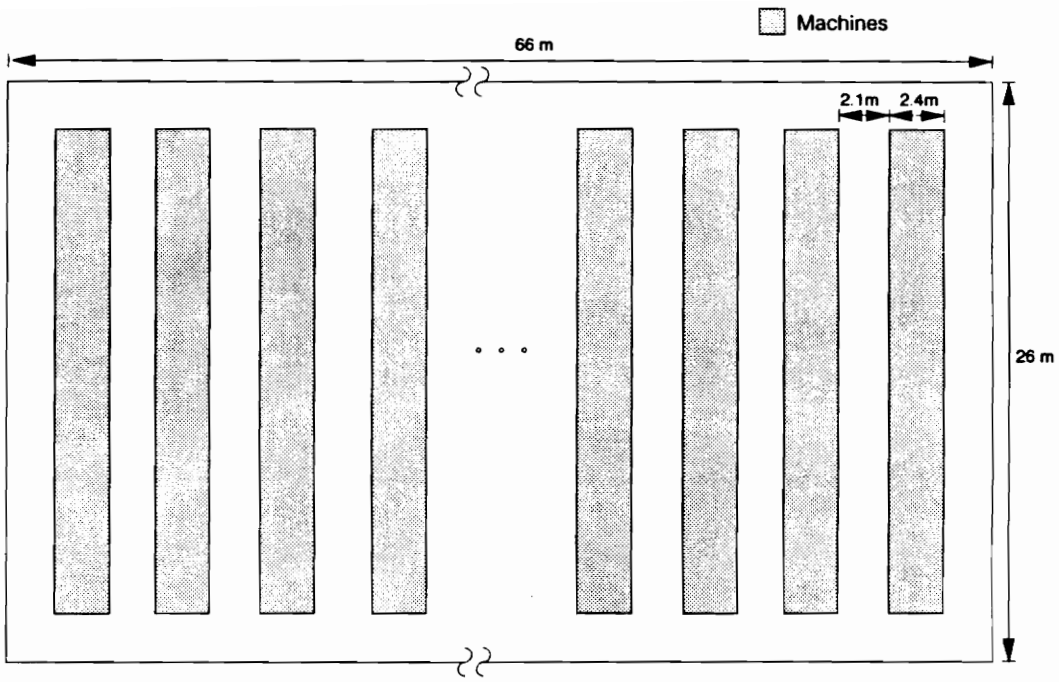

Figure 2.5-1. Overhead sketch of the general layout of the confined areas of Site C.

measurements of Site B, except for the following notable difference. Measurements taken in the open-plan areas of Site C were with the transmitter and receiver typically surrounded by non-reflective textile inventory, while the measurements at Site B were with the terminals surrounded by larger and more reflective metal machinery and inventory. Thus, in a very general way, topographies of the open-plan areas of Site C are loosely comparable to those in the arena of Site A in that they both are in large open areas in which few significant metal reflectors are present. The effective height of the metallic ceiling structure for the open-plan areas of Site C is 6 meters, and the walls are constructed of reinforced concrete cinder blocks.

Representative LOS topographies in the confined areas are with the base station at a corner of the area (potential location for a base station in a communication system) and the mobile at the same end of the rows of machinery. Representative OBS topographies are with the base station at the corner of the area, and the mobile either in an aisle between the machinery or in the end aisle opposite the base station (See Figure 2.5-1). In either case, unlike the OBS topographies of Site B, the direct paths of these OBS topographies are completely obstructed by long, "wall-like" rows of metal machinery. Thus the difference between LOS and OBS topographies is much more severe due to this heavy obstruction for the confined areas of Site C than for any areas of Site B. Representative topographies in the open-plan areas closely resemble the topographies of Site B, except for the noted difference in the amount and composition of typical scatterers in the areas. A total of 8 measurement locations using 2 base station locations were used for both the confined areas and the open-plan areas of Site C. Thus the total number of measurement locations is 16, and the total number of base station locations is 4.

Site D is Whittemore Hall, a closed-plan office building and the electrical engineering building on the campus of Virginia Tech. The building has 6 floors, although measurements were limited to the fifth and sixth floors. A limited amount of data were recorded at Site D due to the limitation in the operating range of the measurement system. This limitation is caused by the severe path loss found at Whittemore Hall, which itself is a significant result and is discussed in Chapter 4. The outside dimensions of Site D are 79 meters long by 27 meters

wide. The insides of the exterior walls and all internal partitioned walls are typically constructed of reinforced concrete (load bearing walls) or drywall supported by vertical metal studs. The outsides of the exterior walls are concrete and stone. The typical topography of the building has offices and laboratories segregated by partitioned walls and accessed to by 2.5 meter wide corridors. The floor is constructed of ceramic tiles mounted on a concrete base, and the ceiling is a standard dropped ceiling structure made of 0.7 meter square, 2 centimeter thick foam ceiling tiles supported by 2 centimeter wide aluminum strips. The height of the dropped ceiling is 2.5 meters above the floor. The actual separation between the floors is a reinforced concrete ceiling located 1.7 meters above the dropped ceiling. Measurements taken at Site D were typically made with the base station located at a sixth floor central point at which three corridors converge (again, a likely potential base station location for future systems), and the mobile located at various positions throughout the corridors of the sixth floor. For two measurement runs, the mobile was in corridors on the fifth floor.

Typical OBS topographies at Site D are with the base station located in one corridor and the mobile located in another. Thus the obstruction is typically one or more partitioned walls, either drywall with metal studs or reinforced concrete. A total of 7 measurement locations using 1 base station location were used at Site D.

2.6 Summary

This chapter presented a detailed discussion of the experimental design employed during the first measurement campaign. The time domain measurement apparatus has been described, as were pertinent system calculations which reveal that thermal and man-made noise levels, and not lack of detector sensitivity, limit weak signal reception. A detailed description of the measurement procedure was presented. The system calibration methods that were used during the measurement campaign were also presented, as were detailed descriptions of the four measurement locations in which propagation data were recorded.

3 File Management and Data Processing

The large database obtained during the measurement phase prompted considerable thought into determining the most efficient, secure, and structured methods to classify and store the raw and processed data files and the calculated results. This chapter illustrates the file classification and storing methods, and fully describes all data reduction and processing procedures.

3.1 File Classification

Following the measurement phase and before the data processing phase, the data files were classified into several categories defined by frequency, topography, T-R separation, building, and receiver antenna height. This classification process was necessary in order to draw accurate and meaningful conclusions from the results. There are two ways to determine all of the above parameters for each measurement run – by an examination of the Microsoft Disk Operating System (MS-DOS) subdirectory in which the file is located and by an examination of the base filename. Each raw data file is located in one of nine subdirectories of a raw data directory according to topography and T-R separation. Figure 3.1-1 illustrates the nine subdirectories in which the data files are located.

Each data file is classified in either a line-of-sight (LOS), obstructed (OBS), or partially obstructed (PAR) topography. The PAR topographies include measurement locations in which the transmitter moves from a LOS topography to an OBS topography, or vice-versa, during one measurement run. The PAR classification consists of less than 10% of the total number of runs. For each of the 3 topographical classifications, there are 3 T-R separation subdirectories. All files from measurement runs in which T-R separations were less than 25 meters are located in the subdirectory called TRLOW. For T-R separations between 25 meters and 50 meters, the subdirectory is called TRMED, and for T-R separations greater than 50 meters, it is called TRHIGH.

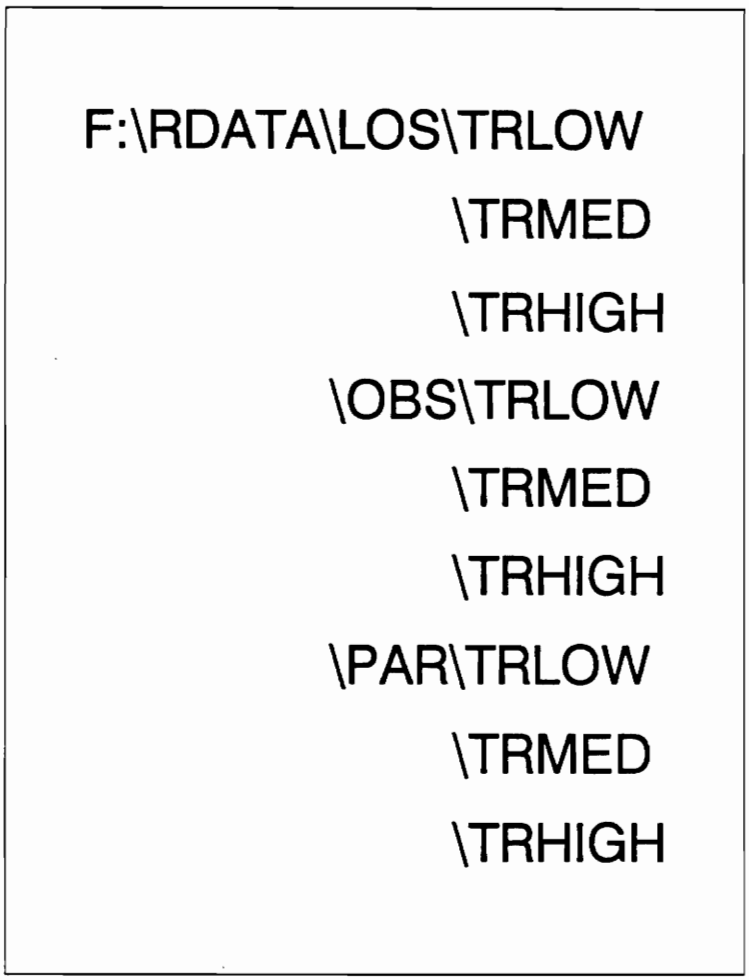

Figure 3.1-1. Listing of the nine subdirectories in which the raw data files are located.

Frequency, building, base station and measurement location, and receiver antenna height can all be determined by a simple examination of the base filename (without the extension). Figure 3.1-2 illustrates how a typical filename, **F1B2A04H**, should be examined to determine the above parameters. Building identifiers B1-B4 in the filename correspond to what previously has been named Sites A-D, respectively.

Measurement locations were selected carefully to ensure the collection of an equal amount of data from LOS and OBS topographies. In total, 201 measurement runs were recorded at 57 measurement locations in 4 buildings. For a few of the measurement locations, due to ceiling height limitations, measurements were made at one antenna height only, causing the total number of measurements for high antennas to be slightly less than for low antennas. The number of measurements taken in the middle T-R separation range (between 25 m and 50 m) exceeded the number of measurements taken in each of the other ranges by approximately a factor of two. The measurements recorded in this range had T-R separations that were evenly dispersed between 25 meters and 50 meters. Table 3.1-1 summarizes the number of runs and the percentage of the overall total for each classification.

3.2 Data Storage

The data acquisition program *capture.c* was written in C and operated on a personal portable computer, which was interfaced with the oscilloscope. The C code for *capture.c* is listed in Appendix B. For each measurement run, the program stored 3 files on the computer's hard disk drive. One file, called *filename.dat*, consists of 256 raw data points for each of 128 power delay profiles recorded by the oscilloscope. These data are stored in block binary format for storage efficiency. The second file, called *filename.hdr*, is also a binary data file which consists of the oscilloscope preamble parameters such as volts/division, time/division, etc. The third file, called *filename.des*, is a descriptive text file which consists of important parameters for the measurement run such as T-R separation, topographical classification, receiver attenuation value, antenna heights, AGV speed and direction, and a brief description of the physical

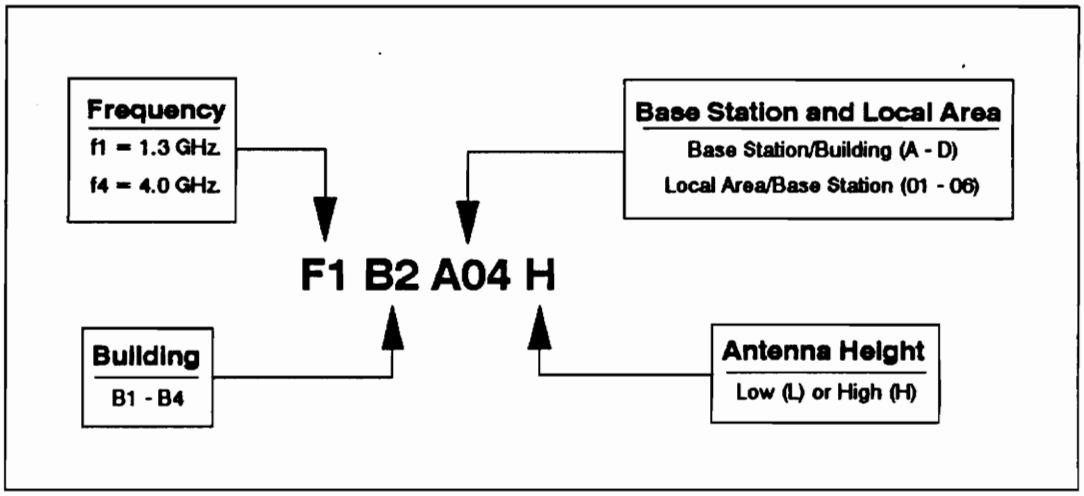

Figure 3.1-2. Breakdown of a typical base filename.

Table 3.1-1. The number of measurement runs and the percentage of the overall total for each measurement classification.

	Number of Runs	% of Total Runs
1.3 GHz.	100	49.8
4.0 GHz.	101	50.2
LOS Topography	93	46.3
PAR Topography	19	9.4
OBS Topography	89	44.3
High Antenna (4.0 m)	92	45.8
Low Antenna (1.7 m)	109	54.2
Site A	50	24.9
Site B	74	36.8
Site C	64	31.8
Site D	13	6.5
T-R < 25m	47	23.4
25m < T-R < 50m	102	50.7
T-R > 50m	52	25.9

environment. An "in-line" software logging feature forced the program operator to complete the description before any data were recorded, and thus eliminated the omission of critical information. Figure 3.2-1 is an example of a typical *.des* file.

Following the measurement phase, the entire database was transferred to a a University Systems 386-25 MHz personal computer and classified into the 9 subdirectories described in the last section. The *.dat* files were stored on the G:\ sector of the hard drive, while the *.hdr* files, *.des* files, and all data reduction and processing files are stored on the F:\ sector. Figure 3.2-2 is the raw data directory containing all *.dat* files recorded in LOS topographies for T-R separations less than 25 meters (LOS\TRLOW). Figure 3.2-3 is a listing of all processing directories in the LOS\TRLOW subdirectory on the F:\ sector of the hard drive. Each of the 16 directories in Figure 3.2-3 contains the same filenames as in Figure 3.2-2, but with different extensions. This insures that all processed data of the same type (i.e. average path loss values) will be in the same directory, and all processed data for one measurement location will have the same base filename. Having the data and results in this format allows for a more controlled, structured approach to the data analysis.

3.3 Data Reduction

Data reduction procedures include those to quantize the raw data into discrete time bins and to threshold the received power profiles. All data reduction and processing programs were written in Pascal. Listings of computer code is in Appendix B.

Quantization of Data into Bins

Each raw data file consists of 256 data points for each of the 128 power delay profiles recorded during a measurement run. Each profile has either a 200, 500, or 1000 ns full scale time window, which correspond to oscilloscope sampling periods of 0.78, 1.95, and 3.91 ns respectively. In order to compare data files for measurement runs taken with different time windows, the raw power delay profiles were converted into discrete profiles with 3.9 ns bins (The approximate RMS duration of the probing pulse). Thus each quantized file, called

F1B3C01L.DES

Number of snapshots: 128
Frequency of operation: 1
Pre-LNA cable (in feet): 6.000000
T-R separation (in feet): 133.000000
LOS present? y
Triggering cable used? y
Receiver attenuation value: 12.000000
Transmitter antenna height: 68.000000
Receiver antenna height: 68.000000
Description of topography:
    Receiver located in inspection area. Large metal cylindrical ceiling ducts about 15ft. Overall ceilingheight of 20 ft. Large open area with carts of non-reflective textile inventory.
Direction of Vehicle: transverse
Vehicle Speed 2.020000

Figure 3.2-1. Typical *.des* file.

```
 Volume in drive F has no label
 Directory of  F:\RDATA\LOS\TRLOW\DAT

F1B1A03H DAT     65536    3-10-90   10:07a
F1B1A03L DAT     65536    3-09-90    7:10p
F4B1A03L DAT     65024    3-09-90    7:19p
F4B1A03H DAT     65536    3-10-90   12:05p
F1B1A04H DAT     65536    3-09-90    9:34p
F4B1A04H DAT     65536    3-09-90    9:08p
F4B2A03L DAT     65536    3-11-90    3:01p
F4B2A03H DAT     65536    3-11-90    3:11p
F1B2A04H DAT     65536    3-11-90    3:54p
F4B2A04H DAT     65536    3-11-90    4:05p
F1B2A04L DAT     65536    3-11-90    4:47p
F4B2A04L DAT     65536    3-11-90    4:56p
F4B2C01L DAT     65536    3-12-90   10:22a
F1B2C01L DAT     65536    3-12-90   10:29a
F1B2C01H DAT     65536    3-12-90   10:39a
F4B2C01H DAT     65536    3-12-90   10:46a
F4B3A04H DAT     65536    3-23-90   10:58p
F4B3A04L DAT     65536    3-23-90   11:08p
F4B3B04H DAT     65536    3-24-90    2:15p
F4B3B04L DAT     65536    3-24-90    2:22p
F1B3B04L DAT     65536    3-24-90    2:43p
F4B4A03L DAT     65536    4-01-90    6:29p
F1B4A03L DAT     65536    4-01-90    6:34p
F1B3D03L DAT     65536    3-25-90   12:05a
F4B3D03L DAT     65536    3-25-90   12:12a
F4B3D03H DAT     65536    3-25-90   12:22a
F1B3D03H DAT     65536    3-25-90   12:27a
F1B3B04H DAT     65536    3-24-90    1:57p
       28 File(s)    888832 bytes free
```

Figure 3.2-2. Raw data directory of all *.dat* files recorded in LOS topographies for T-R separations less than 25 meters (LOS\TRLOW).

```
 Volume in drive F has no label
 Directory of  F:\RDATA\LOS\TRLOW

.             <DIR>       5-29-90   4:36p
..            <DIR>       5-29-90   4:36p
THR           <DIR>       6-07-90   9:31a
TRS           <DIR>       7-08-90   4:32p
AVG           <DIR>       6-26-90   7:10p
JIT           <DIR>       7-01-90   4:26p
ATT           <DIR>       7-08-90   4:32p
DDJ           <DIR>       7-01-90   4:26p
JTS           <DIR>       7-01-90   5:54p
DJS           <DIR>       7-01-90   5:54p
TDP           <DIR>       7-08-90   4:32p
PLS           <DIR>       2-07-91   8:51p
RMS           <DIR>       6-07-90   9:31a
PLD           <DIR>       2-07-91   8:51p
RMD           <DIR>       2-08-91  10:17a
HDR           <DIR>       6-07-90   9:31a
DES           <DIR>       6-07-90   9:31a
       17 File(s)   2725888 bytes free
```

Figure 3.2-3. Listing of all processing directories in the LOS\TRLOW subdirectory.

filename.bin, consists of 128 profiles, each of which are 51, 127, or 255 bins long, for time windows of 200, 500, or 1000 ns respectively. To determine bin amplitudes of each profile, all data points within a designated bin were averaged. For profiles with 200 ns windows (only 1 measurement location), 5 consecutive data points were averaged. For 500 ns windows, 2 points were averaged, and for 1000 ns windows, each data point was designated a bin. An example of the quantization technique used to determine bin amplitudes is illustrated in Figure 3.3-1 for a 500 ns window. The quantization was performed by a computer program called *bindata.pas*.

Display Threshold

In any real-world communication system, measured signals consist of deterministic and stochastic signals, and processed noise. In a wide band radar system, this processed noise can appear as a "false alarm", a falsely detected signal at an arbitrary time and amplitude. An important step in attaining accurate results from wide band propagation experiments is to determine an optimum threshold level for a power delay profile so as to minimize the false alarm rate, and to maximize the probability of detection of a true multipath signal.

Previously used methods to determine the threshold level have been considered for this database. In [30], the threshold level was determined manually after careful visual inspection of profile plots. The unwieldy amount of data collected for this project virtually eliminates this time-consuming technique. In [16], the threshold level was set to the highest point of a small, tail-end portion of each profile, assumed to be only noise power. For our measurements, although careful attention was made to assure that the last 15% of each profile was absent of any multipath components, no guarantee can be made that for every recorded profile (approximately 26,000 total), an occasional late-arriving component wasn't visible at some amplitude higher than the noise floor. If the level is set to the absolute maximum of the last 15% of the profile, these occasional late arriving signals would be lost in the thresholding algorithm. Furthermore, if these signals are strong, the threshold level would be raised to an unreasonable level. Thus, a new threshold technique was investigated.

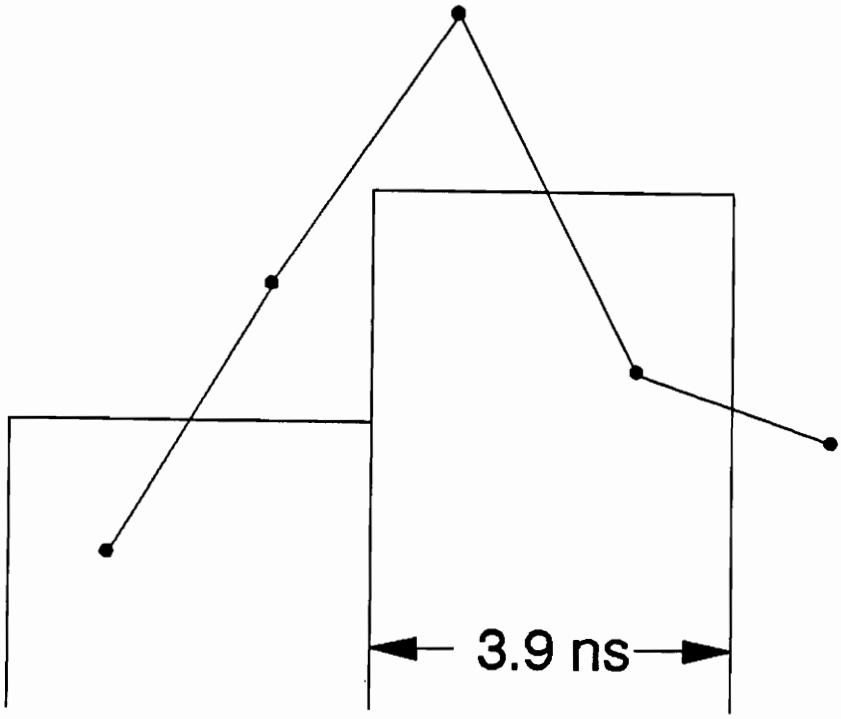

Figure 3.3-1. Illustration of quantization technique used to determine bin amplitudes (500 ns window).

Two experiments were performed in order to gain an understanding of the effects of threshold methods on the false alarm rate and perceived power delay profile parameters such as rms delay spread and path loss. First, a back-to-back noise experiment was performed in which the baseband noise output of the receiver was recorded while the transmitter remained off. The noise level was controlled by adjusting the receiver attenuators. The noise data were quantized into bins and the mean(μ) and standard deviation(σ) were computed for several time windows and attenuator settings. Various threshold levels were then applied to the noise data, and probability of errors were determined from the total number of bins evaluated, of which there were a minimum of 4,350 for each test.

Based on the results from this test, it was determined that a good threshold algorithm is to set the level equal to the mean of the noise plus a factor (C) times the standard deviation of the noise ($\mu + C\sigma$). The noise experiments indicate that for a constant factor C, as the time window and attenuator setting vary (typical of actual recorded data), so does the probability of false alarm. This is most likely due to the nonlinearity of the square law detector. Thus, it was necessary to determine the noise threshold level (factor C) for each profile based on the computed ratio σ/μ, which was empirically found to be a good numerical parameter that represents different time windows and attenuator settings. From an evaluation of the probability of error results for a wide range of values of factor C, it was determined that C should be set to 3.5 for σ/μ less than about 1.3, and 4.0 for σ/μ greater than 1.3.

The second experiment involved the application of our threshold technique to measured data, and the determination of the sensitivity of perceived rms delay spread and path loss values to fluctuations in the factor C. Table 3.3-1 summarizes these results for 2 specific measurement runs, TEST1 and TEST2. A location at which the signal-to-noise ratio is relatively high is represented by TEST1, and a location at which the signal-to-noise ratio is relatively low is represented by TEST2. The results indicate that for TEST2, the average rms delay spread increases 21%, from 131.5 ns to 159.5 ns as C is decreased from 4.0 to 3.0, and path loss decreases 0.5 dB. For TEST1, the rms delay spread increases 8% from 55.1 ns to 59.5 ns and path loss varies only 0.1 dB over the same range of C values. A total of 6 measurement runs were tested for this thresholding

Table 3.3-1. Results from noise threshold experiment which indicate the effect of various noise threshold levels on rms delay spread and path loss.

Location	σ/u	Factor C	Perceived RMS Delay Spread (ns)	Perceived Path Loss (dB) above a 1 m reference
TEST1	1.22	2.5	62.1	31.0
		3.0	59.5	31.0
		3.5	57.1	31.1
		4.0	55.1	31.1
TEST2	1.56	2.5	178.2	37.4
		3.0	159.5	37.8
		3.5	143.5	38.1
		4.0	131.5	38.3

experiment. For the four measurement runs not listed in Table 3.3-1, delay spread and path loss values varied with C between the extreme cases of TEST1 and TEST2.

Received Power Threshold

Although the display threshold method is effective in determining a noise threshold level based on measured statistics of receiver noise power, it does not evaluate the signal-to-noise ratio (SNR) of a measured profile. If the received power is low enough that all multipath components of a profile are nearly or completely lost in the noise floor, subsequent parameter calculations would most certainly be inaccurate. Thus it is necessary to add an additional screening routine to the threshold algorithm to account for profiles with unacceptable signal-to-noise ratios. It was decided that a profile should have a 7 dB ***maximum*** signal to ***maximum*** noise ratio in order for it to be deemed valid for processing. The maximum signal is considered the largest bin amplitude within a profile, and the maximum noise is considered the maximum bin amplitude in the last 15% of the profile. If a profile did not meet this criterion, it was discarded and not considered in computation of the channel parameters. Less than .5% of the data were discarded for inadequate SNR.

Both the display threshold and received power threshold techniques were performed by a computer program called *thrshold.pas*. The program created a binary data file for each measurement run called *filename.thr*. Each *.thr* file consists of 128 thresholded profiles.

3.4 Data Processing

This section describes all data processing procedures. Important multipath channel parameters that were computed include wide band and narrow band path loss and time dispersion parameters such as mean excess delay, rms delay spread, time delay jitter, and differential time delay jitter.

Time Dispersion Parameters

Wide band multipath channels are grossly quantified by their mean excess

delay ($\overline{\tau}$) and rms delay spread (σ_τ) [16,21,23]. Mean excess delay is the first moment of the power delay profile and is defined as

$$\overline{\tau} = \frac{\sum_{k=1}^{N} A_k^2 \, T_k}{G_r} \qquad \text{Where } G_r = \sum_{k=1}^{N} A_k^2 \tag{3.4.1}$$

where A_k^2 is the post-detected voltage of a multipath component in the k^{th} bin, and T_k is the time delay of the k^{th} bin and is measured relative to a first detectable signal arriving at $T_0 = 0$ ns. The rms delay spread is the square root of the second central moment of the power delay profile and is defined as

$$\sigma_\tau = \sqrt{\overline{\tau^2} - (\overline{\tau})^2} \qquad \text{Where } \overline{\tau^2} = \frac{\sum_{k=1}^{N} A_k^2 \, T_k^2}{G_r} \tag{3.4.2}$$

In (3.4.1) and (3.4.2), the index k represents successive temporal bins in a power delay profile and N is the total number of bins for the profile. Since square-law detection is used, the A_k^2 value is obtained from a direct extraction of oscilloscope voltage points, which are directly proportional to the square of the detector input voltage. Since a temporal bin extent of 3.9 ns is used for all measurements for this project, T_k is given by

$$T_k = \frac{3.9(2k - 1)}{2} \qquad (k>0) \tag{3.4.3}$$

Since square law detection is used, the A_k^2 term in (3.4.1) and (3.4.2) can be found by a simple extraction of calculated bin amplitudes.

The rms delay spread is an important parameter in determining bandwidth capacity of a radio channel [5]. Chapter 7 of this thesis discusses the relationship between rms delay spread and bit error rate in a digital signal. Mean excess delay represents the average delay imposed by the multipath as compared to a LOS path. It is used to calculate delay jitter and differential delay jitter, important parameters which give insight into the variation of mean excess delay over a local area and over sub-wavelength physical separations, respectively.

For each measurement run, average values of $\overline{\tau}$ and σ_τ were calculated via

two methods. As in past wide band measurement campaigns [16,23], a spatially averaged profile was computed for each measurement run by computing an average value for each oscilloscope point. The parameters $\overline{\tau}$ and σ_τ were then computed for this average profile, using (3.4.1) and (3.4.2). This method, which we call ***profile averaging***, was used for the database in this project. Also, values of $\overline{\tau}$ and σ_τ were computed for each of the 128 profiles recorded during a measurement run, and average values of $\overline{\tau}$ and σ_τ were found by averaging the individual parameters for each profile. We call this method ***parameter averaging***.

Another computed parameter is excess delay spread < 10 dB, which is defined as the maximum excess delay at which a multipath component is received with an amplitude within 10 dB of the maximum level of the profile. Results for this parameter are presented as the worst case maximum excess delay spread < 10 dB in a measurement run. Figure 3.4-1 is an example of a power delay profile for an OBS topography at a T-R separation of 48 meters. The rms delay spread, mean excess delay, maximum excess delay < 10 dB, and display threshold level are indicated on the plot. A complete data set of spatially averaged profiles similar to Figure 3.4-1 is given in Appendix A of [43].

A program called *rms.pas* computed $\overline{\tau}$ and σ_τ. Values of σ_τ for each profile are stored in block binary format in a *.rmd* file. The average and standard deviation for $\overline{\tau}$ and σ_τ over each run were also computed, as was the maximum excess delay < 10 dB. All five values were stored in a *.tdp* file (tdp stands for time dispersion parameters). Finally, σ_τ was computed for the spatially averaged profile and stored in a *.rms* file, located in the **\avg** subdirectory of Figure 3.2-3.

Time delay jitter and differential delay jitter were also computed. Time delay jitter is found from the mean excess delay for all individual profiles and the spatially averaged profile in a measurement run. Let $\overline{\tau}_a$ denote the mean excess delay of the spatially averaged profile of a measurement run, and $\overline{\tau}_i$ denote the mean excess delay of an individual profile, where i = 1 to 128 for this database. Following the notation of [31], we let J_i represent time delay jitter for a profile, defined by

$$J_i = \overline{\tau}_i - \overline{\tau}_a \tag{3.4.4}$$

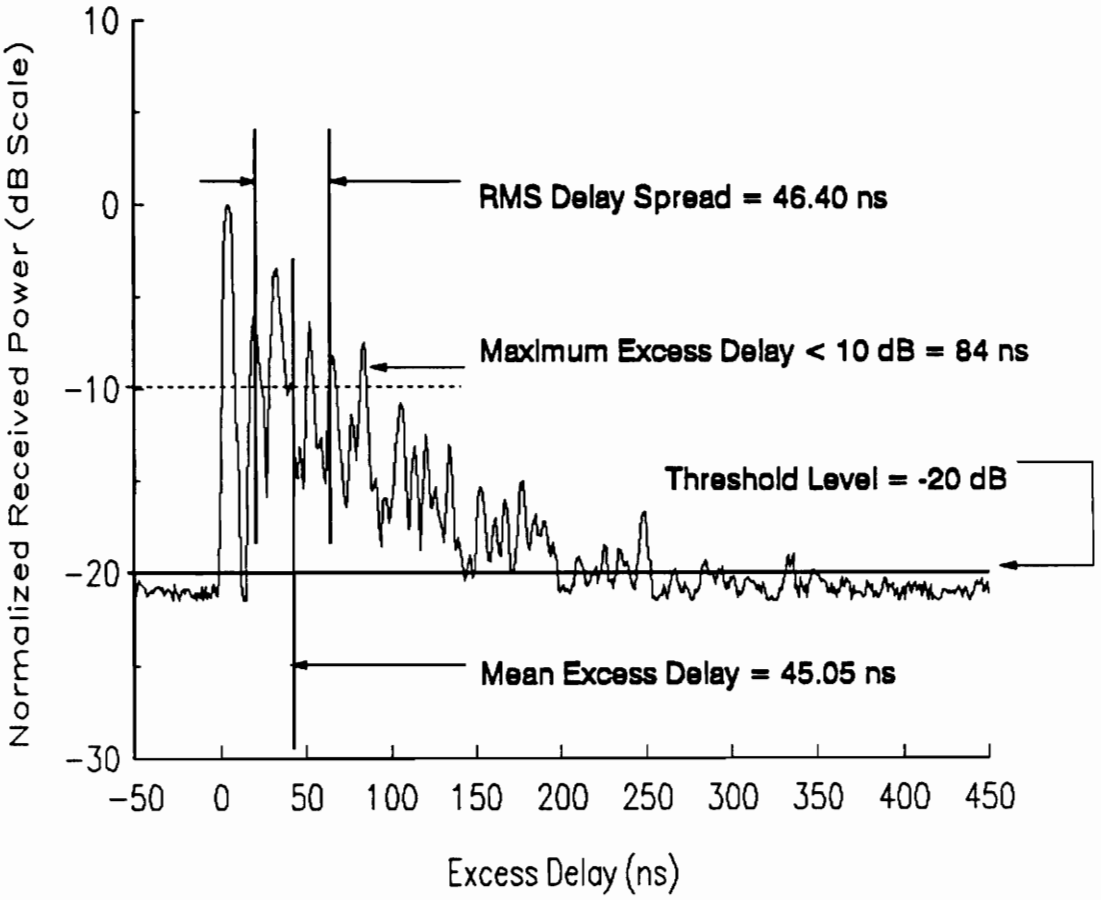

Figure 3.4-1. Example of a power delay profile with a 500 ns time window; rms delay spread, mean excess delay, maximum excess delay < 10 dB, and display threshold level are shown; y-axis is in dB.

J_{MAX} is the magnitude of the maximum delay jitter for all profiles in a measurement run. Differential delay jitter ($\Delta J_k/\Delta s$) and peak-to-peak differential delay jitter $(\Delta J_k/\Delta s)_P$ were introduced in [32]. Differential delay jitter indicates the differences of mean excess delay over small receiver distances Δs, as determined by the spatial increment between successive profiles in a measurement run. For these data, Δs was 0.25λ for all measurements. Differential delay jitter is defined by

$$\Delta J_k/\Delta s = \bar{\tau}_{k+1} - \bar{\tau}_k \qquad k = 1, 127 \tag{3.4.5}$$

$(\Delta J/\Delta s)_{MAX}$ the magnitude of the maximum differential delay jitter for a measurement run. Time delay jitter indicates the variability of multipath fading for a particular measurement location, and differential delay jitter indicates the variability of fading of individual multipath components over sub-wavelength spatial separations.

A program called *jitter.pas* computed time delay jitter and differential delay jitter values for each profile (pair of successive profiles for differential delay jitter) and stored them in *.jit* and *.ddj* files, respectively.

Wide Band Path Loss

In [23], it is shown that the path loss can be estimated from the power delay profile, provided that all detectable multipath components are within the time window of the oscilloscope. G_R, the denominator in equation (3.4.1), is a summation of received powers for each bin in a profile. By multiplying this summation by the total time window of a profile, an integration of the power delay profile, or the total received energy, is found. By referencing this energy to the energy received at a free space reference location, the path loss of the channel is computed. Let $PL(dBr_{10\lambda})$ represent the path loss in dB above the free space path loss reference $PL_{10\lambda}(dB)$, which was measured via an experiment in which the system was taken outdoors into a virtually multipath-free environment and placed at a T-R separation of 10λ (Chapter 2, Section 2.4). Throughout the campaign, the system did not behave exactly the same at all times (i.e. it did not maintain the same transmitter power, amplifier gains, etc). The system varied as

much as 3 dB in received power from one back-to-back calibration to another. Thus, during the measurements, back-to-back calibrations were conducted several times daily, and all path loss calculations were referenced to the appropriate calibration measurement.

Let G_{sub} represent the power summation, A_{sub} represent receiver attenuator settings, and ΔT_{sub} represent temporal bin extents. The subscript **R** represents typical measurements and the subscript **10λ** represents the controlled free space experiment. The subscript **REF** without the superscript $*$ represents the back-to-back calibration taken just prior to the 10λ experiment, and the subscript **REF** with the superscript $*$ represents an appropriate back-to-back calibration taken in the field. $PL(dBr_{10\lambda})$ is then given by

$$PL(dBr_{10\lambda}) = [\overset{*}{A}_{REF}(dB) - A_R(dB)] + 10 \log \frac{\overset{*}{G}_{REF}\overset{*}{\Delta T}_{REF}}{G_R \Delta T_R} - PL_{10\lambda}(dB) \quad (3.4.6)$$

Where,

$$PL_{10\lambda}(dB) = [A_{REF}(dB) - A_{10\lambda}(dB)] + 10 \log \frac{G_{REF}\Delta T_{REF}}{G_{10\lambda}\Delta T_{10\lambda}}$$

Wide band results for path loss were computed with reference to the same physical distance (1 meter) in addition to the same electrical distance (10λ). Let $PL(dBr_{1m})$ represent the path loss in dB above a 1 meter reference. From Friis transmission formula (2.1.1), the relationship between $PL(dBr_{1m})$ and $PL(dBr_{10\lambda})$ for 1.3 GHz and 4.0 GHz is easily determined.

$$PL(dBr_{1m}) = PL(dBr_{10\lambda}) - 7.3 \quad \text{at 1.3 GHz.} \quad (3.4.7a)$$

$$PL(dBr_{1m}) = PL(dBr_{10\lambda}) + 2.5 \quad \text{at 4.0 GHz.} \quad (3.4.7b)$$

A program called *pathloss.pas* computed $PL(dBr_{1m})$ for all profiles of each measurement run, and stored the values in block binary format in a *.pld* file. The mean value of $PL(dBr_{1m})$ was also computed and stored in a *.pls* file. Finally, $PL(dBr_{1m})$ was computed for the spatially averaged profile and stored in a *.pls* file, located in the **\avg** subdirectory.

Narrow Band Path Loss

A narrow band commercial receiver and a strip chart recorder provided CW signal strength measurements at 1.3 GHz. The strip chart recordings represents the CW signal strength of the wide band power delay profiles for each measurement taken at 1.3 GHz.

During measurements, the receiver output voltage (strip chart deflection) was calibrated by connecting the output of the 1.3 GHz signal generator directly to the receiver input. Several known input powers were applied and the strip chart deflections were measured. This calibration technique allowed the researchers to determine received power from the strip chart deflection. Since the transmitted power P_T and the receiver system gain G_R are known, and the received power P_R is found via the above calibration technique, the path loss PL is computed by the following equation.

$$PL = P_T - P_R + G_R \tag{3.4.8}$$

Based on the blueprints, the T-R separations at the start, middle, and finish of each measurement run were determined. Median signal strength values P_R were estimated and manually recorded for each of three portions of the strip chart record. Since the exact location of the transmitter, receiver, and specific obstructions are known, it is possible to obtain 1.3 GHz shadowing information for these obstructions. All CW data is located in the F:\CWSTATS subdirectory and stored in *.sts* files. Each *.sts* file is eight lines long. The first line is either LOS or OBS, depending on the topography of the measurement. The next three lines are the T-R separations in meters for the three portions of the measurement run. The next line contains the receiver attenuation level in dB. The last three lines contain received CW signal strengths in dBm for the three portions of the measurement run.

3.5 Summary

This chapter described all file classification, data storage, data reduction, and data processing techniques that were used to extract useful results from the raw data files. Methods of file classification were discussed. Data reduction

procedures such as quantization of raw data files into bins and methods for display and received power thresholding were discussed. After all data reduction procedures were completed, the reduced *.thr* data files were processed to determine important multipath channel parameters such as mean excess delay($\overline{\tau}$), rms delay spread(σ_τ), maximum excess delay $<$ 10dB, time delay jitter, differential delay jitter, and path loss. Average values of $\overline{\tau}$, σ_τ, and path loss were calculated two ways – by averaging the parameters for each profile in a measurement run (***parameter averaging***) and by calculating the values for a spatially averaged profile of a measurement run (***profile averaging***). A comparison of these two methods is in the next chapter.

4 Results

This chapter presents all results obtained from the initial measurement campaign. Results are presented for the channel parameters defined and discussed in the previous chapter, including mean excess delay, rms delay spread, maximum excess delay < 10 dB, time delay jitter, differential delay jitter, and path loss. Path loss results were obtained from wide band power delay profiles at 1.3 GHz and 4.0 GHz, and from narrow band CW fading data at 1.3 GHz only, which were recorded simultaneously with the wide band profiles. Shadowing effects of typical factory and office building obstructions were estimated from the CW data.

The time dispersion results are presented as scatter plots of the measured parameter versus T-R separation, and as cumulative distribution functions (CDFs). Scatter plots present a complete and concise representation of the measured data, and with computed linear regression lines, illustrate effects of T-R separation on time dispersion parameters. Cumulative distribution functions more clearly present the effects of frequency, antenna height, topography, and building structure, and provide a statistical modeling tool for system designers. Since both representations of the data have advantages, both are presented. A typical figure which illustrates results for time dispersion parameters has a scatter plot as part (a) and a CDF as part (b).

The average values of rms delay spread, mean excess delay, and path loss for a measurement run were computed using two methods described in Chapter 3, ***profile averaging*** and ***parameter averaging.*** Mean excess delay and rms delay spread results obtained from profile averaging are consistently 5–15% higher than those obtained from parameter averaging. Path loss values obtained from profile averaging are consistently lower than, but within 2 dB of, those obtained from parameter averaging. The reason for these slight discrepancies is subtle. Because a triggering cable was employed, all profiles for a measurement run were referenced to a fixed time determined by the length of the cable. Thus, as the

mobile moved during a measurement run, multipath components would shift or "walk" on the oscilloscope screen according to the relative change in T-R separation. For profile averaging, a simple oscilloscope point-by-point averaging technique was used to determine the spatially averaged profile, in which the time shift induced by the moving transmitter was not accounted for. This causes the spatially averaged profile to be slightly spread in time and time dispersion parameters to be slightly but consistently inaccurate for profile averaging. As a result, all results for this campaign are presented using parameter averaging.

4.1 RMS Delay Spread (σ_τ)

The square root of the second central moment of a power delay profile is called the rms delay spread (σ_τ), defined by equation (3.4.2). It is a time dispersion parameter that characterizes multipath channels and can be used to estimate data rate and bandwidth limitations for multipath channels [5].

Figure 4.1-1(a) is a scatter plot of rms delay spread as a function of T-R separation, with linear regression lines for each frequency. Each point represents the rms delay spread computed by ***parameter averaging***. The linear regression lines are computed using a least-squares method to estimate the slope and y-intercept of a "best-fit" line given by

$$\overline{Y} = mX + b \tag{4.1.1}$$

Where $\overline{Y}$ represents the estimate of rms delay spread as a function of T-R separation X. The values of the slope m, y-intercept b, and standard deviation about the linear model, are computed from the aforementioned least-squares technique, described in [33]. The standard deviation about the linear model is a quantifying parameter which gives a measure of the predictability of σ_τ about the distance dependent mean. Figure 4.1-1(b) is a CDF of the data in the scatter plot.

Figure 4.1-1 indicates that rms delay spread generally increases with T-R separation at both frequencies. The slopes of the regression lines are 0.74 ns/meter and 0.83 ns/meter for 1.3 GHz and 4.0 GHz, respectively. Also, rms delay spread values are nearly the same for 1.3 GHz and 4.0 GHz, clearly

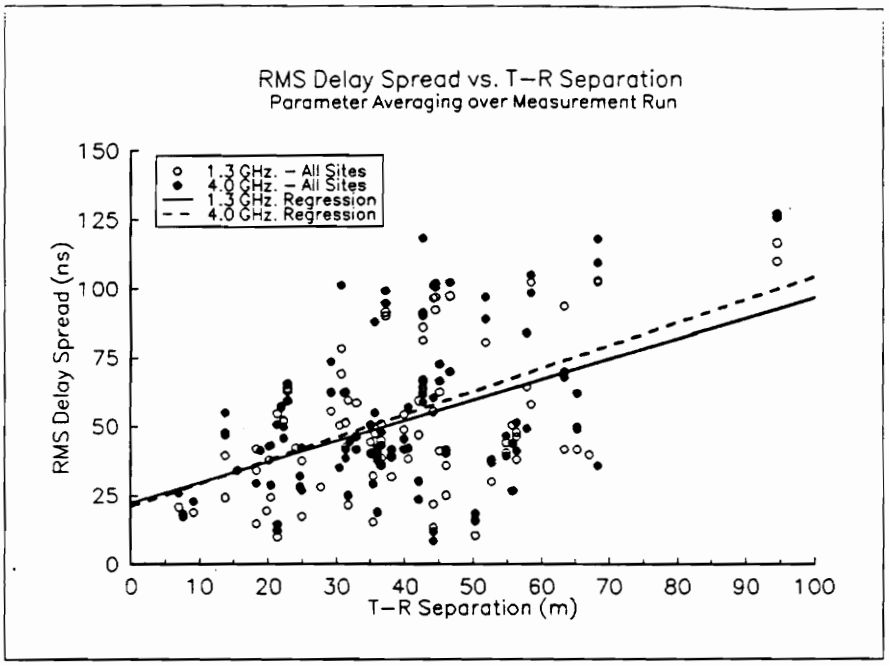

(a) Scatter Plot

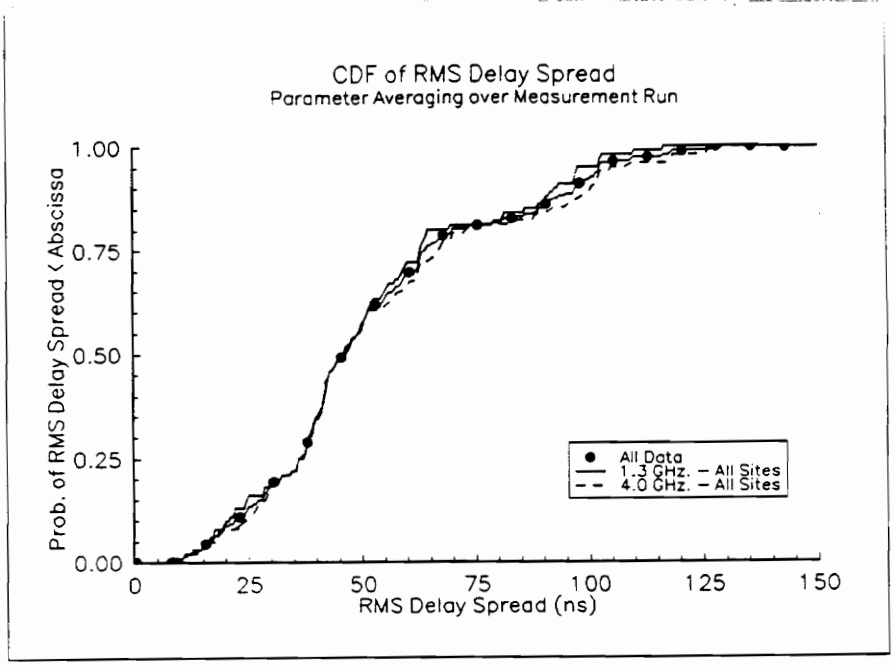

(b) CDF

Figure 4.1-1. (a) Scatter plot and (b) CDF of rms delay spread as a function of frequency only; regression lines for each frequency are given.

illustrated by Figure 4.1-1(b). A comparison of rms delay spread results for two buildings is reported in [20], in which the difference between 910 MHz and 1.75 GHz median rms delay spread values were found to be less than 2 ns for both buildings. Results reported in [19], in which measurements were taken at 850 MHz, 1.7 GHz, and 4.0 GHz in two dissimilar office buildings, also indicate minimal differences in rms delay spread among the three frequencies.

Figure 4.1-2 is a scatter plot(a) and CDF(b) of the same data points, with antenna height as an additional parameter. Low and high antenna height refers to 1.7 and 4.0 meters above the floor, respectively. It was expected that raising the antenna from 1.7 meters to 4.0 meters would, in many cases, change the channel seen by the antennas such that significant differences in σ_τ would be observed. In particular, we expected that with higher antennas, visibility to exterior walls would increase, thereby increasing the delay spread. However, Figure 4.1-2 indicates only a small difference in σ_τ as a function of antenna height. Measurements with a low antenna yield, on average, median values of σ_τ which are about 5 ns lower than those taken with a high antenna.

At Site B, raising the receiver antenna to 4.0 meters often brought the antenna above surrounding obstructions, and in several cases, provided a LOS path to the transmitting mobile that did not exist with the receiver antenna at 1.7 meters. Figure 4.1-3 is a CDF of rms delay spread for Site B only, with antenna height as a parameter. This CDF indicates higher values of σ_τ for the low antenna than for the high antenna at Site B, although the difference is only on the order of 10-20%. Only at certain measurement locations, where a LOS path became evident when the antenna was raised, did σ_τ reduce significantly. For example, for a particular measurement location at Site B, the low antenna was obstructed by several metal tool-making machines, and average values of σ_τ were found to be 89 ns and 88 ns for 1.3 GHz and 4.0 GHz, respectively. When the receiving antenna was raised to 4.0 meters, a very clear LOS path was observed, and average values of σ_τ were reduced to 47 ns and 55 ns for 1.3 GHz and 4.0 GHz, respectively.

Figure 4.1-4 is a scatter plot(a) and CDF(b) of σ_τ as a function of topography (LOS or OBS) and frequency, from which it is evident that σ_τ depends on whether or not a line-of-sight path exists between the transmitter and

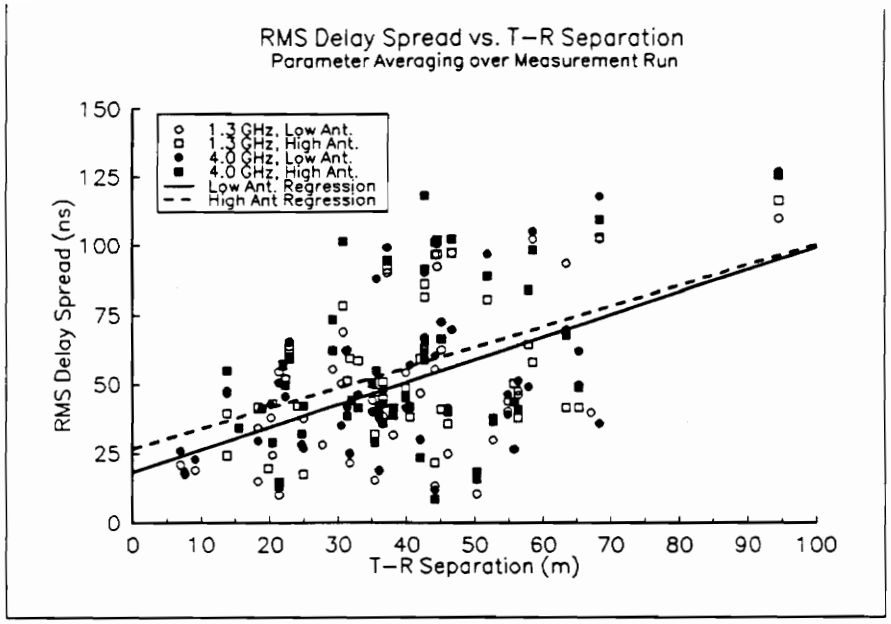

(a) Scatter Plot

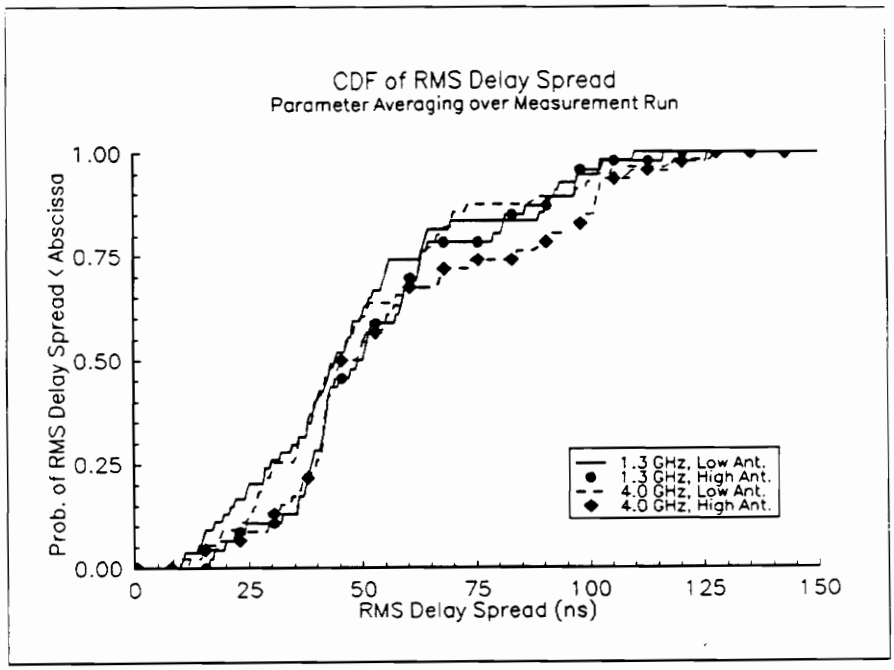

(b) CDF

Figure 4.1-2. (a) Scatter plot and (b) CDF of rms delay spread as a function of frequency and antenna height; regression lines for each antenna height are given.

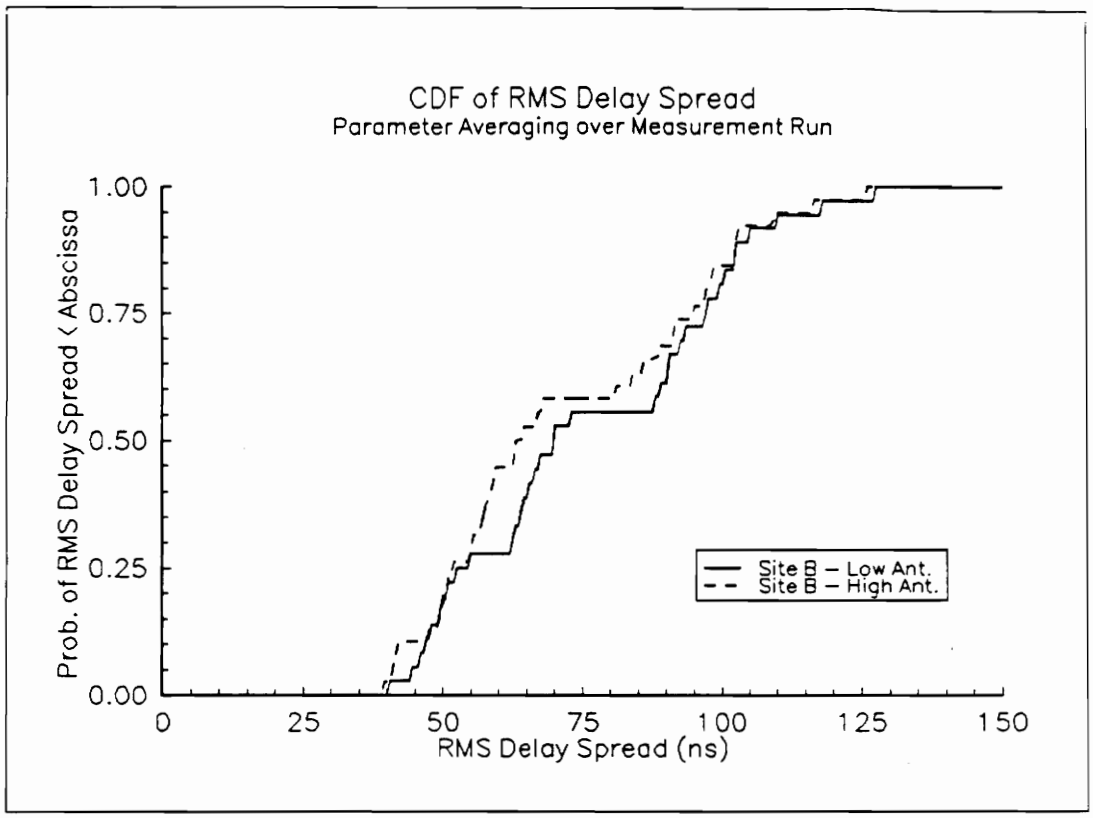

Figure 4.1-3. CDF of rms delay spread for Site B as a function of antenna height.

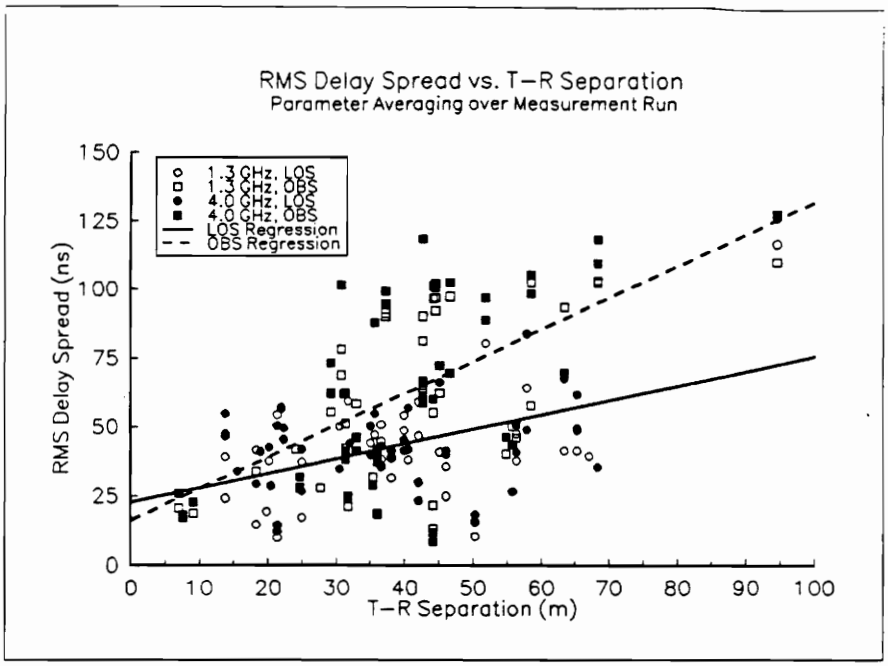

(a) Scatter Plot

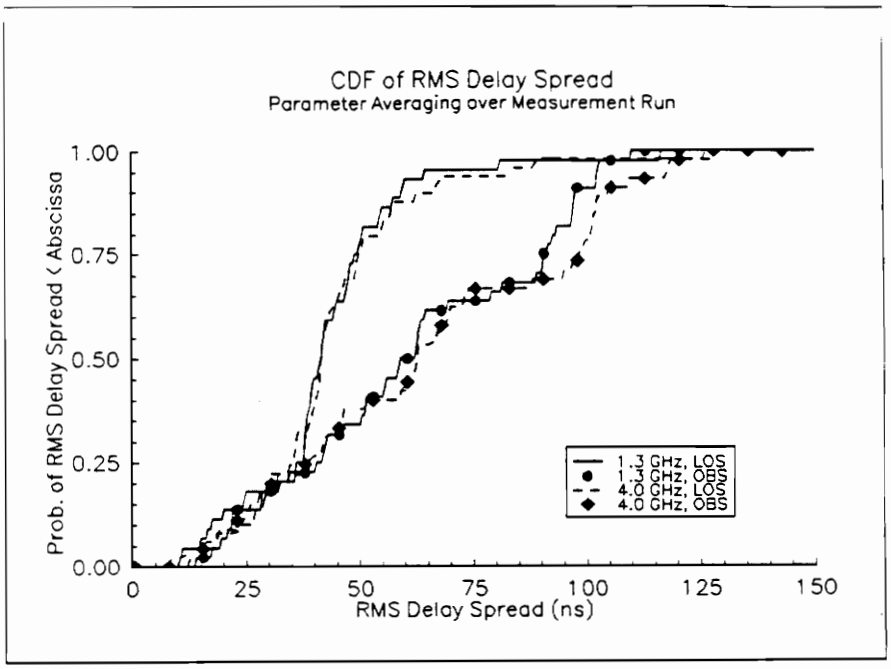

(b) CDF

Figure 4.1-4. (a) Scatter plot and (b) CDF of rms delay spread as a function of frequency and topography; regression lines for LOS and OBS topographies are given.

receiver. The scatter plot illustrates that, with the exception of the single measurement location at a T-R separation of 95 meters, all recorded average values of σ_τ that exceed 90 ns are for OBS topographies. The CDF illustrates, for example, that the probability of delay spread exceeding 75 ns is about 0.1 for LOS topographies and about 0.4 for OBS topographies at both frequencies. This topographical dependence is a significant result in that the performance of future indoor digital systems with high data rate requirements (i.e. radio local area networks) may be significantly dependent on whether a LOS path exists from the transmitter to the receiver.

Figure 4.1-5 is a scatter plot(a) and CDF(b) of σ_τ for individual buildings. Most of the σ_τ values greater than 85 ns are found at Site B, the large open-plan factory filled with metal machinery and inventory. Most of the values at Site D, the closed-plan office building, are less than 50 ns. As the CDFs indicate, the delay spread found in the sports arena (Site A) and the textile manufacturing plant (Site C) are similar. Half of the 16 Site C measurement locations were in relatively uncluttered, large open areas, similar to many locations at Site A. The remaining Site C locations were in smaller, more confined areas with heavy obstruction, similar to many locations at Site D, but with more reflective obstructions. This may partially account for the similarity between the two distributions. Obstructions at Site D were typically partitioned walls and standard dropped ceiling structures, less reflective than the metal machines and construction materials found in the open-plan buildings. Thus, it is reasonable to expect somewhat lower delay spread values at Site D than at Sites A, B, or C.

Worst case values of σ_τ for all profiles are 90 ns for the partitioned office building and 230 ns for the open-plan topographies. Median values range from as low as 22 ns for Site D to 67 ns for Site B. The median rms delay spread value for all individual profiles is 46 ns. In general, values of σ_τ are lower than those reported in [23], in which median values of σ_τ for all profiles were reported to be approximately 100 ns for factory floor environments. This discrepancy may be due, in part, to the lack of noise thresholding for the measurements reported in [23]. Wide band measurements were also conducted on factory floors at 910 MHz using a similar time-domain measurement system [24]. Median σ_τ values for these measurements ranged from 53 ns in a manufacturing environment with many

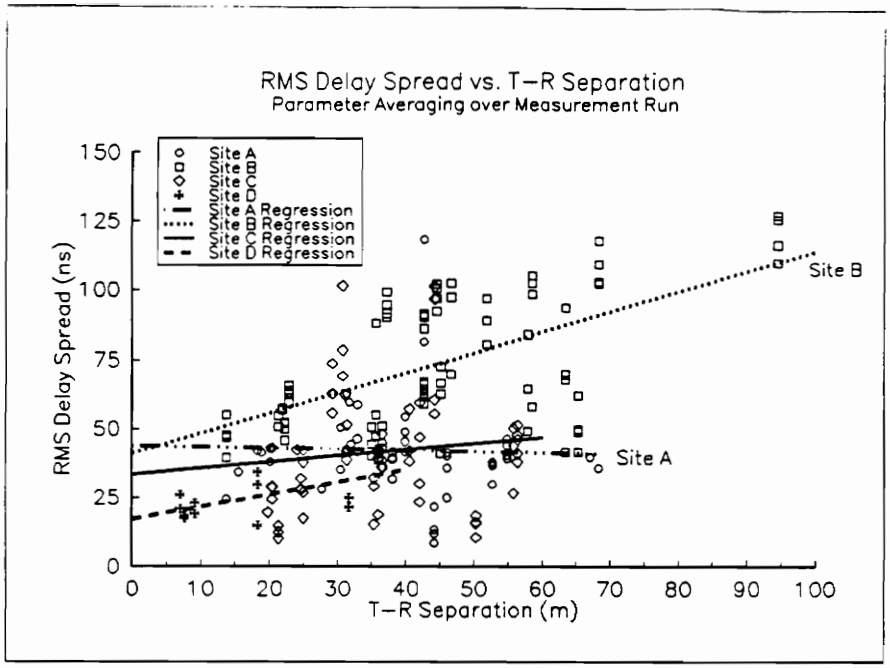

(a) Scatter Plot

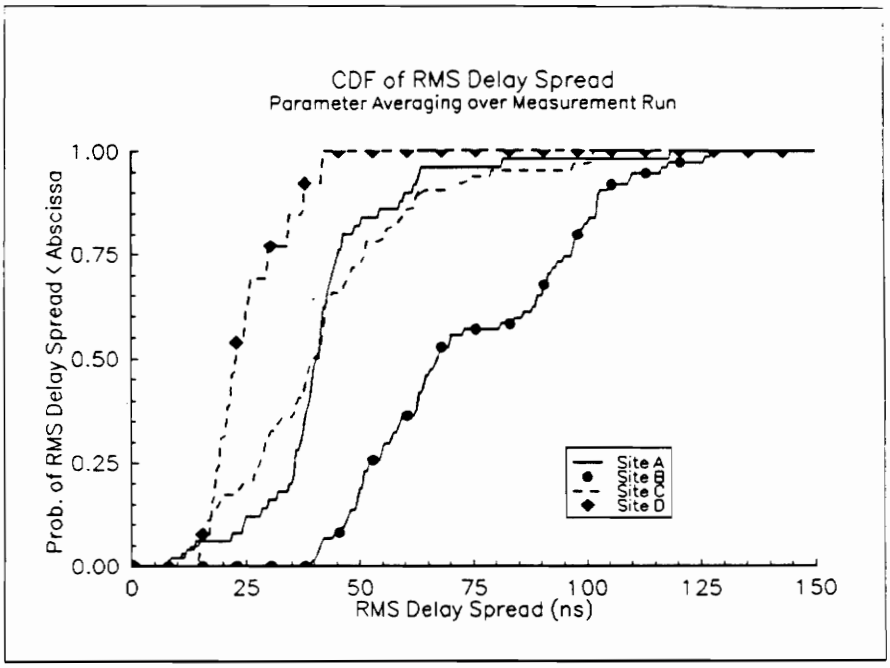

(b) CDF

Figure 4.1-5. (a) Scatter plot and (b) CDF of rms delay spread as a function of frequency and building; regression lines for each building are given.

surrounding scatterers to 15 ns on an electronics shop floor. These median values and their corresponding topographies are comparable to the values of 22 ns and 67 ns for Sites A and D, respectively. The results of measurements recorded at 1.5 GHz inside a meeting room, an office, and a laboratory are reported in [22], in which median values of σ_τ are reported to be 28 ns for the office and meeting room and 34 ns for the laboratory. In [22], maximum values of σ_τ were found to be approximately 75 ns for the office and meeting room, and 130 ns for the laboratory.

Table 4.1-1 summarizes the slopes, y-intercepts, and standard deviations about the linear model for all linear regression lines used on rms delay spread scatter plots. Notice that the standard deviation for the OBS linear regression curve is 24 ns, and the standard deviation for the LOS linear regression curve is 17 ns. This indicates that OBS topographies generally have higher and less predictable rms delay spreads than LOS topographies. Less predictability with increased delay spread is evident for most classifications in Table 4.1-1. This is further indicated by the relatively low standard deviation for Site D (7 ns), as compared with the other sites (19 ns average). This low standard deviation for Site D may indicate a more predictable channel for closed-plan office buildings due to more defined obstructions. However, much more data are needed in closed-plan office buildings before a definitive conclusion can be drawn.

4.2 Mean Excess Delay ($\overline{\tau}$)

The mean excess delay of a power delay profile ($\overline{\tau}$), defined by (3.4.1), is the first moment, or centroid, of the power delay profile, and is a useful parameter to determine the extent of distortion in a narrow band FM system. This is true because phase-locked loop circuitry necessary for coherent-detection receivers (i.e. FM receivers) will phase track as a function of the centroid of the delay profile of a radio channel [34]. The more this centroid varies (as the channel varies), the more phase error exists in the locking circuitry, which results in distortion in the detected audio signal.

The general trends for significant rms delay spread results presented in the previous section are similar to trends for mean excess delay. For example, the effects of frequency and antenna height on $\overline{\tau}$ were very minor, whereas the effects

Table 4.1-1. Slopes, y-intercepts, and standard deviations for all rms delay spread linear regression models presented on the scatter plots.

	Slope (ns/meter)	Y-Intercept (ns)	Standard Error of Estimate (ns)
1.3 GHz - All Files	0.74	22	22
4.0 GHz - All Files	0.83	21	25
Low Antenna	0.81	18	22
High Antenna	0.74	26	24
LOS Topography	0.53	23	17
OBS Topography	1.15	16	24
Site A	-0.04	44	17
Site B	0.73	41	19
Site C	0.22	33	21
Site D	0.45	17	7

of topography and building were significant. Thus, only the notable scatter plots and CDFs for mean excess delay are presented.

Figure 4.2-1 is a scatter plot(a) and CDF(b) of $\overline{\tau}$ as a function of frequency and topography. There is a remarkable similarity between this CDF and Figure 4.1-4(b), the CDF for rms delay spread as a function of frequency and topography. Figure 4.2-2 is a scatter plot(a) and CDF(b) of $\overline{\tau}$ for individual buildings. All average values of $\overline{\tau}$ greater than 100 ns are from Site B, and all Site D values are lower than 55 ns. One notable difference between σ_τ and $\overline{\tau}$ is that as many as seven $\overline{\tau}$ values exceed 125 ns, with the highest at approximately 135 ns. Recall that no value of σ_τ exceeded 125 ns. Table 4.2-1 summarizes the slopes, y-intercepts, and standard deviations about the computed linear regression models for mean excess delay. A comparison between Tables 4.1-1 and 4.2-1 indicate the standard deviations for mean excess delay are higher than standard deviations for rms delay spread, which indicates less predictability for mean excess delay than for rms delay spread. Worst case and median values of mean excess delay for all individual profiles are about 230 ns and 35 ns, respectively.

4.3 Maximum Excess Delay < 10 dB

The maximum excess delay < 10 dB was computed for each measurement run, and is defined as the largest excess delay at which a multipath component has an amplitude within 10 dB of the strongest component in a profile. Results are presented as the maximum excess delay < 10 dB for all profiles in a measurement run.

Figure 4.3-1 is a scatter plot(a) and CDF(b) of maximum excess delay as a function of frequency. Unlike rms delay spread and mean excess delay, maximum excess delay appears to be slightly dependent on frequency. The CDF indicates that on average, 4.0 GHz produces slightly higher maximum excess delays than 1.3 GHz. However, this result may be partially biased by the fact that, at several measurement locations, less signal-to-noise was present at 4.0 GHz than at 1.3 GHz, which may have resulted in the detection of occasional noise false alarms at high excess delays. Since the parameter has been defined as the maximum time in which a multipath component (< 10 dB) is detected over all 128 profiles in a measurement run, just one occurrence of this noise detection for a given

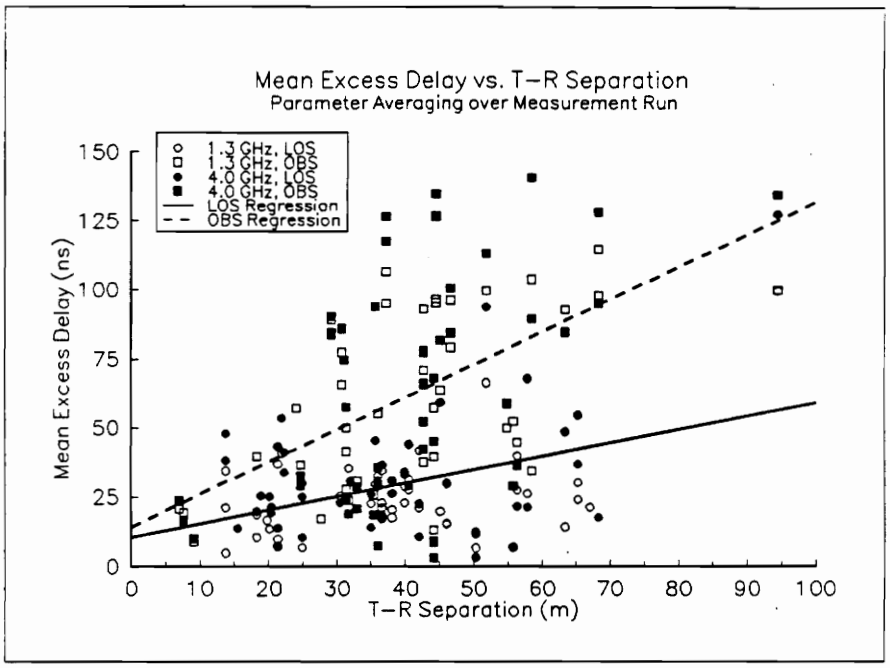

(a) Scatter Plot

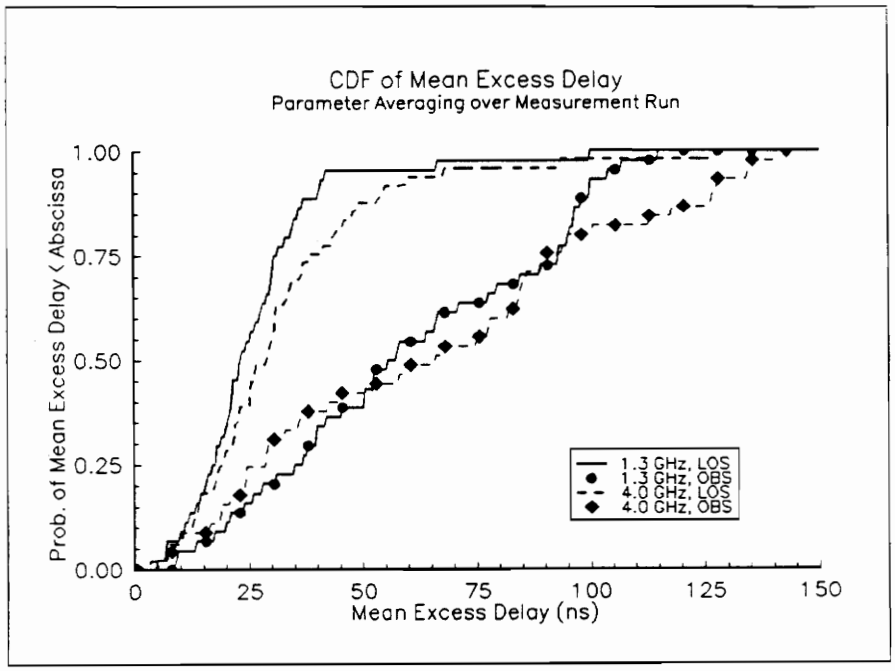

(b) CDF

Figure 4.2-1. (a) Scatter plot and (b) CDF of mean excess delay as a function of frequency and topography; regression lines for LOS and OBS topographies are given.

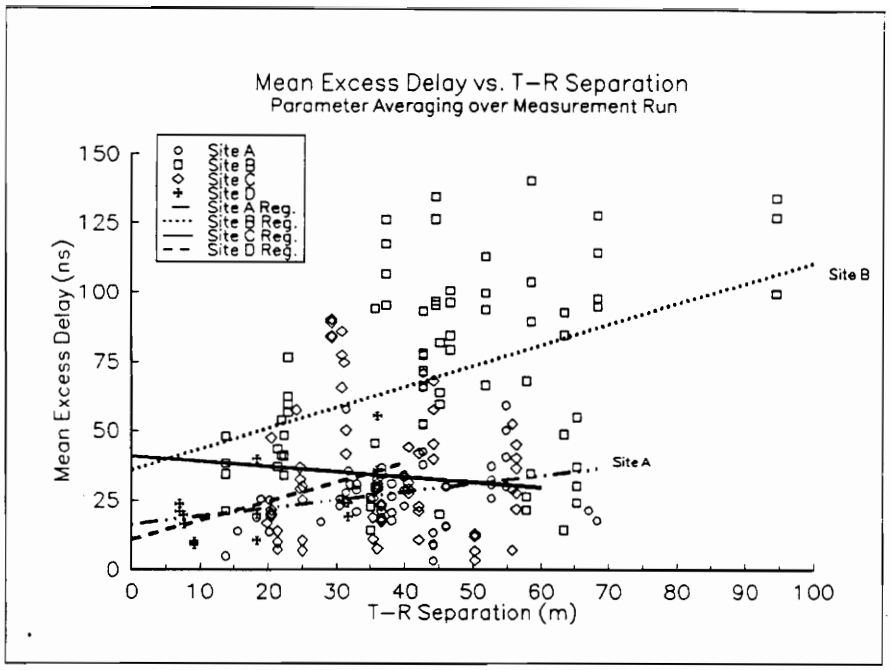

(a) Scatter Plot

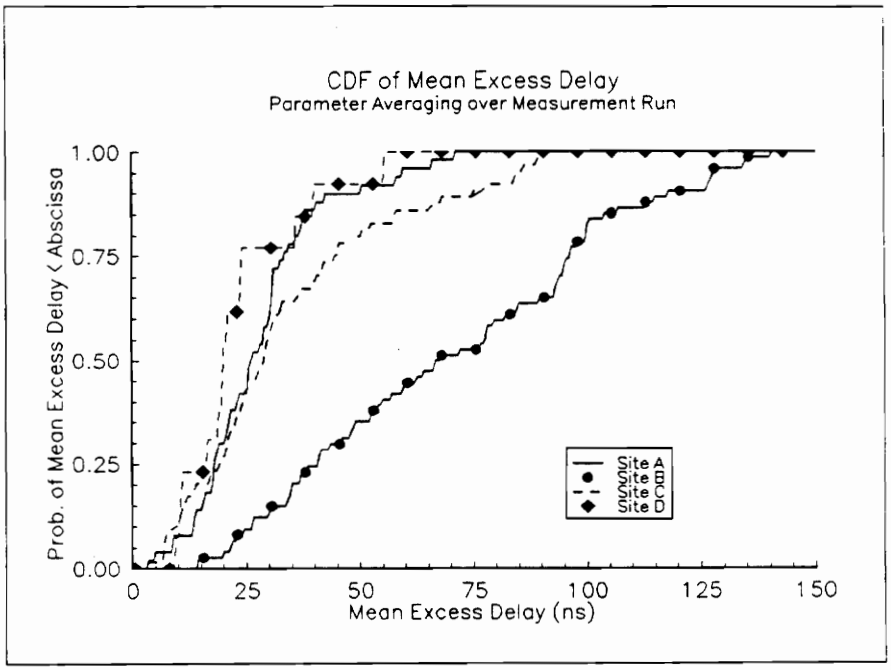

(b) CDF

Figure 4.2-2. (a) Scatter plot and (b) CDF of mean excess delay as a function of frequency and building; regression lines for each building are given.

Table 4.2-1. Slopes, y-intercepts, and standard deviations for all mean excess delay linear regression models presented on the scatter plots.

	Slope (ns/meter)	Y-intercept (ns)	Standard Error of Estimate (ns)
1.3 GHz - All Files	0.66	17	27
4.0 GHz - All Files	0.92	11	32
Low Antenna	0.89	11	31
High Antenna	0.66	19	28
LOS Topography	0.49	10	18
OBS Topography	1.17	14	31
Site A	0.29	16	14
Site B	0.75	36	31
Site C	-0.18	41	23
Site D	0.69	11	11

measurement run would result in an incorrect value for maximum excess delay.

Figure 4.3-2 is a scatter plot(a) and CDF(b) of maximum excess delay as a function of antenna height and frequency. As for the σ_τ and $\overline{\tau}$ results, results for maximum excess delay indicate little to no dependence on antenna height.

Figure 4.3-3 is a scatter plot(a) and CDF(b) of maximum excess delay as a function of topography. Figure 4.3-3 indicates that maximum excess delay is highly dependent on topography. For example, the probability that maximum excess delay exceeds 500 ns is about 0.35 for OBS topographies, but nearly 0 for LOS topographies. In OBS topographies, the earliest arriving signals are relatively weak, and later signals, which typically arrive at the receiver via reflection or scattering, will often have amplitudes within 10 dB of the weak early arriving signals.

Figure 4.3-4 is a scatter plot(a) and CDF(b) of maximum excess delay as a function of building. Most maximum excess delay values greater than 500 ns were recorded at Site B. This location is probably most capable of providing high energy paths in excess of 500 ns excess delay due to the large, open-plan highly reflective environment. Maximum delay spread values found at Site D, the closed-plan office building did not exceed 300 ns for any location. This result is reasonable considering the close confinements and less reflective building materials (drywall and ceiling tile) at Site D. Table 4.3-1 summarizes the linear regression characteristics for all maximum excess delay scatter plots.

4.4 Time Delay Jitter and Differential Delay Jitter

Time delay jitter is the difference between the mean excess delay of each individual profile for a measurement run and the mean excess delay of the spatially averaged profile for a measurement run and is given by equation (3.4.4). Scatter plots for delay jitter are presented for all individual profiles as a function of T-R separation. Delay jitter values for a given measurement run are represented by a vertical line on scatter plots. Thus the overall extent of delay jitter values for a measurement run, denoted as the peak-to-peak time delay jitter, is represented by the length of the corresponding vertical line on a scatter plot.

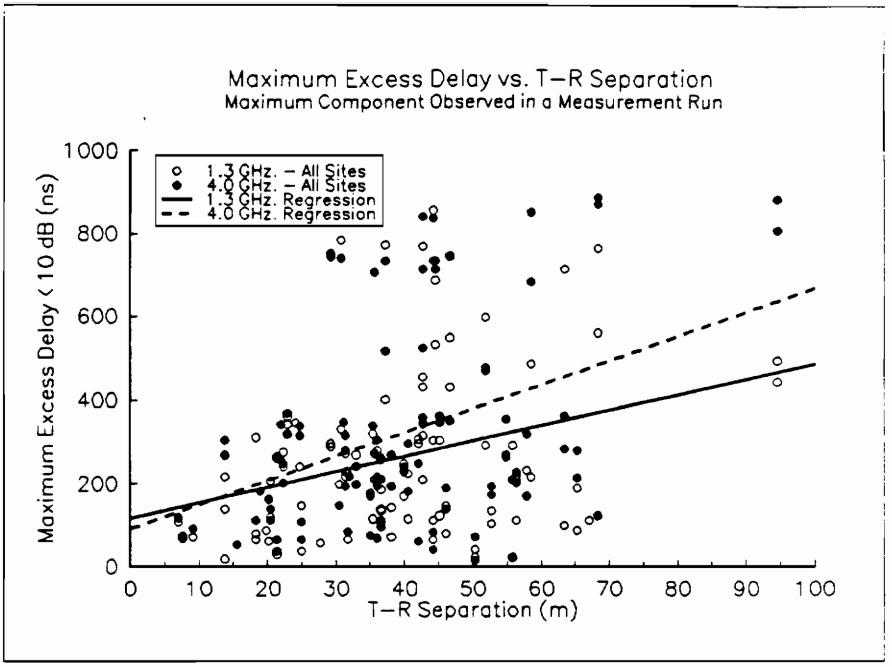

(a) Scatter Plot

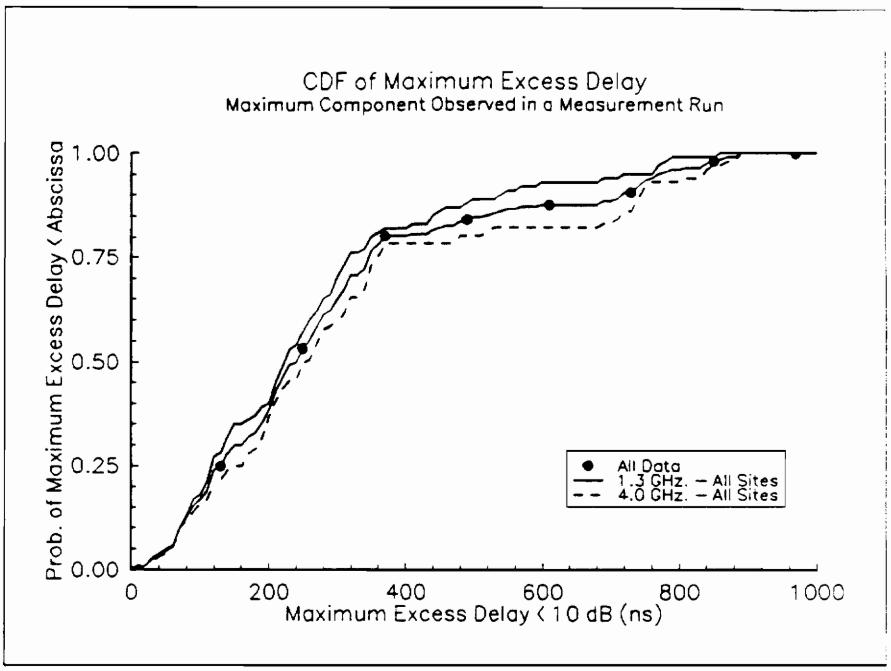

(b) CDF

Figure 4.3-1. (a) Scatter plot and (b) CDF of maximum excess delay as a function of frequency only; regression lines for each frequency are given.

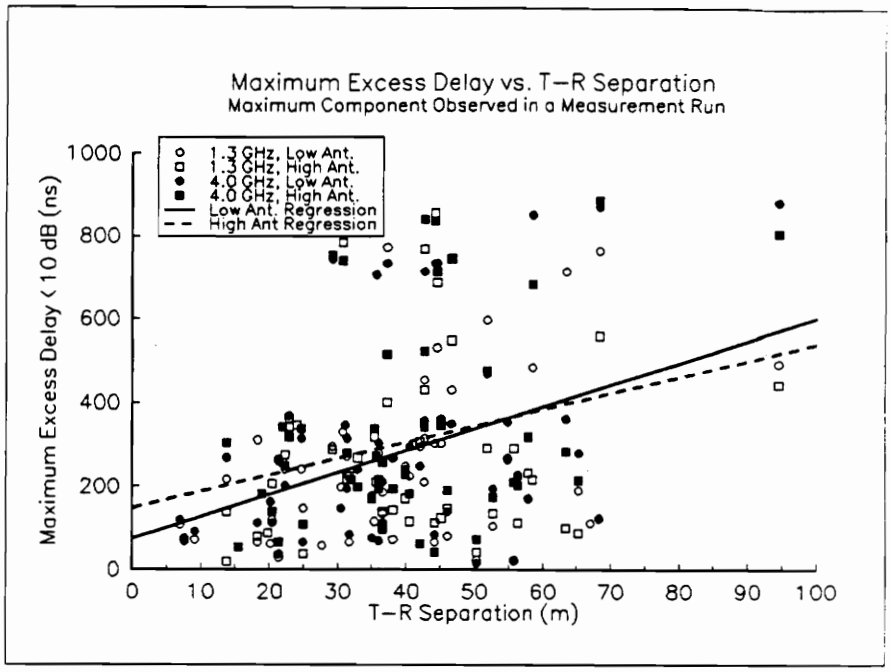

(a) Scatter Plot

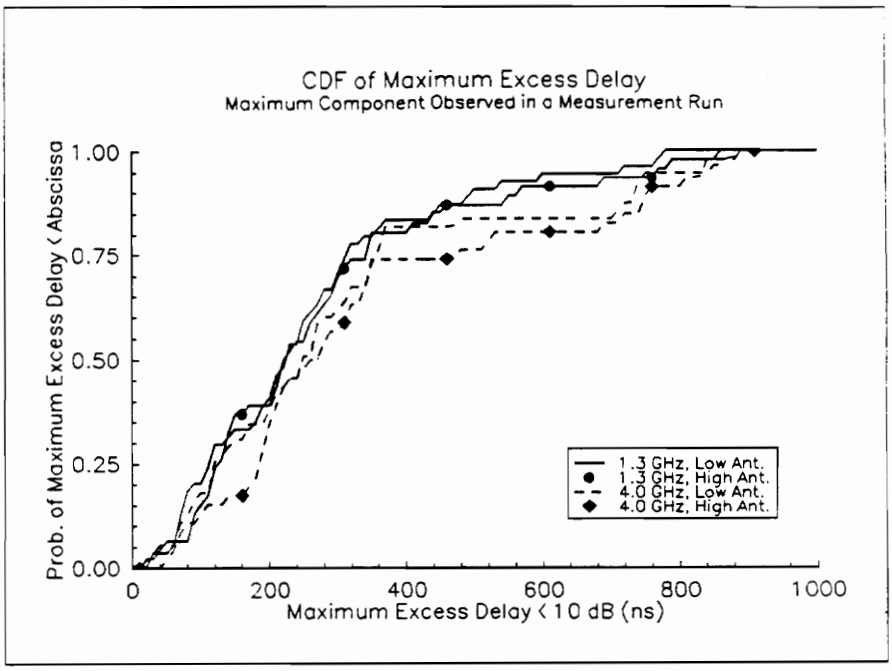

(b) CDF

Figure 4.3-2. (a) Scatter plot and (b) CDF of maximum excess delay as a function of frequency and antenna height; regression lines for each antenna height are given.

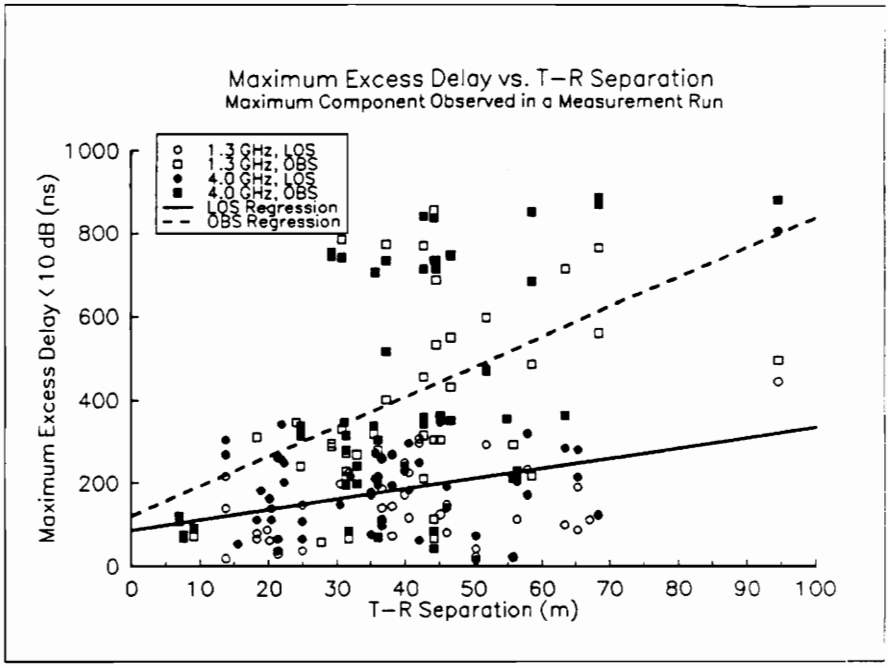

(a) Scatter Plot

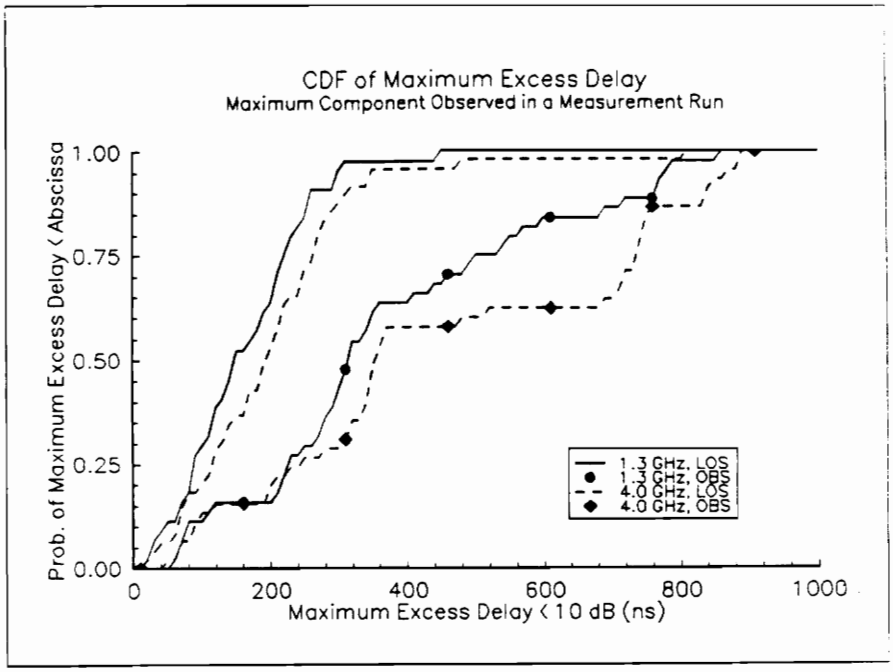

(b) CDF

Figure 4.3-3. (a) Scatter plot and (b) CDF of maximum excess delay as a function of frequency and topography; regression lines for LOS and OBS topographies are given.

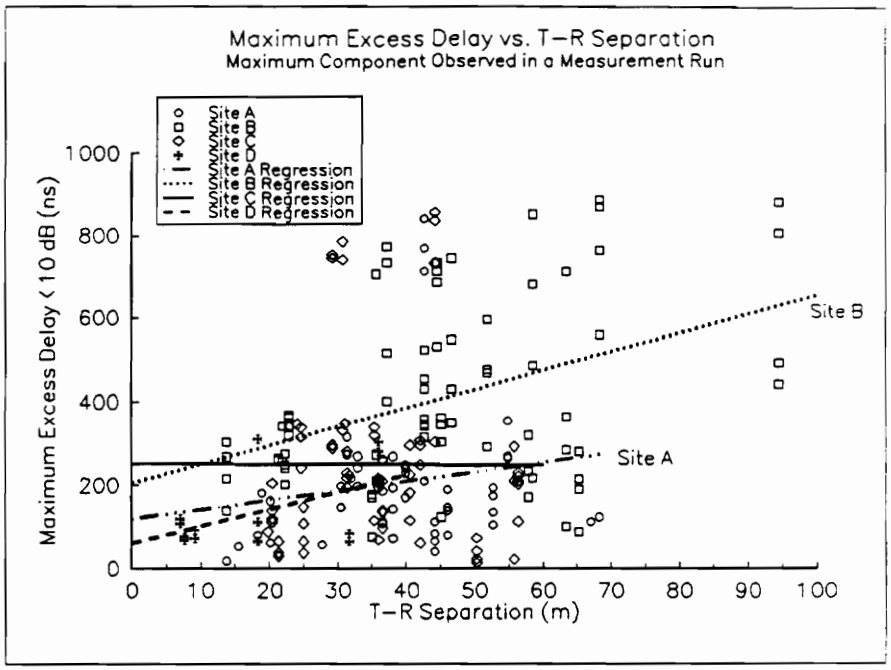

(a) Scatter Plot

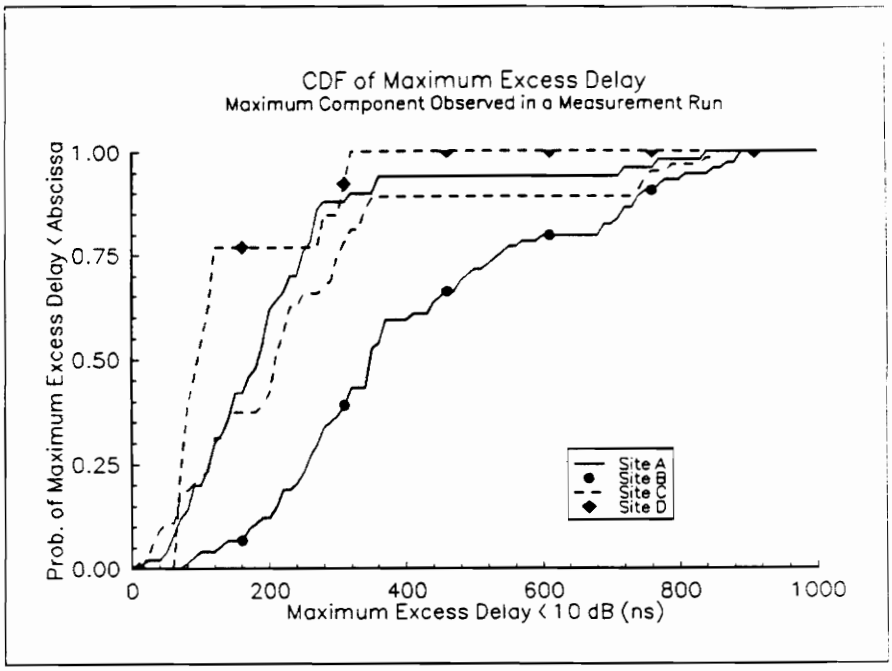

(b) CDF

Figure 4.3-4. (a) Scatter plot and (b) CDF of maximum excess delay as a function of frequency and building; regression lines for each building are given.

Table 4.3-1. Slopes, y-intercepts, and standard deviations for all maximum excess delay linear regression models presented on the scatter plots.

	Slope (ns/meter)	Y-intercept (ns)	Standard Error of Estimate (ns)
1.3 GHz - All Files	3.7	116	181
4.0 GHz - All Files	5.8	92	222
Low Antenna	5.3	73	192
High Antenna	3.9	148	218
LOS Topography	2.5	86	107
OBS Topography	7.2	120	223
Site A	2.2	119	165
Site B	4.5	204	199
Site C	-0.1	250	212
Site D	4.1	60	86

Figure 4.4-1 is a scatter plot of time delay jitter for all 1.3 GHz/low antenna measurements, with topography (LOS/OBS) as a parameter. Scatter plots which illustrate delay jitter for the other three measurement runs at each location are virtually identical to the one presented, which indicates minimal effects of frequency and antenna height on time delay jitter. Worst case peak-to-peak delay jitter for any measurement run does not exceed 180 ns, and less than 1% exceeds 120 ns. Careful observation of Figure 4.4-1 indicates that most peak-to-peak delay jitter values in excess of 80 ns are for OBS topographies. Overall results for delay jitter are similar to those reported in [32].

Figure 4.4-2, probability density functions (pdfs) of delay jitter for LOS and OBS topographies, illustrates that absolute values of delay jitter for OBS topographies are statistically greater than those for LOS topographies. This is indicated by the sample standard deviations of 11.1 ns and 18.1 ns for LOS and OBS topographies, respectively. Figure 4.4-3 is a pdf of delay jitter as a function of building. Absolute values of delay jitter are generally the highest at Site B and the lowest at Site D, while the extent of delay jitter for Sites A and C are very similar. This follows the trend for all time dispersion parameters discussed thus far.

Differential delay jitter is defined as the difference between mean excess delay values for successive profiles in a measurement run and is given by equation (3.4.5). It is used to determine the variation of the centroid of a power delay profile over sub-wavelength spatial separations. For these data, the spatial separation was approximately 0.25λ for all measurements. Scatter plots and pdfs indicate very similar results between differential delay jitter and time delay jitter. This is indicated by Figures 4.4-4 and 4.4-5, and Table 4.4-1. Figure 4.4-4 illustrates pdfs of differential delay jitter for LOS and OBS topographies, and Figure 4.4-5 illustrates pdfs of differential delay jitter as a function of building. Table 4.4-1 lists calculated standard deviations (σ) of all time delay jitter and differential delay jitter values about their respective means as a function of classification. Worst case peak-to-peak differential delay jitter values are approximately 190 ns, and less than 1% of the values exceed 140 ns.

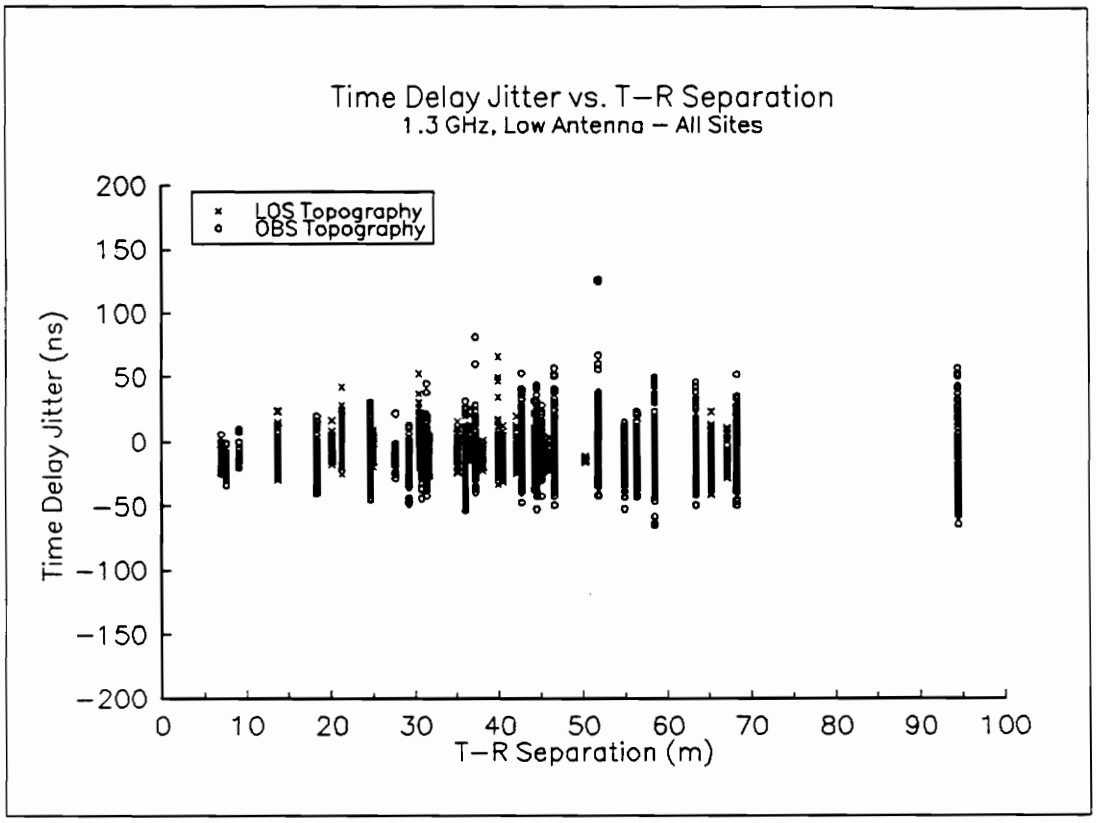

Figure 4.4-1. Scatter plot of time delay jitter values for all measurement runs performed at 1.3 GHz with a low antenna configuration as a function of topography.

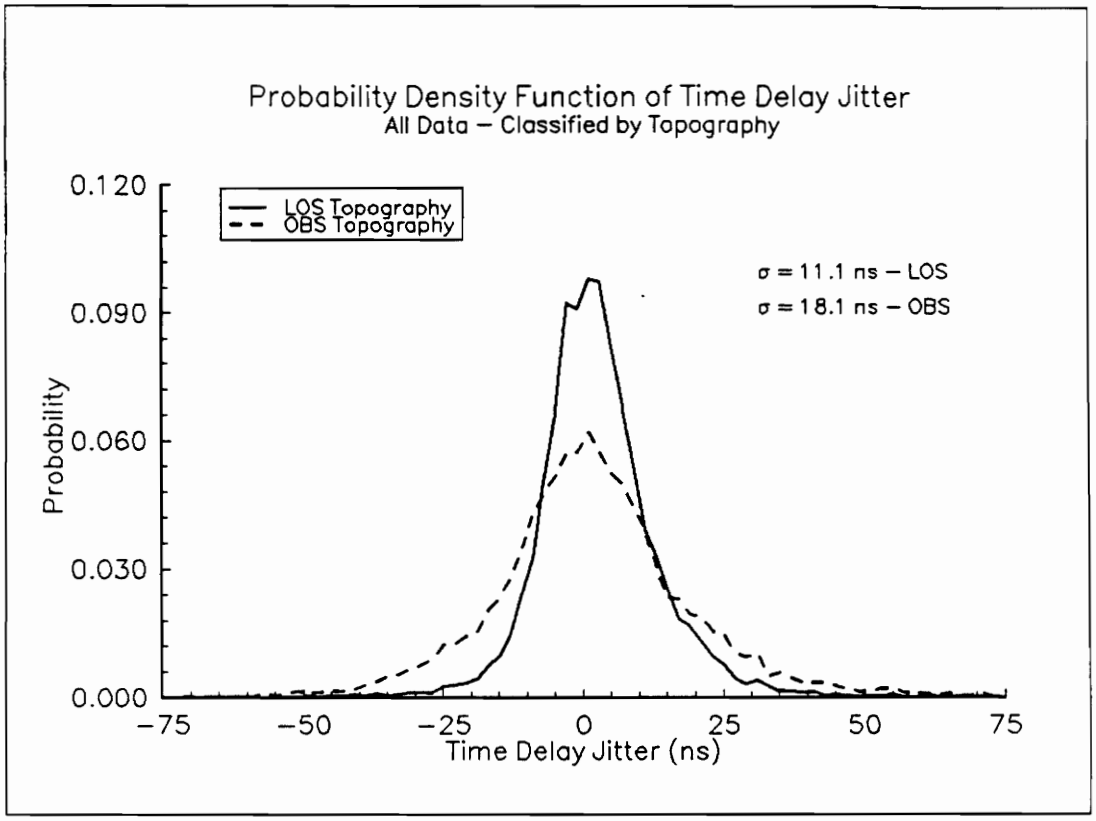

Figure 4.4-2. Probability density function of time delay jitter values for all measurement runs as a function of topography.

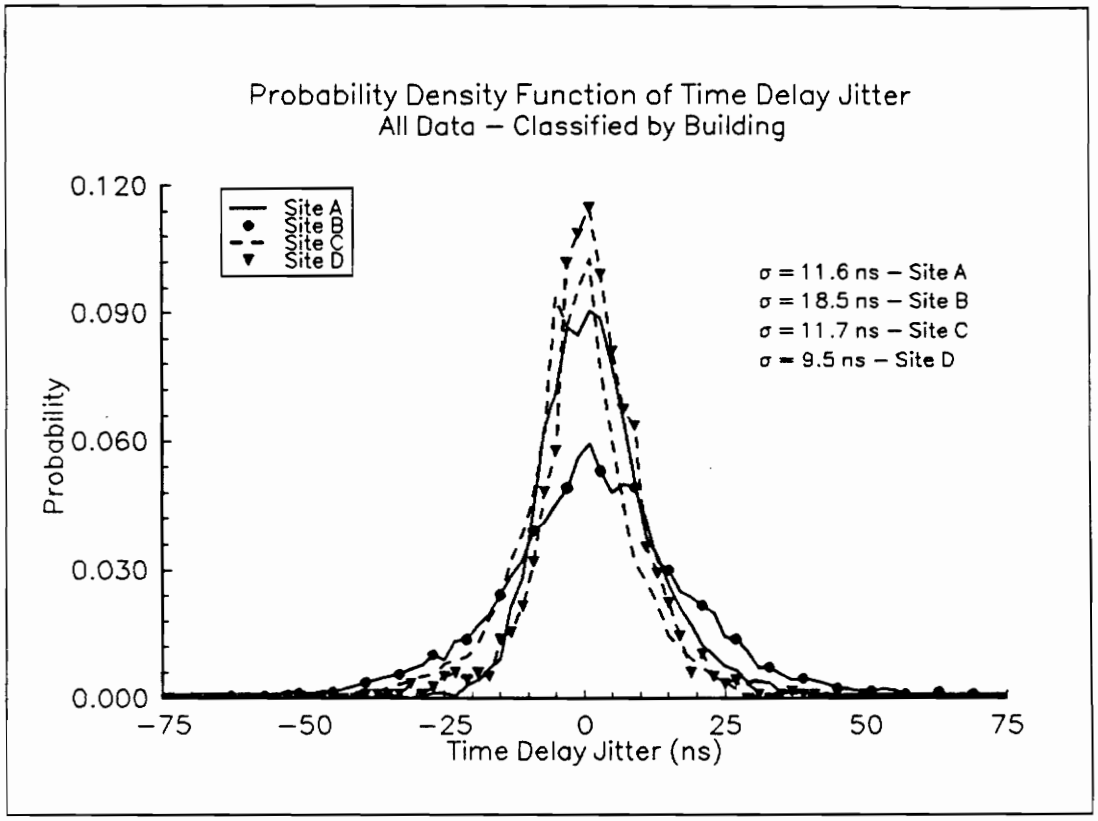

Figure 4.4-3. Probability density function of time delay jitter values for all measurement runs as a function of building.

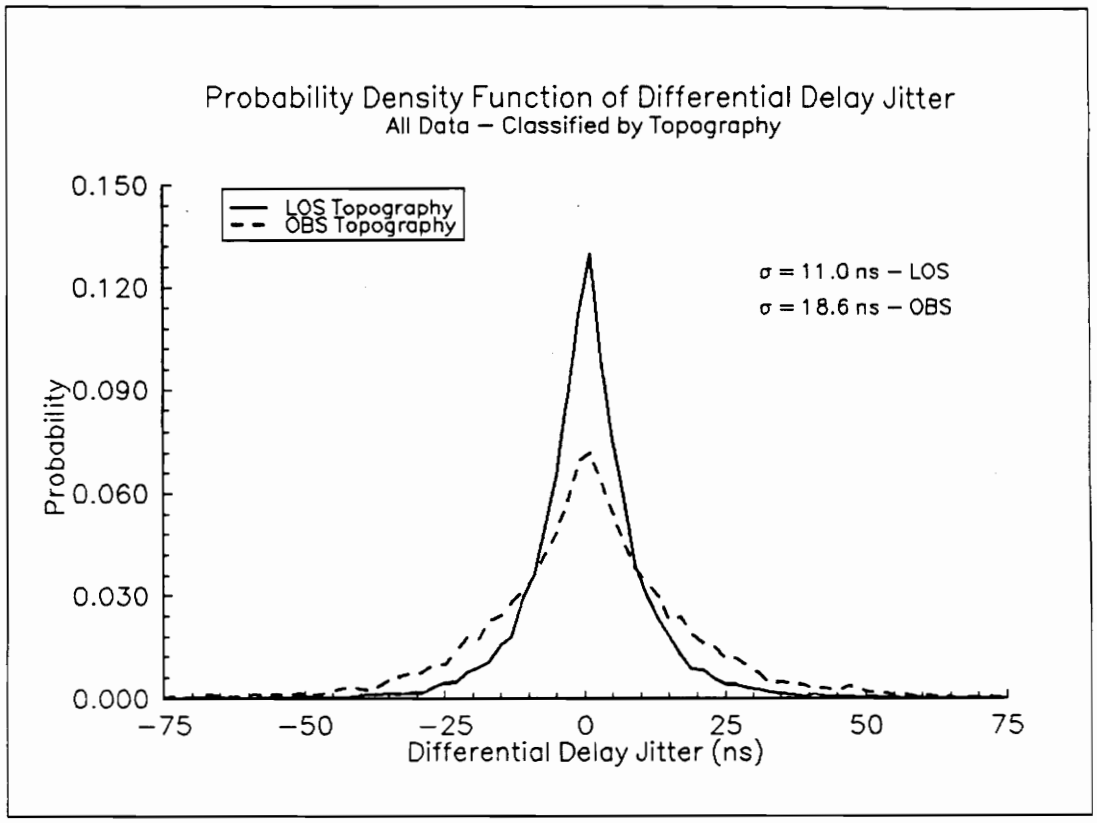

Figure 4.4-4. Probability density function of differential delay jitter values for all measurement runs as a function of topography.

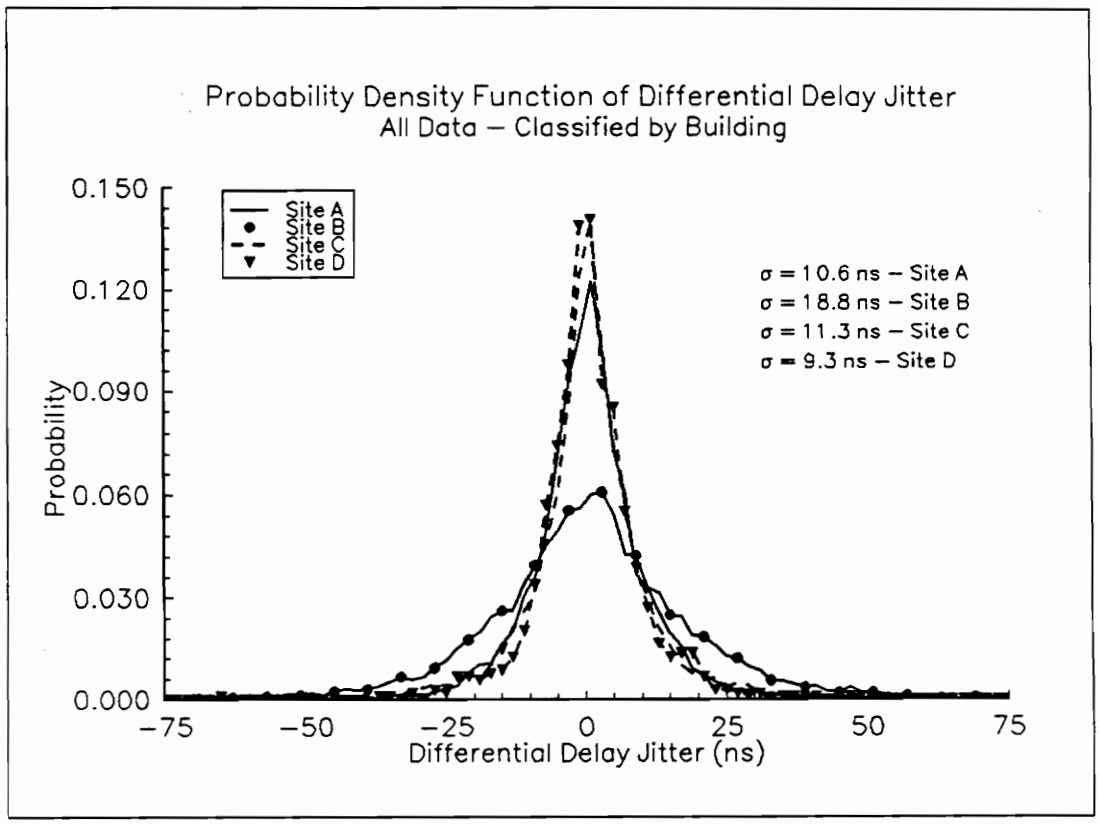

Figure 4.4-5. Probability density function of differential delay jitter values for all measurement runs as a function of building.

Table 4.4-1. Computed values of the sample standard deviation σ for time delay jitter and differential delay jitter as a function of classification.

	Time Delay Jitter standard deviations (ns)	Diff. Delay Jitter standard deviations (ns)
1.3 GHz - All Files	13.8	13.4
4.0 GHz - All Files	15.6	15.7
Low Antenna	14.3	14.4
High Antenna	15.2	14.8
LOS Topography	11.1	11.0
OBS Topography	18.1	18.6
Site A	11.6	10.6
Site B	18.5	18.8
Site C	11.7	11.3
Site D	9.5	9.3
ALL DATA	14.7	14.6

4.5 Path Loss

Techniques to determine path loss from wide band power delay profiles and CW fading data were described in Chapter 3. All wide band results are presented first, followed by narrow band results, which include a section with estimates of the shadowing effects induced by some common factory and office building equipment. Results are given as scatter plots of path loss versus the T-R separation displayed on a logarithmic scale. Path loss results are given in dB above a reference free space path loss at 1 meter. A comparison of 1.3 GHz results obtained from the wide band and narrow band methods is given.

It has been shown that the total power contained in a locally-averaged received multipath power delay profile at a T-R separation d is well described by a log-normal distribution (normal distribution in dB) about a mean path loss law of the form d^n [23]. The computation of the d^n model is based on Friis transmission formula (2.1.1). A minimum squared error linear fit is calculated for all data points on a plot in the following manner. The left end point of a best fit d^n regression line is fixed at path loss value corresponding to n = 2 (free space loss) at a T-R separation of 1 meter. Values of n are then incremented from 1.0 to 7.0, and the d^n path loss values $\overline{L}(n,d)$ above the free space loss at one meter are computed from

$$\overline{L}(n,d) = 10n \log_{10}(d) \tag{4.5.1}$$

Where $\overline{L}(n,d)$ is the mean power law estimate for the path loss. The square of the difference between the value of a path loss point and the corresponding point on the d^n model is called the the squared error. The value of n which yields the lowest summation of squared errors for the entire data set determines the optimum d^n fit. The standard deviation (σ, in dB) of path loss about the optimum fit is also a minimum for the calculated value of n, and is a measure of the predictability of path loss values. The standard deviation for a data set of length N is computed from

$$\sigma = \sqrt{\frac{\sum_{k=1}^{N} \left(L_k - \overline{L}_k\right)^2}{N-1}} \tag{4.5.2}$$

Where,

L_k = measured path loss value (dB).

$\overline{L}_k$ = corresponding path loss value of d^n model (dB).

N = total number of points evaluated.

Computed values of n and σ are given for each frequency on all scatter plots, and tables which summarize best fit values of n and σ are presented.

Wide Band Results

Figure 4.5-1 is a scatter plot of all wide band path loss results excluding the few made in Site D. Due to unusually high loss environments at Site D, results for this partitioned office building are presented separately. Each point on the plot represents the ***parameter averaged*** value of path loss in dB above theoretical free space loss at 1 meter. One result is the similarity of the power law models for 1.3 GHz and 4.0 GHz. The calculated values of n are 2.09 for all open-plan (Sites A-C) 1.3 GHz data and 2.13 for all open-plan 4.0 GHz data. Values of σ are 7.6 dB for both frequencies. Although Figure 4.5-1 indicates nearly identical results for both frequencies, subsequent results indicate a slight advantage of one frequency over the other, depending on the environment.

Figure 4.5-2 illustrates path loss results for measurements taken for (a) 1.7 meter base station antenna height and (b) 4.0 meter base station antenna height. At 1.3 GHz, values of n and σ are 2.09 and 7.7 dB for high and low base station antennas. However, at 4.0 GHz, a slight difference is noticed between high and low antenna heights. At 4.0 GHz, values of n and σ are 2.14 and 8.6 dB for a low base station antenna, and 2.11 and 6.7 dB for a high base station antenna. Figure 4.5-2(a) illustrates that 1.3 GHz has slightly less path loss than 4.0 GHz when the low antenna is used. Figure 4.5-2(b), illustrates that a high antenna configuration is less sensitive to frequency than a low antenna configuration. The combination of 4.0 GHz and 1.7 meter antenna height has the highest values of n and σ. This results in a lower coverage area for this configuration, given the same transmitter power and receiving equipment. Coverage areas and other system design issues are addressed in Chapter 7.

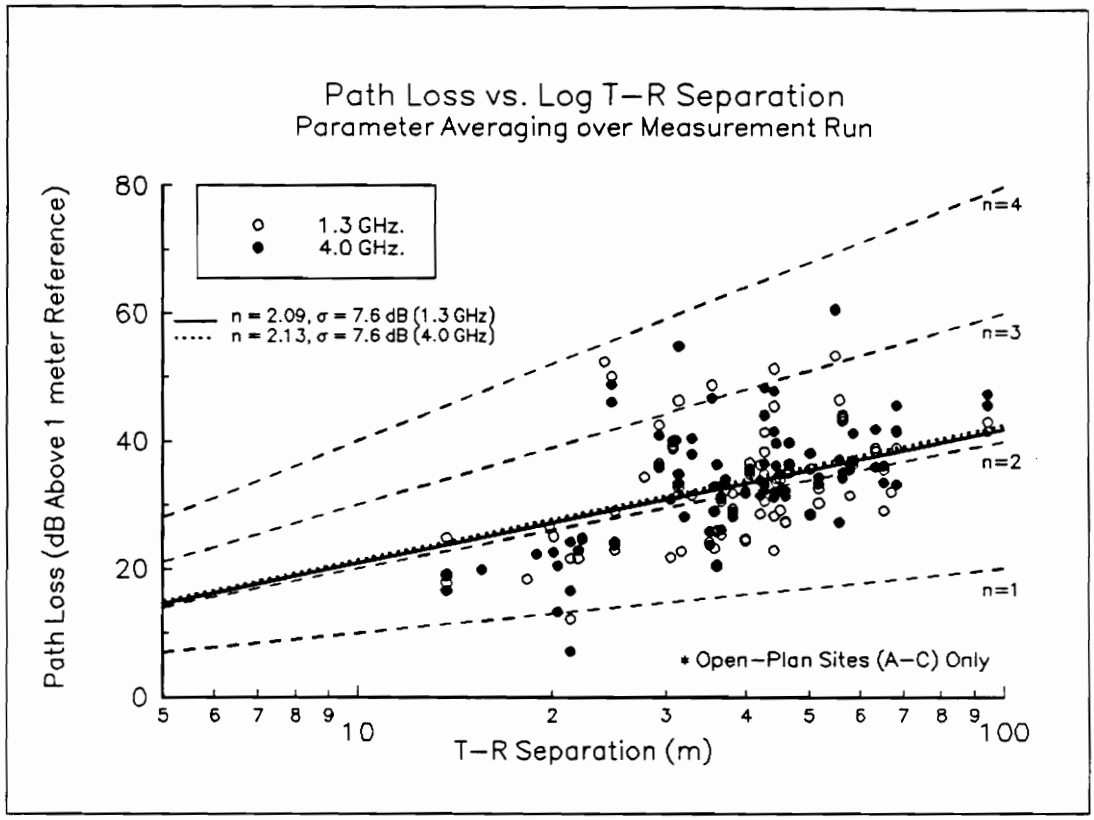

Figure 4.5-1. Scatter plot of all wide band path loss results at open-plan sites as a function of frequency.

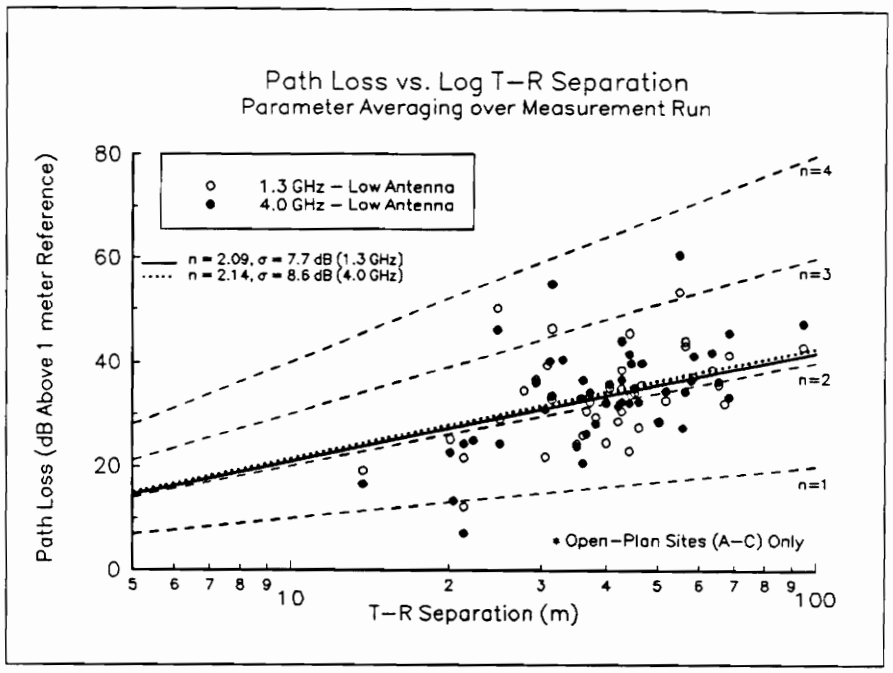

(a) Low Antenna (1.7m)

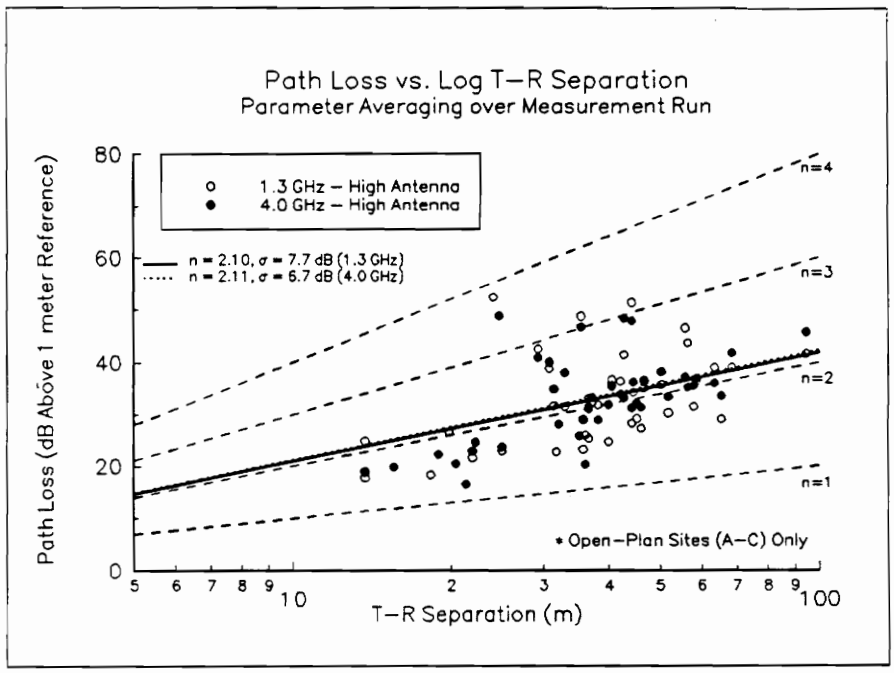

(b) High Antenna (4.0m)

Figure 4.5-2. Scatter plots of wide band path loss results at open-plan sites for (a) low antenna (1.7m) and (b) high antenna (4.0m) as a function of frequency.

Figure 4.5-3 illustrates path loss in (a) LOS and (b) OBS topographies. In LOS topographies, many path loss values were slightly below that of free space propagation; for several cases, this enhanced propagation is significant. The two lowest path loss values on Figure 4.5-3(a) ($\sim$21 meter T-R separation) were recorded in a confined area of Site C. Values of n were below 1.0 for both frequencies at this location, which was bounded by a brick wall several feet to one side, a row of metallic bins 6 feet high on the other side, a concrete floor, and metal ceiling ducts at a height of approximately 4 meters. The waveguide effect, in which energy is directed from the transmitter to the receiver by the rectangular structure of the main reflectors, may be why the path loss is lower than free space loss at this and other similar locations. Also, the physical characteristics of the environment may be such that a surface wave is launched on one of the walls or ceiling, which would also result in path loss values lower than free space.

A comparison of LOS and OBS results illustrates that topography has a significant effect on path loss. In LOS topographies, values of n are 1.84 for both frequencies, while σ is 4.9 dB and 4.8 dB at 1.3 GHz and 4.0 GHz, respectively. In OBS topographies, n is 2.35 for 1.3 GHz and 2.44 for 4.0 GHz, while σ is 7.9 dB and 7.1 dB at 1.3 GHz and 4.0 GHz, respectively. In OBS topographies, path loss is on average, slightly higher at 4.0 GHz than at 1.3 GHz, while in LOS environments, no difference exists between frequencies. Thus, for LOS paths, no real advantage is gained by using one frequency over the other. However, if a system must operate in an environment in which reliable communications will be required over heavily obstructed, spacious (no waveguide effects) areas, 1.3 GHz may be more desirable.

Figure 4.5-4 illustrates path loss results taken in Sites A-D. There is a notable difference among results for each building, and between the two frequencies at each location. Path loss recorded at Site B (large, open-plan factory) is close to free space propagation, as n is 1.97 at 1.3 GHz and 2.09 at 4.0 GHz. Values of σ at Site B are only 3.7 dB and 4.0 dB at 1.3 GHz and 4.0 GHz, respectively. The cause of the drastic reduction in σ is the large-scale geometrical consistency for all Site B measurements. At the other three sites, measurements were made in several different types of environments. For example, environments at Site C consisted of open-plan environments similar to Site B, and also confined

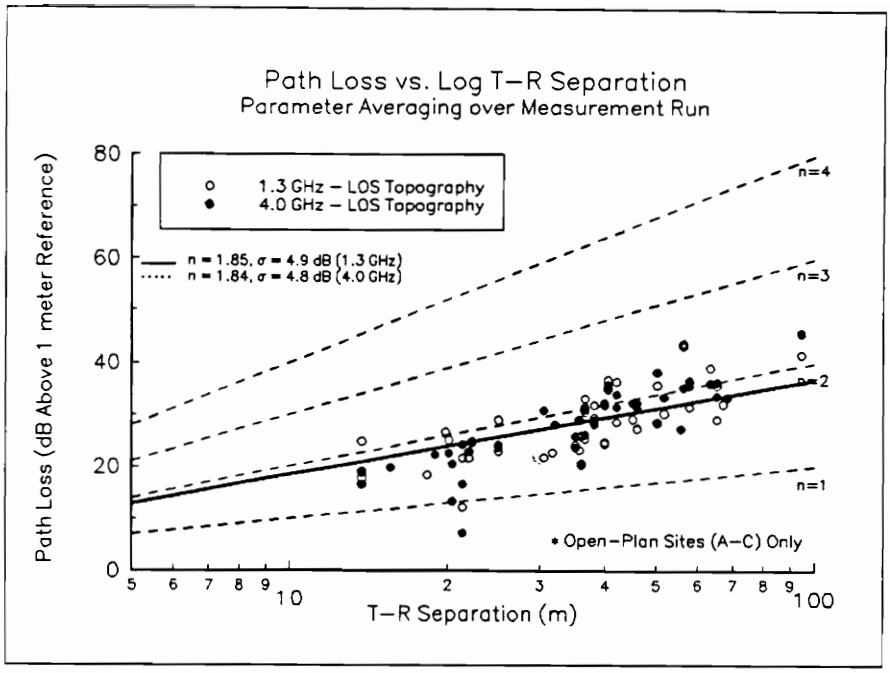

(a) LOS Topography

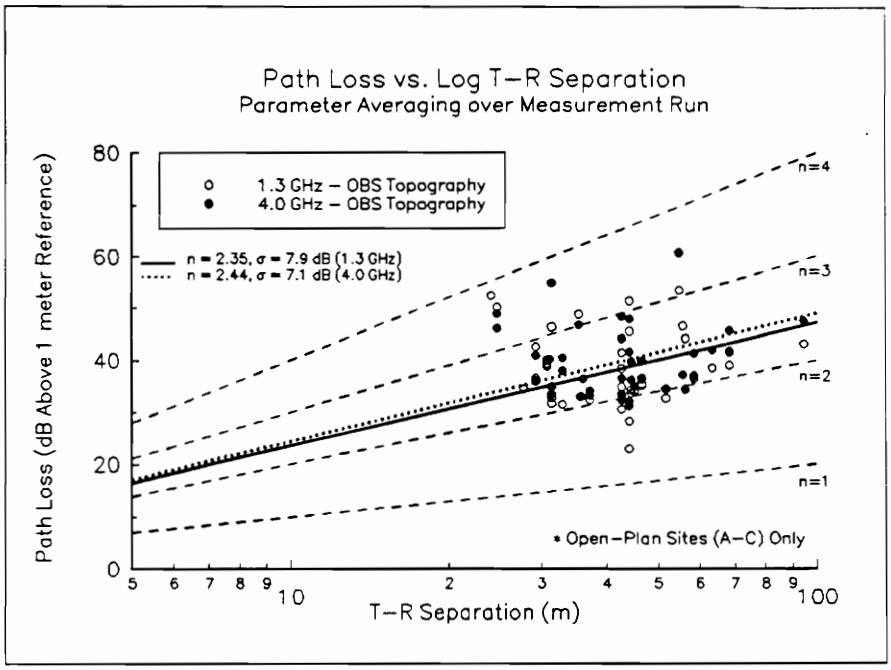

(b) OBS Topography

Figure 4.5-3. Scatter plots of wide band path loss results at open-plan sites for (a) LOS topography and (b) OBS topography as a function of frequency.

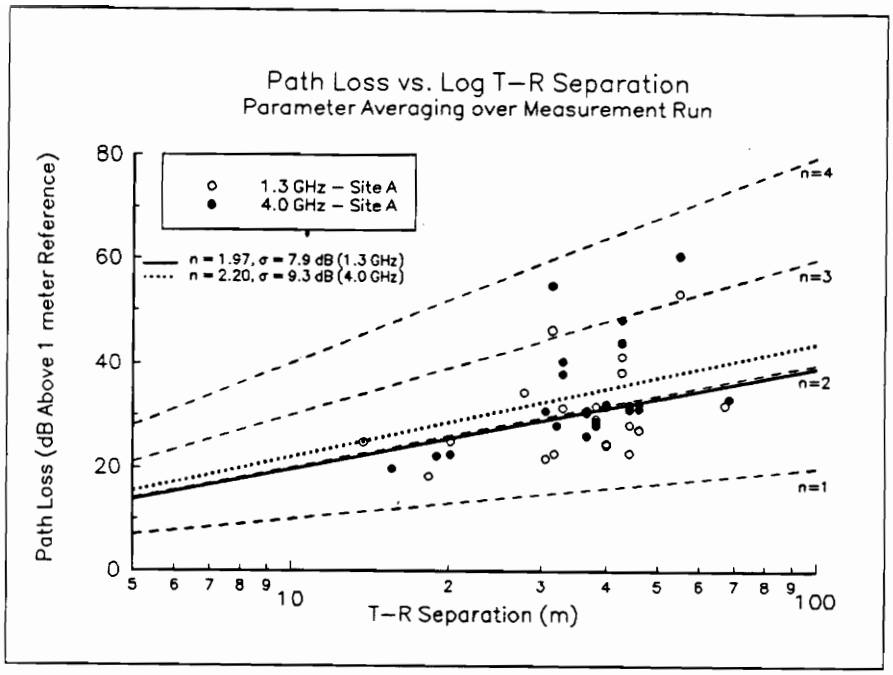

(a) Site A

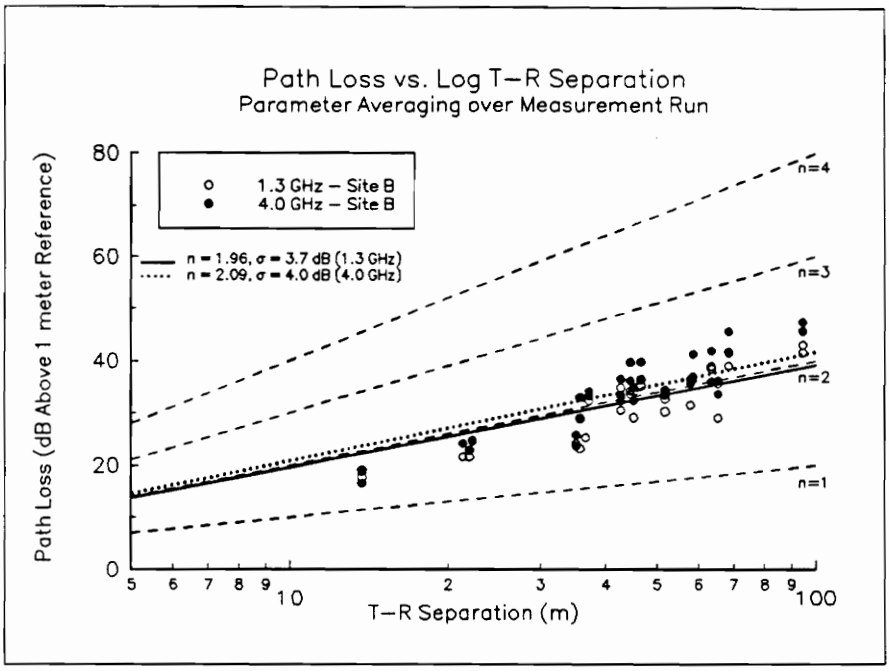

(b) Site B

Figure 4.5-4. Scatter plots of wide band path loss results for Sites A-D as a function of frequency. Figure continued on next page (Sites C and D).

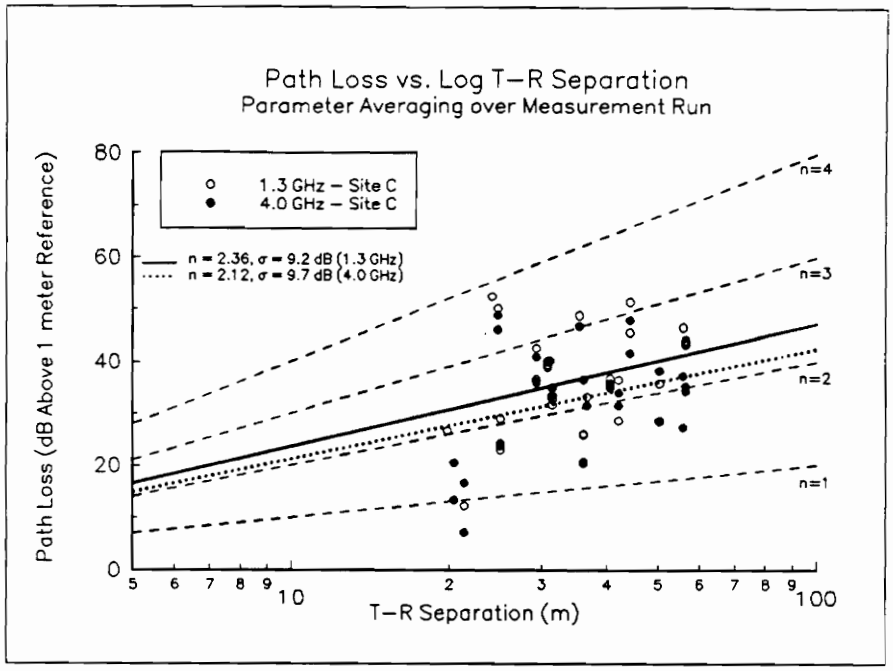

(c) Site C

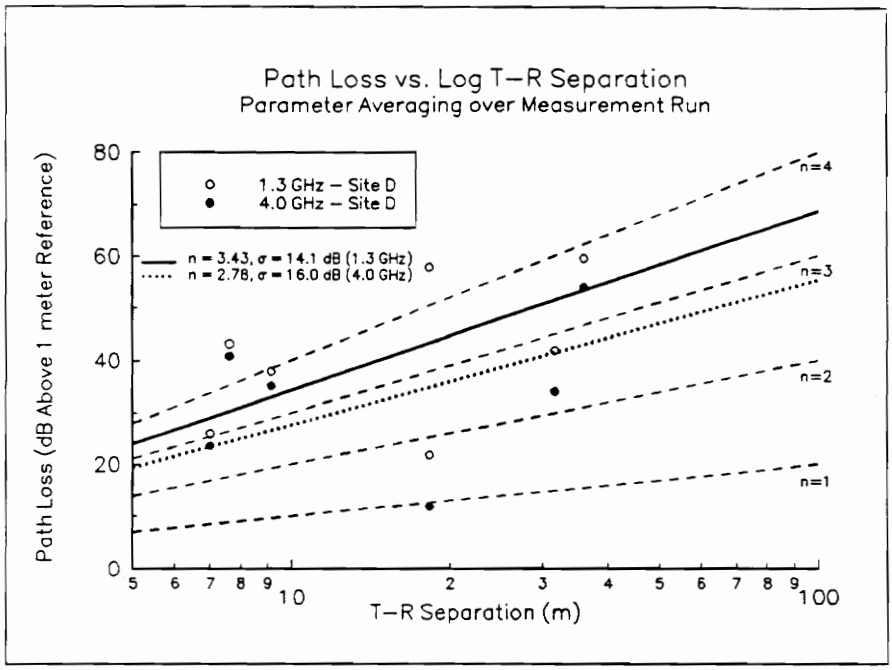

(d) Site D

Figure 4.5-4. – Continued.

environments with low ceilings and long rows of metal machinery. It is expected that path loss values in OBS topographies for these two environments would differ. Relatively high σ values of 9.2 dB at 1.3 GHz and 9.7 dB at 4.0 GHz support this expectation. This provides motivation to more carefully classify the data in terms of geometrical consistencies based on building blueprints, which is a first step in developing accurate site-specific propagation models. This topic is discussed in more detail in Chapter 6.

Path loss at Site A (sports arena) is typically higher than at Site B for both frequencies. At Site B, all measurements were recorded in one large room, with OBS paths impeded by highly reflective machinery and inventory, while many measurements taken at Site A were between two distinctly different areas of the building (i.e. from the ground floor inside the spectators arena to the outer concourse which surrounds the arena). Direct paths for these types of measurements are typically obstructed by walls, with little chance of energy diffraction around objects. This explains higher path loss values at Site A than at Site B. The higher path loss values observed at 4.0 GHz versus 1.3 GHz at Site A could be explained by the fact that some of the "wall" obstructions like block walls, concrete, and wooden seats may be more penetrable by 1.3 GHz signals than by 4.0 GHz signals.

Path loss results at Site D were significantly higher (n=3.43 at 1.3 GHz, n=2.77 at 4.0 GHz) than for the open-plan locations, although wide band measurements were limited to six locations at Site D. As opposed to most open-plan locations, OBS locations at Site D were primarily with the transmitter and receiver separated by one or more hallways. Direct paths are more heavily obstructed in this environment than for typical obstructions in open-plan topographies. Also, materials at Site D include drywall partitions, tile floors, and standard foam dropped ceiling structures, nominally less reflective materials than the primarily metallic machinery, inventory, walls, and ceiling at the open-plan locations. These conditions will result in higher path loss values at Site D, particularly for OBS topographies.

For each of the six Site D measurement locations, 4.0 GHz path loss results were lower than 1.3 GHz results at the same measurement location. A possible explanation for this result is that some obstructions at Site D (typically drywall)

may be more reflective at 4.0 GHz relative to 1.3 GHz, and may actually guide these signals around corners and down corridors, whereas some or all of the 1.3 GHz power may be absorbed or heavily attenuated by the obstructions. The Site D location which indicates better than free space propagation (See Figure 4.5-4d, T-R separation 19m) is LOS along an enclosed corridor. This may be another example the waveguide effect or the launching of surface waves. Notice how much more the effect is present at 4.0 GHz than 1.3 GHz. Values of n for this location are approximately 1.0 and 1.7 at 4.0 GHz and 1.3 GHz, respectively. This further supports the claim of higher reflectivity at 4.0 GHz for typical Site D materials. Table 4.5-1 summarizes computed values of n and σ values for all wide band path loss scatter plots presented. The values of n calculated from this measurement campaign agree closely with those reported in [23], which reports an overall average value of 2.18 for n, computed from 1.3 GHz wide band profiles recorded in 5 factory buildings.

Narrow Band Results

In addition to wide band path loss results, narrow band CW signal strength results are presented to compare with wide band results. Also, the CW fading is used to estimate shadowing effects of typical factory and office building obstructions. Figure 4.5-5 is a scatter plot for all open-plan (a) CW and (b) wide band data. For the CW data, three points are represented for each measurement run, one each at the beginning, the middle, and the end of the run. Thus each point represents the median path loss over a 10.7λ measurement track. The CW path loss parameters are remarkably similar to the wide band results. For all open-plan CW data, best fit n and σ are 2.11 and 9.0 dB, respectively. This compares to 2.09 and 7.6 dB for all open-plan 1.3 GHz wide band data. Figure 4.5-6 is a scatter plot for Site D (a) CW and (b) wide band data. Only one point represents the wide band path loss, while three points corresponding to 10.7λ segments represents the CW path loss. With the exception of the location with the lowest path loss (T-R separation ~ 21 meters), the CW and wide band results are again similar. Table 4.5-2 lists n and σ for CW results and a relative comparison to wide band results for each classification. The relative comparison is presented as CW values subtracted from wide band values. Values of n for CW

Table 4.5-1. Computed values of power law exponent n and standard deviation σ about the path loss model for wide band path loss results.

	1.3 GHz. n	1.3 GHz. σ (dB)	4.0 GHz. n	4.0 GHz. σ (dB)
All Files	2.09	7.6	2.13	7.6
Low Antenna	2.09	7.7	2.14	8.6
High Antenna	2.09	7.7	2.11	6.7
LOS	1.84	4.9	1.84	4.8
OBS	2.35	7.9	2.44	7.1
Site A	2.00	7.9	2.20	9.3
Site B	1.97	3.7	2.09	4.0
Site C	2.36	9.2	2.12	9.7
Site D	3.43	14.1	2.77	16.0

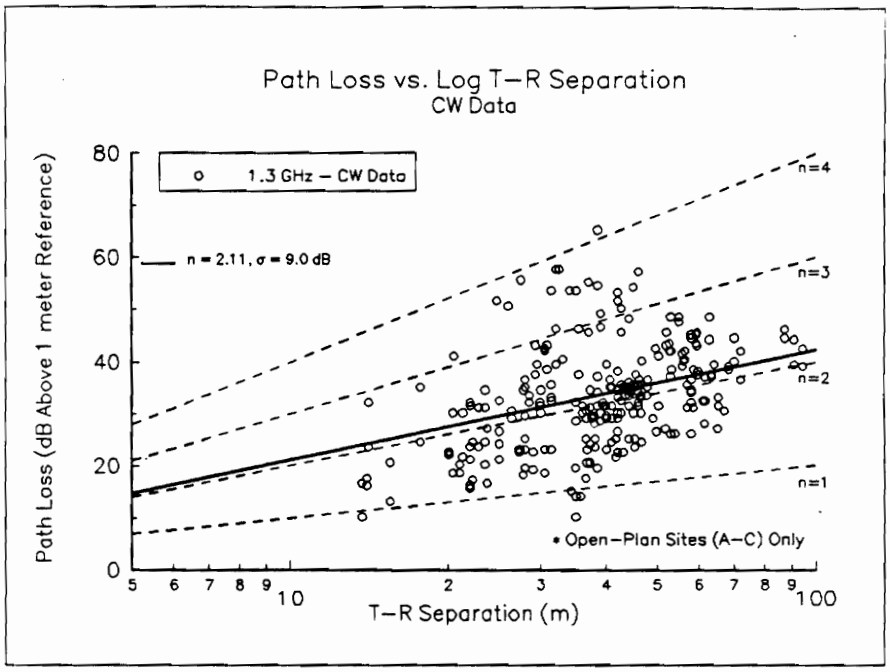

(a) Narrow Band (CW) Path Loss

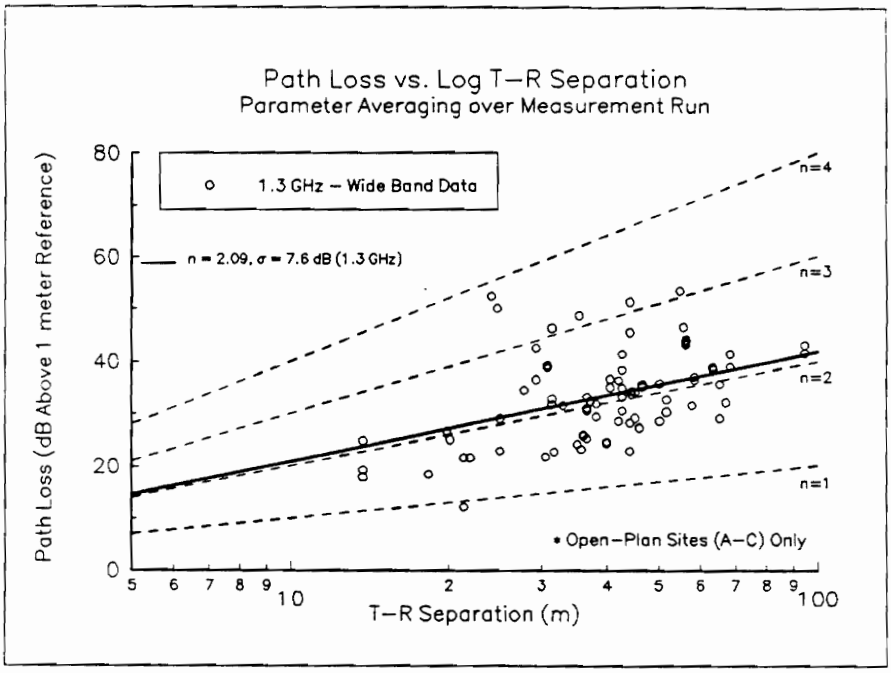

(b) Wide Band Path Loss

Figure 4.5-5. Scatter plot of all 1.3 GHz (a) CW and (b) wide band path loss results at open-plan sites.

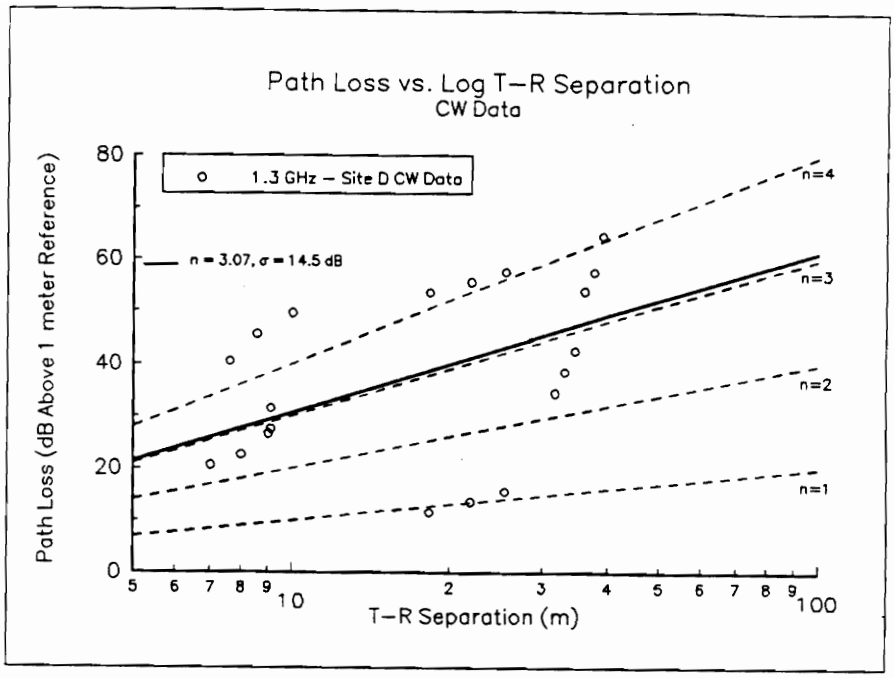

(a) Narrow Band (CW) Site D Path Loss

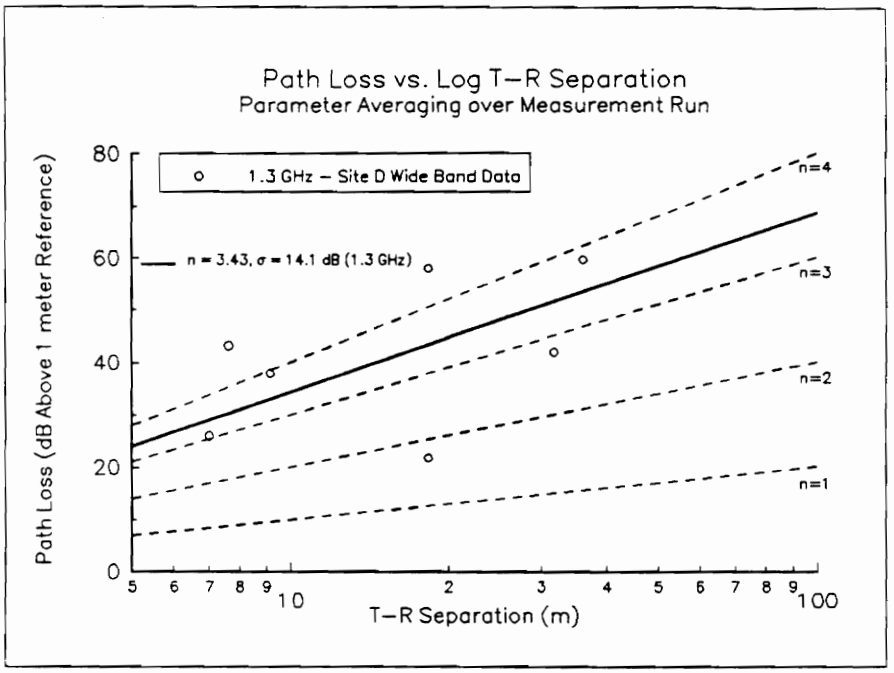

(b) Wide Band Site D Path Loss

Figure 4.5-6. Scatter plot of all 1.3 GHz (a) CW and (b) wide band path loss results at Site D.

Table 4.5-2. Computed values of power law exponent n and standard deviation σ about the path loss model for narrow band path loss results; and their values relative to the wide band results of Table 4.5-1.

	1.3 GHz. n	Relative to Wide Band	1.3 GHz. σ (dB)	Relative to Wide Band
All Files	2.11	+0.02	9.0	+1.4
Low Antenna	2.16	+0.07	9.0	+1.3
High Antenna	2.06	-0.03	8.8	+1.1
LOS	1.83	-0.01	6.6	+1.7
OBS	2.43	+0.08	9.2	+1.3
Site A	2.11	+0.11	11.1	+3.2
Site B	1.92	-0.05	5.7	+2.0
Site C	2.35	-0.01	8.8	-0.4
Site D	3.07	-0.36	14.7	+0.6

and wide band measurements are remarkably similar for all classifications, except for Site D, where only seven locations were measured. In [23], it was proven that average CW and wide band power measurements are equivalent, provided that the path phases are independent and uniformly distributed over $[0,2\pi)$, or the path amplitudes are uncorrelated. A situation in which neither of these conditions are met is highly unlikely [23]. The similarity between CW and wide band results supports this proof. Relative values of σ for CW results are consistently higher than those for wide band results. This result is due to the independence of the phase of each multipath component in a wide band profile. For CW, the phase of each component is critical since the phasor sum of all components determines the received power at a specific location. This phase dependence causes rapid changes in received power over short distances for CW measurements in the presence of multipath propagation. For the wide band measurements, the components generally remain specular, and thus the received power will not rapidly change over small distances.

Shadowing

Detailed records of the exact transmitter and receiver locations were kept throughout the first measurement campaign. By using building blueprints, shadowing effects of particular building obstructions were estimated. At locations where obstructions were known to exist, the strip chart recordings were examined to determine 1.3 GHz attenuation estimates for particular obstructions. Attenuation estimates for typical obstructions in the factories (Sites B and C) are listed in Table 4.5-3, and attenuation estimates for common objects in a partitioned office building (Site D) are listed in Table 4.5-4.

Table 4.5-3. Shadowing effects of typical factory obstructions.

	Loss (dB)		Loss (dB)
Light Textile inventory	3-5	Heavy Textile inventory	8-11
Chain link fenced in area 20 ft. high which contains tools, inventory, and people	5-12	area where workers inspect metal finished products for defects	3-12
Metal Blanker 12 square feet	4-7	metallic inventory	4-7
Metallic Hoppers which hold scrap metal for recycling 10 square feet	3-6	Large I-beam 16-20 in.	8-10
Small Metal Pole 6 in. diameter	3	Metallic inventory racks 8 square feet	4-9
Metal Pulley System used to hoist metal inventory 4 sq. ft.	6	Empty Cardboard inventory boxes	3-6
Light Machinery < 10 square feet	1-4	Concrete Block Wall	13-20
General Machinery 10-20 square feet	5-10	Ceiling Duct	1-8
Heavy Machinery > 20 square feet	10-12		
Metal catwalk/stairs	5		
Light Textile	3-5		

Table 4.5-4. Shadowing effects of typical office building obstructions.

Item	Loss (dB)
Concrete Block Wall	13
Loss From One Floor	20-30
Loss From One Floor and One Wall	40-50
Fade observed when transmitter turned a right angle corner in a corridor	10-15

4.6 Summary

This chapter examined statistical results obtained during the initial measurement campaign. Results were presented for the following time dispersion parameters: rms delay spread, mean excess delay, maximum excess delay, time delay jitter, and differential delay jitter. Wide band and narrow band path loss results were obtained. Results were presented as scatter plots, cumulative distribution functions (CDFs), probability density functions (pdfs), and in tabular form.

In general, it was found that frequency and antenna height did not significantly affect any of the computed time dispersion parameters, although at a few locations where the antenna was raised to 4 meters, and a LOS path clearly became visible, delay spread was reduced by as much as 60%. It was determined that topography (LOS/OBS) has an impact on all time dispersion parameters studied. With a LOS path, rms delay spread values exceeded 75 ns only about 10% of the time, while for OBS topographies, 75 ns was exceeded nearly 40% of the time. Mean excess delay, maximum excess delay $<$ 10 dB, and time delay jitter values also significantly increased when OBS channels were measured.

Measurements made in Site B, the open-plan, large factory with large, metal machinery surrounding all aisles yielded highest values of rms delay spread, maximum excess delay, and time delay jitter. The lowest time dispersion values were found at Site D, the closed-plan office building.

Path loss results indicated that for large areas in which many reflective obstructions exist between and surrounding the terminals, 1.3 GHz propagation was less shadowed by the obstructions than 4.0 GHz propagation, which causes slightly less path loss for the lower frequency in environments of this type. Power law exponents less than the free space value (n=2) were observed at certain locations in which a LOS existed in an enclosed environment. In general, the highest path loss values were observed for the closed-plan office building. Large-scale path loss results for wide band and narrow band measurements yielded similar d^n models.

5 Polarization Measurements and Results

This chapter describes a second measurement campaign, which was initiated to determine the effects of antenna polarization and directivity on rms delay spread and path loss inside an office building and a supermarket. Included is a description of the experiment design and file naming and storage procedures, and a discussion of all rms delay spread and path loss results. Since the experiment design differs little from the original campaign, it is discussed only briefly.

5.1 Motivation

Wide band measurements were taken using omni-directional linearly polarized (LP) antennas, circularly polarized (CP) directional antennas, and at a few locations in one building, LP directional antennas. The purpose of this campaign was to determine the effects of antenna polarization and antenna directivity on signal coverage and time dispersion.

Circular polarization is attractive because a CP signal may undergo a polarization sense reversal after each reflection. A CP wave can be decomposed into two orthogonal wave components (i.e. horizontal and vertical), in which one component leads the other by 90°. At a boundary between free space and a good conductor, all electric field components which are tangential to the boundary undergo a 180° phase shift upon reflection, and all components normal to the boundary do not undergo a phase shift [44]. For CP, the 180° phase shift at a reflection boundary results in a reversal of the polarization sense. Although it would be too optimistic to expect each CP multipath component in typical indoor environments to undergo a polarization sense reversal (scattering, depolarization, double reflections, etc), in general, it its expected that CP may reduce multipath propagation.

5.2 Measurement System and Procedure

The wide band system used for the polarization measurements nearly identical to the one described in Chapter 2, with two notable exceptions. The first exception is the employment of a more powerful Tektronix 11402 digitizing oscilloscope for the polarization study. This scope has a finer vertical resolution and faster data logging capability than the HP 52503 used in the original measurements. The second exception is the use of the CP helical antennas.

The measurement procedure for the polarization study differed from that used in experiments from the first campaign. First, since the primary purpose of these measurements is to study the effects of polarization, and since a large database of measurements using different frequencies and base station antenna heights was obtained in the first campaign, all polarization measurements were taken at a carrier frequency of 1.3 GHz, with mobile and base station antenna heights of 1.7 meters. Also, for the first campaign, 128 impulse response estimates were recorded over a distance of 32λ at each measurement location, and all delay spread and path loss results were presented as ***parameter averaged*** values for each measurement (Chapter 4 – Introduction). For the polarization study, only 1 impulse response estimate was recorded at a stationary location for each measurement. For this single recording, the oscilloscope averaging was set to 64. Appendix A illustrates each snapshot recorded during the polarization campaign. Eight different polarization combinations were recorded at *each* measurement location, with the primary objective to directly compare results for the polarization combinations at many locations. To implement spatial averaging for each of these combinations would have greatly increased the amount of time required to complete measurements at one location, and the total number of locations would have been greatly reduced. Spatial averaging was used at several locations that were revisited for the purpose of decoupling the effects of antenna directivity and antenna polarization.

Polarization measurements were recorded in two buildings – Whittemore Hall (Site D from the first campaign) and Kroger supermarket. In Whittemore Hall, two base station locations were used, one on the second floor and one on the third floor. Nine measurement locations were used for the second floor base station, while seven were used for the third floor base station. Measurements in

the supermarket were made using one base station, located in a corner of the shopping area, while 16 measurement locations were selected between and around aisles of produce. A total of 32 measurement locations were used during the polarization campaign.

Initially, eight measurements were made at each of the 32 locations to determine the effects of signal polarization on rms delay spread and path loss. By comparing measurements between vertical and horizontal LP, any advantages in signal strength and delay spread of one polarization over the other were found. These measurements may also be useful for studying the reflective and scattering behavior of specific objects and materials. From linear cross-polarized measurements (i.e. base station vertical polarization, mobile horizontal polarization), the strength and temporal extent of multipath components which arrive at the receiver with the opposite sense of LP were obtained. Measurements using a directive, CP base station antenna and a LP omni-directional mobile antenna were made. Finally, measurements were made with directive, CP antennas at the base station and mobile, with the base station antenna oriented toward the mobile and 45 degrees offset from the mobile in each azimuthal direction. Vertical and horizontal polarization measurements were made using the omni-directional discone antennas from the first campaign, and the CP measurements were made using endfire helical antennas, which have gains and 3 dB beamwidths of approximately 9 dBi and 30°. Table 5.2-1 is a description of the measurement types, including a 2 letter code to identify each type.

The initial polarization measurement phase compares omni-directional LP antennas with directional CP antennas. In order to decouple effects due to antenna directivity from those due to antenna polarization, a limited set of measurements were recorded using directional, LP log-periodic antennas in addition to the LP discone and CP helical antennas. These measurements are referred to as the "final phase" of the polarization campaign. The final phase is only preliminary as it was conducted at only six locations throughout Whittemore Hall. Since only a few locations were revisited, a spatial averaging technique was implemented to provide a better comparison between antenna configurations. For each measurement, ten impulse response estimates were recorded at $\lambda/4$ intervals over a distance of 2.5λ. Results for rms delay spread are presented as the average

Table 5.2-1. Descriptions of the eight polarization measurements performed at each location for the initial polarization measurements.

VV– Base Station and Mobile using Vertical Polarization.

HH– Base Station and Mobile using Horizontal Polarization.

VH– Base Station using Vertical Polarization, Mobile using Horizontal Polarization. Commonly referred to as Linear Cross-pol.

CV– Base Station using Circular Polarization with the helical always pointed in the direction of the Mobile, Mobile using Vertical Polarization.

CH– Base Station using Circular Polarization with the helical always pointed in the direction of the Mobile, Mobile using Horizontal Polarization.

C1– Base Station and Mobile using Circular Polarization with both helical antennas always pointed in the direction of each other. Will be commonly referred to as CP - On Axis

C2– Base Station and Mobile using Circular Polarization. Mobile helical pointed in the direction of the Base Station; Base Station helical pointed $\sim 45^{\circ}$ to the right of directly toward the Mobile.

C3– Base Station and Mobile using Circular Polarization. Mobile helical pointed in the direction of the Base Station; Base Station helical pointed $\sim 45^{\circ}$ to the left of directly toward the Mobile.

of ten computed values for each measurement (***parameter averaging*** from Chapters 3 and 4).

The log-periodic antennas have gains of 7 dBi and a 3 dB beamwidth of 55°. Figure 5.2-1 compares the azimuth plane radiation patterns of the LP log-periodic and CP helical antennas, and indicates that the helical antennas are slightly more directive than the log-periodic antennas. This results in two azimuthal "areas of uncertainty", where the gain of the log-periodic antennas is significantly higher than the gain of the helical antennas. For measurements taken in a wide array of topographies, this may cause significant multipath components which arrive from one of these areas of uncertainty to be more attenuated using the helical antennas, which would result in an unfair bias which favors the helical antennas for reduced rms delay spread. However, for our limited data base, all measurements were taken in narrow corridors, in which the field of vision for potential significant components rarely exceeds 15° in any plane (excepting back wall reflections, which are eliminated for the helical and log-periodic antennas). Thus, the probability of having significant components which arrive in an area of uncertainty for *these* measurements is low. This is especially true for the three LOS measurements, which were recorded straight down a narrow corridor.

Should the opportunity to conduct a more extensive polarization campaign arise, it is strongly recommended that measurements using all three antennas (CP directive, LP directive, and LP omni-directional) be made. Also, it is suggested that the number of turns on the present helical antennas be reduced in order to make the antennas less directive, and thus more comparable to the log-periodic antennas.

5.3 File Classification and Data Storage

Figure 5.3-1 illustrates the file naming technique for a typical base filename, WHL2BVH. From each filename, the building, type of topography, base station and measurement locations, and antenna configuration can be determined. Similar to the initial campaign, the data acquisition program stored 3 files on a computer hard disk at the time of each measurement run. One file, *filename.dat*, consists of 1024 raw data points, which represent the single impulse

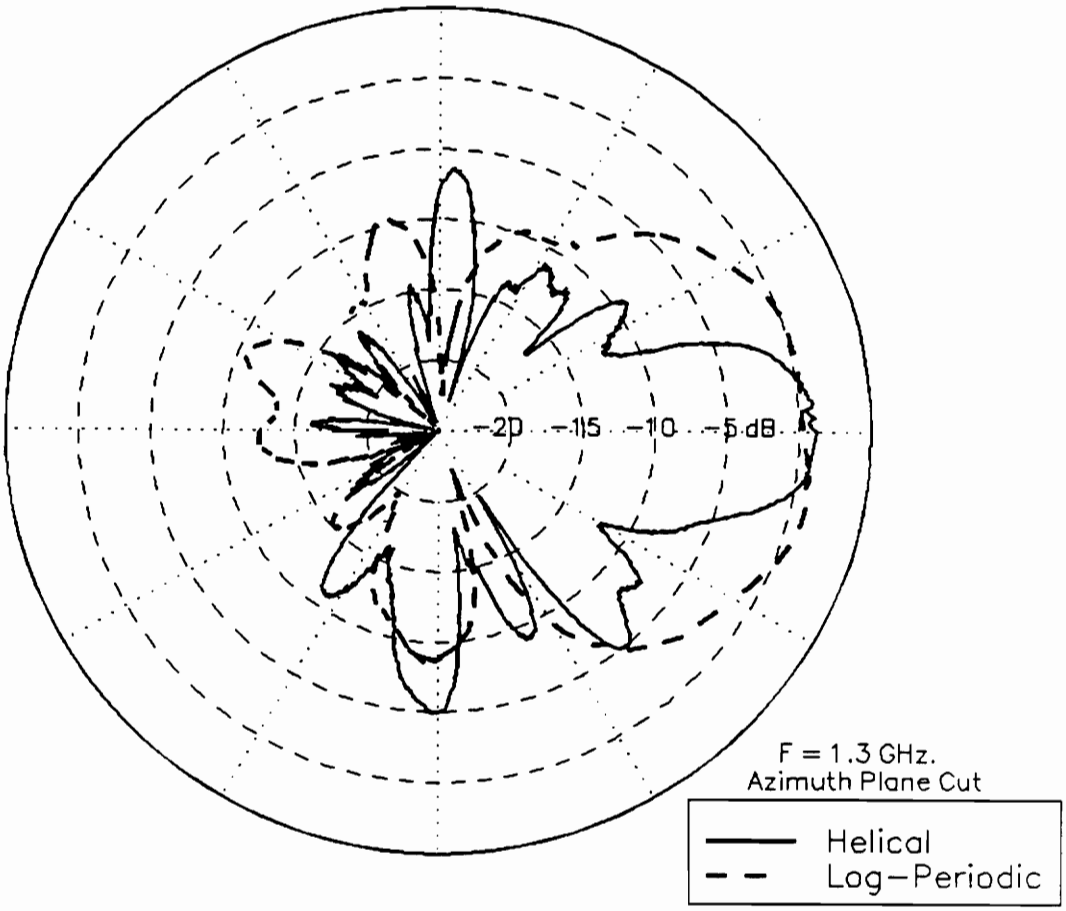

Figure 5.2-1. Azimuth plane radiation patterns for CP helical antenna (solid) and LP log-periodic (dashed) antennas at 1.3 GHz. Pattern is in the H-plane for the log-periodic antenna.

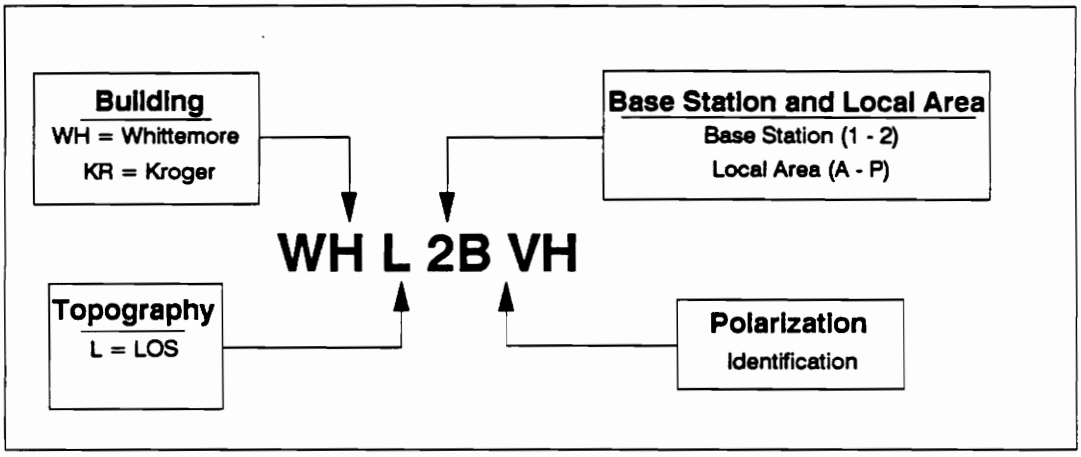

Figure 5.3-1. Breakdown of a typical base filename for polarization measurement campaign.

response estimate corresponding to the measurement described by *filename*. These raw data points are stored in block binary format for storage efficiency. The second file, *filename.hdr*, is a text file, which consists of oscilloscope preamble parameters, and is accessed during processing to obtain information such as volts/div, time/div, etc. The third file, *filename.des*, is a text file which gives the measurement details such as T-R separation, receiver attenuation, and polarization. A typical *.des* file, **WHL2BVH.DES**, is shown in Figure 5.3-2.

The *.dat* files are stored in 1 of 2 subdirectories on a personal computer. All *.dat* files recorded in Whittemore Hall are stored in the C:\ WIDEBAND\WHIT\REALRUNS\RAWDATA\DAT subdirectory, and all *.dat* files recorded in Kroger supermarket are stored in a similar subdirectory, with \WHIT\ replaced by \KROG\. The *.hdr* and *.des* files are stored in one of two similar subdirectories each, with \DAT replaced by \HDR and \DES, respectively. All *.dat* files were thresholded using a similar method described in Chapter 3. The thresholded files are called *filename.thr*, and are stored similarly to the three "measurement" files, with \RAWDATA\XXX replaced by \THRSHOLD.

For each data file, three channel parameters were computed: rms delay spread (σ_τ), mean excess delay ($\overline{\tau}$), and path loss above a 1 meter free space reference PL(dBr_{1m}). A complete discussion of these parameters, and there significance in mobile radio system design was presented in Chapter 3. Values of σ_τ are located in the text file *filename.rms*. The *.rms* files are stored similarly to the *.thr* files, with \THRSHOLD replaced by \RMSDELAY. Values of $\overline{\tau}$ and PL(dBr_{1m}) are located in text files *filename.med* and *filename.pls*, respectively. The *.med* and *.pls* files are stored similarly to the *.rms* files, with \RMSDELAY replaced by \MEANEXES and \PATHLOSS, respectively. In each of the *.rms*, *.med*, and *.pls* files, two values are stored. The first value in each file is the T-R separation in meters, and the second value is the parameter value. For example, if the file **WHL2BVH.RMS** were viewed, the numbers 31.39 and 11.21 would be seen in an unformatted list structure. This indicates that an rms delay spread of 11.21 ns was computed for this measurement, which was taken at a T-R separation of 31.39 meters.

All files for the final phase of the polarization campaign were stored exactly

```
WHO2ECH
T-R SEPARATION (IN METERS):    22.6
RECEIVER ATTENUATION (IN dB):   20
MEASUREMENT LOCATION : WHITTEMORE HALL
TYPE OF TOPOGRAPHY   : OBSTRUCTED
TYPE OF POLARIZATION:  CH

OFFSET:     -1.00000000000051E-0002
SENSITIVITY: 1.99999999999889E-0003
TIMEBASE:    9.99999999999482E-0008
NUMPOINTS:  1024
MAINPOS:    -9.00000000000076E-0008
#AVG POINTS:  16
XINCR        1.00000000000050E-0009
XZERO       -9.00000000000076E-0008
YMULT        3.12499999999879E-0007
YZERO       -1.00000000000051E-0002
t(n)=XZERO+XINCR*n   v(n)=YZERO+YMULT*dat(n)
```

Figure 5.3-2. Typical *.des* file for polarization measurement campaign.

as described in the previous two paragraphs, with the directory C:\WIDEBAND\WHIT replaced by C:\WIDEBAND\WHIT3RD.

5.4 RMS Delay Spread Results

Figure 5.4-1 is a CDF of rms delay spread using omni-directional discone antennas for vertical, horizontal, and linear cross-pol for all 32 second campaign measurement locations. No significant difference in σ_τ is found for one sense of LP over the other, as the median value of σ_τ for both polarizations is between 27 and 30 ns. This independence of polarization sense holds when results from the office building and the supermarket are examined independently. Although not severe, Figure 5.4-1 indicates on average, a slight delay spread increase for cross-polarized measurements. The median value of σ_τ for the cross-polarized measurements is approximately 35 ns.

For co-polarized measurements, the overall median values of σ_τ for the office building and supermarket are about 20 ns and 32 ns, respectively. Worst case values for the office building and supermarket are about 85 ns and 55 ns, respectively. Although the office building has the lower median rms delay spread, it has several values higher than the maximum value in the supermarket. This can be attributed to the extreme differences from one topography to another in the office building compared to the supermarket. Most topographies in the office building are relatively simple – LOS down a hallway or OBS around a single corner, and a few are more complicated – OBS around more than 1 corner. These more complicated paths would not be dominated by a few closely spaced temporal components, which would yield significantly higher values of σ_τ relative to the "LOS – hallway" locations. Conversely, all measurement locations in the supermarket are in the same large-scale topography, which may be why the overall range of σ_τ values at this location is smaller. Median and worst-case values of delay spread in the office building from the original campaign agree closely with those measured in the second campaign.

Figure 5.4-2 compares CP On Axis (C1 from Table 5.2-1), CP 45° Off-Axis (C2 and C3), Base Circular to Mobile Linear (CH and CV), and LP (VV and HH) measurements for all measurement locations in LOS (a) and OBS (b) topographies. For LOS and OBS channels, there is a significant reduction in σ_τ

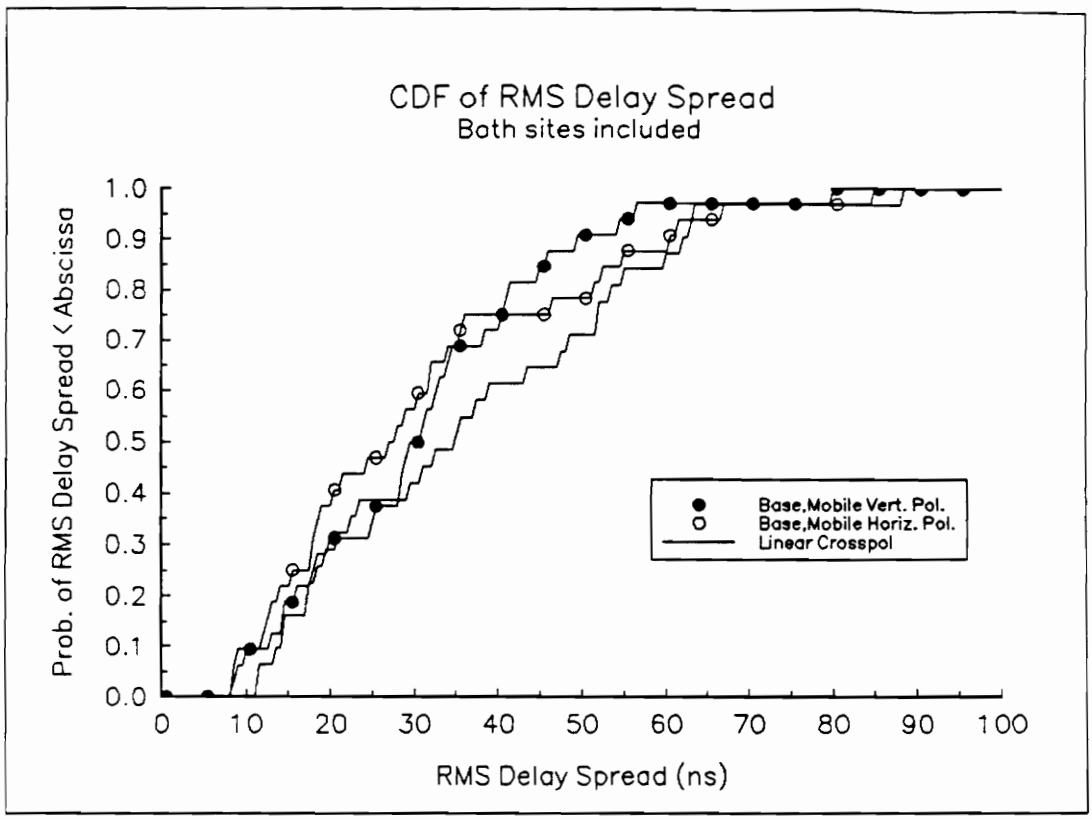

Figure 5.4-1. CDF of rms delay spread for vertical, horizontal, and linear cross-pol measurements, using omni-directional discone antennas at transmitter and receiver. f = 1.3 GHz.

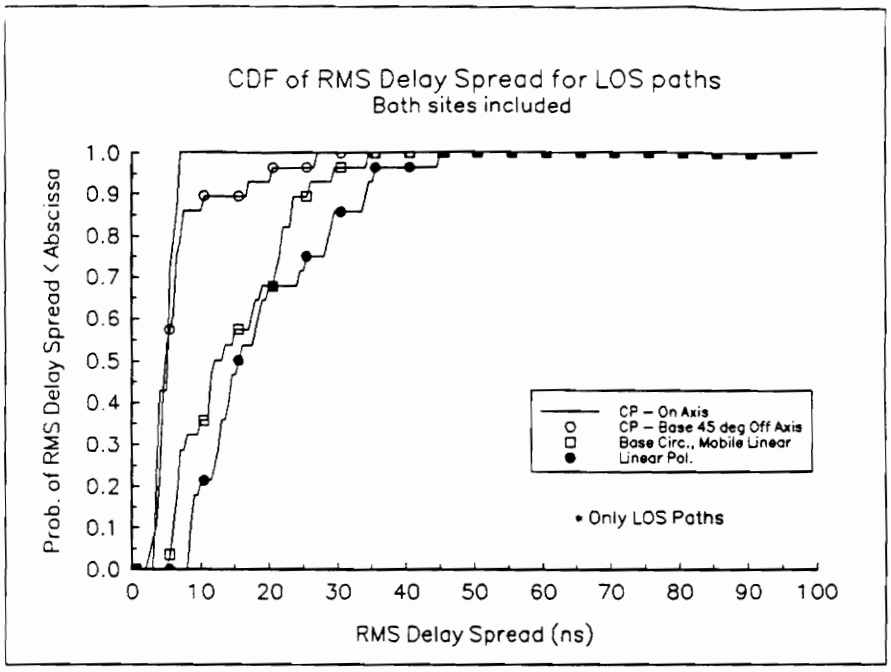

(a) LOS Topography

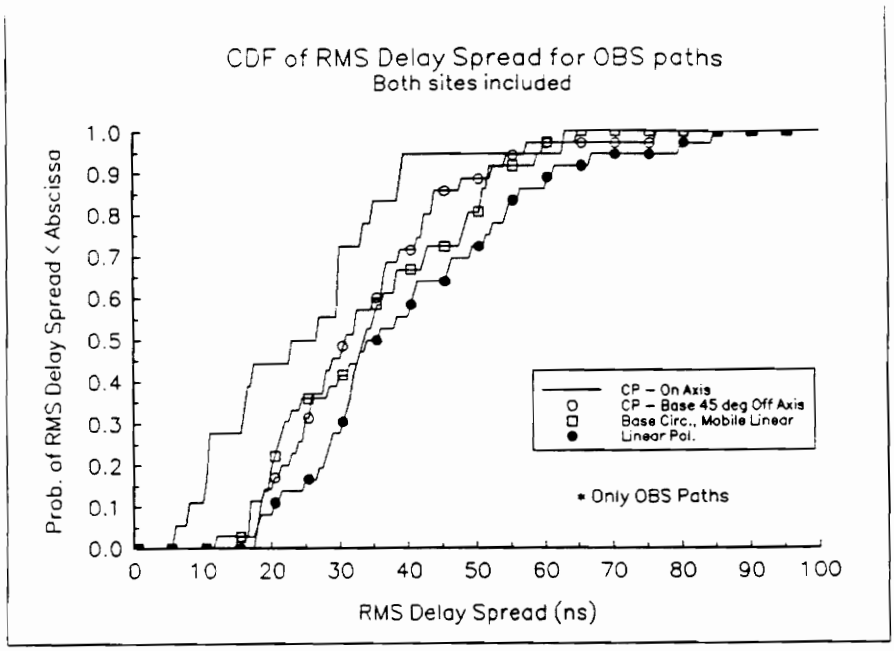

(b) OBS Topography

Figure 5.4-2. CDF of rms delay spread as a function of polarization for (a) LOS and (b) OBS topographies. CP refers to helical antennas; Linear refers to discone antennas. f = 1.3 GHz.

for CP directive antennas compared to LP omni-directional antennas. This reduction is more significant for LOS topographies. Less significant rms delay spread reductions are noticed when the base station antenna is CP pointed 45° off-axis and the mobile antenna is CP pointed on-axis, and when the base station antenna is CP on-axis and the mobile antenna is LP omni-directional.

To isolate the delay spread reduction offered by linear and CP directional antennas, several "final phase" polarization measurements were made using log-periodic LP antennas in addition to the discone and helical antennas. The six measurement locations were carefully marked on a Whittemore hall blueprint during the first polarization measurements, and returned to when the log-periodic antennas became available. Table 5.4-1 compares values of σ_τ for vertically-polarized omni-directional, horizontally-polarized omni-directional, vertically-polarized directional, horizontally-polarized directional, and circularly-polarized directional antennas at these six locations. All five antenna configurations represented in Table 5.4-1 were with identical antennas at the transmitter and receiver. Although measurements were recorded with the base station directive antennas pointed on-axis and 45° off-axis in each direction, the data in Table 5.4-1 were with the transmitter and receiver antennas pointed on-axis. All six locations were made with transmitters and receivers in hallways. The first three locations in Table 5.4-1 are in LOS environments along a corridor. The last three locations are in OBS channels, in which the transmitter and receiver are located in different corridors on the same floor.

Values of σ_τ for the three LOS locations using directive CP antennas were between 2.2 ns and 2.7 ns, and consistently lower than those using either horizontal or vertical directive LP antennas. The rms delay spread calculation was with the time of the peak of the first detectable pulse set to t=0. This accounts for values of σ_τ less than the rms pulse width of ~ 4 ns. No consistent delay spread reduction exists for the three OBS topographies. These limited measurements suggest that in certain LOS environments, some multipath components within 10-15 dB of the direct component are cross-polarized and thus reduced when using CP. But for OBS channels, Table 5.4-1 suggests that σ_τ may or may not be reduced when using CP.

There may be several reasons why CP does not always show delay spread

Table 5.4-1. Comparison of rms delay spread for LP omni-directional (vertical and horizontal), LP directional (vertical and horizontal), and CP directional results. All directional measurements were made with antennas on-axis.

	σ_τ(ns) Omni LP - Vert.	σ_τ(ns) Omni LP - Horiz.	σ_τ(ns) Directive LP - Vert.	σ_τ(ns) Directive LP - Horiz.	σ_τ(ns) Directive CP
LOS - 9.40 m	8.2	13.6	4.0	8.1	2.3
LOS - 15.2 m	15.0	19.6	6.3	4.8	2.7
LOS - 31.1 m	12.1	9.3	3.5	3.7	2.2
OBS - 13.6 m	34.9	37.3	21.4	21.4	20.8
OBS - 31.7 m	57.3	50.3	34.5	28.7	22.0
OBS - 34.1 m	41.2	48.9	29.1	39.2	37.2

reduction in OBS channels. First, large multipath components will have a tendency to undergo multi-hop reflections since there is no single strong direct component dominating the power delay profile. In this case, even if CP undergoes a complete polarization reversal after each reflection, whether or not it is cross-polarized at the receiver strictly depends on the total number of reflections between terminals. Second, in well obstructed channels, propagation from transmitter to receiver is typically via various reflectors and scatterers. In such cases, LP tends to become depolarized, in which the received power for the opposite sense of LP is on the order of the received power for the same sense. This linear depolarization will cause a CP signal to not undergo a polarization sense reversal. Rather, a CP signal may reflect the same sense of polarization or may become elliptically polarized.

The values given in Table 5.4-1 are average values of rms delay spread for 10 impulse responses over 2.5 wavelengths. The table fails to indicate the behavior of σ_τ from one $\lambda/4$ interval to the next. Figure 5.4-3 illustrates the variation of σ_τ over 2.5 wavelengths for the five antenna configurations listed in Table 5.4-1 (omni horizontal and vertical, directive horizontal and vertical, and directive circular – directive antennas on-axis) for the three LOS measurement locations (a-c). For all three locations, σ_τ using omni-directional antennas varies severely over sub-wavelength intervals. This is due to two or more multipath components which arrive at the receiver within a time period of 5 ns, or the width of the probing pulse. Thus, these components are not resolvable, and will fade in and out depending on the relative phases of each component. This behavior is called non-resolvable component fading, and is what causes the severe differences in σ_τ over sub-wavelength intervals. Hypothetically, if the measurement system could achieve infinitely small time resolution, this variation of delay spread over small distances would certainly not exist, since non-resolvable component fading would be eliminated. In Figure 5.4-3 (c), the rms delay spread consistently rises and falls with each $\lambda/4$ movement of the transmitter for both omni-directional antenna configurations (vertical and horizontal). Figure 5.4-4 shows 3-dimensional power delay profiles for the (a) omni-directional vertical and (b) omni-directional horizontal results of Figure 5.4-3(c). From either 3-D plot, it is clear that a multipath component at an excess delay of approximately 150 ns

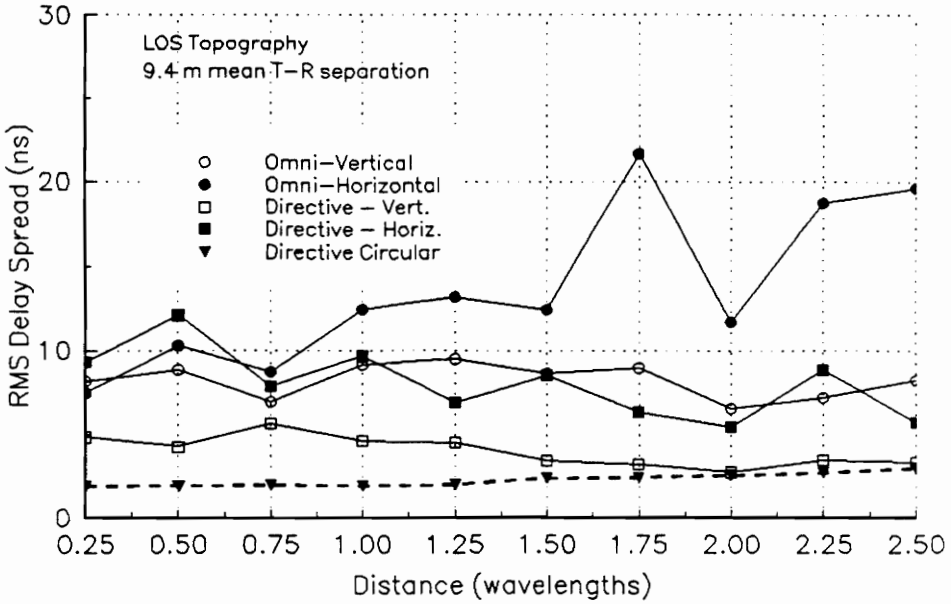

(a)

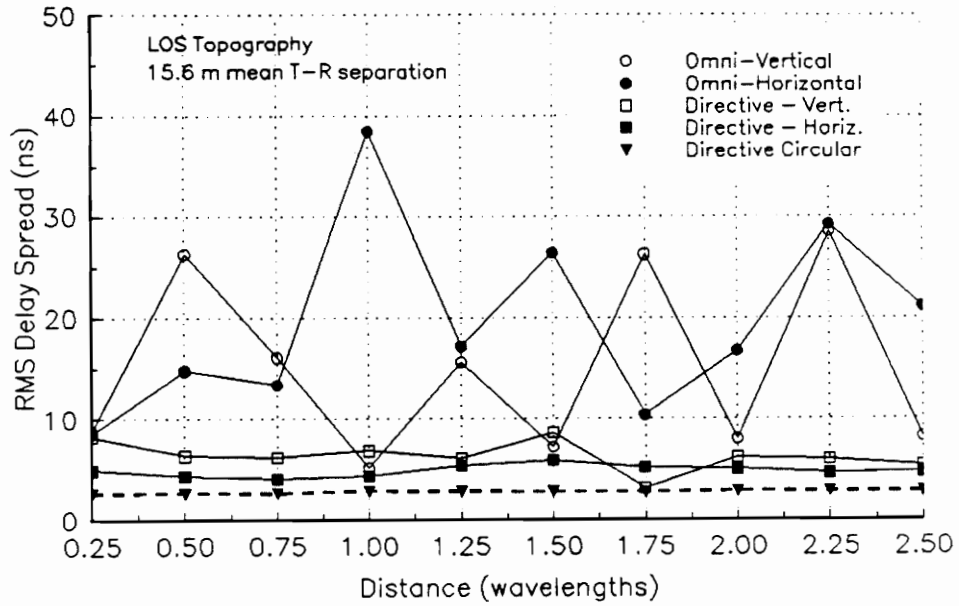

(b)

Figure 5.4-3. Variation of rms delay spread over 2.5λ for LP omni-directional (V and H), LP directional (V and H), and CP directional, for the 3 LOS (a-c) locations. f = 1.3 GHz. Part (c) is on the following page.

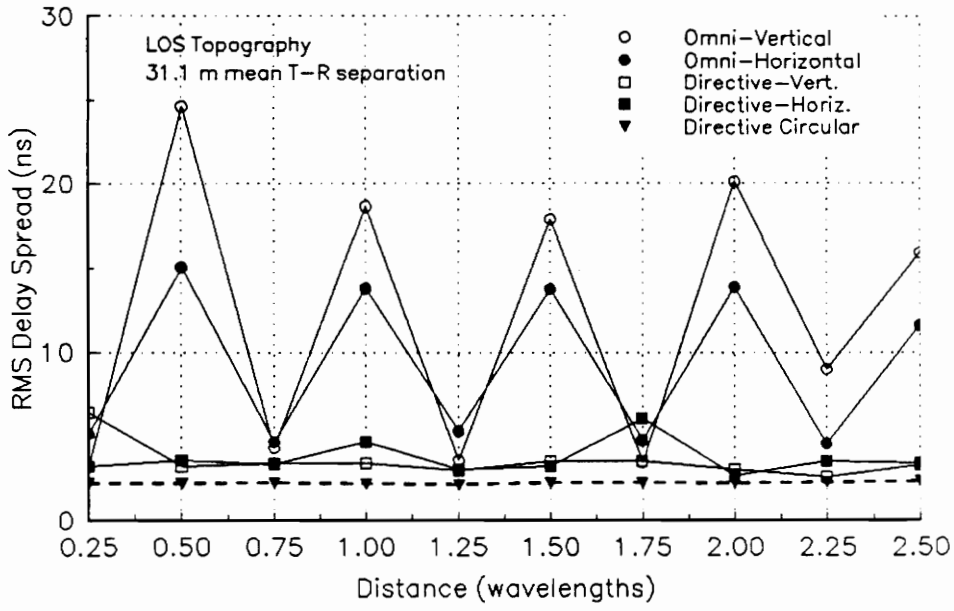

(c)

Figure 5.4-3. – Continued.

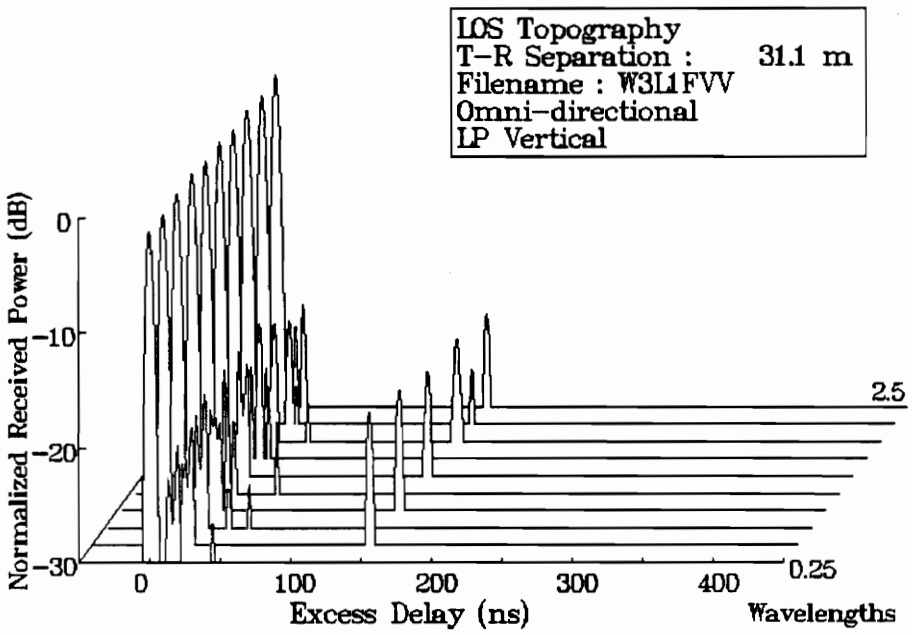

(a) Omni-directional Vertical

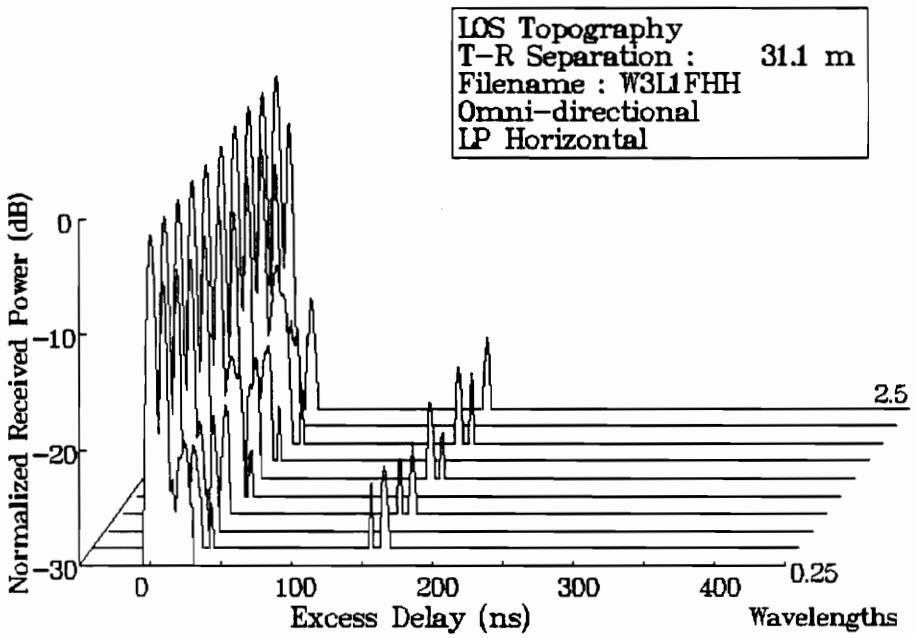

(b) Omni-directional Horizontal

Figure 5.4-4. 3-dimensional views of 10 power delay profiles for omni-directional vertical (a) and omni-directional horizontal (b) recorded in a corridor (LOS) for "final phase" polarization measurements.

appears and disappears with each $\lambda/4$ movement of the transmitter, causing the rms delay spread to fluctuate accordingly. Further, the amplitude of this component is higher for vertical polarization than for horizontal polarization, which gives rise to the higher rms delay spread peaks for vertical polarization in Figure 5.4-3(c). The likely reason for this periodic fluctuation is the existence of two multipath components which undergo non-resolvable component fading.

For each LOS location, the variation of σ_τ is greatly diminished when directive LP antennas are used, and when directive CP antennas are used, the rms delay spread remains virtually unchanged over 2.5 wavelengths. This indicates that CP not only consistently reduces rms delay spread in the LOS hallway topographies, but it also causes the rms delay spread to be remarkably consistent over several wavelength intervals. This is due to the directivity of the antenna and the cross-polarization of multipath components, both of which help diminish non-resolvable component fading.

Figure 5.4-5 illustrates the variation of σ_τ for the three OBS topographies (a-c). For certain OBS topographies, CP again reduces the variation of delay spread over 2.5λ, as clearly indicated by Figure 5.4-5 (a). However, in other locations, it illustrates little to no improvement over directive LP antennas, as indicated by Figure 5.4-5 (b). In Figure 5.4-5 (c), although the mean rms delay spread for directive circular antennas is similar to the mean for the horizontal and vertical directive antenna configurations, the variation over 2.5λ is still smaller for the CP antennas.

Figures 5.4-6 and 5.4-7 illustrate rms delay spread as function of distance for six directive off-axis antenna configurations (45° left and right of on-axis for LP vertical, LP horizontal, and CP) for the three LOS and OBS topographies, respectively. For all off-axis measurements, the base station antenna was oriented 45° left or right of on-axis while the mobile antenna remained on-axis. Figure 5.4-3 (b) and Figure 5.4-6 (b) together contain graphs of rms delay spread as a function of distance for a total of 11 antenna configurations for one "final phase" measurement location. Figure 5.4-8 (a-k) contains 3-D power delay profiles for these 11 measurement runs. A comparison of the LP omni-directional antennas (a and b) with the on-axis LP directional antennas (c and d) indicates a significant reduction in multipath when the directional antennas are used. In particular,

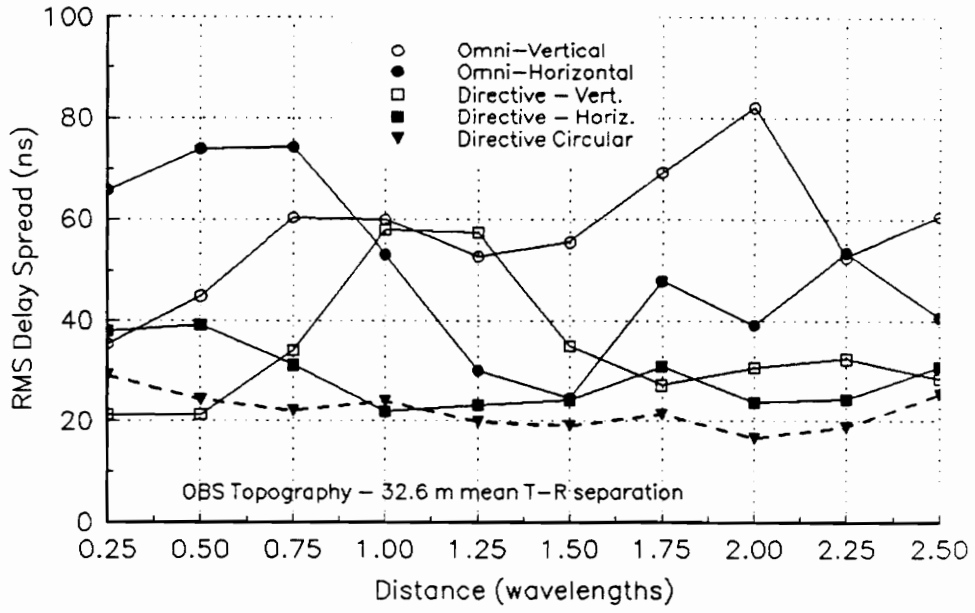

(a)

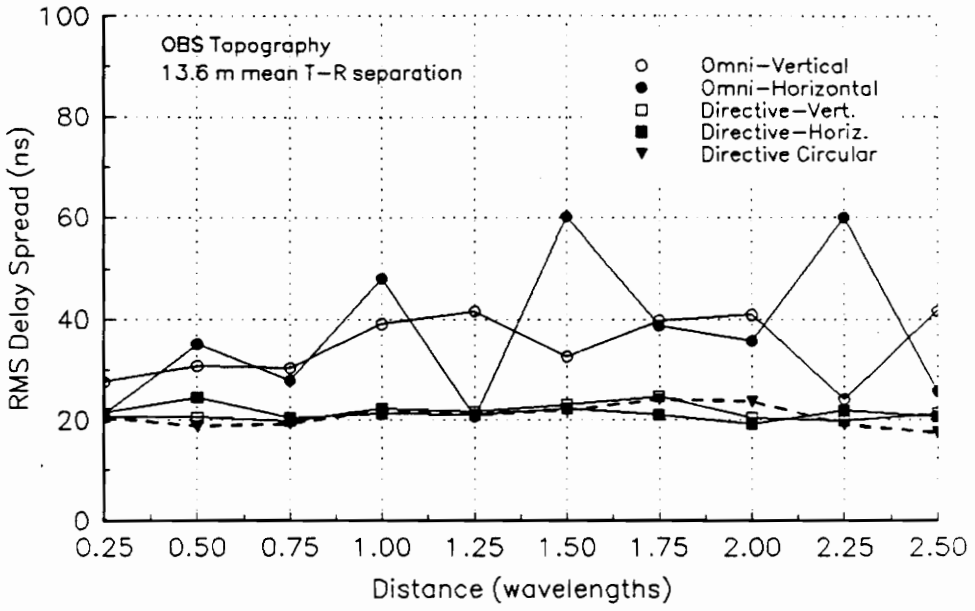

(b)

Figure 5.4-5. Variation of rms delay spread over 2.5λ for LP omni-directional (V and H), LP directional (V and H), and CP directional, for the 3 OBS (a-c) locations. f = 1.3 GHz. Part (c) is on the following page.

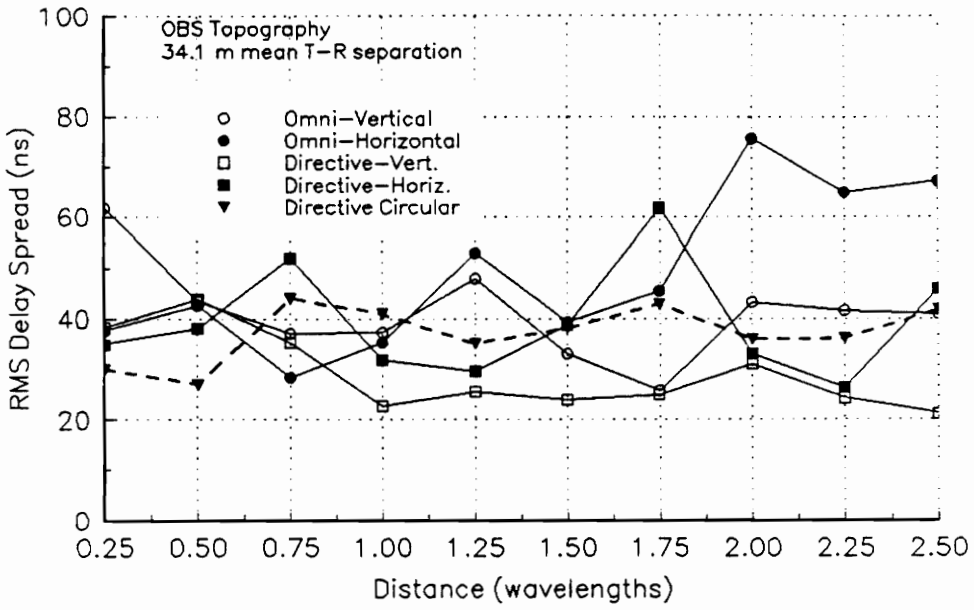

(c)

Figure 5.4-5. – Continued.

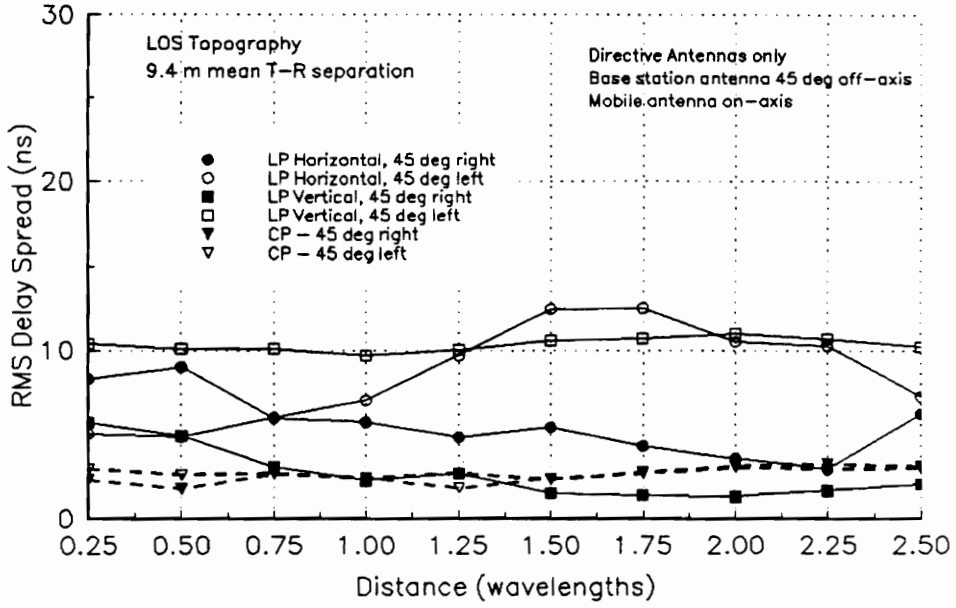

(a)

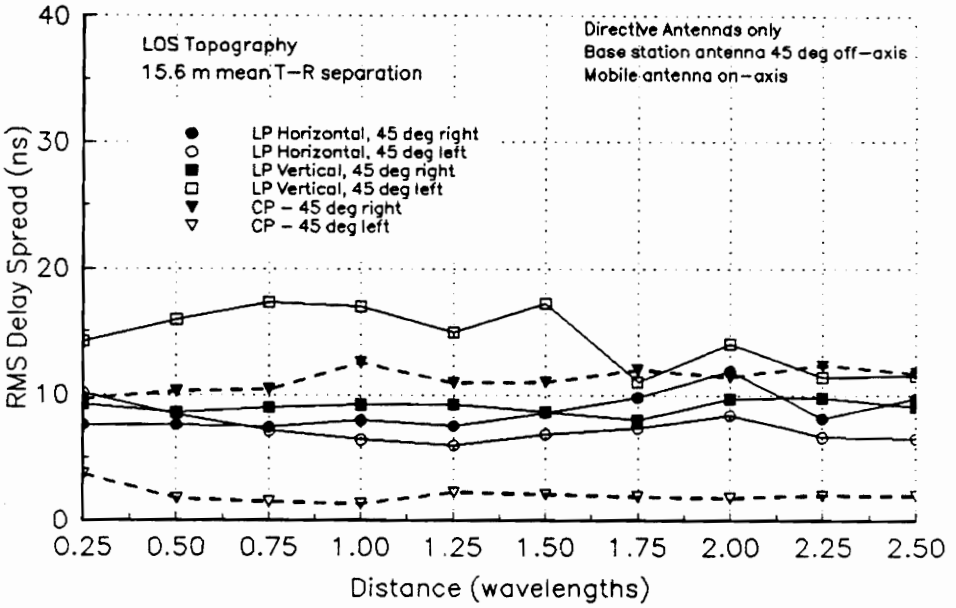

(b)

Figure 5.4-6. Variation of rms delay spread over 2.5λ for LP directional 45° off-axis (V and H), and CP directional 45° off-axis, for the 3 LOS (a-c) locations. f = 1.3 GHz. Part (c) is on the following page.

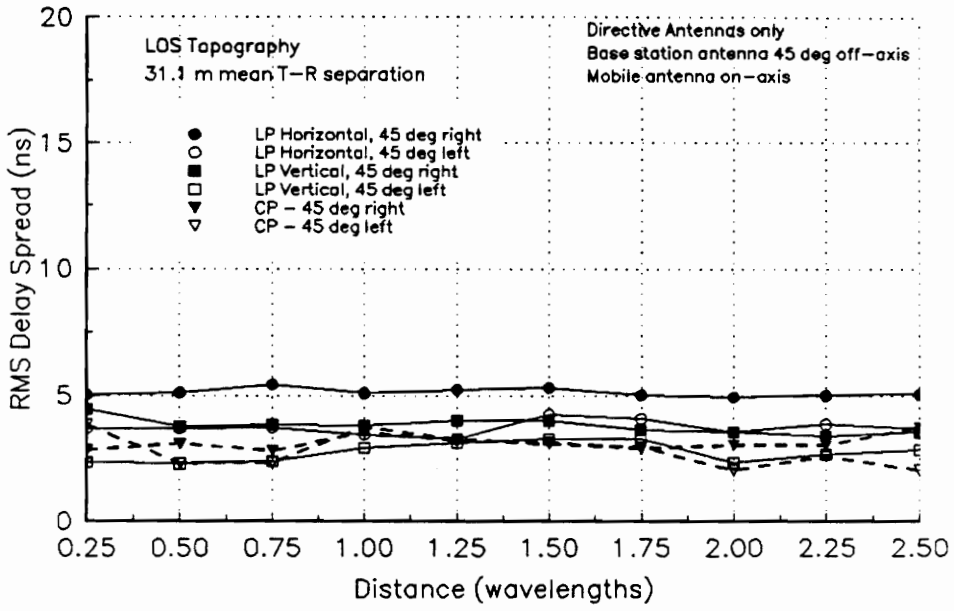

(c)

Figure 5.4-6. - Continued.

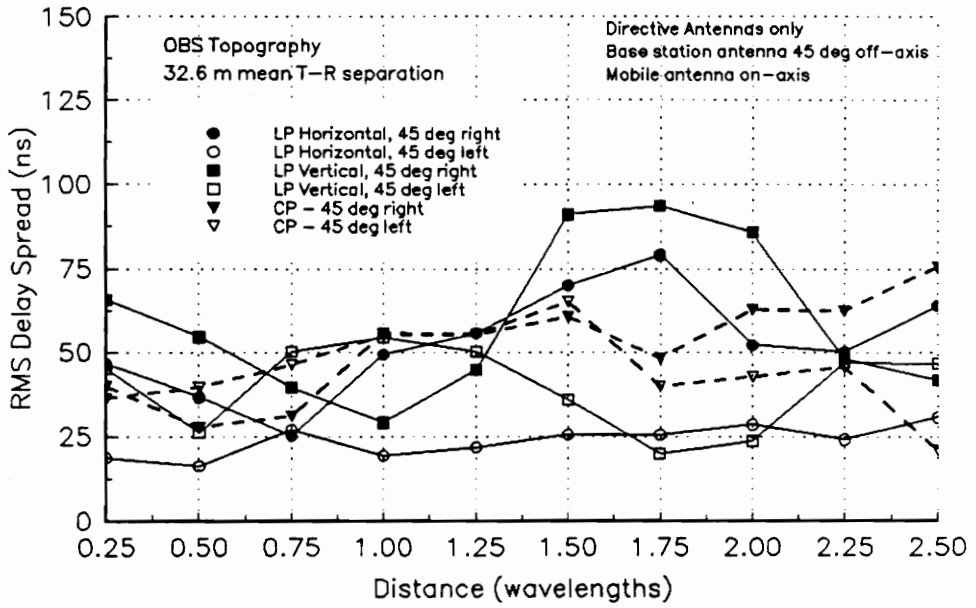

(a)

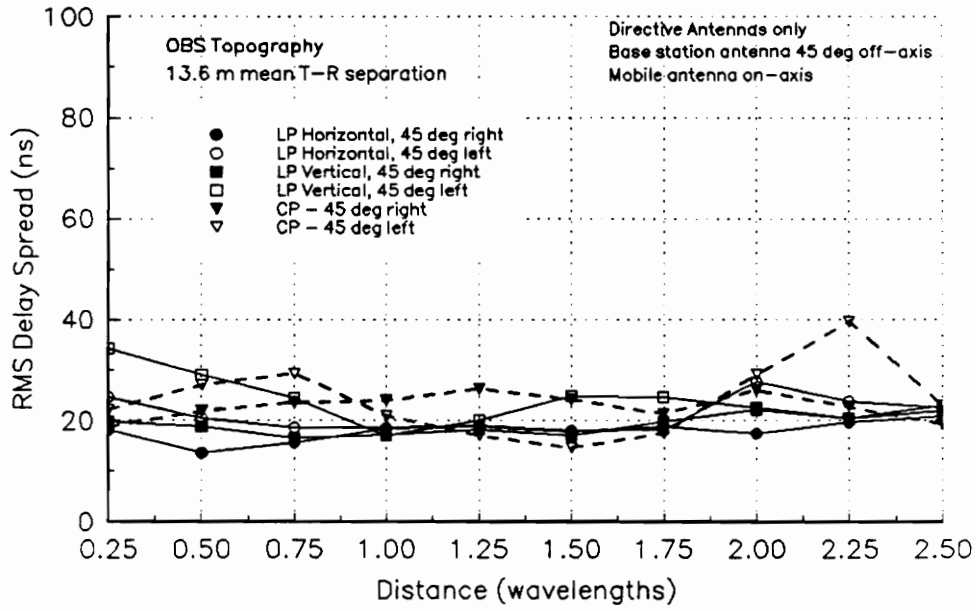

(b)

Figure 5.4-7. Variation of rms delay spread over 2.5λ for LP directional 45° off-axis (V and H), and CP directional 45° off-axis, for the 3 OBS (a-c) locations. f = 1.3 GHz. Part (c) is on the following page.

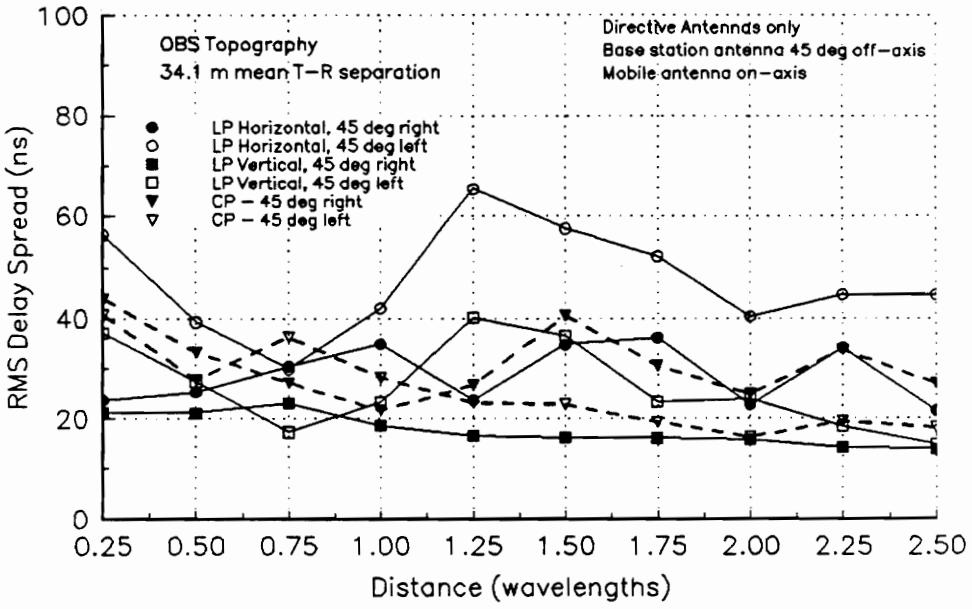

(c)

Figure 5.4-7. – Continued.

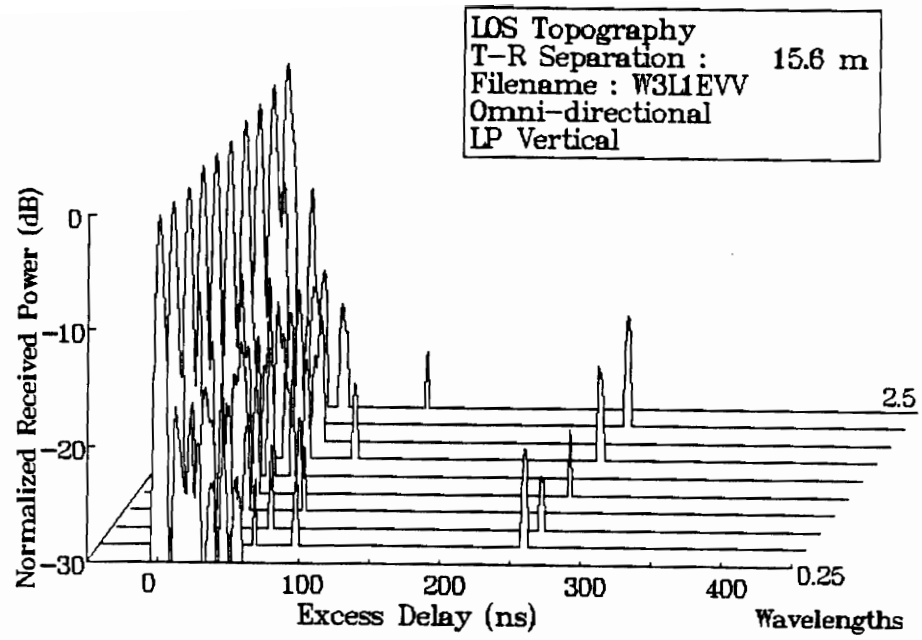

(a)

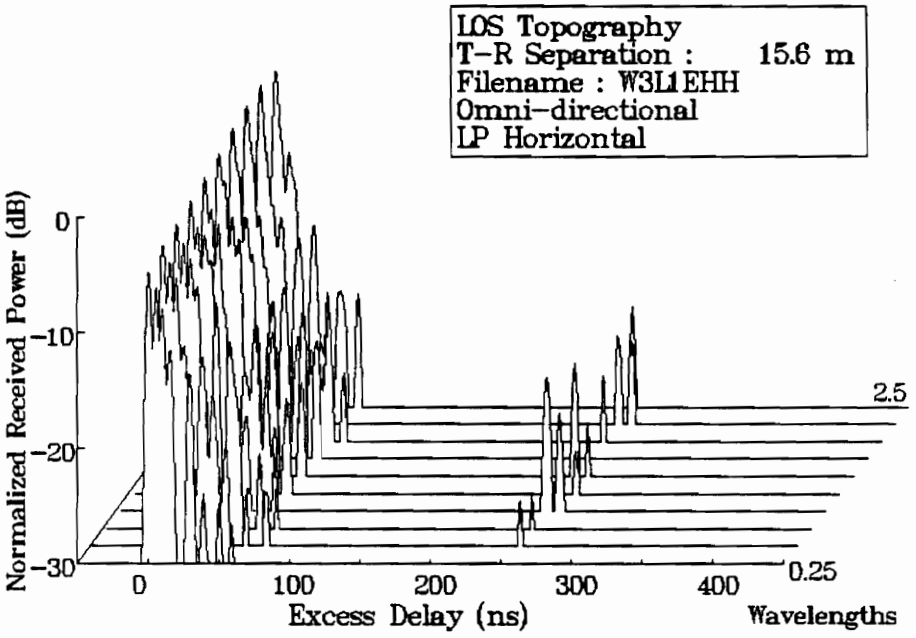

(b)

Figure 5.4-8. 3-dimensional views of ten power delay profiles for all 11 antenna configurations (a–k) for one "final phase" polarization measurement location. Figure continued on the next five pages (parts c–k).

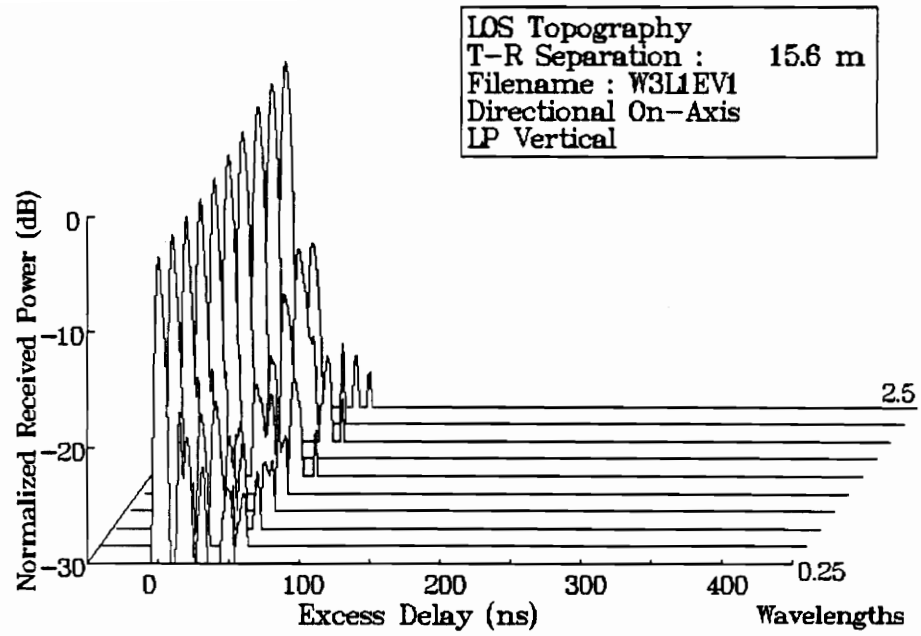

(c)

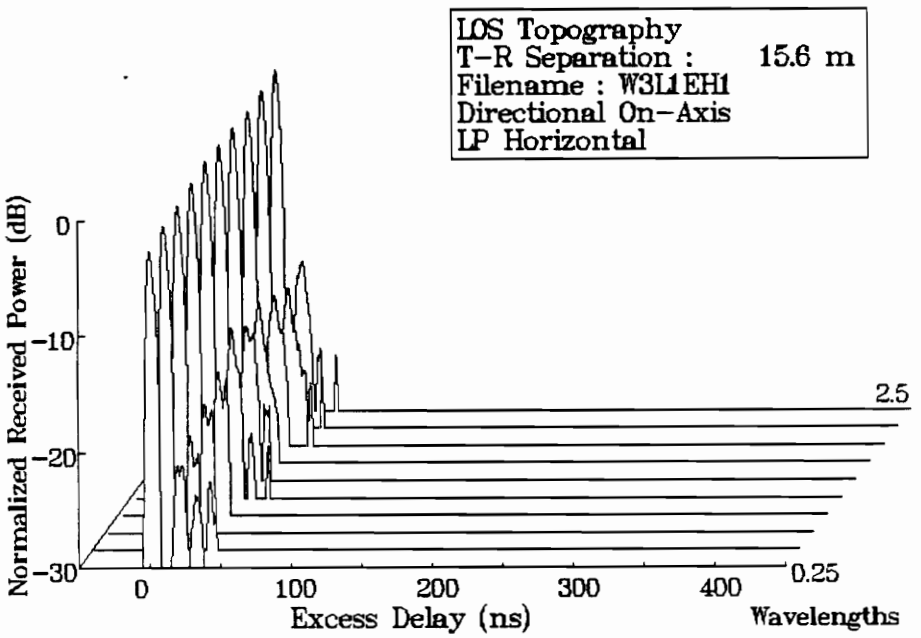

(d)

Figure 5.4-8. – Continued.

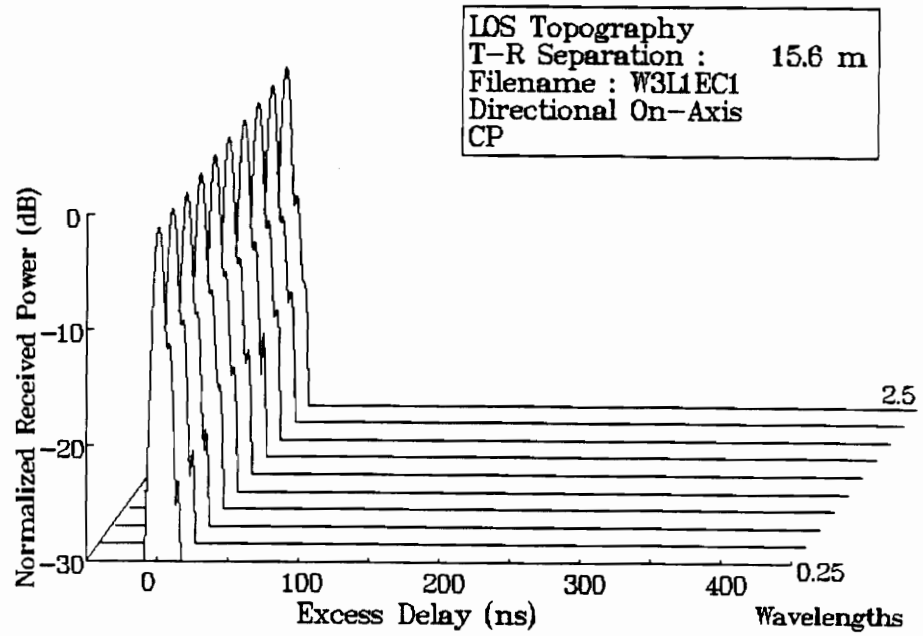

(e)

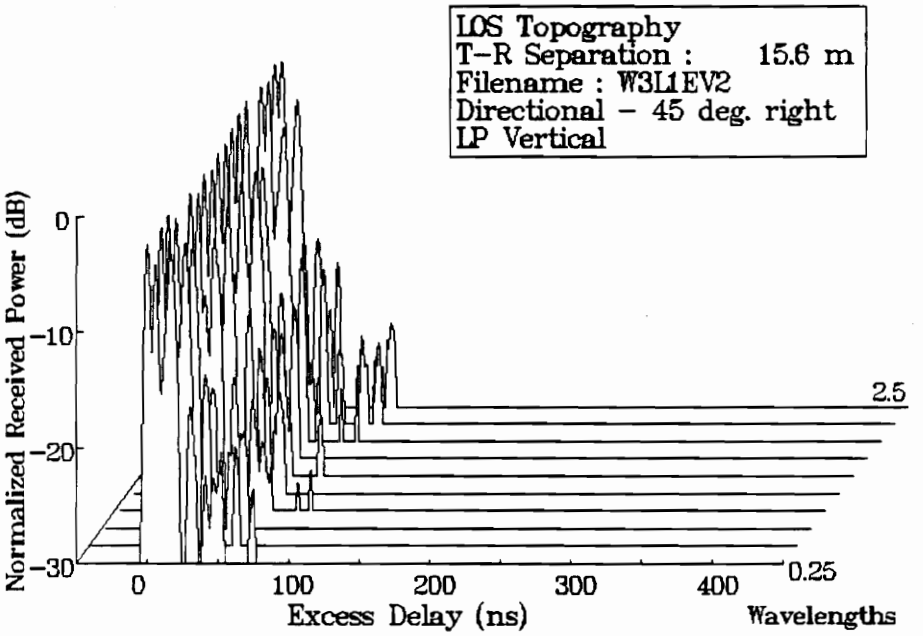

(f)

Figure 5.4-8. – Continued.

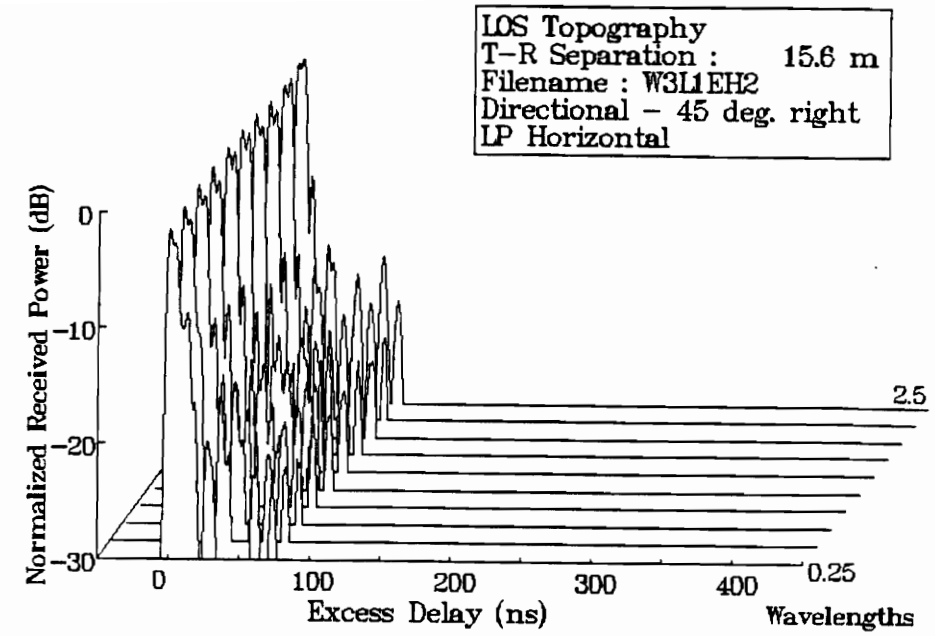

(g)

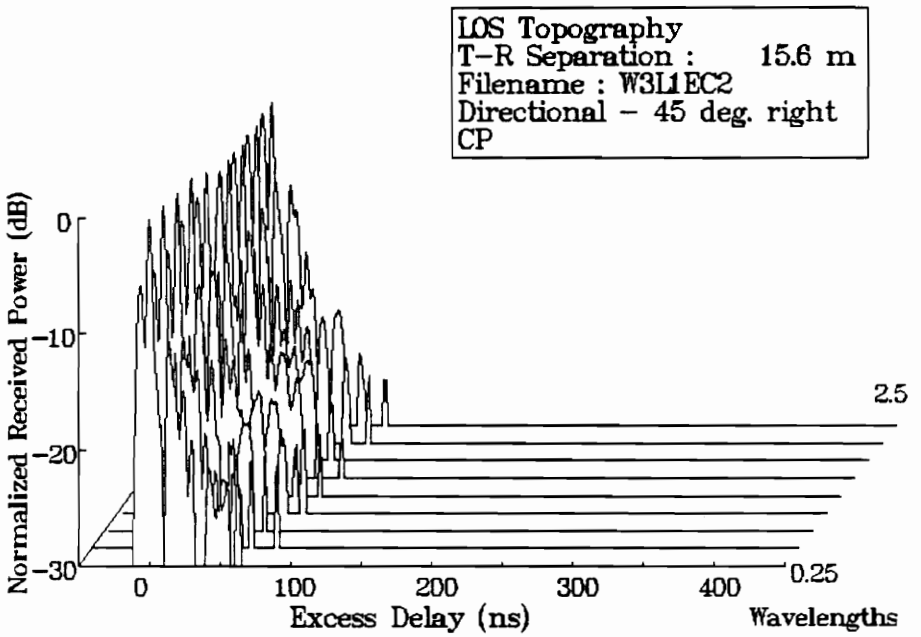

(h)

Figure 5.4-8. – Continued.

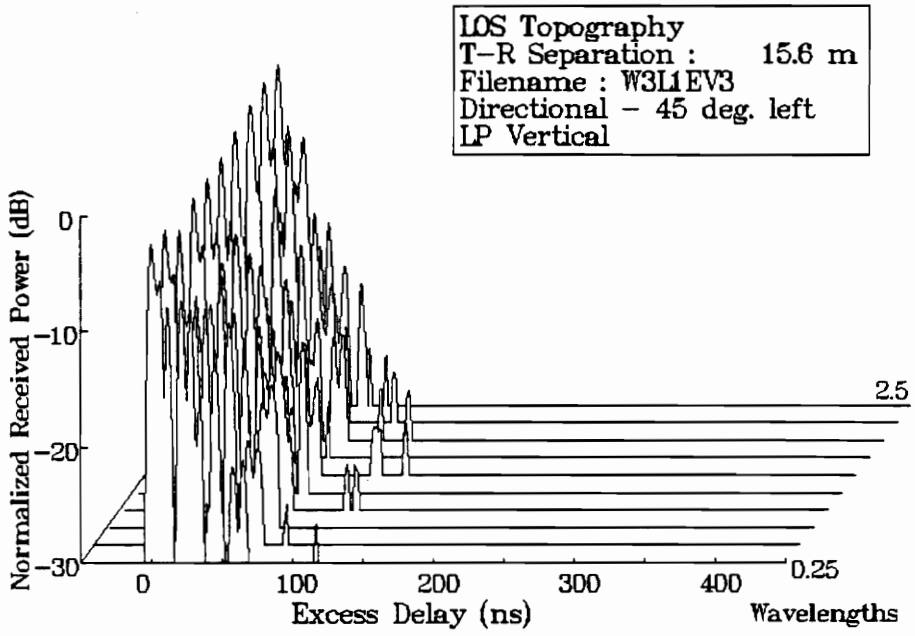

(i)

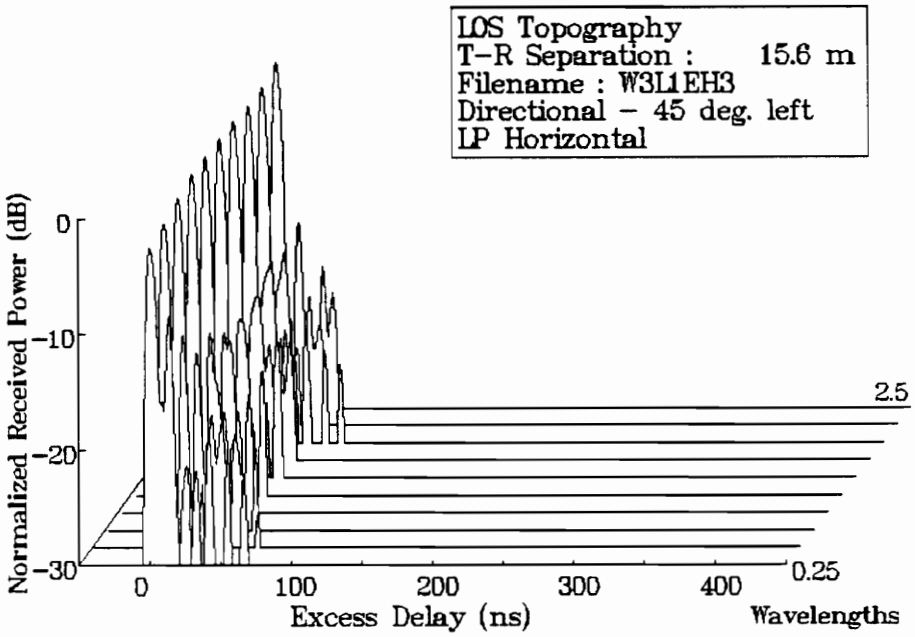

(j)

Figure 5.4-8. – Continued.

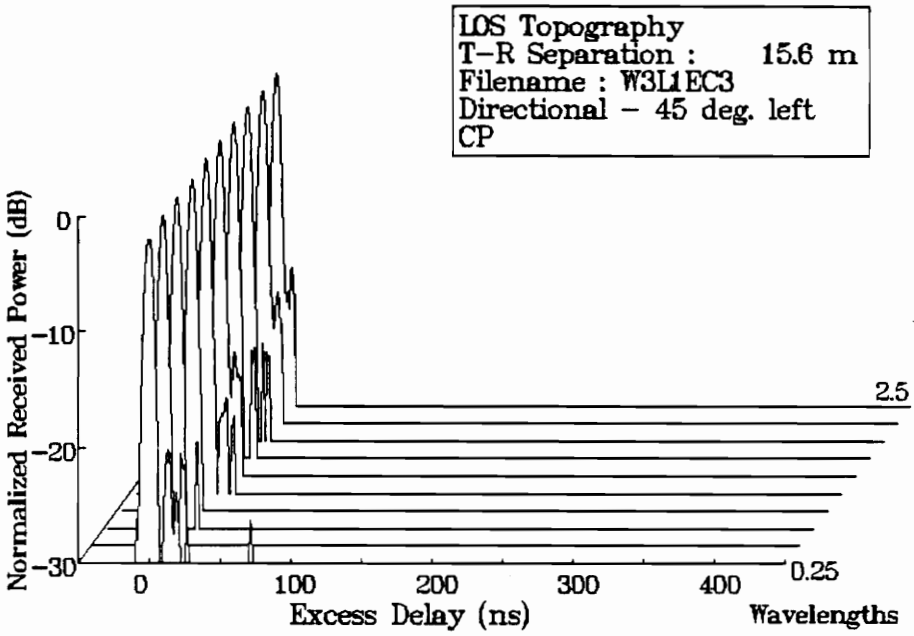

(k)

Figure 5.4-8. – Continued.

notice that the components at an excess delay of approximately 250 ns using the omni-directional antennas disappear when the directional antennas are used, confirming that a back wall reflection is the source of these components. Figure 5.4-8 (e) illustrates an even greater reduction when CP on-axis antennas were used, as the power delay profiles consist of primarily the LOS component for all 10 profiles in the measurement run.

5.5 Path Loss and Cross-pol Discrimination Results

The method of calculating path loss from a wide band impulse response estimate was described in Chapter 3. Figure 5.5-1 is a scatter plot of path loss values for horizontal, vertical, and linear cross-pol omnidirectional antennas. Similar to the results for delay spread, path loss values are relatively independent of linear polarization sense. The calculated values of power law exponent n for all polarization campaign measurements are 2.20 and 2.23 for vertical and horizontal polarization, respectively. The standard deviations σ about the d^n model are 8.6 dB and 10.4 dB for vertical and horizontal polarization, respectively. The cross-pol results indicate greater path loss, since n=2.63 and σ=7.1 dB, and can be explained by some polarization isolation offered by the channels.

Figure 5.5-2 illustrates the cross-pol discrimination between discone antennas as a function of co-pol path loss. Each point indicates the path loss in the opposite sense of polarization with respect to the path loss for the linear co-pol measurements at a single location. For example, the highest point on the plot indicates at that LOS location, the cross-pol path loss was 17 dB higher than the average co-pol path loss, which is 20 dB above a 1 meter free space reference. The mean values of cross-pol discrimination for LOS and OBS topographies are 8.3 dB and 2.8 dB, respectively. In LOS environments, the received signal is dominated by the LOS component, which is not depolarized. Conversely, in OBS topographies, the received signal is primarily composed of multipath components from reflecting, diffracting, and scattering objects, which have a greater tendency to depolarize the transmitted signal.

The standard deviation of cross-pol discrimination results is 3.4 dB for LOS topographies and 2.5 dB for OBS topographies. The three LOS locations that exhibit the highest discrimination causes the LOS standard deviation to be

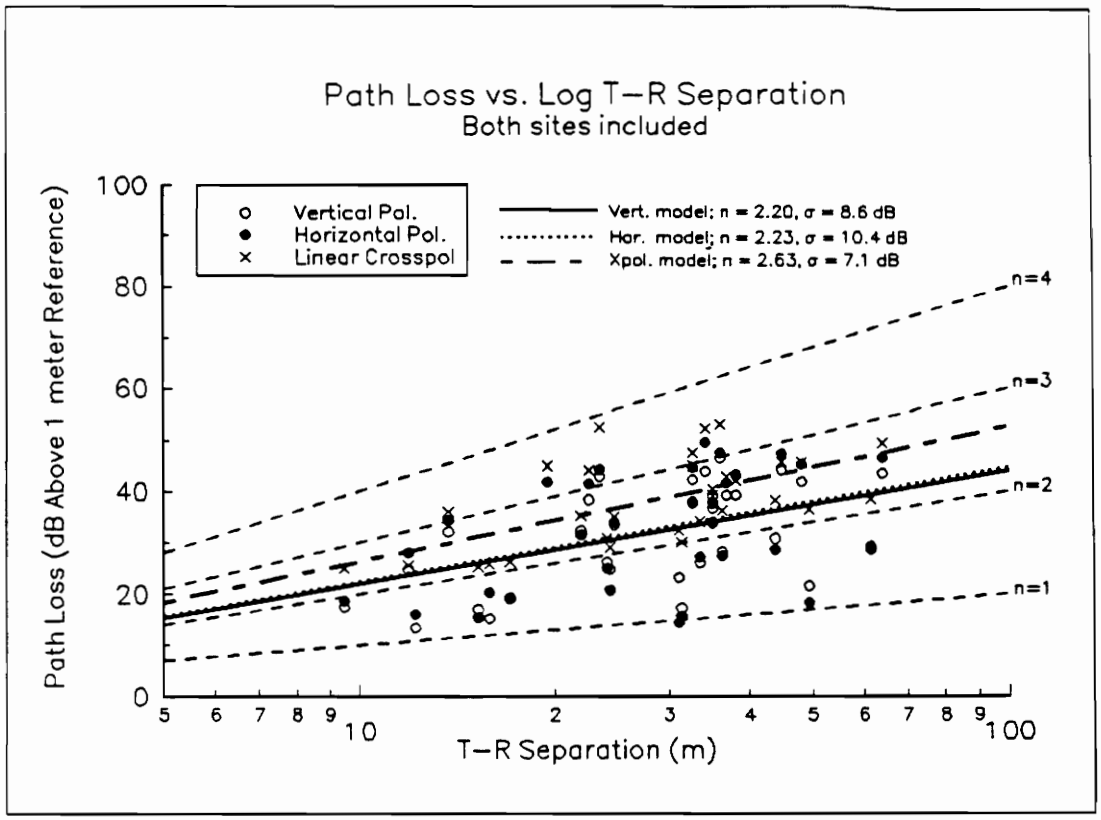

Figure 5.5-1. Scatter plot of path loss for vertical, horizontal, and linear cross-pol measurements, using omni-directional discone antennas at transmitter and receiver. f = 1.3 GHz.

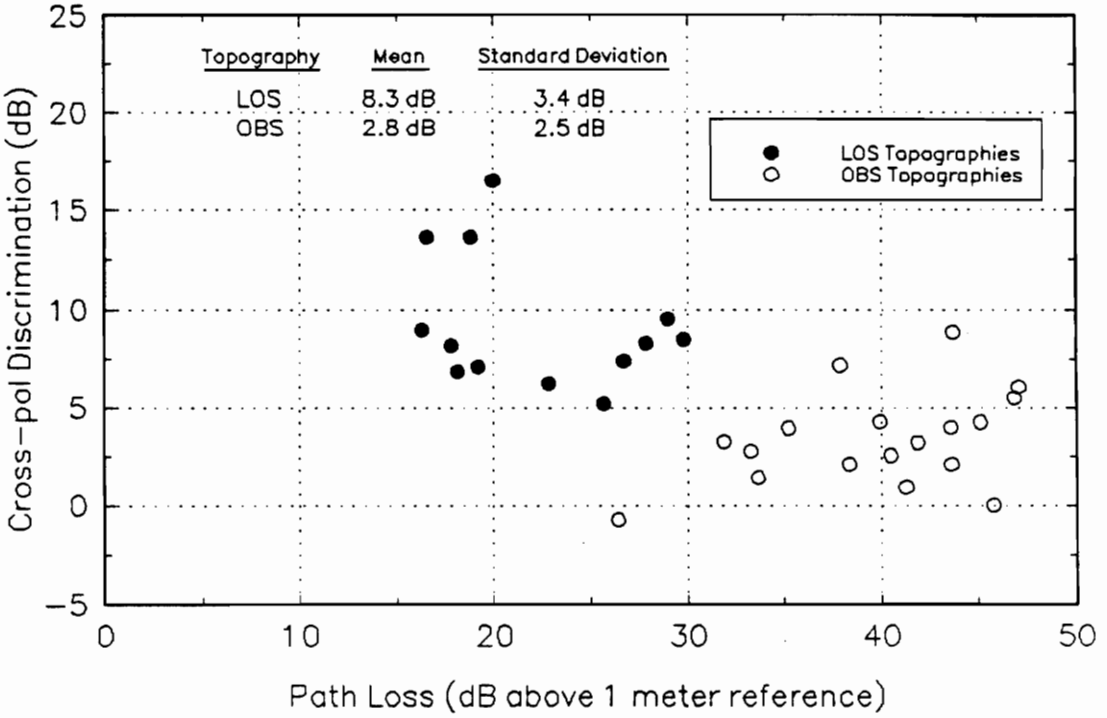

Figure 5.5-2. Cross-pol discrimination using omni-directional discone antennas as a function of co-pol path loss for all polarization measurement locations. Discrimination significantly greater in LOS than OBS environments.

greater than for OBS, as all other LOS discrimination values range between 5 and 10 dB. Measurements recorded down hallways in the closed-plan office building account for these three large discrimination values. In such environments, strong multipath components are due to single-hop reflections from relatively smooth surfaces (walls and floor) – objects which would tend to depolarize the signal less than objects which appear finite in size with rough surfaces.

Cross-pol measurements in two laboratories are reported in [7], in which cross-pol discrimination measurements were conducted at 800 MHz. Mean values of cross-pol discrimination were found to be –0.2 dB for the smaller of two buildings, and –2.2 dB for the larger. That is, measurements in [7] found that signals received using the opposite sense of polarization were stronger than using the same sense. In both buildings we measured, signal strengths were found to be on average, slightly higher using the same sense of linear polarization than in the opposite sense. However, as path loss increases, our data show degradation of cross-pol discrimination. Measurements in [7] used transmitters and receivers on different floors, which lead to obstructed topographies with large path loss values. Our data and [7] suggest that as the multipath channels become more obstructed and path loss increases, cross-pol discrimination becomes lower. Note, however, that in LOS topographies, Figure 5.5-2 shows cross-pol discrimination is much better than reported in [7], which suggests that in LOS channels, CP could offer reductions in delay spread due to the preservation of polarization. This also suggests that CP is effective for decreasing delay spread in LOS channels, which is confirmed experimentally in Table 5.4-1.

Figure 5.5-3 is a scatter plot comparing path loss results for directional CP (On Axis) and omni-directional LP in LOS (a) and OBS (b) topographies. For the directive CP antennas, the on-axis antenna gains have been factored out of the path loss calculations to fairly compare to path loss measurements using omni-directional antennas. Although delay spread values improve, wide band path loss becomes greater using directive CP antennas. For all LOS results, n values are 1.74 and 1.54 for CP and LP data, respectively. This path loss difference is much more significant in OBS topographies, in which n values are 3.50 and 2.70 for CP and LP, respectively. The path loss is more severe for OBS topographies since propagation in these environments is typically via many paths in many directions,

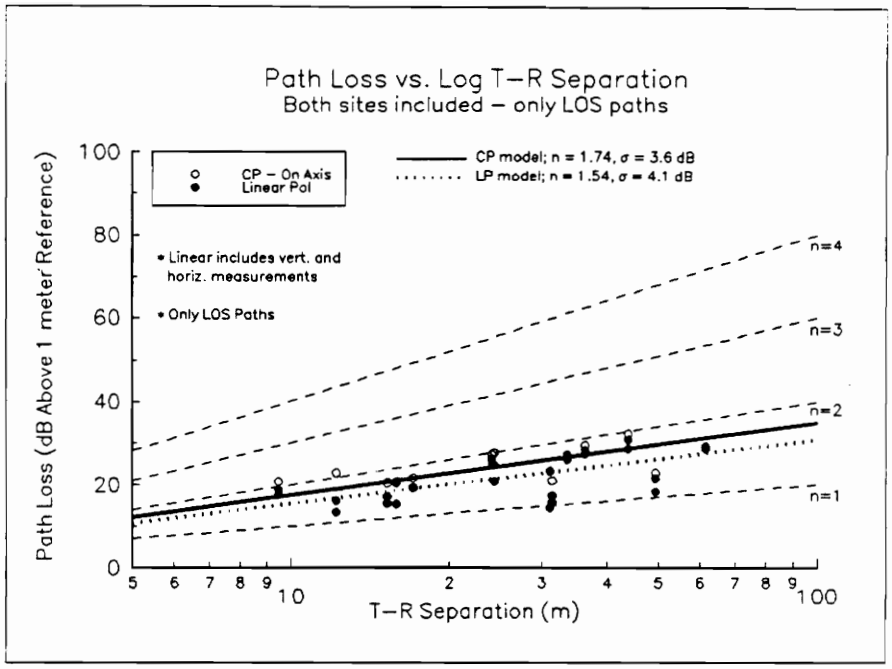

(a) LOS Topography

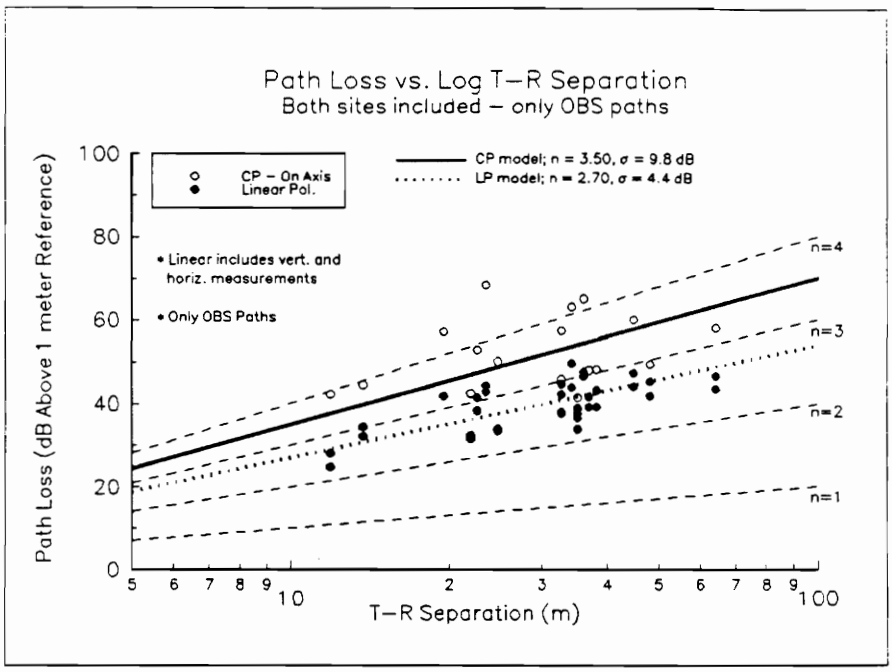

(b) OBS Topography

Figure 5.5-3. Scatter plot of path loss for CP antennas pointed on-axis and omni-directional LP antennas for (a) LOS and (b) OBS topographies. Illustrates higher path loss for CP antennas in OBS topographies. f = 1.3 GHz.

whereas in LOS environments, the power delay profile is typically dominated by the direct LOS component. Thus, when a directive antenna is employed and pointed on-axis, power delay profiles recorded in OBS topographies lack significant components from paths not illuminated by the antenna. This increases the path loss with respect to omni-directional antennas at the same locations.

5.6 Summary

This chapter presented path loss and delay spread results for a second measurement campaign, in which the effects of antenna directivity and polarization were studied. Delay spread results indicated no significant difference between vertical and horizontal polarization using omni-directional antennas. Although not very striking, there was a slight increase ($\sim 15\%$) in delay spread for linear cross-polarized measurements with respect to linear co-polarized measurements, using omni-directional antennas. A significant reduction in delay spread was achieved when CP directional helical antennas were used. This reduction was greatest when the antennas were on-axis, or pointed directly towards the other terminal. However, on average, a less significant reduction was found when the base station antenna was pointed 45° to the right or left of the mobile. A slight reduction also was found when the base station CP antenna is pointed on axis, and the mobile uses the omni-directional linear antenna. This final scenario may well represent a future indoor microcellular system, in which directional antennas are used base stations located in corners of a building, and simple omni-directional monopoles are used on the mobile transceivers. Similar results for wide band measurements taken across a large college campus are reported in [45].

For CP directional antennas, a better delay spread reduction was noticed for LOS measurements versus OBS measurements. A preliminary set of measurements which compared CP directional helical and LP directional log-periodic antennas revealed that most of the reduction is probably due to antenna directivity and a simple channel geometry. At all three LOS locations, a slight delay spread reduction using CP antennas was noticed. However, at the three OBS environments, although there was a delay spread reduction for LP directive over LP omni-directional, there may or may not have been additional reductions

for CP directive, depending on the specific behavior of the channel.

Similar to delay spread, path loss results indicated little difference for vertical and horizontal polarization. The amount of cross-pol discrimination was significantly greater for LOS environments than for OBS environments using omni-directional antennas. Since directive antennas eliminate multipath components which are not illuminated by the antenna, results indicate more path loss for directional antennas than omni-directional antennas, after the on-axis antenna gains are normalized. This is especially true in OBS topographies, in which the power delay profile is not dominated by the LOS component.

6. Site-Specific Propagation Prediction

This chapter introduces ideas and methods in which the wide band propagation data can be used to develop site-specific propagation prediction models. General comments concerning ray-tracing and site-specific propagation are presented, along with a suggested step-by-step approach to implement ray-tracing methods. As a first step to develop site-specific models, measurements from each campaign have been classified into eight categories based on geometric consistencies. For example, all LOS measurements recorded in hallways or corridors are classified independently from LOS measurements recorded in open areas. Path loss and rms delay spread results from these eight classifications are presented.

6.1 Introduction

Propagation results presented in Chapters 4 and 5 can be used to determine the effects of frequency, topography (LOS/OBS), building, and antenna height, gain, and polarization, based on statistical analyses of a large database. However, if reliable indoor systems are to be designed and installed efficiently with out the luxury of measured propagation data, accurate models based on descriptive physical properties of specific locations must be developed. Since the location of the transmitter and receiver were carefully documented on building blueprints during each measurement campaign reported in this thesis, a case-by-case study of recorded impulse response estimates and corresponding blueprint information can be initiated. Thus, the data obtained during the measurement campaigns provides a platform for the development of site-specific models. With such models, the long-term objective of developing a fast, reliable, automated system design tool can be realized.

6.2 Proposed Ray-Tracing Approach

In this section, a step-by-step approach for the development of accurate site-specific models, based on the data, is suggested. This is only one possible approach, and not a proven technique. It is presented to provide a researcher with an example of guidelines to follow for developing site-specific propagation models. The first few steps of this approach force the researcher to thoroughly examine one or two very simple locations initially, rather than attempt to study the entire data set "in parallel".

Step 1.

The first step in developing site-specific models is to classify the measurement locations according to geometric consistencies. A first attempt at this classification has been completed and is described in the next section. The eight geometric categories presented in the following sections will most likely be updated, rearranged, and added to, as insight into site-specific propagation behavior evolves. By continually updating the geometric classifications as better models are developed, forward progress in the overall objective of better site-specific modeling techniques can be made. Specifically, although it should remain the ultimate goal, it is unreasonable to expect, for any mobile and base station location in any building, the impulse response and path loss of a channel to be predicted with 100% accuracy. If ray-tracing algorithms are developed in conjunction with carefully selected geometric classifications, a methodical modeling technique which uses both theoretical modeling using ray-tracing algorithms and statistical modeling based on the geometric classifications may be developed.

Step 2.

After the data has been classified, the next step is to select one location with a simple geometry, and carefully examine the measured impulse responses and blueprints of this location to determine the source of significant multipath components. It is suggested that one of the "final phase" measurements of the polarization campaign be studied first. These measurements were recorded in corridors on the second and third floors of Whittemore Hall (relatively simple

geometries – measurements made in hallways with smooth walls and floor). Impulse response estimates were recorded at $\lambda/4$ intervals as the transmitter traversed a 2.5λ track. Figures 5.4-3 and 5.4-5 were plots of rms delay spread over the 2.5λ distance for the six final phase polarization measurement locations, using LP omni-directional, LP directional on-axis, and CP directional on-axis antenna configurations. These figures indicate that profiles can change considerably over sub-wavelength intervals because of fading due to non-resolvable components. In order to account for this fading, or at least be aware of its existence, the behavior of impulse response estimates over small distances must be taken into account in order to correlate the measured data with physical channel characteristics.

Step 3.

After the sources of significant multipath components have been determined, the next step is to model these sources using theoretical reflection, scattering, and diffraction models. For example, if a multipath component is caused by a wall reflection, the reflection coefficient (from electromagnetic field theory) which results in the approximate measured amplitude could be determined. If the reflection coefficient "model" yields reasonable results, then this model may work well for smooth wall reflections of this type, and should consequently be tested on similar cases. If the results for several cases are unreasonable, then a scattering model, in which a radar cross section for a multipath source is determined, may better model reflections of this type.

Step 4.

Once the behavior of propagation in a few simple locations is understood, the next step is to develop a ray-tracing program which combines the theoretical models (reflection, scattering, and diffraction) and statistical results based on the geometric classifications. The program will combine theoretical models with accumulated statistics to yield a hybrid theoretical/statistical modeling technique. The program should have the flexibility to weight the influences of the theoretical and statistical models. For example, if a measurement location can be classified (with confidence) into a category in which statistical modeling proves to be effective (i.e. low values of σ in the d^n path loss models), then the program should

weight the statistical influences more than the theoretical influences. Conversely, if a measurement location is such that statistical modeling for the geometric category in which this location is placed is ineffective, or if there is not a good match between this measurement topography and those for any geometric classification, then the program should rely more on theoretical modeling. The researcher should apply the ray tracing programs to the simple locations which were studied and recreate the impulse responses and path loss for these locations. Finally, one would need to expand the program to include measurements with more complex topographies. At this time, the knowledge base and the tools should be refined to the point that, with the addition of new locations, the theoretical modeling parameters and the geometrical classifications can be continuously updated.

6.3 Geometric Classification

In this thesis, an attempt to classify the measurement locations according to geometric consistencies has been completed. All measurements from both campaigns have been classified into eight categories. Three of the eight categories are for LOS topographies, and five are for OBS topographies. Table 6.3-1 gives physical descriptions for each classification. As a better understanding of the site-specific propagation behavior evolves, these classifications will be rearranged, and new classifications are likely to evolve.

Path loss and rms delay spread results for these classifications are presented in the next section. The *.rms* and *.pls* files which contain these results are stored in one of 16 subdirectories on a personal computer, eight subdirectories each for *.rms* and *.pls* files for the eight classifications. For example, files which contain rms delay spread results (*.rms* extension) for category #1 are stored in the C:\WIDEBAND\CATGORY1\RMSDELAY\ subdirectory. For each other category, \CATGORY1 is replaced with \CATGORY2, \CATGORY3, etc., and for files which contain path loss results (*.pls* extension), \RMSDELAY is replaced by \PATHLOSS.

6.4 Results from Geometric Classification

Figure 6.4-1 illustrates cumulative distribution functions (CDFs) of rms

Table 6.3-1. Descriptions for each of the eight categories that were developed based on geometric consistencies in measurement locations for each campaign.

CATEGORY 1–LOS:	Hallways and hallway-like environments. Includes measurements between rows of machinery, if the machines extend from floor to ceiling. **EXAMPLE:** All LOS measurements in the corridors of Whittemore Hall.
CATEGORY 2–LOS:	Open areas in which few potential scatterers surround the transmitter and receiver – "light clutter areas". **EXAMPLE:** LOS measurements on the playing surface of Cassell Coliseum.
CATEGORY 3–LOS:	Open areas in which many potential scatterers surround the transmitter and receiver – "heavy clutter areas". **EXAMPLE:** LOS measurements in the large, open-plan factory with much metal machinery and inventory.
CATEGORY 4–OBS:	Hallways and hallway-like environments with the transmitter and receiver obstructed by a single 90° turn in a corridor. **EXAMPLE:** OBS measurements in Whittemore Hall in which the receiver is around a corner with respect to the transmitter.
CATEGORY 5–OBS:	Completely separate areas of the same building, separated by at least one wall. **EXAMPLE:** OBS measurments at Cassell Coliseum in which the transmitter is on the playing surface and the receiver is in the concourse which surrounds the arena.
CATEGORY 6–OBS:	Open areas in which few objects obstruct the transmitter from the receiver – "light obstruction". **EXAMPLE:** OBS measurements at Site C in which the obstruction is one or two machines.
CATEGORY 7–OBS:	Open areas in which many objects obstruct the transmitter from the receiver – "heavy obstruction". **EXAMPLE:** OBS measurements at Site B in which the obstruction is many large, various-shaped machines.
CATEGORY 8–OBS:	Open areas in which the obstruction is a series of one or more rows of inventory, food, etc. which may act as a knife-edge diffractor. **EXAMPLE:** Almost exclusively consists of OBS measurements in the supermarket in which the obstruction is food aisles 2.5 meters high.

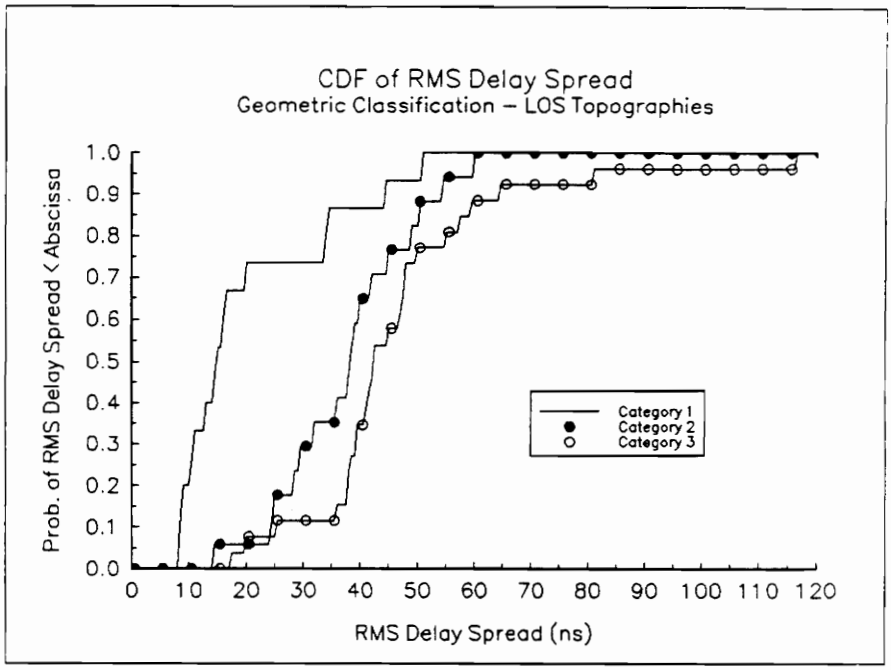

(a) LOS Topographies

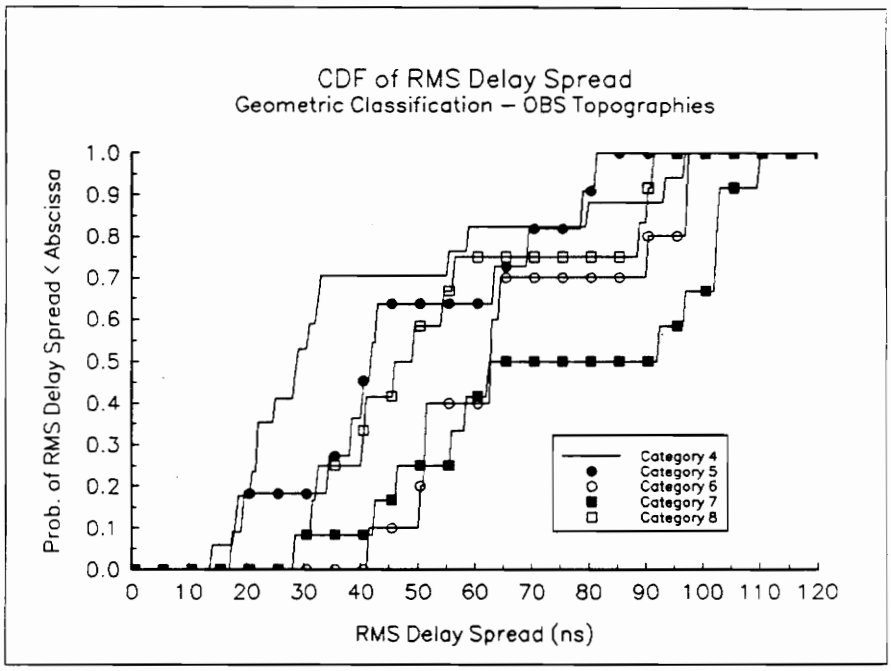

(b) OBS Topographies

Figure 6.4-1. CDFs for geometric classification for (a) LOS and (b) OBS topographies. Categories 1-3 are LOS and Categories 4-8 are OBS.

delay spread using parameter averaging for (a) LOS and (b) OBS categories from the geometric classification. Although the CDFs contain discontinuities due to the insufficient number of data points for certain categories, each plot clearly indicates significant differences among categories within the more general LOS and OBS classifications. For example, in the median rms delay spread values for LOS measurements in hallways (Category 1) is significantly lower than those for LOS measurements in open areas (Categories 2 and 3). For Category 1, the median rms delay spread value is 15 ns, and for Categories 2 and 3, median values are 39 ns and 43 ns, respectively. Although not as significant, median rms delay spread values for LOS measurements in relatively uncluttered open areas (Category 2) are lower than for LOS measurements in cluttered open areas (Category 3). The worst case parameter-averaged value of rms delay spread in LOS environments was 116 ns, found in Category 3. This value was recorded in the large open-plan factory during the first campaign (Site B).

Figure 6.4-1(b) indicates that the lowest median rms delay spread value for OBS topographies is found in hallways (Category 4); the median rms delay spread value for Category 4 is 29 ns. Measurements in this category were recorded with the transmitter and receiver separated by one 90° turn in a corridor. The OBS categories with the highest median rms delay spread values were for measurements in which the transmitter and receiver are in the same large area but obstructed by machinery, inventory, etc (Categories 6 and 7). Category 6 is for lightly-obstructed topographies and Category 7 is for heavily-obstructed topographies. Although the median values for each of these categories are the same (63 ns), the worst case value is higher for Category 7 than for Category 6 – 110 ns and 98 ns, respectively. The worst case OBS delay spread value (110 ns) was recorded at the same Site B measurement location as the worst case LOS value. At this location, the topography became LOS when the base station antenna was raised to 4.0 meters, but was heavily obstructed with the low antenna configuration. Table 6.4-1 summarizes the median and worst case rms delay spread values for the eight classifications.

Table 6.4-2 gives computed values of n and σ for d^n path loss models for the geometric classifications. Path loss results indicate that the overall lowest values found in LOS topographies were for Category 1 (LOS-Hallways). Power

Table 6.4-1. Median and worst case values of rms delay spread for the eight geometric classifications.

	Median value of σ_τ	Maximum value of σ_τ	Number of Locations
CATEGORY 1 - LOS	15	51	15
CATEGORY 2 - LOS	39	60	17
CATEGORY 3 - LOS	43	116	26
CATEGORY 4 - OBS	29	97	17
CATEGORY 5 - OBS	42	82	11
CATEGORY 6 - OBS	63	98	10
CATEGORY 7 - OBS	63	110	12
CATEGORY 8 - OBS	46	92	12

Table 6.4-2. Values of power law exponent n and standard deviation σ about the path loss model for the eight geometric classifications.

	n	σ (dB)	Number of Locations
CATEGORY 1 - LOS	1.55	4.8	15
CATEGORY 2 - LOS	1.76	3.2	17
CATEGORY 3 - LOS	1.92	4.9	26
CATEGORY 4 - OBS	2.58	8.6	17
CATEGORY 5 - OBS	3.11	11.2	11
CATEGORY 6 - OBS	2.18	3.8	10
CATEGORY 7 - OBS	2.42	9.4	12
CATEGORY 8 - OBS	2.35	3.9	12

law exponent values for the three LOS categories are 1.55, 1.76, and 1.92 for Categories 1-3, respectively. The lowest path loss results for OBS categories (n=2.18) were found in topographies in which the transmitter and receiver were in the same area but lightly obstructed by machinery, inventory, etc (Category 6), which is reasonable since measurements in this category are usually only obstructed by one or two objects. Category 5 contains measurements in which the transmitter and receiver are in completely different areas of the building, separated by at least 1 wall. The power law exponent for Category 5 is 3.11, the highest for any category.

For one LOS category and two OBS categories, values of σ are less than 4 dB; for the other two LOS categories, values of σ are less than 5 dB. This indicates that path loss values for measurement locations which clearly fall in one of these 5 categories may be predicted with reasonable accuracy from a pure statistical approach. In a theoretical/statistical site-specific propagation prediction program, the weighting between statistical and theoretical influences would probably favor statistics for measurements which are classified in one of these five categories. Conversely, for three OBS categories, values of σ exceed 8 dB; for Category 5, σ is 11.2 dB. Path loss values for these categories are less predictable since the variations of physical characteristics among measurements within each classification are greater. For example, Category 5 includes measurements made between the playing surface and the concourse at Cassell Coliseum (Chapter 2, Section 2.5 gives a complete physical description of Cassell Coliseum), between the fifth and sixth floors of Whittemore Hall, and between rooms at Site C, separated by one concrete block wall. For such categories, a more careful classification is needed.

6.5 Summary

This chapter introduced site-specific propagation issues. A general outline of one approach which may lead towards the development of site-specific propagation prediction models has been suggested. As a first step, measurements from each campaign have been classified into eight categories according to geometric consistencies. All LOS measurements have been divided into three categories, and all OBS categories have been divided into five categories. Median

and worst case rms delay spread and path loss results for these categories have been presented, and indicate significant difference among the categories within the more general LOS and OBS classifications.

7. System Design Considerations

This chapter presents some important system design issues that can be applied to propagation results to provide system designers with useful tools as future indoor wireless systems evolve. Methods in which propagation models are related to system design parameters such as bit error rate and path loss outage probability are discussed. The intent here is not to delve into the fine details of system design, for this is a completely separate engineering discipline. The purpose is to provide immediate insight into preliminary relationships between propagation results and design parameters, and to provide several key literature references that present more exact, rigorous details of system design considerations. The first section discusses the relationship between rms delay spread (σ_τ) and bit error rate. The second section uses the propagation power law model parameters n and σ and an assumption concerning the mobile user density within the spatial boundaries of a proposed coverage region, to develop approximations of the probability of path loss within the proposed region.

7.1 Outage Due to RMS Delay Spread

RMS delay spread (σ_τ) induces intersymbol interference (ISI) in a digital signal, which consequently causes bit errors. The effect of σ_τ on the bit error rate (BER) of a digital signal depends on the symbol period T. The longer the symbol period, the less likely multipath components will exist at an excess time delay such that they interfere with subsequent symbol transmissions. In order to eliminate T as a variable in determining the relationship between σ_τ and BER, σ_τ is normalized to the symbol period. The normalized rms delay spread is defined as

$$\mathrm{d} = \frac{\sigma_\tau}{\mathrm{T}} \tag{7.1.1}$$

The difference between symbol period T and bit period T_b is a function of the method by which a digital signal is modulated. For simple bilevel modulation techniques such as binary–phase shift keying (BPSK), the symbol rate is equal to the bit rate. For more sophisticated multilevel modulation techniques such as quadrature-phase shift keying (QPSK), offset quadrature-phase shift keying (OQPSK), and minimum shift keying (MSK), the bit period and the symbol period are related by [35]

$$T = nT_b \tag{7.1.2}$$

where n is the number of bits per symbol. We define the rms delay spread normalized to the bit period T_b as

$$d' = \frac{\sigma_\tau}{T_b} \tag{7.1.3}$$

The need for this relationship will become evident when the effects of σ_τ on BER for different types of modulation are presented.

Glance and Greenstein [6] analyzed the effects of frequency selective fading, which is related to σ_τ, on the BER of a signal. Their results are presented as a set of performance curves that reveal the influences of channel parameters such as d (rms delay spread normalized to the symbol period) and the number of modulation levels (2 and 4 level PSK techniques were studied). An important result from their analyses indicate that for $d < 0.25$, the BER becomes mostly a function of the delay spread of the channel, rather than the spectral shape (frequency domain) of the pulse response. The spectral shape is shown to have a profound influence on BER for values of $d > 0.3$. Other studies of frequency selective fading indicate similar results [4,36,37]. This is an important result in that adaptive equalization techniques can be applied to partially combat spectral shape influences on BER. However, the effects of delay spread on BER may induce an irreducible bit error rate, which will impose an upper limit on the data symbol rate.

Chuang, on the basis of the above conclusion, assumed a value of $d \leq 0.2$, and concentrated on the impact that modulation and detection techniques have

on the irreducible bit error rate [38]. To minimize the irreducible BER, Chuang found that coherent detection is more effective than differential detection. For example, for BPSK modulation and d=0.1, the average irreducible BER is approximately 1.5×10^{-3} for coherent detection and approximately 4.0×10^{-3} for differential detection. Only coherent detection schemes were analyzed in detail.

Chuang also quantified a relationship between modulation schemes and the effect of d on irreducible BER. He concludes that the multilevel modulation techniques are superior to the bilevel techniques, and out of the multilevel techniques (QPSK, OQPSK, 4-level MSK), QPSK is most resistant to delay spread. Both OQPSK and 4-level MSK have a timing offset, in which the two bits of a symbol are transmitted individually with a time difference between them equal to half the symbol period (T/2). This induces interference between the bits of a symbol, which effectively raises the average irreducible BER. This offset is not present in QPSK, which causes this type of modulation to be the most resistant to delay spread. In order to compare effects of the multilevel modulation methods to the bilevel methods, it is more fair to study the irreducible bit error rate as a function of σ_τ normalized to the bit period, or d′ as defined in (7.1.3).

A method of differential detection of BPSK and QPSK was studied, in which an intermediate frequency (IF) hard limiter was placed in the receiver prior to detection [39]. For this detection scheme and $d \leq 0.2$, bit error rates on the order of 5×10^{-4} can be achieved for both BPSK and QPSK. However, for $d > 0.2$, the BER degrades rapidly for both techniques. In [39], all bit error rate results are presented as a function of τ/T, where τ is the time difference between the rays of a proposed two ray model. A two ray model assumes there are only two multipath components in the channel: a direct LOS path and a reflected path which has a certain signal level relative to the direct path. For worst case analysis, the signal level of the delayed ray is usually assumed equal to the direct ray. Thus, the value of σ_τ for this two ray model is equal to half the time difference between rays, or $\tau/2$. Therefore, a value of 0.4 for τ/T in [39] corresponds to a value of 0.2 for d.

In summary, it seems that this hard-limiting/differential detection scheme may be most suitable for system performance in multipath environments, and that adaptive equalization techniques can be avoided if d is less than about 0.2.

As an example, a system transmits 2 Mb/sec and uses differential QPSK (DQPSK) modulation with an IF hard-limiting stage for detection. For this system, recall that the irreducible BER is approximately 5×10^{-4} for d less than 0.2, which corresponds to σ_τ less than 200 ns. Propagation results indicate that rms delay spread values greater than 200 ns were observed less than 0.5% of the time. However, when σ_τ becomes greater than 200 ns (d>0.2), then the BER quickly degrades to as high as about 0.05 at d=0.25. Thus, the "critical" value of σ_τ, above which the BER begins to rapidly degrade is about 200 ns for the system. For larger values of σ_τ, an equalizer or antenna polarization diversity would be needed to maintain the BER of 5×10^{-4}. If the bit rate of the system is lowered to 1 Mb/sec, then this "critical" rms delay spread increases to about 400 ns. Values of rms delay spread greater than 230 ns were not observed at any measurement location.

7.2 Outage Due to Path Loss

This section utilizes the path loss model parameters n and σ and some basic assumptions concerning the mobile user density within a proposed coverage region, to develop approximations of the probability of path loss for any point in the region. The coverage region used for calculations in this section is a circular region with the base station at the center of the circle. A minimum radius (T-R separation) of 1 meter and a maximum radius of 100 meters is assumed. The technique to determine this probability of path loss is described, and results are presented as distribution curves from which the probability of path loss which exceeds a given value can be immediately determined. From these curves and a knowledge of system parameters such as transmitter power, receiver noise and interference levels, and signal-to-interference (SIR) threshold level, the probability of outage within a given coverage region can be determined. The term "outage" means that the path loss exceeds a specified level, and communication is lost over that particular channel. An example in which these parameters are proposed and the probability of outage computed is presented.

Technique

Based on the assumption that path loss over a region is well described over

a region by a log-normal distribution about a mean power law path loss model, the probability of path loss as a function of T-R separation and model parameters can be found. The purpose of this section is to discuss a method in which a user distribution is assumed, and condition of T-R separation (denoted as the radius r for the circular region) is eliminated, which yields the probability of path loss as a function of model parameters only. The probability density function (pdf) of path loss conditioned on propagation model parameters n and σ and radius r is denoted as f[L|n,σ,r]. From the equation of the well-known normal density function [40,41], we obtain

$$f[L|n,\sigma,r] = \frac{1}{\sqrt{2\pi}\sigma} e^{-\frac{1}{2}\left[\frac{L-\overline{L}(n,r)}{\sigma}\right]^2} \tag{7.2.1}$$

Where, $\overline{L}(n,r) = 10n \log_{10}(r)$ is the d^n model used to fit the path loss data for various classifications discussed in previous chapters, and L represents measured path loss in dBr_{1m}. In order to determine the pdf for path loss conditioned solely on model parameters, denoted f(L|n,σ), we make use of the total probability theorem [40]

$$f(L|n,\sigma) = \int_{r_{MIN}}^{r_{MAX}} f[L|n,\sigma,r]\, f(r)\, dr \tag{7.2.2}$$

Where f(r) is the pdf of users over a circular coverage region with radius r. The limits of integration r_{MIN} and r_{MAX} are the radial limits of the proposed circular region.

In order to determine f(r), we assume that all users within the coverage region are distributed uniformly in **area** over the region. This certainly differs from the assumption that the probability of a user at any one **radius** is the same as at any other radius, which is not a valid assumption in a real system. For example, the probability of a user located between 60 and 70 meters from the base

station is higher than the probability of a user located between 10 and 20 meters since the coverage area in the former range is higher than than in the latter range. Using the theory of functions of one random variable, which is completely described in [40], we arrive at the following equation for f(r) based on a circular coverage region with a uniform density of users

$$f(r) = \frac{2r}{r_{MAX}^2} \tag{7.2.3}$$

Substituting (7.2.1) and (7.2.3) into (7.2.2), we obtain a closed-form expression for the pdf of path loss conditioned solely on model parameters

$$f(L|n,\sigma) = \int_{r_{MIN}}^{r_{MAX}} \frac{1}{\sqrt{2\pi}\sigma} e^{-\frac{1}{2}\left[\frac{L\text{-}10n\log_{10}(r)}{\sigma}\right]^2} \frac{2r}{r_{MAX}^2} dr \tag{7.2.4}$$

A computer program was written to integrate the above equation numerically for a range of path loss values between 0 dBr_{1m} and 110 dBr_{1m}, and thus compute $f(L|n,\sigma)$, from which the cumulative conditional distribution $F(L|n,\sigma)$ can be determined. The program applies the trapezoidal rule for numerical integration [42]. The program name is ***outage.pas***; a listing can be found in Appendix B.

Results

Figure 7.2-1 represents the probability of path loss (in dBr_{1m}) based on n and σ of Figure 4.5-1. Figure 7.2-1 indicates that the path loss values which correspond to 0.1% outage are approximately 63.5 dBr_{1m} for 1.3 GHz and 4.0 GHz open-plan measurements. The path loss values which correspond to 1.0% outage are 56.4 dBr_{1m} and 57.2 dBr_{1m} for 1.3 GHz and 4.0 GHz respectively. Table 7.2-1 lists the 10%, 1%, and 0.1% probabilities that path loss exceeds the table value for all classifications from Table 4.5-1, as well as from the 8 site-specific categories introduced in Chapter 6. For example, Table 7.2-1 indicates that a system which in an open-plan location with a 1.7 meter base station antenna height at 1.3 GHz will experience a path loss greater than 63.1 dBr_{1m} 0.1% of the time and a path

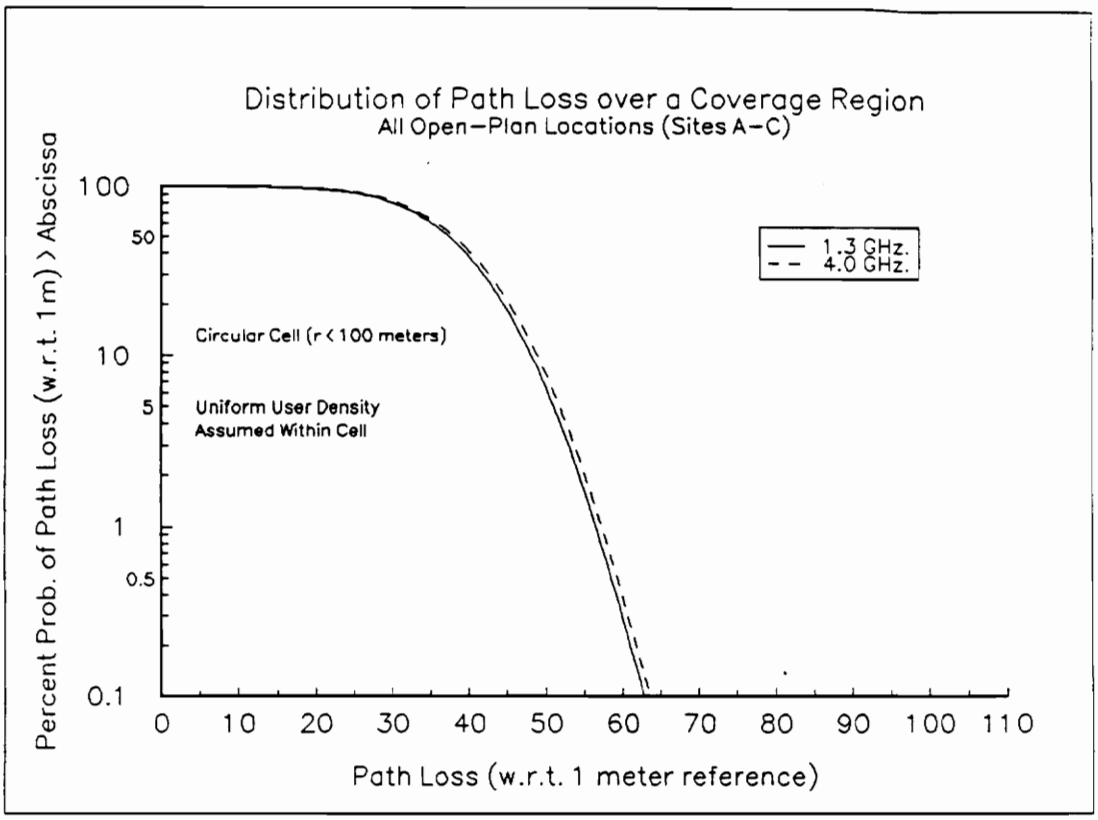

Figure 7.2-1. Distribution of path loss for a proposed circular cell (r<100m) at all open-plan sites as a function of frequency.

Table 7.2-1. Tabulation of likelihood that path loss (in dBr_{1m}) is exceeded for 10%, 1%, and 0.1% of the users in a circular cell.

	1.3 GHz			4.0 GHz		
	10 %	1.0 %	0.1 %	10 %	1.0 %	0.1 %
All Open-Plan Sites	48.0	56.4	63.3	48.7	57.2	63.5
Low (1.7m) Antenna	48.7	56.6	63.1	50.1	59.5	66.8
High (4.0m) Antenna	48.7	56.6	63.1	47.6	54.8	60.4
LOS Topography	40.2	45.7	49.8	40.1	45.5	49.5
OBS Topography	53.2	62.0	68.6	54.1	62.0	68.0
Site A	46.8	55.5	61.9	52.1	62.4	70.0
Site B	41.6	45.7	48.7	44.0	48.7	52.0
Site C	55.0	65.0	72.8	51.7	61.6	69.9
Site D	80.9	96.3	108.5	70.0	88.5	105.7
Category 1 - LOS	34.5	39.9	43.9			
Category 2 - LOS	36.8	40.5	43.1			
Category 3 - LOS	41.7	47.3	51.3			
Category 4 - OBS	58.4	68.0	75.2			
Category 5 - OBS	71.5	83.4	93.4			
Category 6 - OBS	45.5	50.0	53.2			
Category 7 - OBS	56.4	66.5	74.6			
Category 8 - OBS	48.8	53.5	56.8			

Path Loss > Table Value x % of the time
Path Loss in dB above 1 meter reference.

loss greater than 48.7 dBr_{1m} 10% of the time.

Figure 7.2-2 illustrates the curves for two classifications from Table 7.2-1 – 1.3 GHz measurements at Site C, and Category 8 measurements from Chapter 6. Although the computed values of n are 2.35 for both classifications, the standard deviation is significantly less (σ = 3.9 dB) for Category 8 than for 1.3 GHz at Site C (σ = 9.2 db). Consequently, the 0.1% probability point is 72.8 dBr_{1m} for Site C and only 56.8 dBr_{1m} for Category 8, a 16 dB difference. This example clearly illustrates the importance of achieving a low standard deviation when using a d^n model, and thus the importance of prudent data classification based on site-specific geometrical consistencies.

The following is an example in which base station transmitter power, receiver interference level, and the signal-to-interference (SIR) threshold level of a system are proposed, and the probability of outage is determined from a path loss distribution curve. The general open-plan building distribution (Figure 7.2-1) is used for this example, although the technique can easily be applied to any distribution represented by the points in Table 7.2-1. An effective isotropic radiated power at the base station of +7 dBm (5 milliwatts) at 1.3 GHz is proposed. A 3 dB gain receiving antenna is used. A noise floor of −100 dBm @ 20 MHz baseband bandwidth, and a co-channel interference level of −90 dBm is estimated. Thus the total receiver noise and interference level is approximately −90 dBm, with nearly the entire contribution due to co-channel interference. A relationship between path loss (in dBr_{1m}) and signal-to-interference ratio (SIR) can be found and is given by the following equation

$$SIR\ (dB) = P_{EIRP\ @\ 1m}\ (dBm) - P_{LOSS}\ (dBr_{1m}) - P_I\ (dBm) + G_R \quad (7.2.5)$$

Where,

SIR (dB) = Signal-to-Interference Ratio

$P_{EIRP\ @\ 1m}$ (dBm) = Effective Radiated Power referred to 1 meter (−24.7 dBm)

P_I (dBm) = Interference Level at receiver (−90 dBm)

G_R = Receiver Antenna Gain

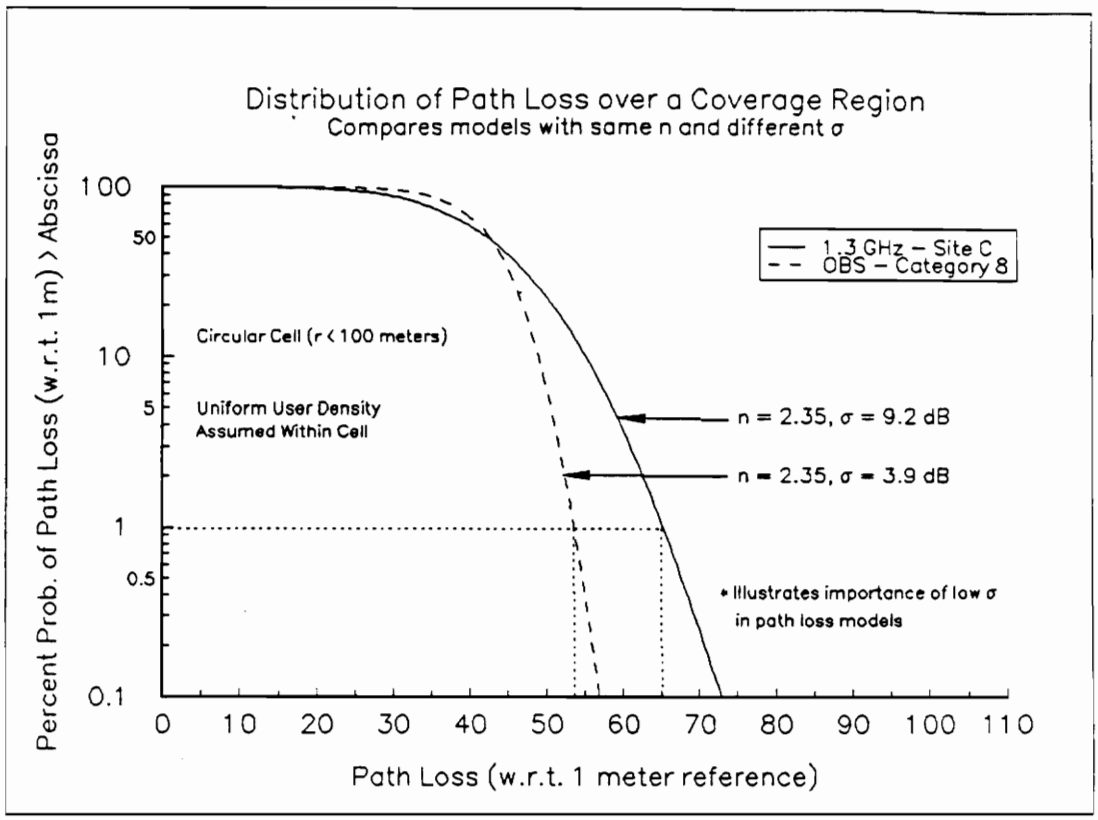

Figure 7.2-2. Distribution of path loss for a proposed circular cell. Compares models with the same n and different σ. Illustrates the importance of low values of σ in d^n path loss models.

Making the appropriate substitutions, we find

$$\text{SIR (dB)} = 65.3 - P_{\text{LOSS}}\,(\text{dBr}_{1\text{m}}) \qquad (7.2.6)$$

An SIR threshold of +10 dB to determine the probably of outage is proposed. Any link with an SIR less than +10 dB will experience outage. Figure 7.2-3 is the distribution function for SIR corresponding to the 1.3 GHz path loss distribution of Figure 7.2-1, using equation (7.2.6). The probability of outage is less than 2% based on the proposed system parameters. Several changes in the system can be made in order to reduce this outage. If the transmitter power is increased by 5 dB, the probability of outage is reduced to less than 0.3%. Also, the coverage region has an impact on the probability of outage. If a circular region with a 75 meter radius rather than a 100 meter radius is assumed, the probability of outage is decreased by approximately a factor of 2, from about 1.3% to about 0.6%. To determine this, the integral of equation (7.2.4) is evaluated over the range from r_{MIN} of 1 meter to r_{MAX} of 75 meters, and a new path loss distribution function is determined, from which the SIR function is determined from equation (7.2.6).

7.3 Summary

In this chapter, the important issue of transforming propagation parameters such as rms delay spread and path loss into meaningful system design parameters such as bit error rate and probability of outage was addressed.

In the first section, the effects of rms delay spread on bit error rate for a digital signal were examined. It has been reported that for a normalized rms delay spread (d) less than about 0.25, the delay spread may induce an irreducible bit error rate, which will impose an upper limit on the data symbol rate. For values of d greater than 0.25, the spectral shape of the pulse response has a profound effect on bit error rate, and adaptive equalization techniques to combat this effect will be needed. The effects of detection and modulation on the bit error rate for $d < 0.2$ were briefly discussed. In [38], it was determined that multilevel modulation techniques for coherent detection were more desirable than

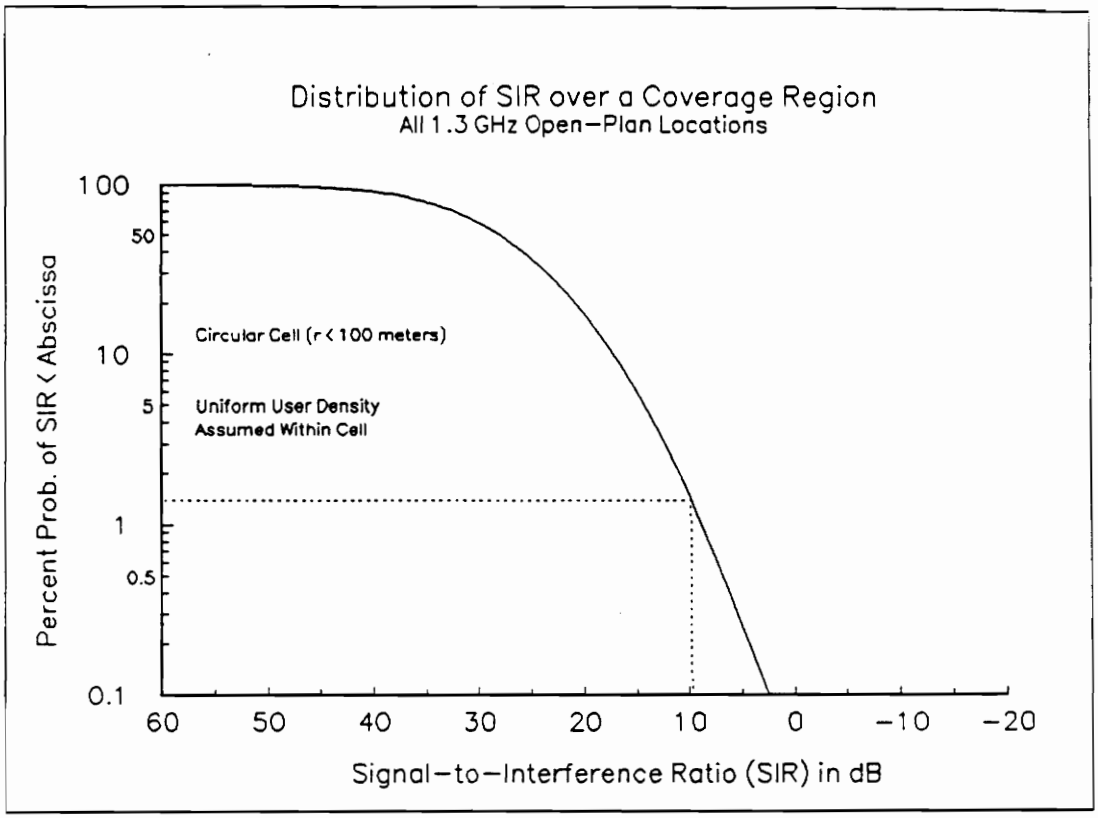

Figure 7.2-3. Distribution function of Signal-to-Interference ratio which corresponds to the proposed system applied to the 1.3 GHz distribution of Figure 7.2-1.

differential detection, and out of the multilevel techniques, QPSK modulation was most resistant to delay spread. However, it was shown in [39] that a differential detection scheme in which a hard limiter is placed in the IF stage of the receiver prior to PSK modulation yields lower bit error rates (5×10^{-4} for d<0.2) than the best results from [38].

In the second section, the path loss model parameters n and σ were used to develop approximations of the probability of path loss over a coverage region. A uniform user density within a proposed circular coverage region with a maximum radius of 100 meters was assumed, and probabilities of path loss which correspond to computed models were presented. From the probability of path loss and reasonable assumptions for system parameters such as transmitter power and receiver noise and interference levels, path loss probabilities can be converted into probabilities of signal-to-interference ratios (SIR). An example using proposed values of system parameters was given, and a distribution curve for SIR derived from this example was presented.

8 Conclusions

In general, no significant differences exist between rms delay spread at 1.3 GHz and 4.0 GHz. As a result, no distinct advantage in terms of improving the bit error rate of a digital signal is gained from using one frequency over the other. Similarly, antenna height does not significantly affect rms delay spread. Only at a few locations where the base station was raised to 4 meters, and a LOS path clearly became visible, did a significant decrease in rms delay spread occur.

However, rms delay spread is a strong function of topography (LOS/OBS) and building. Values of rms delay spread exceed 75 ns about 10% of the time in LOS topographies, but nearly 40% of the time in OBS topographies. Worst case rms delay spread values for individual profiles were found to be about 90 ns for the closed-plan office building and about 230 ns for open-plan topographies. Median values ranged from as low as 20 ns for the closed-plan office building to about 70 ns for the open-plan factory with many reflective obstructions. The median value for all individual profiles is about 45 ns.

The significant results concerning the impact of frequency, antenna height, topography, and building on rms delay spread are similar to the same results for all other time dispersion parameters. Worst case and mean values of mean excess delay for all individual profiles are about 230 ns and 35 ns, respectively. Worst case values for maximum excess delay with an amplitude within 10 dB of the maximum signal of a power delay profile are about 900 ns for the open-plan environments and about 440 ns for the closed-plan office building. Worst case time delay jitter and differential delay jitter are approximately 180 ns and 190 ns respectively. All time dispersion parameters are slightly less random at 1.3 GHz than at 4.0 GHz, and the randomness is much less for the closed-plan office building than for open-plan factories. However, more data are needed in closed-plan office buildings before a definitive conclusion can be drawn.

Path loss values have been determined and quantified by computing the best fit d^n models for data of various classifications and tabulating the values for the power law exponent n and for the standard deviation (σ, in dB) about the d^n model. Results for the **entire data set** indicate little relationship between frequency and path loss. Computed values of n are 2.09 and 2.13 for all 1.3 GHz and 4.0 GHz data, respectively. A more thorough examination of the data indicate that one frequency may, on average, encounter slightly less path loss than the other, depending on the building. For the large open-plan areas, 1.3 GHz experienced less path loss than 4.0 GHz. However, for topographies such as those in the closed-plan office building and the confined areas of Site C, in which successful data transmission from one terminal to the other depends on propagation through small corridors and around corners, 4.0 GHz seems to be more desirable. For example, values of n for Site B are 1.97 and 2.09 for 1.3 GHz and 4.0 GHz, respectively, and values of n for Site D are 3.43 and 2.77 for 1.3 GHz and 4.0 GHz, respectively. This also indicates a very significant increase in path loss from the open-plan topography at Site B to the closed-plan topography at Site D. The amount of path loss variation (quantified by σ) was also lowest for Site B; where values of σ are 3.7 dB and 4.0 dB for 1.3 GHz and 4.0 GHz, respectively. This compares to values of 7.6 dB for all 1.3 GHz and 4.0 GHz results. In general, values of σ are slightly higher for 4.0 GHz than for 1.3 GHz, indicating slightly less randomness of path loss at the lower frequency.

A second measurement campaign was initiated, in which the effects of antenna directivity and polarization on rms delay spread and path loss were studied. Delay spread results indicate no significant difference between vertical and horizontal polarization using omni-directional antennas. A significant reduction in rms delay spread was achieved when CP directional helical antennas were used. This reduction was greatest when the antennas were on-axis, or pointed directly towards the other terminal. A less significant reduction was found when the base station antenna was pointed 45° to the right or left of the mobile.

For CP directional antennas, a better rms delay spread reduction was noticed for LOS measurements versus OBS measurements. A preliminary set of measurements which compared CP directional helical and LP directional log-

periodic antennas revealed that most of the reduction is probably due to antenna directivity. Although, a slight reduction using CP was noticed at all 3 LOS locations, and CP was found to greatly reduce the variation of rms delay spread over sub-wavelength intervals for all LOS locations and certain OBS locations. Linear cross-pol discrimination was greater for LOS environments than for OBS environments, which may account for this delay spread reduction using CP, since single-hop CP reflections will be more cross-polarized in environments with more cross-pol discrimination.

Similar to delay spread, path loss results indicated little difference for vertical and horizontal polarization. Since directive antennas eliminate multipath components which are not illuminated by the antenna, results indicate more path loss for directional antennas than omni-directional antennas. This is especially true in OBS topographies, in which the power delay profile is not dominated by the direct LOS component.

The more predictable path loss behavior at Site B indicates the importance of carefully classifying data into categories based on geometric consistencies. All Site B measurements were taken in one open-plan area with the same large-scale geometrical properties. In Chapter 6, all 1.3 GHz data recorded during both campaigns were classified into eight categories, based on consistent physical properties. From this second classification, values of σ were found to be as low as 3.2 dB, and less than 5 dB for five of the eight categories.

Chapter 7 first discussed the relationship between rms delay spread and bit error rate (BER). It was determined for example, that if a normalized rms delay spread value of 0.2 is assumed for a 2 Mb/s bit rate DQPSK signal, then the maximum tolerable value for rms delay spread is about 200 ns for an unequalized channel. Recall that the normalized rms delay spread is simply the computed rms delay spread divided by the symbol rate of the digital signal. Values of rms delay spread greater than 200 ns were observed only in very rare cases (less than 0.5%). It was shown that for normalized rms delay spread values above 0.2, adaptive equalization may be necessary to prohibit a significant and unacceptable increase in BER [6]. This indicates that for the 2 Mb/s proposed system, adaptive equalization is necessary only about 0.1% of the time.

A statistical operation was used to compute the probability density function (pdf) of users with respect to the separation of the mobile and the base station within a proposed coverage region. This pdf combined with the d^n power law models computed from the path loss results provide the information necessary to calculate the probability of path loss for any point in a proposed region. Resultant distribution functions then can be applied to a particular system, in which the transmitter power, receiver noise floor, antenna gains and signal-to-interference threshold are known parameters, to determine the probability of outage for a given coverage region. It is this probability of outage that is most useful to mobile communication system designers. An example using this technique is presented in Chapter 7.

The results and conclusions obtained from this comprehensive study of indoor radio wave propagation gives insight into the design and installation limitations of indoor mobile wireless communication systems. A statistical knowledge of the effects of frequency, topography, antenna height, and building characteristics on propagation have been obtained from the results and can be used as a tool for system design for future mobile systems. Further, the data collected in this work may be used to develop better site-specific channel models which may someday permit fast, accurate, automated wireless system design.

References

[1] D.C. Cox, "Universal portable radio communications," *IEEE Trans. Veh. Technol.*, vol. VT-34, no. 3, pp. 117-121, Aug. 1985.

[2] T.S. Rappaport, "Indoor radio communications for factories of the future," *IEEE Commun. Mag.*, vol. 27, no. 5, pp. 15-24, May 1989.

[3] D.M.J. Devasirvatham, "Multipath time delay spread in the digital portable radio environment," *IEEE Commun. Mag.*, vol. 25, no. 6, pp. 13-21, June 1987.

[4] P.A. Bello and B.D. Nelin, "The effects of frequency selective fading on the binary error probabilities of incoherent and differentially coherent matched filter receivers," *IEEE Trans. Commun. Syst.*, vol. CS-11, pp. 170-186, June 1963.

[5] W. Jakes, Jr., *Microwave Mobile Communications*, Wiley-Interscience, 1974.

[6] B. Glance and L.J. Greenstein, "Frequency-selective fading effects in digital mobile radio with diversity combining," *IEEE Trans. Commun.*, vol. COM-31, no. 9, pp. 1085-1094, September 1983.

[7] D.C. Cox, *et. al.*, "Cross polarization coupling measured for 800 MHz radio transmission in and around houses and large buildings," *IEEE Trans. Ant. Prop.*, vol. AP-34, no. 1, pp. 83-87, Jan. 1986.

[8] D.C. Cox, R.R. Murray, and A.W. Norris, "800 MHz attenuation measured in and around suburban houses," *AT&T Tech. J.*, vol. 63, no. 6, pp. 921-954, July 1984.

[9] D.C. Cox, R.R. Murray, and A.W. Norris, "Measurements of 800 MHz radio transmission into buildings with metallic walls," *BST J.*, vol. 62, no. 9, pp. 2695-2717, Nov. 1983.

[10] H.H. Hoffman and D.C. Cox, "Attenuation of 900 MHz radio waves propagating into a metal building," *IEEE Trans. Ant. Prop.,* vol. AP-30, no. 4, pp. 808-811, July 1982.

[11] T.S. Rappaport and C.D. McGillem, "UHF fading in factories," *IEEE J. Select. Areas Commun.*, vol. SAC-7, no. 1, pp. 40-48, Feb. 1989.

[12] S.E. Alexander, "Radio propagation within buildings at 900 MHz," *Electron. Lett.*, vol. 19, no. 20, p. 860, Sept. 1983.

[13] R.J.C. Bultitude, "Measurement, characterization and modeling of indoor 800/900 MHz radio channels for digital communications," *IEEE Commun. Mag.*, vol. 25, no. 6, pp. 5-12, June 1987.

[14] J. Horikoshi, *et. al.*, "1.2 GHz band wave propagation measurements in concrete building for indoor radio communications," *IEEE Trans. Veh. Technol.*, vol. VT-35, no. 4, pp. 146-152, Nov. 1986.

[15] P. Karlsson, "Investigation of radio propagation and macroscopic diversity in indoor microcells at 1700 MHz" *in Proc. of 40th IEEE Veh. Technol. Conf.*, pp. 390-395, Orlando, FL, May 1990.

[16] D.M.J. Devasirvatham, "Time delay spread and signal level measurement of 850 MHz radio waves in building environments," *IEEE Trans. Ant Prop.*, vol. AP-34, no. 11, pp. 1300-1305, Nov. 1986.

[17] D.M.J. Devasirvatham, "A comparison of time delay spread measurements within two dissimilar office buildings," *Proc. of 1986 Intnl. Conf. on Communications*, vol. 2, June 1986.

[18] D.M.J. Devasirvatham, "Multipath time delay spread in the digital portable radio environment," *IEEE Commun. Mag.,* vol. 25, no. 6, pp. 13-21, June 1987.

[19] D.M.J. Devasirvatham, *et. al.,* "Radio propagation measurements at 850 MHz, 1.7 GHz, and 4.0 GHz inside two dissimilar office buildings", *Electron. Lett.*, vol. 26, no. 7, pp. 445-447, March 1990.

[20] R.J.C. Bultitude, *et. al.*, "A comparison of indoor radio propagation characteristics at 910 MHz and 1.75 GHz," *IEEE J. Select. Areas Commun.*, vol. 7, no. 1, pp. 20-30, Jan. 1989.

[21] A.A.M. Saleh and R.A. Valenzuela, "A statistical model for indoor multipath propagation," *IEEE J. Select. Areas Commun.*, vol. SAC-5, no. 2, pp. 128-137, Feb. 1987.

[22] T. Takeuchi, *et. al.*, "Multipath delay estimation for indoor wireless communication" *in Proc. of 40th IEEE Veh. Technol. Conf.*, pp. 401-406, Orlando, FL, May 1990.

[23] T.S. Rappaport, "Characterization of UHF multipath radio channels in factory buildings," *IEEE Trans. Ant. Prop.*, vol. 37, no. 8, pp. 1058-1069, Aug. 1989.

[24] K. Pahlavan, *et. al.*, "Multipath propagation measurements on manufacturing floors at 910 MHz", *Electron. Lett.*, vol. 25, no. 3, pp. 225-227, Feb. 1989.

[25] L. Ailes, *et. al.*, "Development of an autonomous guided vehicle for indoor propagation measurements" *in Proc. of 40th IEEE Veh. Technol. Conf.*, pp. 119-123, Orlando, FL, May 1990.

[26] M. I. Skolnik, *Introduction to Radar Systems*, Second Edition, McGraw-Hill, 1980.

[27] T.S. Rappaport, "Wide-band test antennas," *RF Design*, pp. 37-41, April 1988.

[28] E.N. Skomal, *Man-Made Radio Noise*, Van Nostrand Reinhold Company, 1978.

[29] H.L. Krauss, C.W. Bostian, and F.H. Raab, *Solid State Radio Engineering,* John Wiley & Sons, 1980.

[30] S.Y. Seidel, "UHF Indoor Radio Channel Models for Manufacturing Environments," *Masters Thesis*, Virginia Polytechnic Institute and State University, August 1989.

[31] D.M.J. Devasirvatham, "Multipath time delay jitter measured at 850 MHz in the portable radio environment," *IEEE J. Select. Areas Commun.*, vol. SAC-5, no. 5, pp. 855-861, June 1987.

[32] T.S. Rappaport, "Delay spread and time delay jitter for the UHF factory multipath channel," *in Proc. of 38th IEEE Veh. Technol. Conf.*, pp. 186-189, Philadelphia, PA, June 1988.

[33] W.J. Dixon and F.J. Massey, Jr., *Introduction to Statistical Analysis*, Fourth Edition, McGraw-Hill, 1983.

[34] J.S. Engel, "Effects of multipath transmission on the measured propagation delay of an FM signal," *IEEE Trans. Veh. Technol.*, vol. VT-18, pp. 44-52, May 1969.

[35] L.W. Couch II, *Digital and Analog Communication Systems*, Third Edition, Macmillan, 1990.

[36] S. Ariyavisitakul *et al.*, "Fractional-bit differential detection of MSK: A scheme to avoid outages due to frequency-selective fading," *IEEE Trans. Veh. Technol.*, vol. VT-36, no. 1, pp. 36-42, Feb. 1987.

[37] S. Yoshida and F. Ikegami, "A comparison of multipath distortion characteristics among digital modulation techniques," *IEEE Trans. Veh. Technol.*, vol VT-34, no. 3, p. 128, Aug. 1985.

[38] J. C-I Chuang, "The effects of time delay spread on portable radio communications channels with digital modulation," *IEEE J. Select. Areas Commun.*, vol. SAC-5, no. 5, pp. 879-889, June 1987.

[39] S. Ariyavisitakul, *et. al.*, "An improvement effect by a hard-limiter on differential detection performance of PSK in frequency-selective fading," IEEE Trans. Veh. Technol., vol. VT-36, no. 4, pp. 193-200, Nov. 1987.

[40] A. Papoulis, *Probability, Random Variables, and Stochastic Process*, McGraw-Hill, 1984.

[41] J.S. Milton and J.C. Arnold, *Probability and Statistics in the Engineering and Computing Sciences*, McGraw-Hill, 1986.

[42] K. Atkinson, *Elementary Numerical Analysis*, John Wiley & Sons, 1985.

[43] T.S. Rappaport and D.A. Hawbaker, "Indoor radio propagation measurements and modeling at 1.3 GHz and 4.0 GHz in four dissimilar buildings, *MPRG–TR–90–5 Technical Report,* Bradley Department of Electrical Engineering, Virginia Tech, Blacksburg, VA. Prepared for AICOMM, Inc., Raleigh, NC., August 15, 1990.

[44] H.P. Neff, Jr., *Basic Electromagnetic Fields,* Second Edition, Harper & Row, 1987.

[45] T.S. Rappaport and B. Tuch, "The effects of antenna gain and polarization on multipath delay spread and path loss at 918 MHz across a large college campus," 1991 IEEE Globecom Proceedings, Phoenix, AZ, December 4, 1991.

Appendix A. Impulse Responses from Polarization Campaign

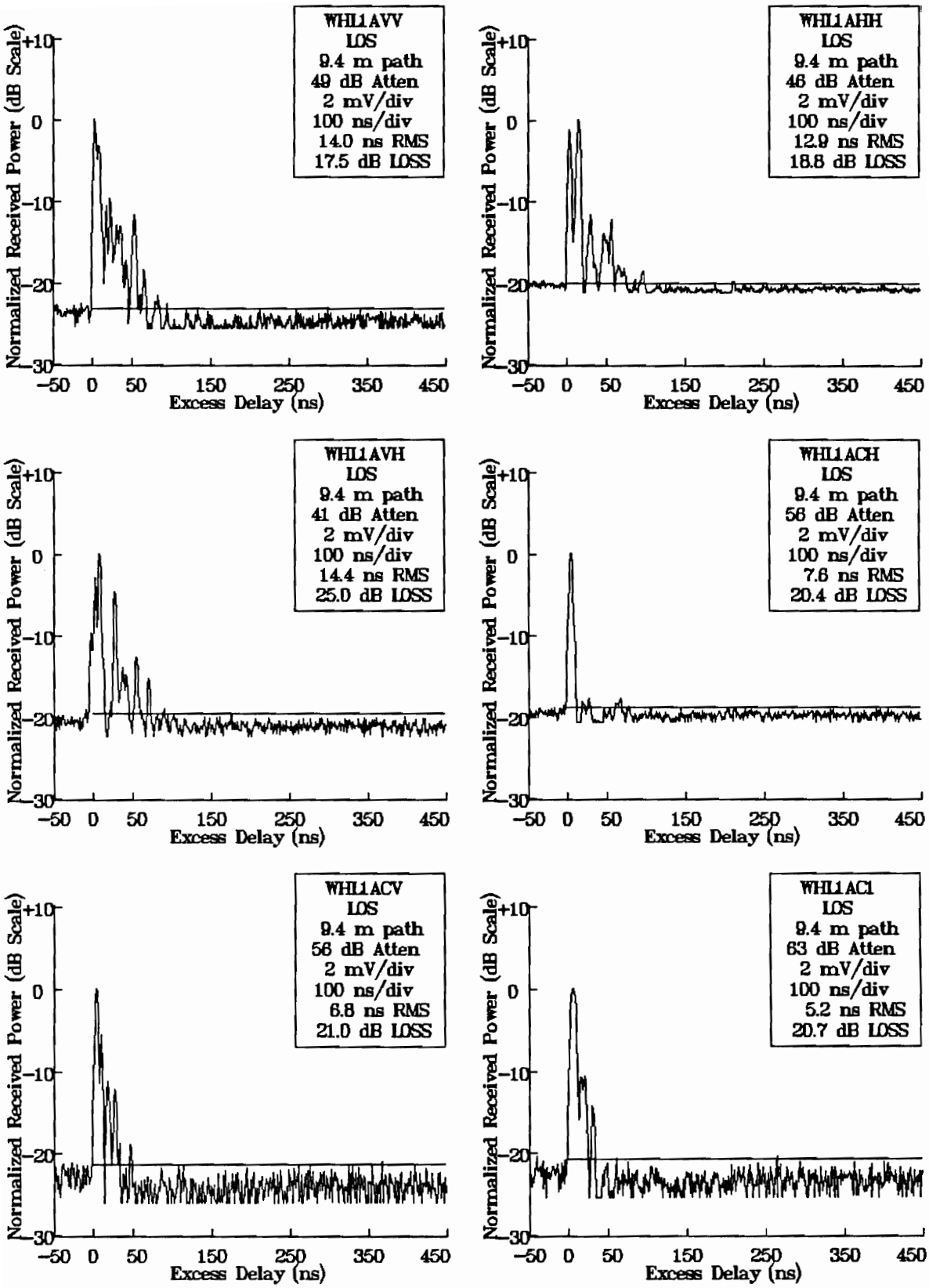
WHL1AVV
LOS
9.4 m path
49 dB Atten
2 mV/div
100 ns/div
14.0 ns RMS
17.5 dB LOSS
WHL1AHH
LOS
9.4 m path
46 dB Atten
2 mV/div
100 ns/div
12.9 ns RMS
18.8 dB LOSS
WHL1AVH
LOS
9.4 m path
41 dB Atten
2 mV/div
100 ns/div
14.4 ns RMS
25.0 dB LOSS
WHL1ACH
LOS
9.4 m path
56 dB Atten
2 mV/div
100 ns/div
7.6 ns RMS
20.4 dB LOSS
WHL1ACV
LOS
9.4 m path
56 dB Atten
2 mV/div
100 ns/div
6.8 ns RMS
21.0 dB LOSS
WHL1AC1
LOS
9.4 m path
63 dB Atten
2 mV/div
100 ns/div
5.2 ns RMS
20.7 dB LOSS
Normalized Received Power (dB Scale)
+10
0
-10
-20
-30
-50 0 50 150 250 350 450
Excess Delay (ns)

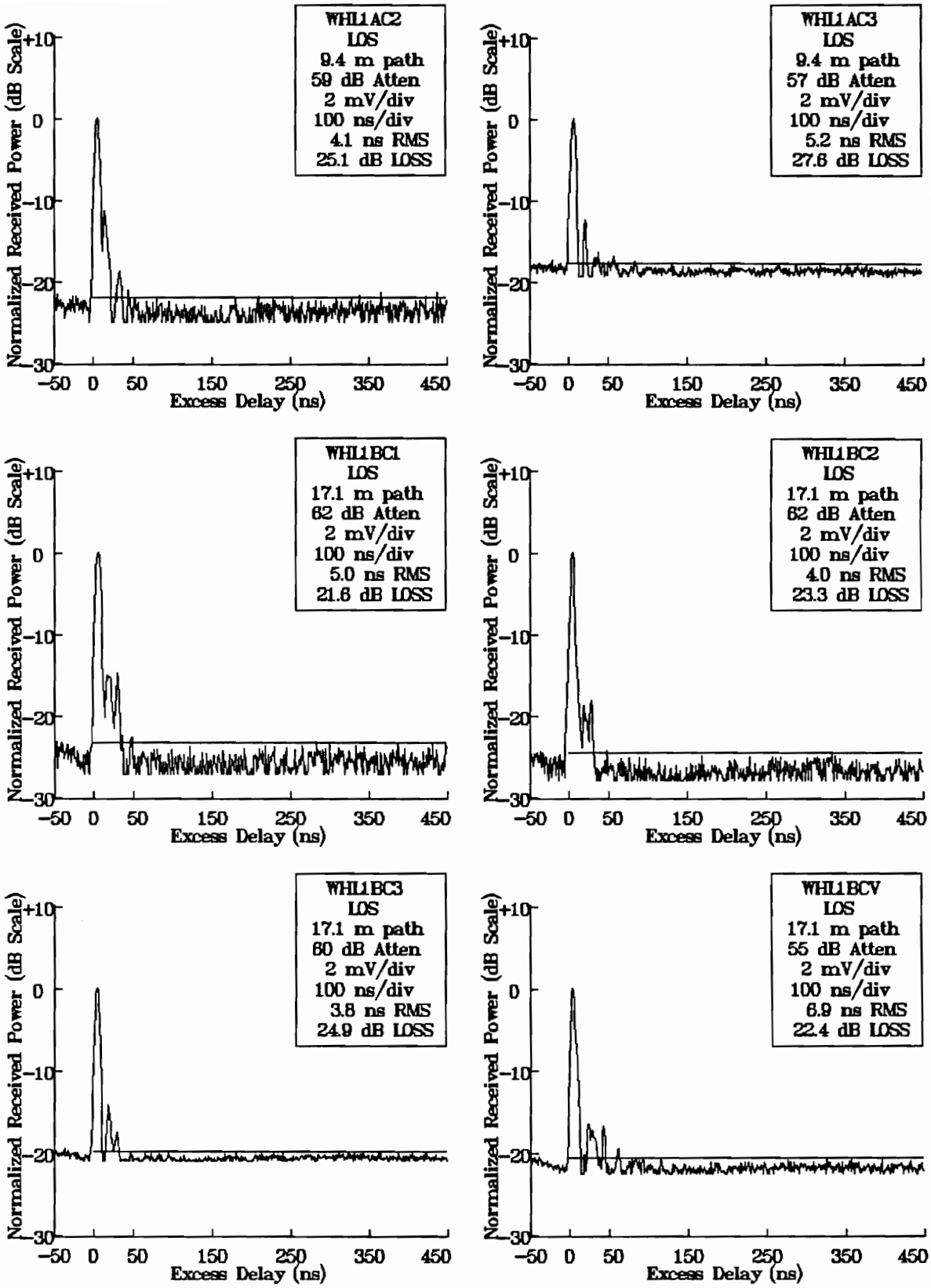
WHL1AC2
LOS
9.4 m path
59 dB Atten
2 mV/div
100 ns/div
4.1 ns RMS
25.1 dB LOSS
WHL1AC3
LOS
9.4 m path
57 dB Atten
2 mV/div
100 ns/div
5.2 ns RMS
27.6 dB LOSS
WHL1BC1
LOS
17.1 m path
62 dB Atten
2 mV/div
100 ns/div
5.0 ns RMS
21.6 dB LOSS
WHL1BC2
LOS
17.1 m path
62 dB Atten
2 mV/div
100 ns/div
4.0 ns RMS
23.3 dB LOSS
WHL1BC3
LOS
17.1 m path
60 dB Atten
2 mV/div
100 ns/div
3.8 ns RMS
24.9 dB LOSS
WHL1BCV
LOS
17.1 m path
55 dB Atten
2 mV/div
100 ns/div
6.9 ns RMS
22.4 dB LOSS
Normalized Received Power (dB Scale)
+10
0
-10
-20
-30
-50 0 50 150 250 350 450
Excess Delay (ns)

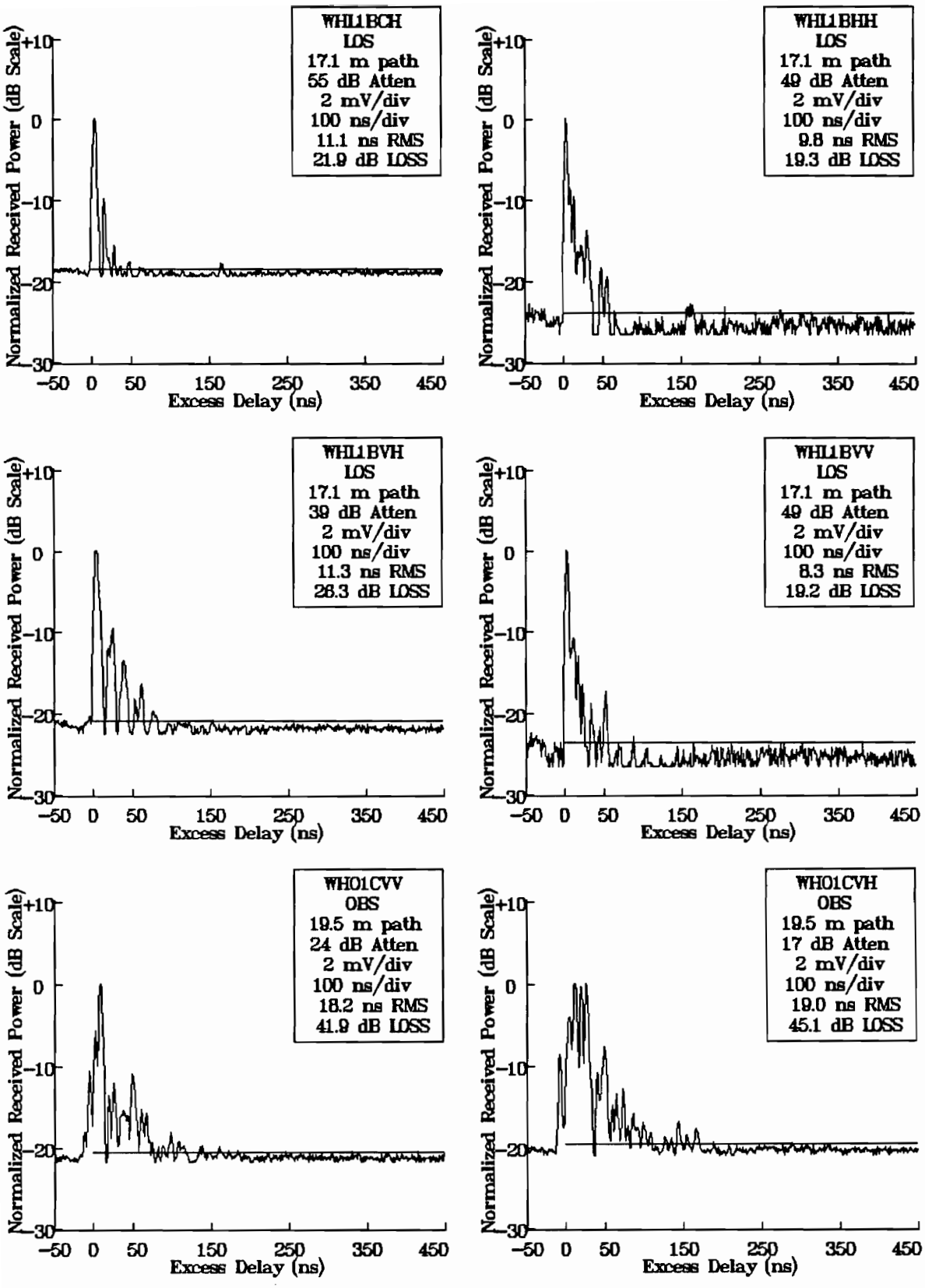
WHL1BCH
LOS
17.1 m path
55 dB Atten
2 mV/div
100 ns/div
11.1 ns RMS
21.9 dB LOSS
WHL1BHH
LOS
17.1 m path
49 dB Atten
2 mV/div
100 ns/div
9.8 ns RMS
19.3 dB LOSS
WHL1BVH
LOS
17.1 m path
39 dB Atten
2 mV/div
100 ns/div
11.3 ns RMS
26.3 dB LOSS
WHL1BVV
LOS
17.1 m path
49 dB Atten
2 mV/div
100 ns/div
8.3 ns RMS
19.2 dB LOSS
WHO1CVV
OBS
19.5 m path
24 dB Atten
2 mV/div
100 ns/div
18.2 ns RMS
41.9 dB LOSS
WHO1CVH
OBS
19.5 m path
17 dB Atten
2 mV/div
100 ns/div
19.0 ns RMS
45.1 dB LOSS
Normalized Received Power (dB Scale)
+10
0
-10
-20
-30
-50 0 50 150 250 350 450
Excess Delay (ns)

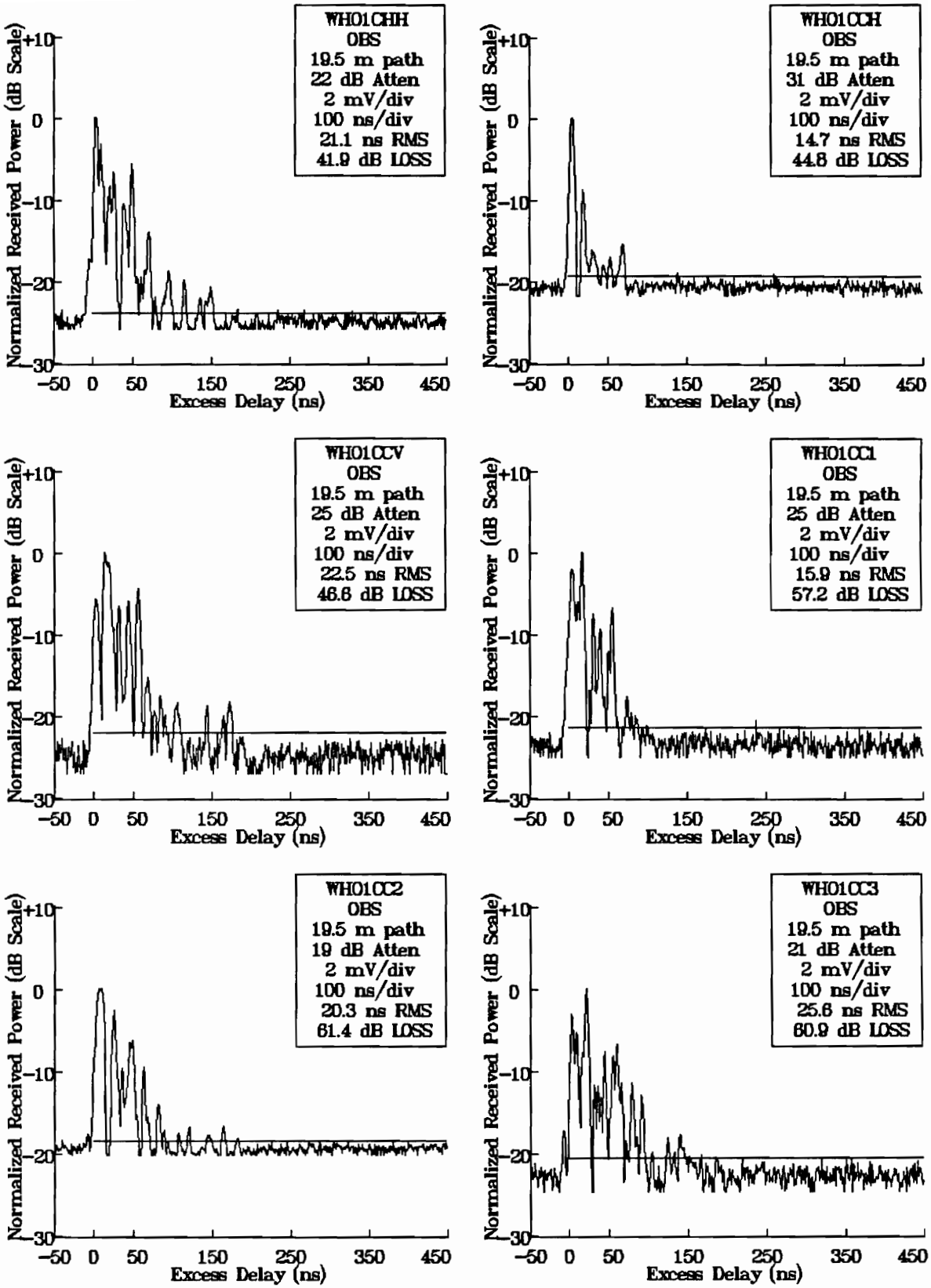
WH01CHH
OBS
19.5 m path
22 dB Atten
2 mV/div
100 ns/div
21.1 ns RMS
41.9 dB LOSS
WH01CCH
OBS
19.5 m path
31 dB Atten
2 mV/div
100 ns/div
14.7 ns RMS
44.8 dB LOSS
WH01CCV
OBS
19.5 m path
25 dB Atten
2 mV/div
100 ns/div
22.5 ns RMS
46.6 dB LOSS
WH01CC1
OBS
19.5 m path
25 dB Atten
2 mV/div
100 ns/div
15.9 ns RMS
57.2 dB LOSS
WH01CC2
OBS
19.5 m path
19 dB Atten
2 mV/div
100 ns/div
20.3 ns RMS
61.4 dB LOSS
WH01CC3
OBS
19.5 m path
21 dB Atten
2 mV/div
100 ns/div
25.6 ns RMS
60.9 dB LOSS
Normalized Received Power (dB Scale)
+10
0
-10
-20
-30
-50 0 50 150 250 350 450
Excess Delay (ns)

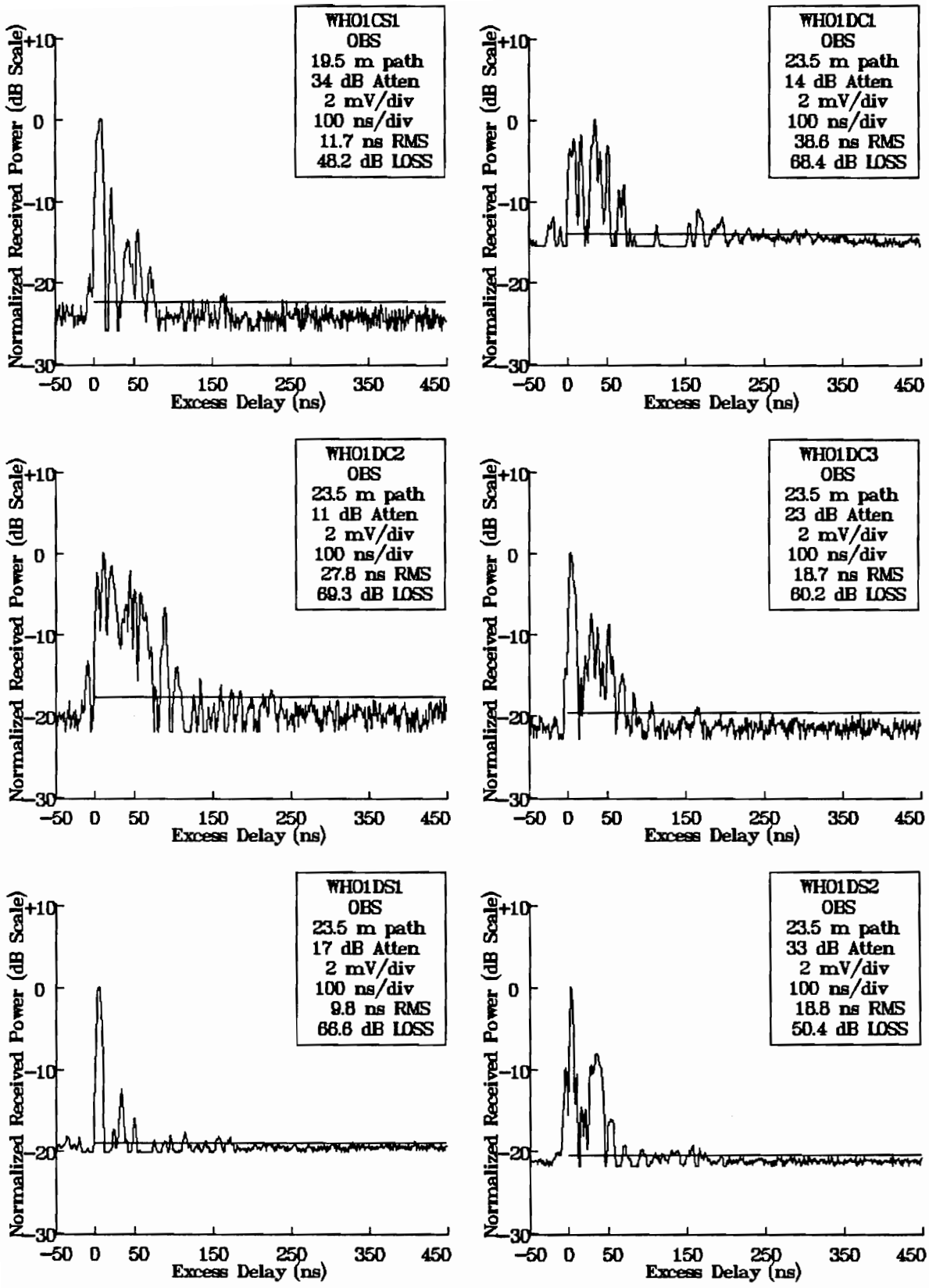
WH01CS1
OBS
19.5 m path
34 dB Atten
2 mV/div
100 ns/div
11.7 ns RMS
48.2 dB LOSS
WH01DC1
OBS
23.5 m path
14 dB Atten
2 mV/div
100 ns/div
38.6 ns RMS
68.4 dB LOSS
WH01DC2
OBS
23.5 m path
11 dB Atten
2 mV/div
100 ns/div
27.8 ns RMS
69.3 dB LOSS
WH01DC3
OBS
23.5 m path
23 dB Atten
2 mV/div
100 ns/div
18.7 ns RMS
60.2 dB LOSS
WH01DS1
OBS
23.5 m path
17 dB Atten
2 mV/div
100 ns/div
9.8 ns RMS
66.6 dB LOSS
WH01DS2
OBS
23.5 m path
33 dB Atten
2 mV/div
100 ns/div
18.8 ns RMS
50.4 dB LOSS
Normalized Received Power (dB Scale)
+10
0
-10
-20
-30
-50 0 50 150 250 350 450
Excess Delay (ns)

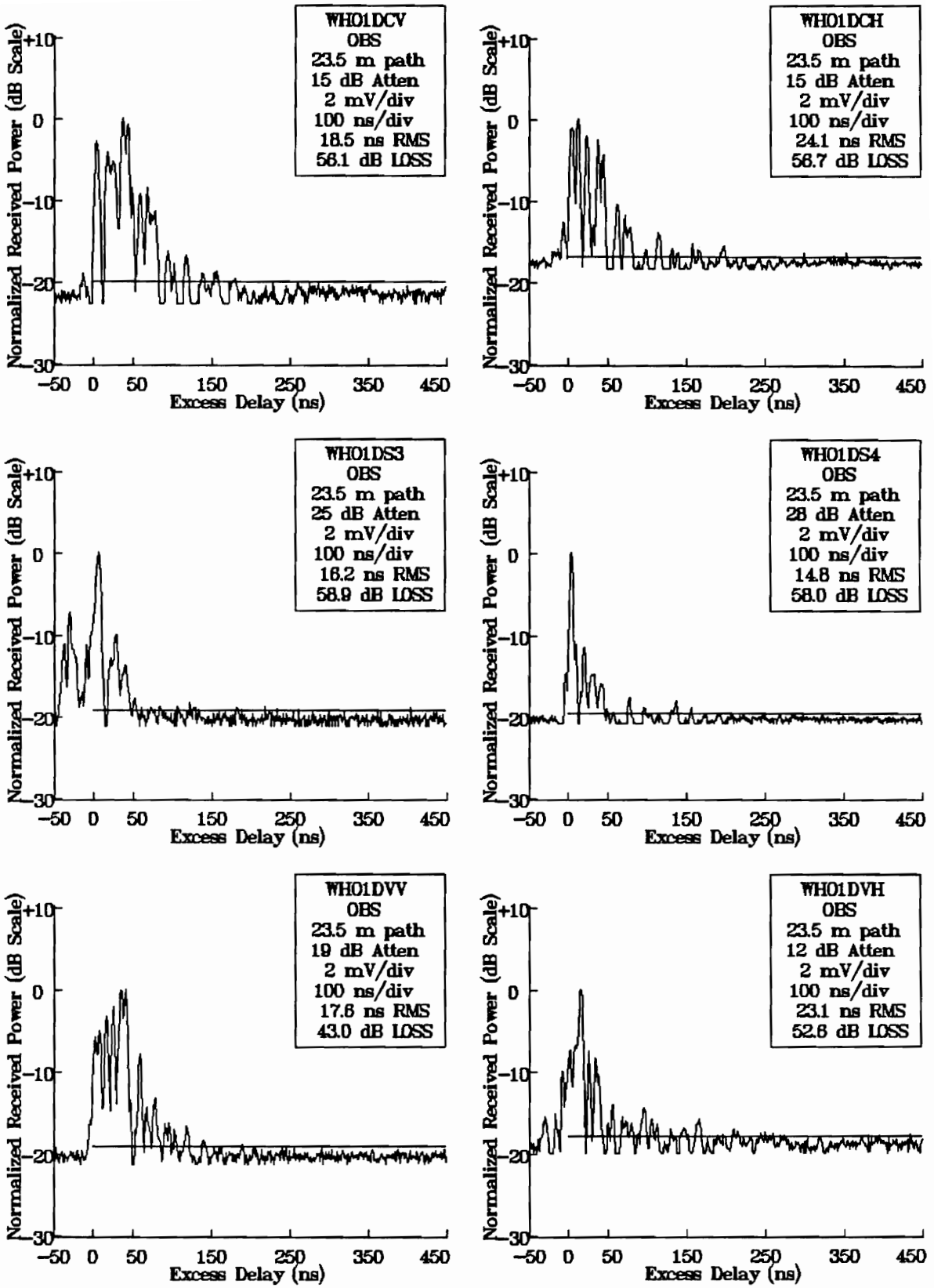
WHO1DCV
OBS
23.5 m path
15 dB Atten
2 mV/div
100 ns/div
18.5 ns RMS
56.1 dB LOSS
WHO1DCH
OBS
23.5 m path
15 dB Atten
2 mV/div
100 ns/div
24.1 ns RMS
56.7 dB LOSS
WHO1DS3
OBS
23.5 m path
25 dB Atten
2 mV/div
100 ns/div
16.2 ns RMS
58.9 dB LOSS
WHO1DS4
OBS
23.5 m path
28 dB Atten
2 mV/div
100 ns/div
14.8 ns RMS
58.0 dB LOSS
WHO1DVV
OBS
23.5 m path
19 dB Atten
2 mV/div
100 ns/div
17.6 ns RMS
43.0 dB LOSS
WHO1DVH
OBS
23.5 m path
12 dB Atten
2 mV/div
100 ns/div
23.1 ns RMS
52.6 dB LOSS
Normalized Received Power (dB Scale)
+10
0
-10
-20
-30
-50 0 50 150 250 350 450
Excess Delay (ns)

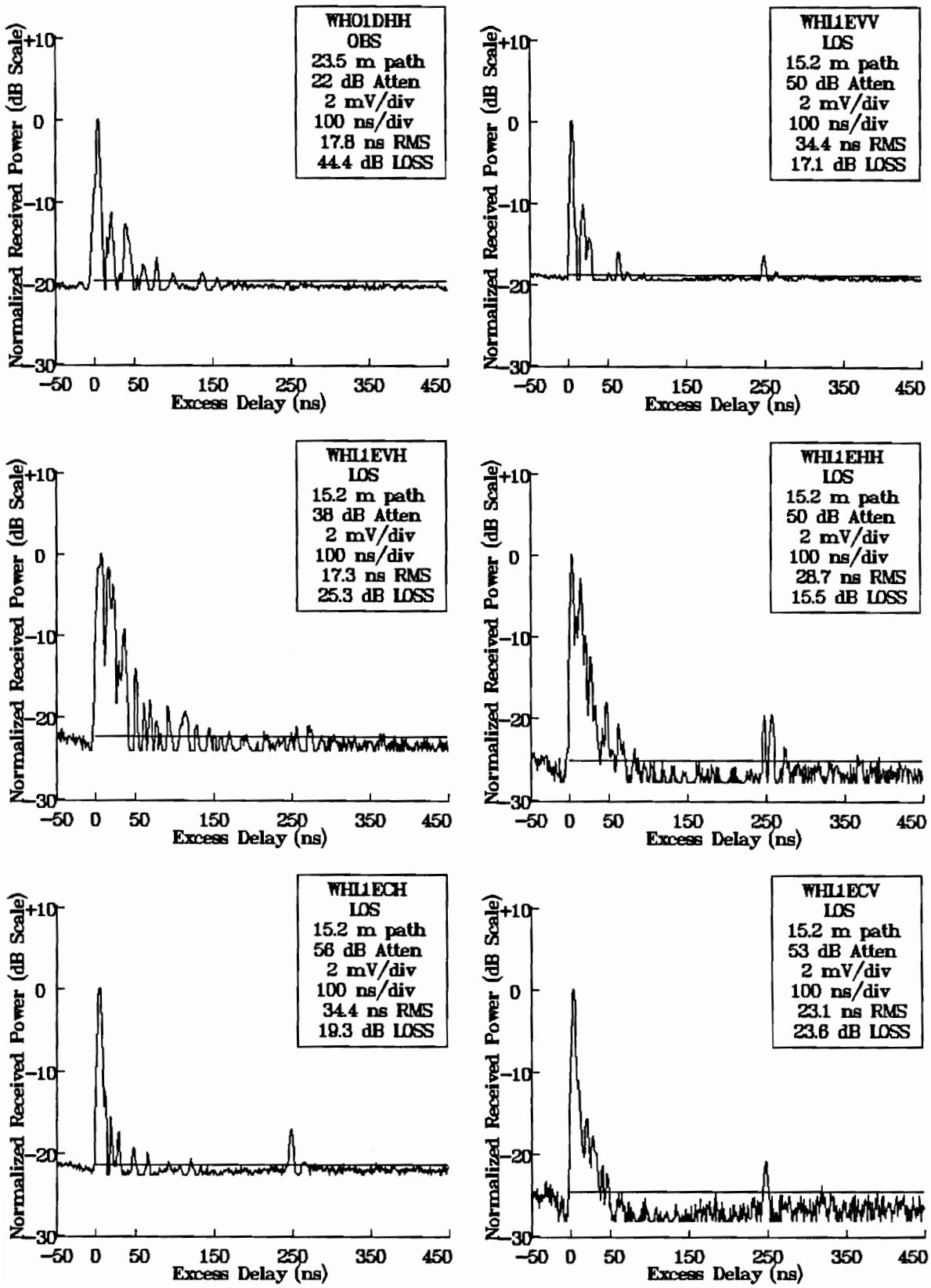
WH01DHH
OBS
23.5 m path
22 dB Atten
2 mV/div
100 ns/div
17.8 ns RMS
44.4 dB LOSS
WHL1EVV
LOS
15.2 m path
50 dB Atten
2 mV/div
100 ns/div
34.4 ns RMS
17.1 dB LOSS
WHL1EVH
LOS
15.2 m path
38 dB Atten
2 mV/div
100 ns/div
17.3 ns RMS
25.3 dB LOSS
WHL1EHH
LOS
15.2 m path
50 dB Atten
2 mV/div
100 ns/div
28.7 ns RMS
15.5 dB LOSS
WHL1ECH
LOS
15.2 m path
56 dB Atten
2 mV/div
100 ns/div
34.4 ns RMS
19.3 dB LOSS
WHL1ECV
LOS
15.2 m path
53 dB Atten
2 mV/div
100 ns/div
23.1 ns RMS
23.6 dB LOSS
Normalized Received Power (dB Scale)
+10
0
-10
-20
-30
-50 0 50 150 250 350 450
Excess Delay (ns)

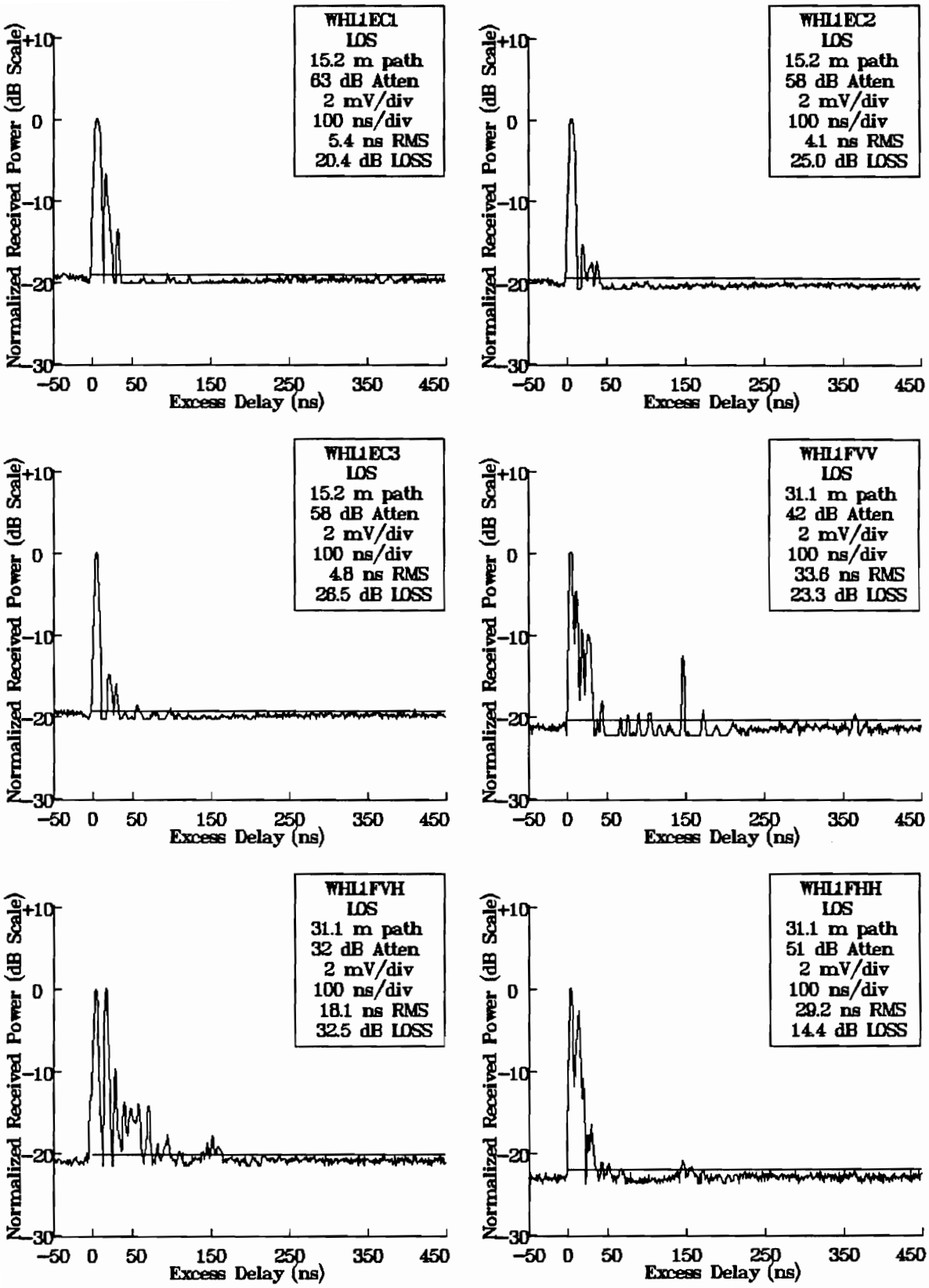
WHL1EC1
LOS
15.2 m path
63 dB Atten
2 mV/div
100 ns/div
5.4 ns RMS
20.4 dB LOSS
WHL1EC2
LOS
15.2 m path
58 dB Atten
2 mV/div
100 ns/div
4.1 ns RMS
25.0 dB LOSS
WHL1EC3
LOS
15.2 m path
58 dB Atten
2 mV/div
100 ns/div
4.8 ns RMS
26.5 dB LOSS
WHL1FVV
LOS
31.1 m path
42 dB Atten
2 mV/div
100 ns/div
33.6 ns RMS
23.3 dB LOSS
WHL1FVH
LOS
31.1 m path
32 dB Atten
2 mV/div
100 ns/div
18.1 ns RMS
32.5 dB LOSS
WHL1FHH
LOS
31.1 m path
51 dB Atten
2 mV/div
100 ns/div
29.2 ns RMS
14.4 dB LOSS
Normalized Received Power (dB Scale)
+10
0
-10
-20
-30
-50 0 50 150 250 350 450
Excess Delay (ns)

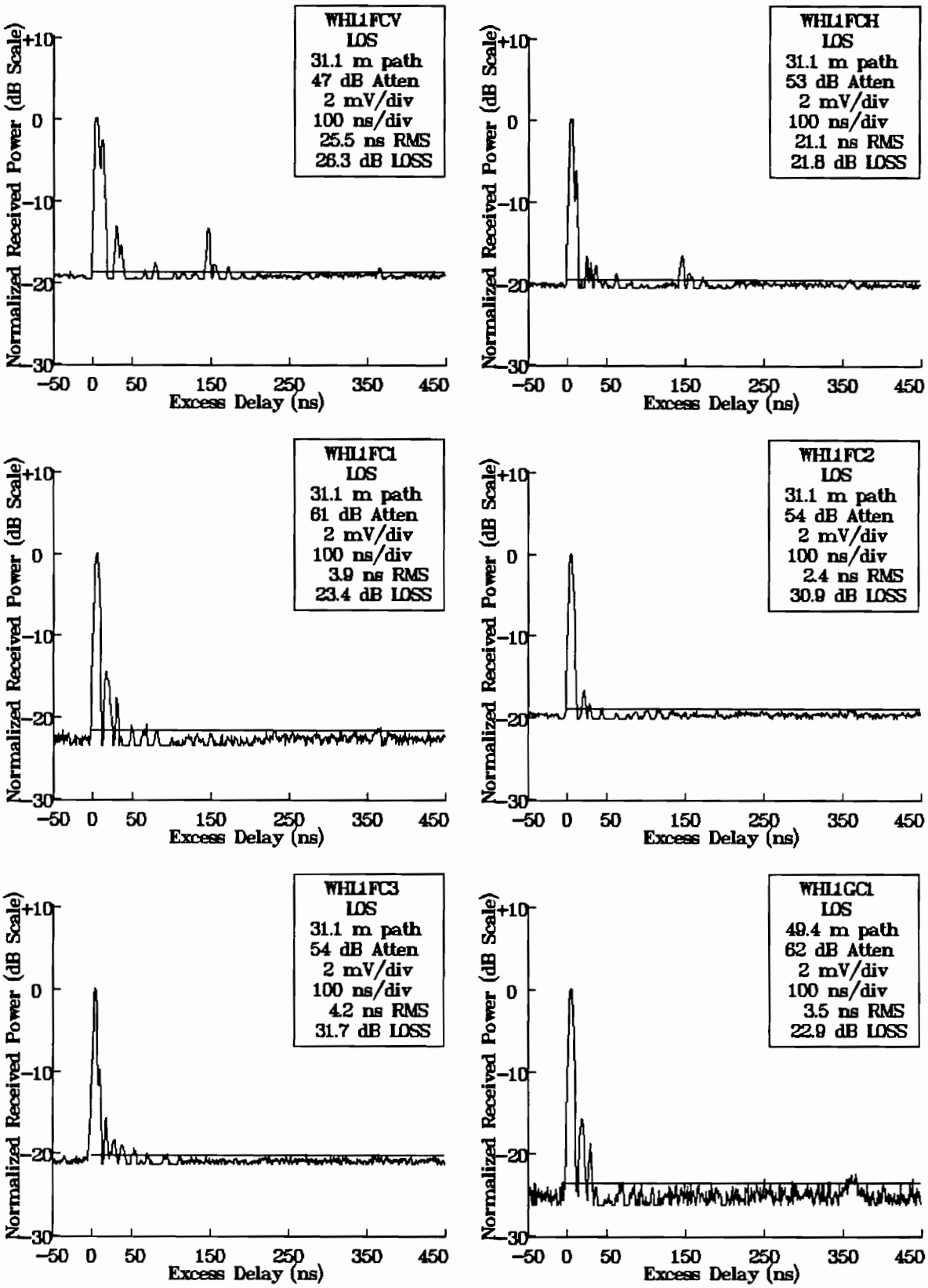
WHL1FCV
LOS
31.1 m path
47 dB Atten
2 mV/div
100 ns/div
25.5 ns RMS
26.3 dB LOSS
WHL1FCH
LOS
31.1 m path
53 dB Atten
2 mV/div
100 ns/div
21.1 ns RMS
21.8 dB LOSS
WHL1FC1
LOS
31.1 m path
61 dB Atten
2 mV/div
100 ns/div
3.9 ns RMS
23.4 dB LOSS
WHL1FC2
LOS
31.1 m path
54 dB Atten
2 mV/div
100 ns/div
2.4 ns RMS
30.9 dB LOSS
WHL1FC3
LOS
31.1 m path
54 dB Atten
2 mV/div
100 ns/div
4.2 ns RMS
31.7 dB LOSS
WHL1GC1
LOS
49.4 m path
62 dB Atten
2 mV/div
100 ns/div
3.5 ns RMS
22.9 dB LOSS
Normalized Received Power (dB Scale)
+10
0
-10
-20
-30
-50 0 50 150 250 350 450
Excess Delay (ns)

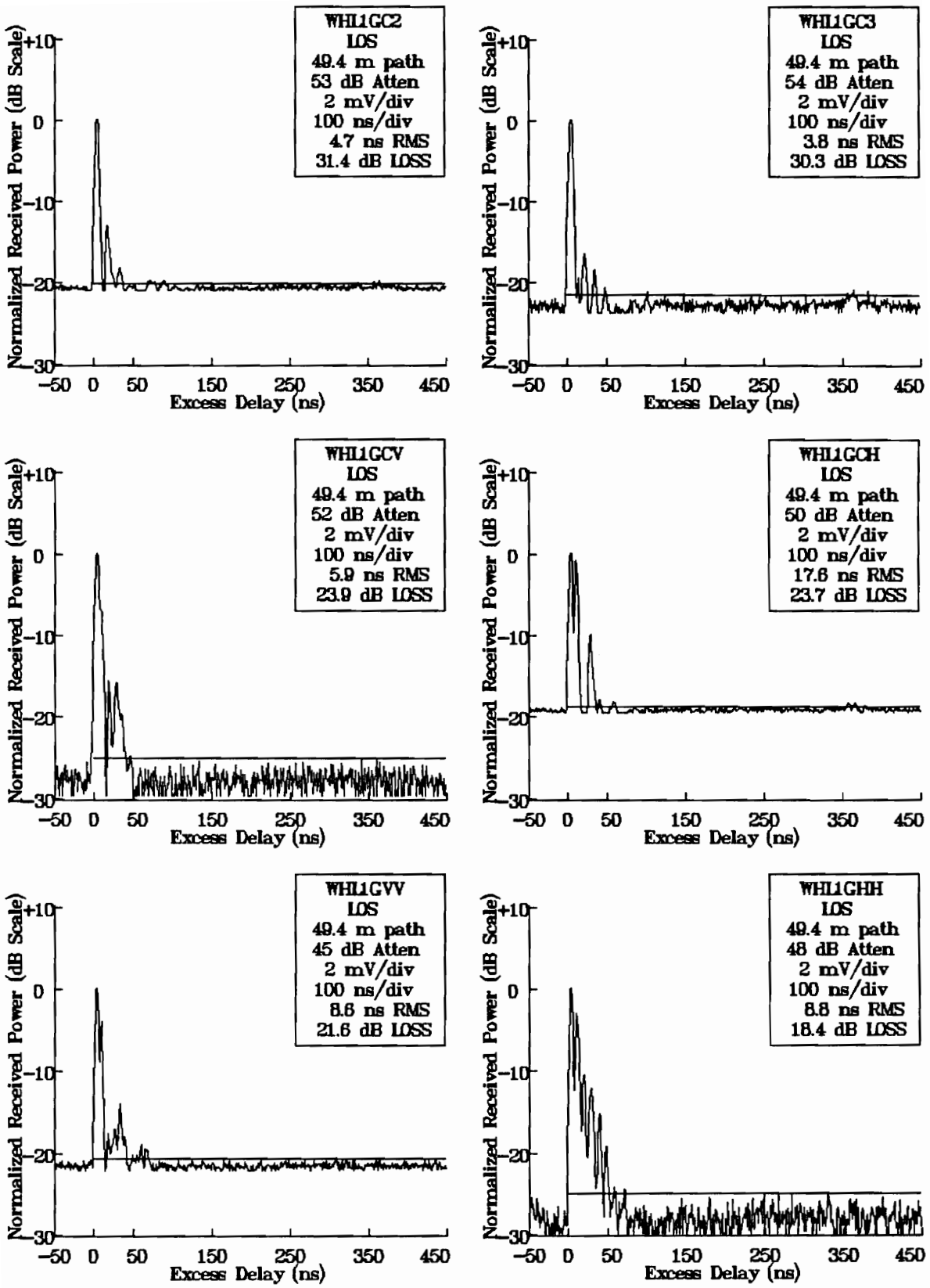
WHL1GC2
LOS
49.4 m path
53 dB Atten
2 mV/div
100 ns/div
4.7 ns RMS
31.4 dB LOSS
WHL1GC3
LOS
49.4 m path
54 dB Atten
2 mV/div
100 ns/div
3.8 ns RMS
30.3 dB LOSS
WHL1GCV
LOS
49.4 m path
52 dB Atten
2 mV/div
100 ns/div
5.9 ns RMS
23.9 dB LOSS
WHL1GCH
LOS
49.4 m path
50 dB Atten
2 mV/div
100 ns/div
17.6 ns RMS
23.7 dB LOSS
WHL1GVV
LOS
49.4 m path
45 dB Atten
2 mV/div
100 ns/div
8.6 ns RMS
21.6 dB LOSS
WHL1GHH
LOS
49.4 m path
48 dB Atten
2 mV/div
100 ns/div
8.8 ns RMS
18.4 dB LOSS
Normalized Received Power (dB Scale)
+10
0
-10
-20
-30
-50 0 50 150 250 350 450
Excess Delay (ns)

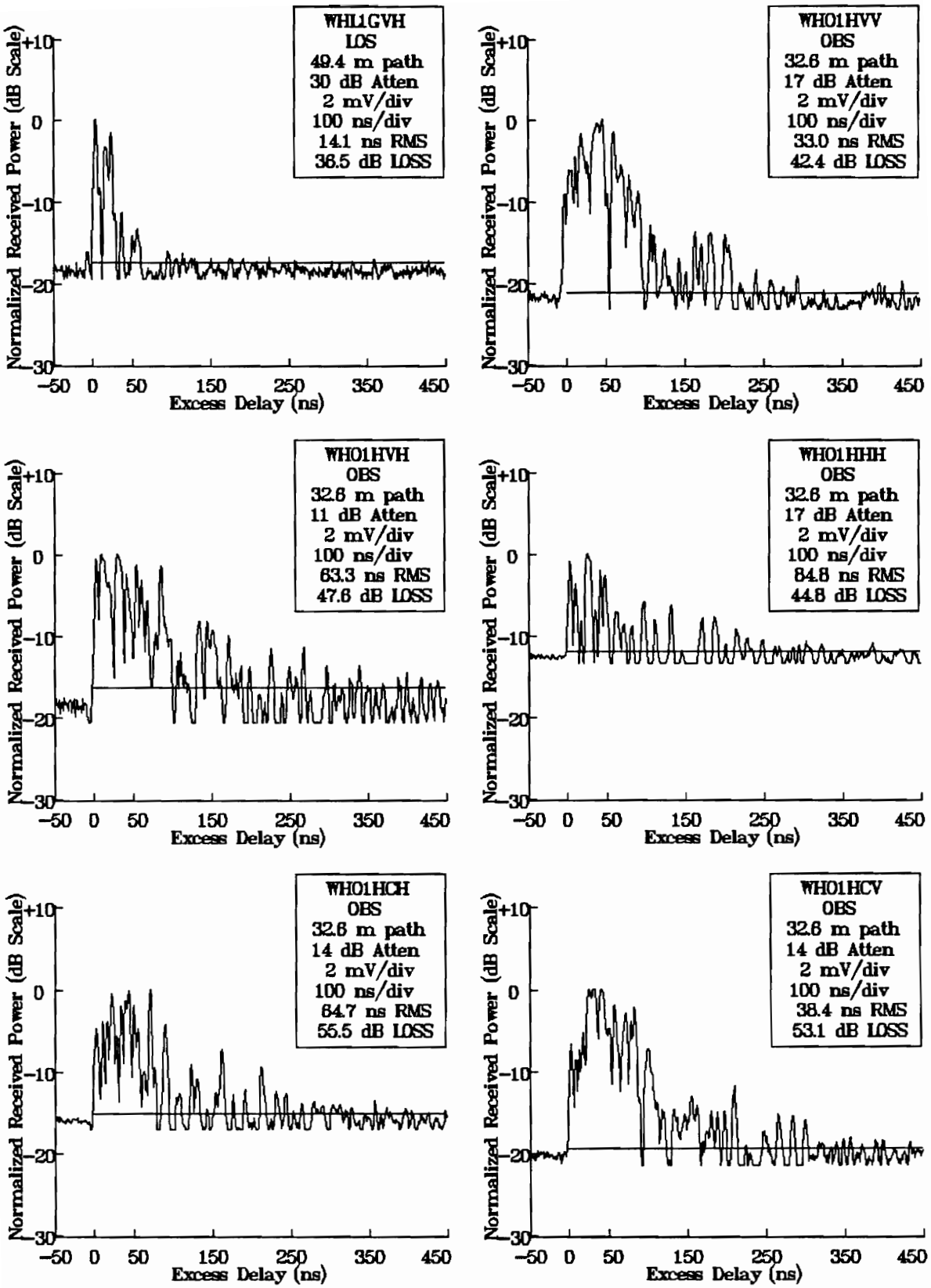
WHL1GVH
LOS
49.4 m path
30 dB Atten
2 mV/div
100 ns/div
14.1 ns RMS
36.5 dB LOSS
WHO1HVV
OBS
32.6 m path
17 dB Atten
2 mV/div
100 ns/div
33.0 ns RMS
42.4 dB LOSS
WHO1HVH
OBS
32.6 m path
11 dB Atten
2 mV/div
100 ns/div
63.3 ns RMS
47.6 dB LOSS
WHO1HHH
OBS
32.6 m path
17 dB Atten
2 mV/div
100 ns/div
84.8 ns RMS
44.8 dB LOSS
WHO1HCH
OBS
32.6 m path
14 dB Atten
2 mV/div
100 ns/div
64.7 ns RMS
55.5 dB LOSS
WHO1HCV
OBS
32.6 m path
14 dB Atten
2 mV/div
100 ns/div
38.4 ns RMS
53.1 dB LOSS
Normalized Received Power (dB Scale)
+10
0
-10
-20
-30
-50 0 50 150 250 350 450
Excess Delay (ns)

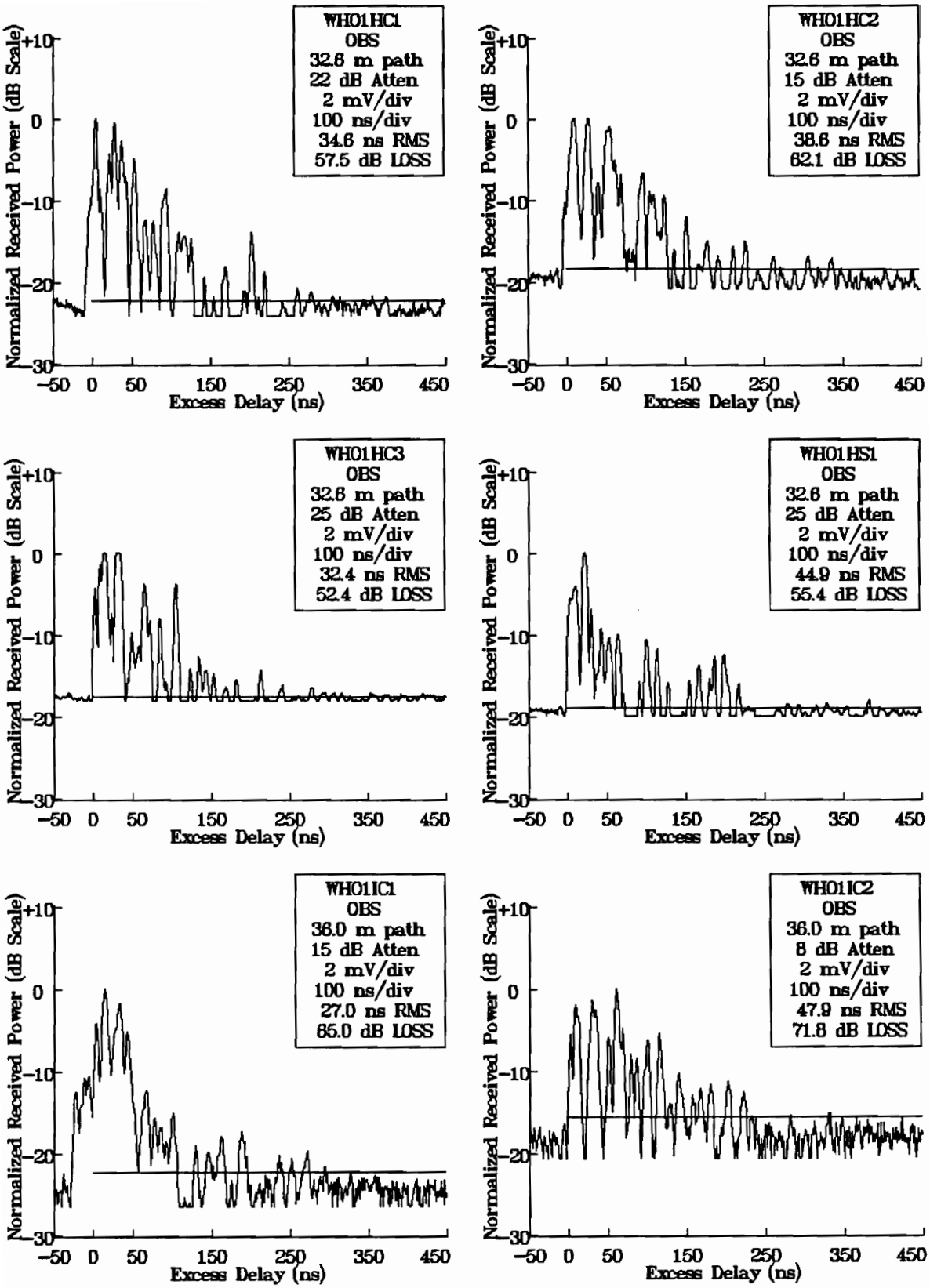
WH01HC1
OBS
32.6 m path
22 dB Atten
2 mV/div
100 ns/div
34.6 ns RMS
57.5 dB LOSS
WH01HC2
OBS
32.6 m path
15 dB Atten
2 mV/div
100 ns/div
38.6 ns RMS
62.1 dB LOSS
WH01HC3
OBS
32.6 m path
25 dB Atten
2 mV/div
100 ns/div
32.4 ns RMS
52.4 dB LOSS
WH01HS1
OBS
32.6 m path
25 dB Atten
2 mV/div
100 ns/div
44.9 ns RMS
55.4 dB LOSS
WH01IC1
OBS
36.0 m path
15 dB Atten
2 mV/div
100 ns/div
27.0 ns RMS
65.0 dB LOSS
WH01IC2
OBS
36.0 m path
8 dB Atten
2 mV/div
100 ns/div
47.9 ns RMS
71.8 dB LOSS
Normalized Received Power (dB Scale)
+10
0
-10
-20
-30
-50 0 50 150 250 350 450
Excess Delay (ns)

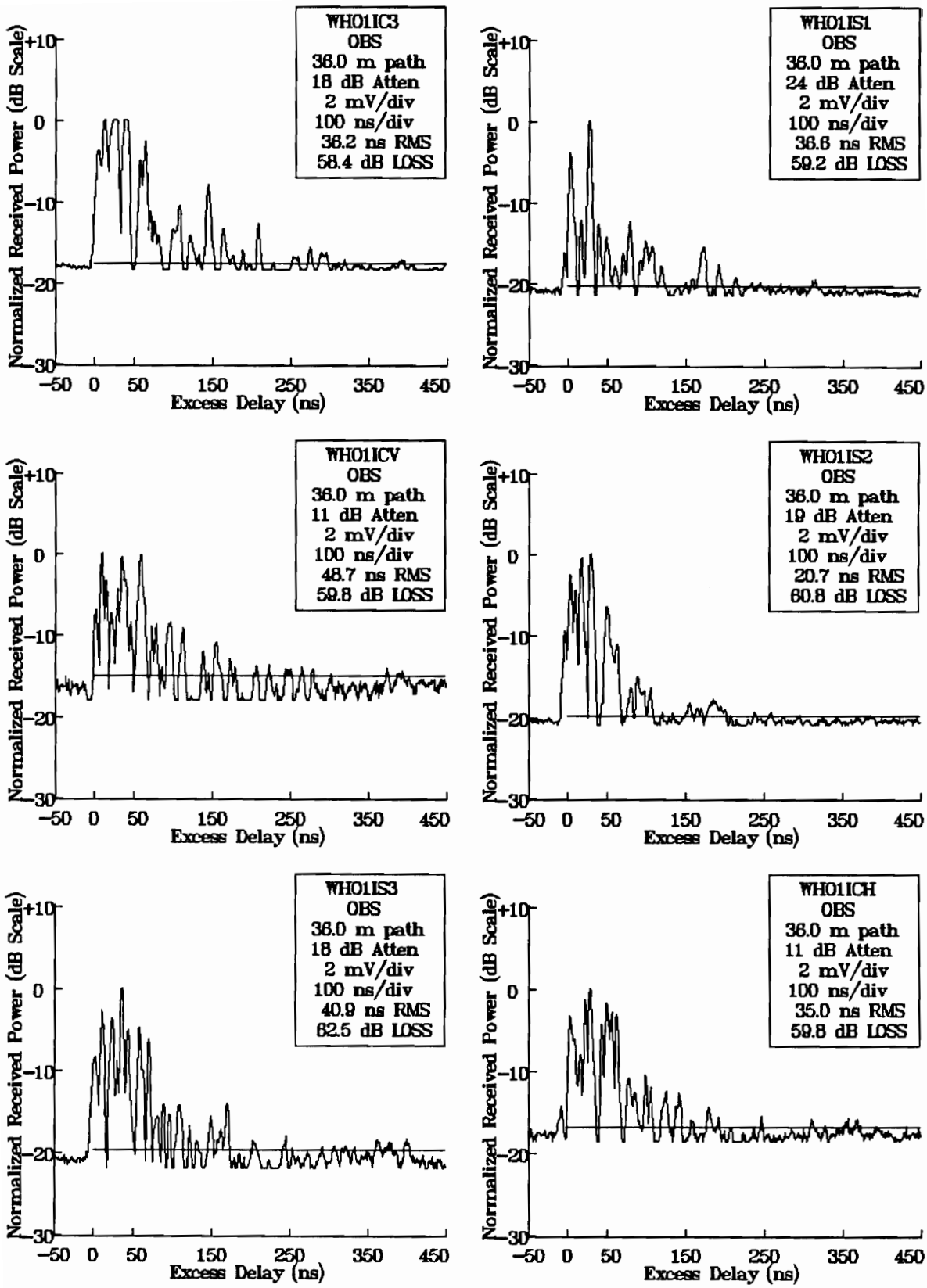
WH01IC3
OBS
36.0 m path
18 dB Atten
2 mV/div
100 ns/div
36.2 ns RMS
58.4 dB LOSS
WH01IS1
OBS
36.0 m path
24 dB Atten
2 mV/div
100 ns/div
36.6 ns RMS
59.2 dB LOSS
WH01ICV
OBS
36.0 m path
11 dB Atten
2 mV/div
100 ns/div
48.7 ns RMS
59.8 dB LOSS
WH01IS2
OBS
36.0 m path
19 dB Atten
2 mV/div
100 ns/div
20.7 ns RMS
60.8 dB LOSS
WH01IS3
OBS
36.0 m path
18 dB Atten
2 mV/div
100 ns/div
40.9 ns RMS
62.5 dB LOSS
WH01ICH
OBS
36.0 m path
11 dB Atten
2 mV/div
100 ns/div
35.0 ns RMS
59.8 dB LOSS
Normalized Received Power (dB Scale)
+10
0
-10
-20
-30
-50 0 50 150 250 350 450
Excess Delay (ns)

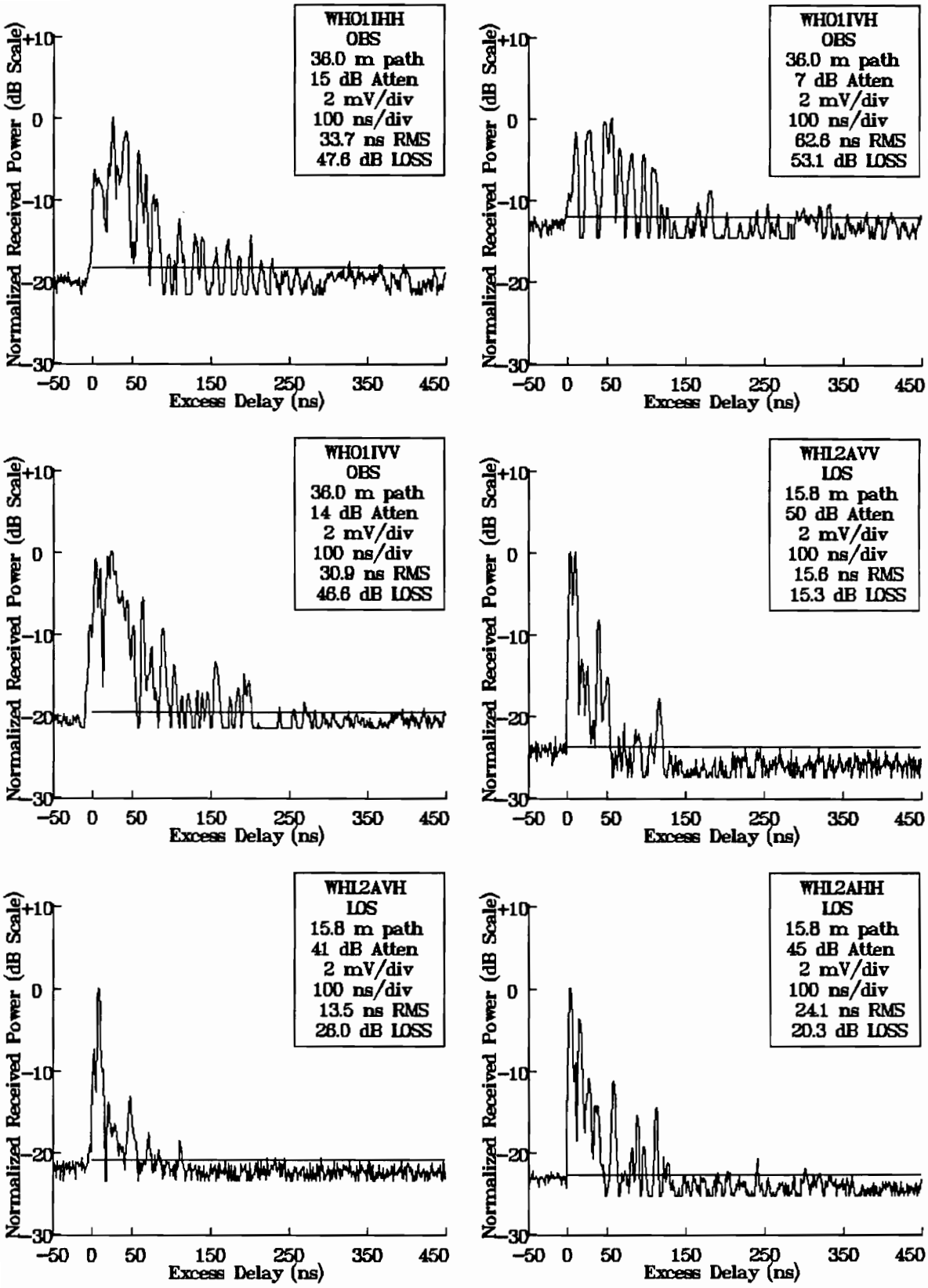
WH01IHH
OBS
36.0 m path
15 dB Atten
2 mV/div
100 ns/div
33.7 ns RMS
47.6 dB LOSS
WH01IVH
OBS
36.0 m path
7 dB Atten
2 mV/div
100 ns/div
62.6 ns RMS
53.1 dB LOSS
WH01IVV
OBS
36.0 m path
14 dB Atten
2 mV/div
100 ns/div
30.9 ns RMS
46.6 dB LOSS
WHL2AVV
LOS
15.8 m path
50 dB Atten
2 mV/div
100 ns/div
15.6 ns RMS
15.3 dB LOSS
WHL2AVH
LOS
15.8 m path
41 dB Atten
2 mV/div
100 ns/div
13.5 ns RMS
26.0 dB LOSS
WHL2AHH
LOS
15.8 m path
45 dB Atten
2 mV/div
100 ns/div
24.1 ns RMS
20.3 dB LOSS
Normalized Received Power (dB Scale)
+10
0
-10
-20
-30
-50 0 50 150 250 350 450
Excess Delay (ns)

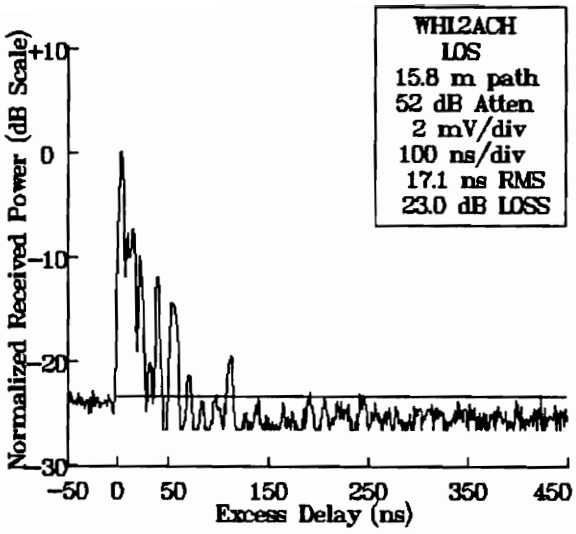
WHI2ACH
LOS
15.8 m path
52 dB Atten
2 mV/div
100 ns/div
17.1 ns RMS
23.0 dB LOSS
Normalized Received Power (dB Scale)
+10
0
-10
-20
-30
-50 0 50 150 250 350 450
Excess Delay (ns)

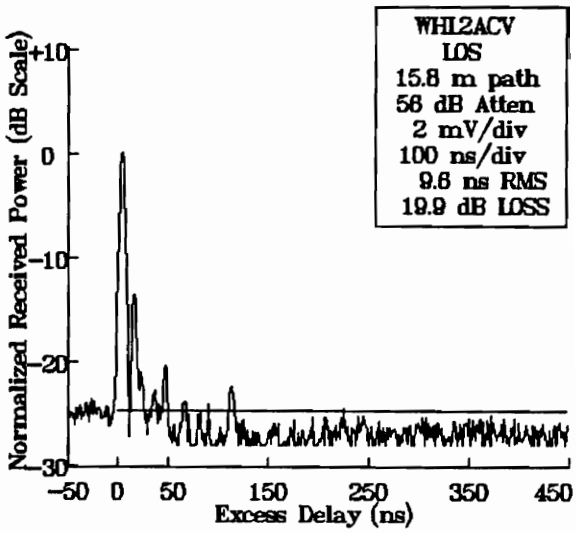
WHI2ACV
LOS
15.8 m path
56 dB Atten
2 mV/div
100 ns/div
9.6 ns RMS
19.9 dB LOSS
Normalized Received Power (dB Scale)
+10
0
-10
-20
-30
-50 0 50 150 250 350 450
Excess Delay (ns)

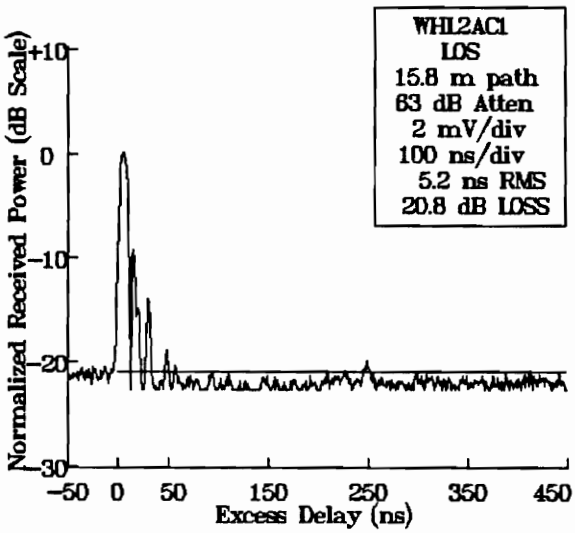
WHI2AC1
LOS
15.8 m path
63 dB Atten
2 mV/div
100 ns/div
5.2 ns RMS
20.8 dB LOSS
Normalized Received Power (dB Scale)
+10
0
-10
-20
-30
-50 0 50 150 250 350 450
Excess Delay (ns)

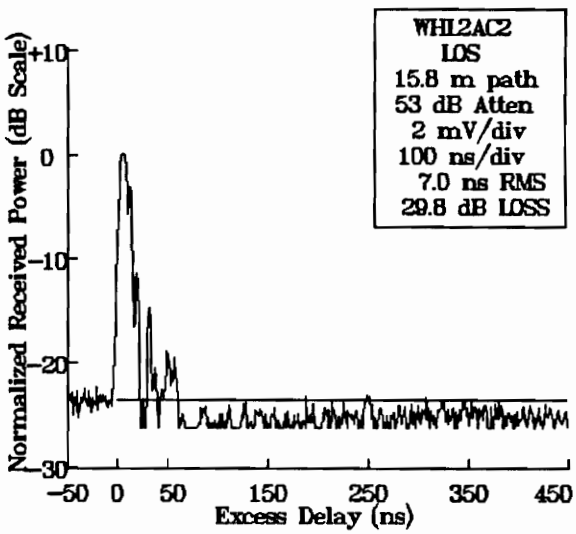
WHI2AC2
LOS
15.8 m path
53 dB Atten
2 mV/div
100 ns/div
7.0 ns RMS
29.8 dB LOSS
Normalized Received Power (dB Scale)
+10
0
-10
-20
-30
-50 0 50 150 250 350 450
Excess Delay (ns)

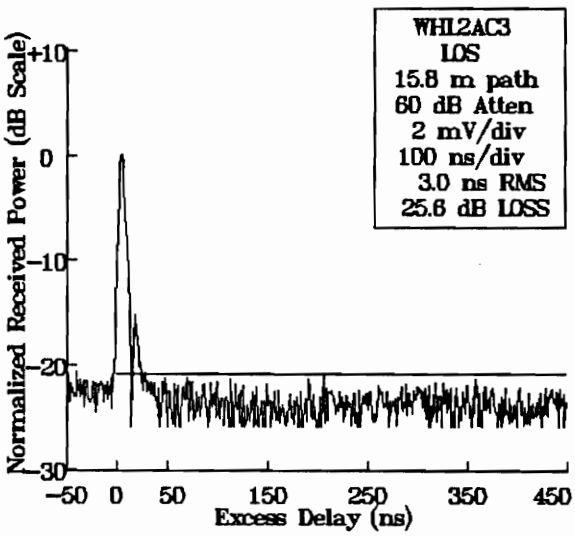
WHI2AC3
LOS
15.8 m path
60 dB Atten
2 mV/div
100 ns/div
3.0 ns RMS
25.6 dB LOSS
Normalized Received Power (dB Scale)
+10
0
-10
-20
-30
-50 0 50 150 250 350 450
Excess Delay (ns)

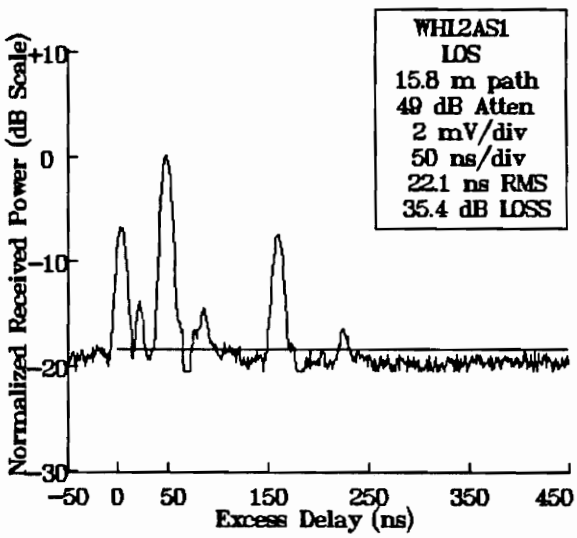
WHI2AS1
LOS
15.8 m path
49 dB Atten
2 mV/div
50 ns/div
22.1 ns RMS
35.4 dB LOSS
Normalized Received Power (dB Scale)
+10
0
-10
-20
-30
-50 0 50 150 250 350 450
Excess Delay (ns)

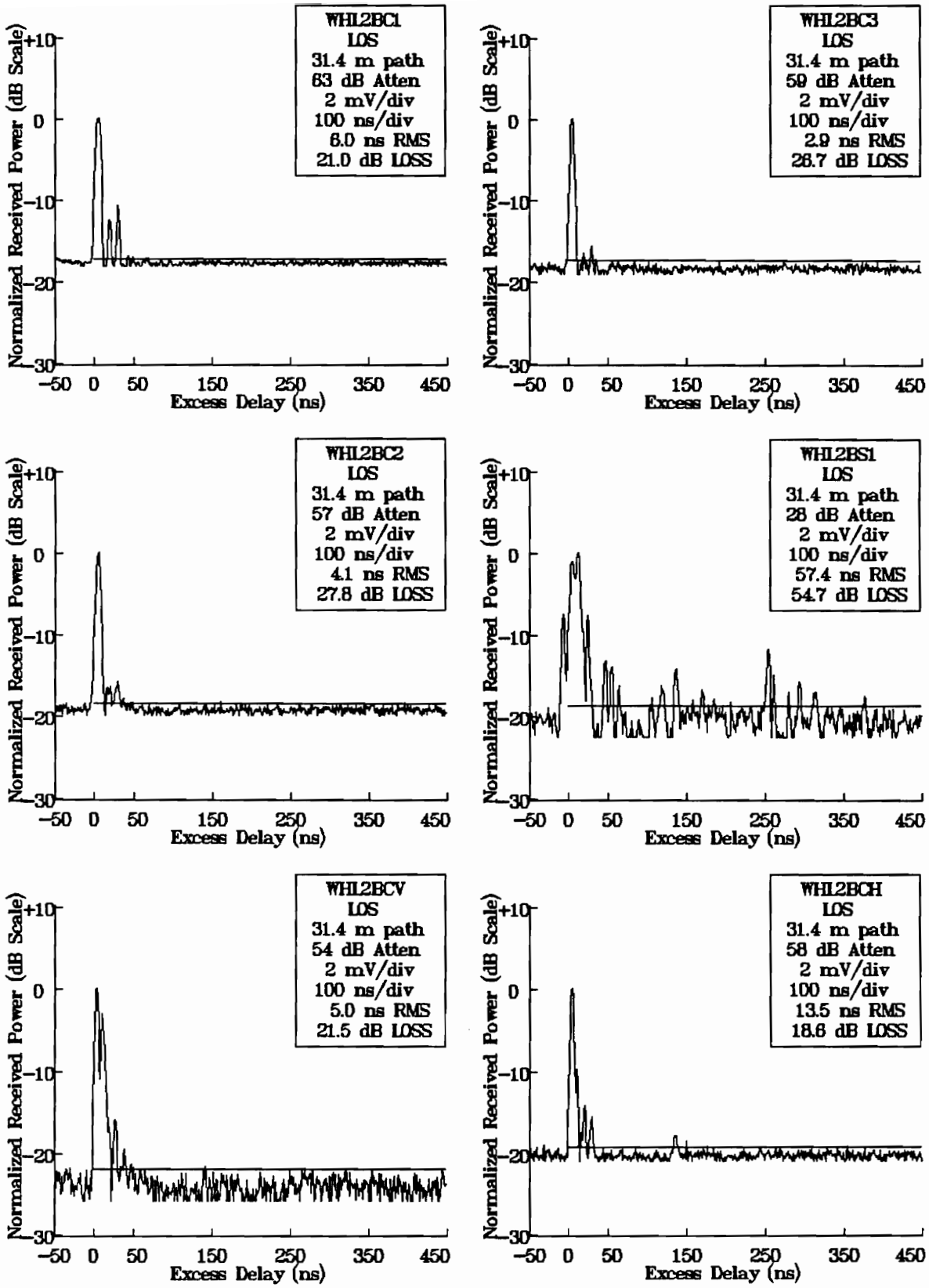
WHI2BC1
LOS
31.4 m path
63 dB Atten
2 mV/div
100 ns/div
6.0 ns RMS
21.0 dB LOSS
WHI2BC3
LOS
31.4 m path
59 dB Atten
2 mV/div
100 ns/div
2.9 ns RMS
26.7 dB LOSS
WHI2BC2
LOS
31.4 m path
57 dB Atten
2 mV/div
100 ns/div
4.1 ns RMS
27.8 dB LOSS
WHI2BS1
LOS
31.4 m path
28 dB Atten
2 mV/div
100 ns/div
57.4 ns RMS
54.7 dB LOSS
WHI2BCV
LOS
31.4 m path
54 dB Atten
2 mV/div
100 ns/div
5.0 ns RMS
21.5 dB LOSS
WHI2BCH
LOS
31.4 m path
58 dB Atten
2 mV/div
100 ns/div
13.5 ns RMS
18.6 dB LOSS
Normalized Received Power (dB Scale)
+10
0
-10
-20
-30
-50 0 50 150 250 350 450
Excess Delay (ns)

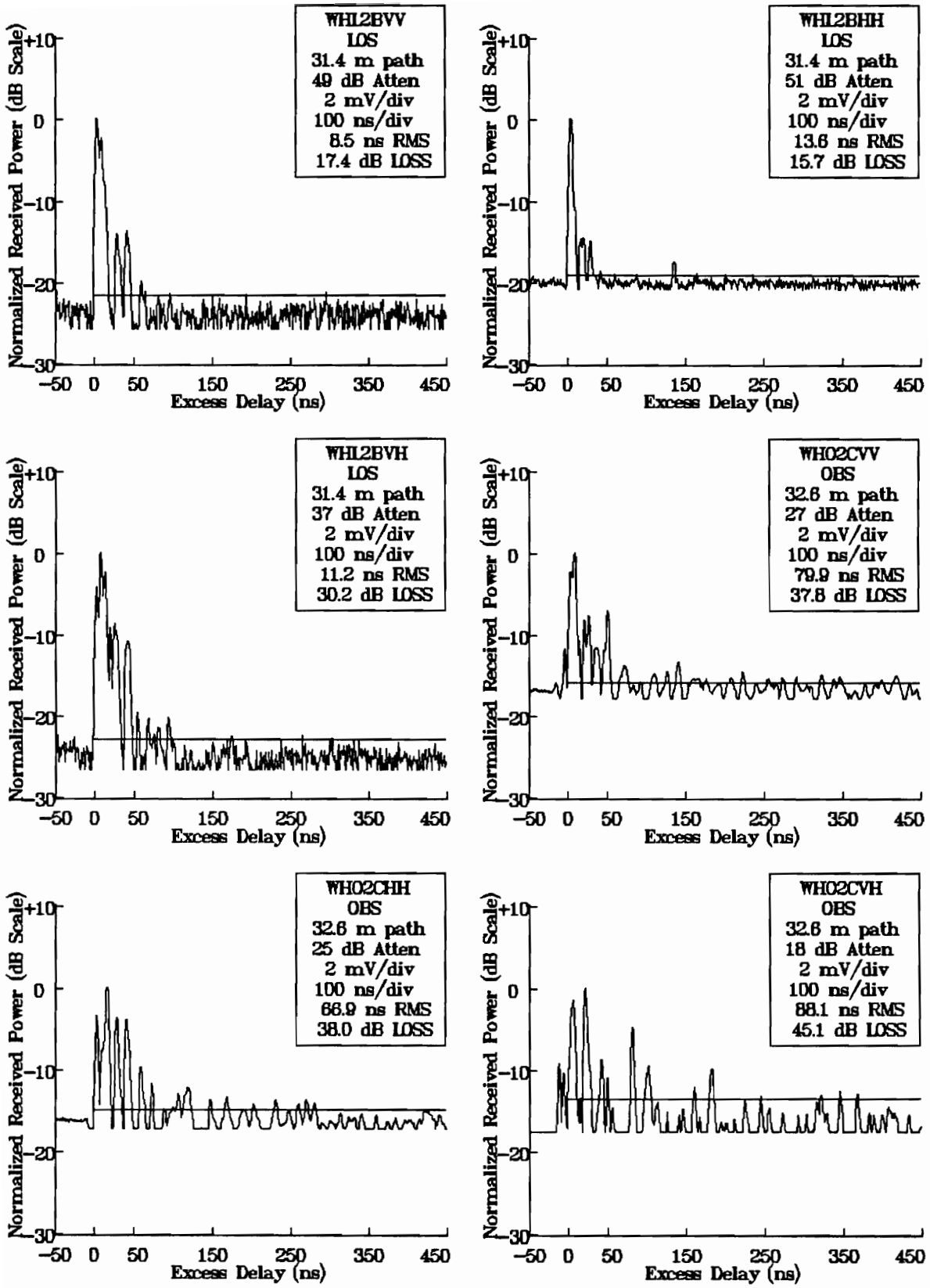
WHL2BVV
LOS
31.4 m path
49 dB Atten
2 mV/div
100 ns/div
8.5 ns RMS
17.4 dB LOSS
WHL2BHH
LOS
31.4 m path
51 dB Atten
2 mV/div
100 ns/div
13.6 ns RMS
15.7 dB LOSS
WHL2BVH
LOS
31.4 m path
37 dB Atten
2 mV/div
100 ns/div
11.2 ns RMS
30.2 dB LOSS
WH02CVV
OBS
32.6 m path
27 dB Atten
2 mV/div
100 ns/div
79.9 ns RMS
37.8 dB LOSS
WH02CHH
OBS
32.6 m path
25 dB Atten
2 mV/div
100 ns/div
66.9 ns RMS
38.0 dB LOSS
WH02CVH
OBS
32.6 m path
18 dB Atten
2 mV/div
100 ns/div
88.1 ns RMS
45.1 dB LOSS
Normalized Received Power (dB Scale)
+10
0
-10
-20
-30
-50 0 50 150 250 350 450
Excess Delay (ns)

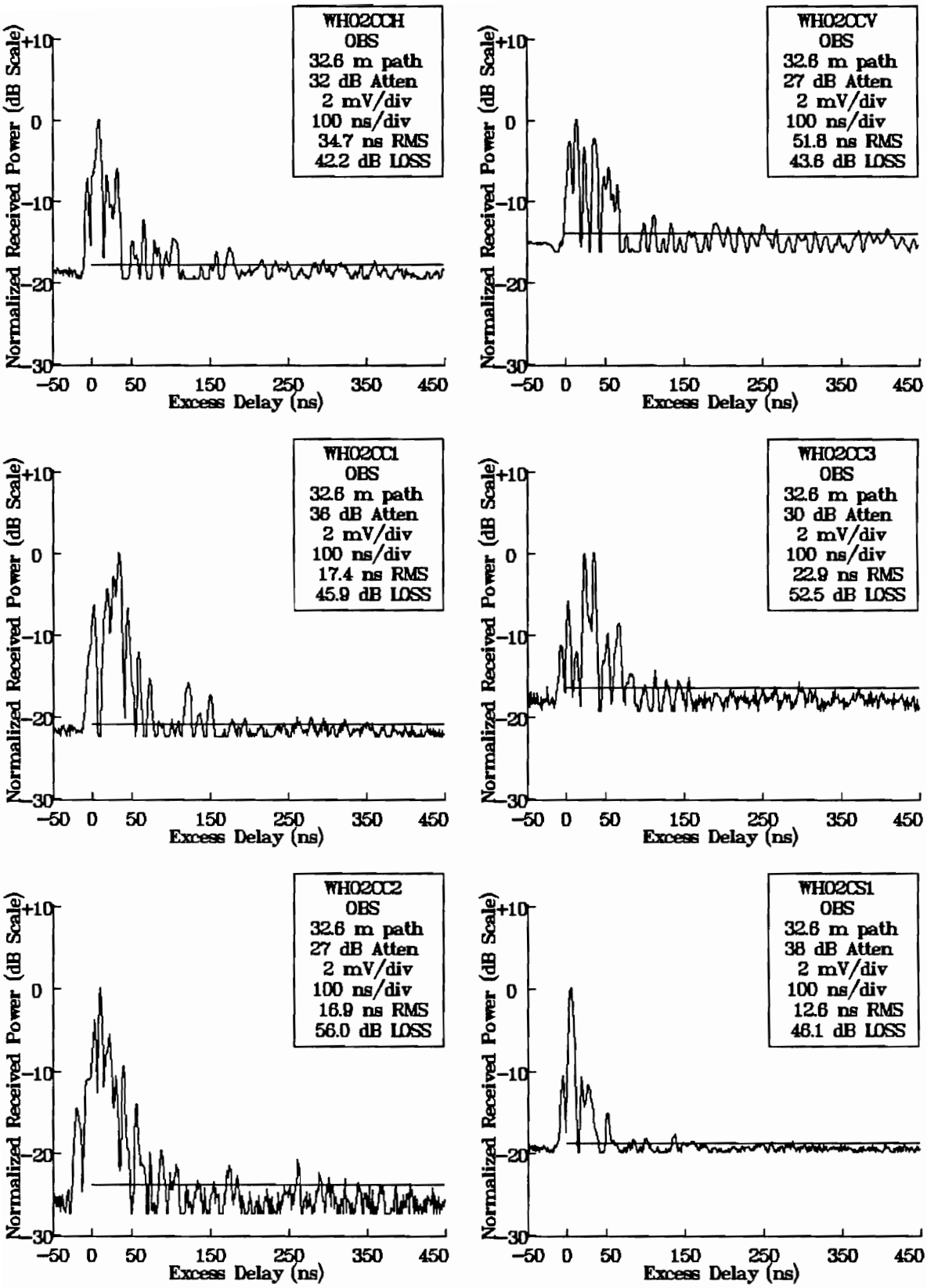
WH02CCH
OBS
32.6 m path
32 dB Atten
2 mV/div
100 ns/div
34.7 ns RMS
42.2 dB LOSS
WH02CCV
OBS
32.6 m path
27 dB Atten
2 mV/div
100 ns/div
51.8 ns RMS
43.6 dB LOSS
WH02CC1
OBS
32.6 m path
36 dB Atten
2 mV/div
100 ns/div
17.4 ns RMS
45.9 dB LOSS
WH02CC3
OBS
32.6 m path
30 dB Atten
2 mV/div
100 ns/div
22.9 ns RMS
52.5 dB LOSS
WH02CC2
OBS
32.6 m path
27 dB Atten
2 mV/div
100 ns/div
16.9 ns RMS
56.0 dB LOSS
WH02CS1
OBS
32.6 m path
38 dB Atten
2 mV/div
100 ns/div
12.6 ns RMS
46.1 dB LOSS
Normalized Received Power (dB Scale)
+10
0
-10
-20
-30
-50 0 50 150 250 350 450
Excess Delay (ns)

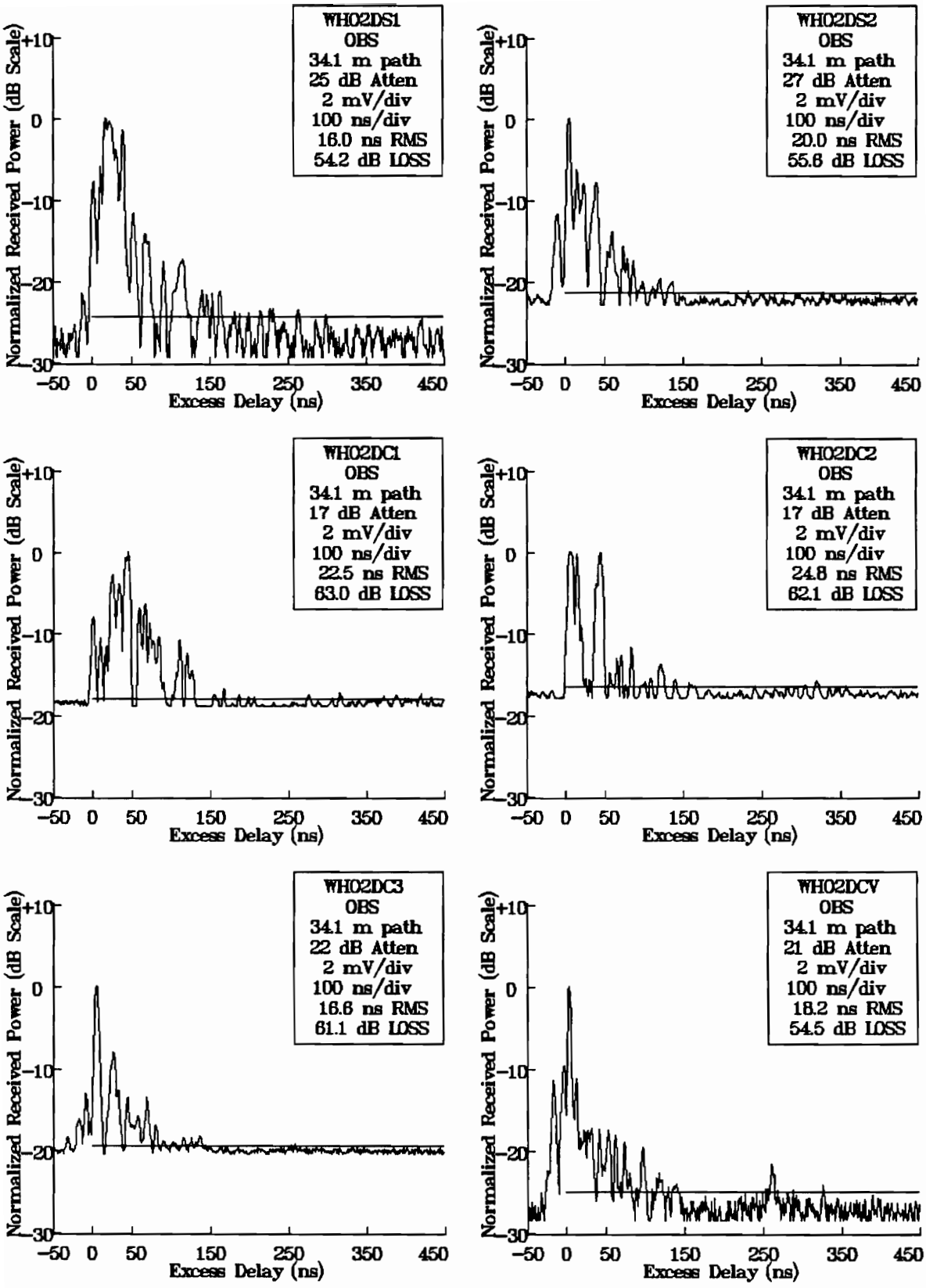
WH02DS1
OBS
34.1 m path
25 dB Atten
2 mV/div
100 ns/div
16.0 ns RMS
54.2 dB LOSS
WH02DS2
OBS
34.1 m path
27 dB Atten
2 mV/div
100 ns/div
20.0 ns RMS
55.6 dB LOSS
WH02DC1
OBS
34.1 m path
17 dB Atten
2 mV/div
100 ns/div
22.5 ns RMS
63.0 dB LOSS
WH02DC2
OBS
34.1 m path
17 dB Atten
2 mV/div
100 ns/div
24.8 ns RMS
62.1 dB LOSS
WH02DC3
OBS
34.1 m path
22 dB Atten
2 mV/div
100 ns/div
16.6 ns RMS
61.1 dB LOSS
WH02DCV
OBS
34.1 m path
21 dB Atten
2 mV/div
100 ns/div
18.2 ns RMS
54.5 dB LOSS
Normalized Received Power (dB Scale)
+10
0
-10
-20
-30
-50 0 50 150 250 350 450
Excess Delay (ns)

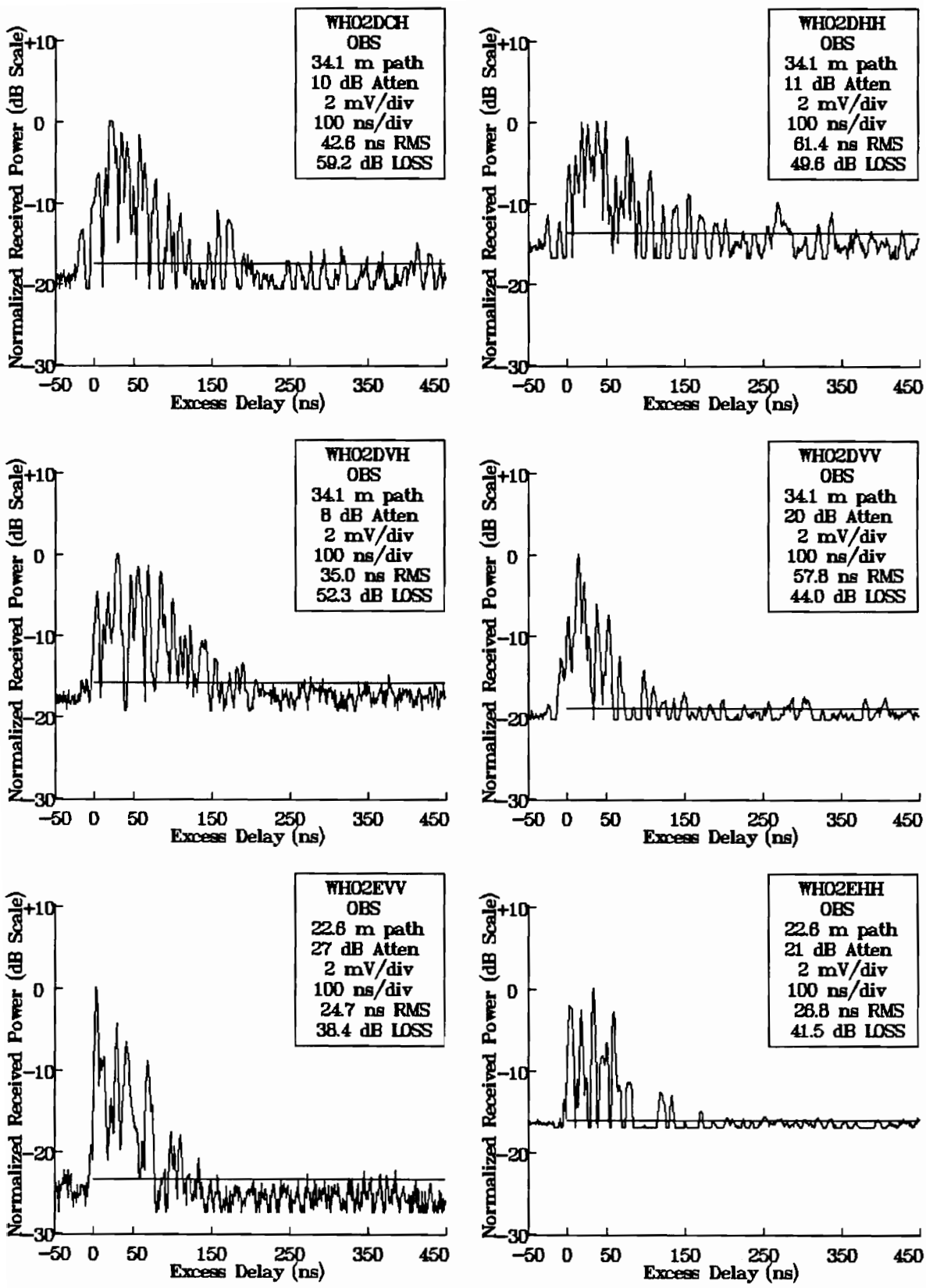
WH02DCH
OBS
34.1 m path
10 dB Atten
2 mV/div
100 ns/div
42.6 ns RMS
59.2 dB LOSS
WH02DHH
OBS
34.1 m path
11 dB Atten
2 mV/div
100 ns/div
61.4 ns RMS
49.6 dB LOSS
WH02DVH
OBS
34.1 m path
8 dB Atten
2 mV/div
100 ns/div
35.0 ns RMS
52.3 dB LOSS
WH02DVV
OBS
34.1 m path
20 dB Atten
2 mV/div
100 ns/div
57.8 ns RMS
44.0 dB LOSS
WH02EVV
OBS
22.6 m path
27 dB Atten
2 mV/div
100 ns/div
24.7 ns RMS
38.4 dB LOSS
WH02EHH
OBS
22.6 m path
21 dB Atten
2 mV/div
100 ns/div
26.8 ns RMS
41.5 dB LOSS
Normalized Received Power (dB Scale)
+10
0
-10
-20
-30
-50 0 50 150 250 350 450
Excess Delay (ns)

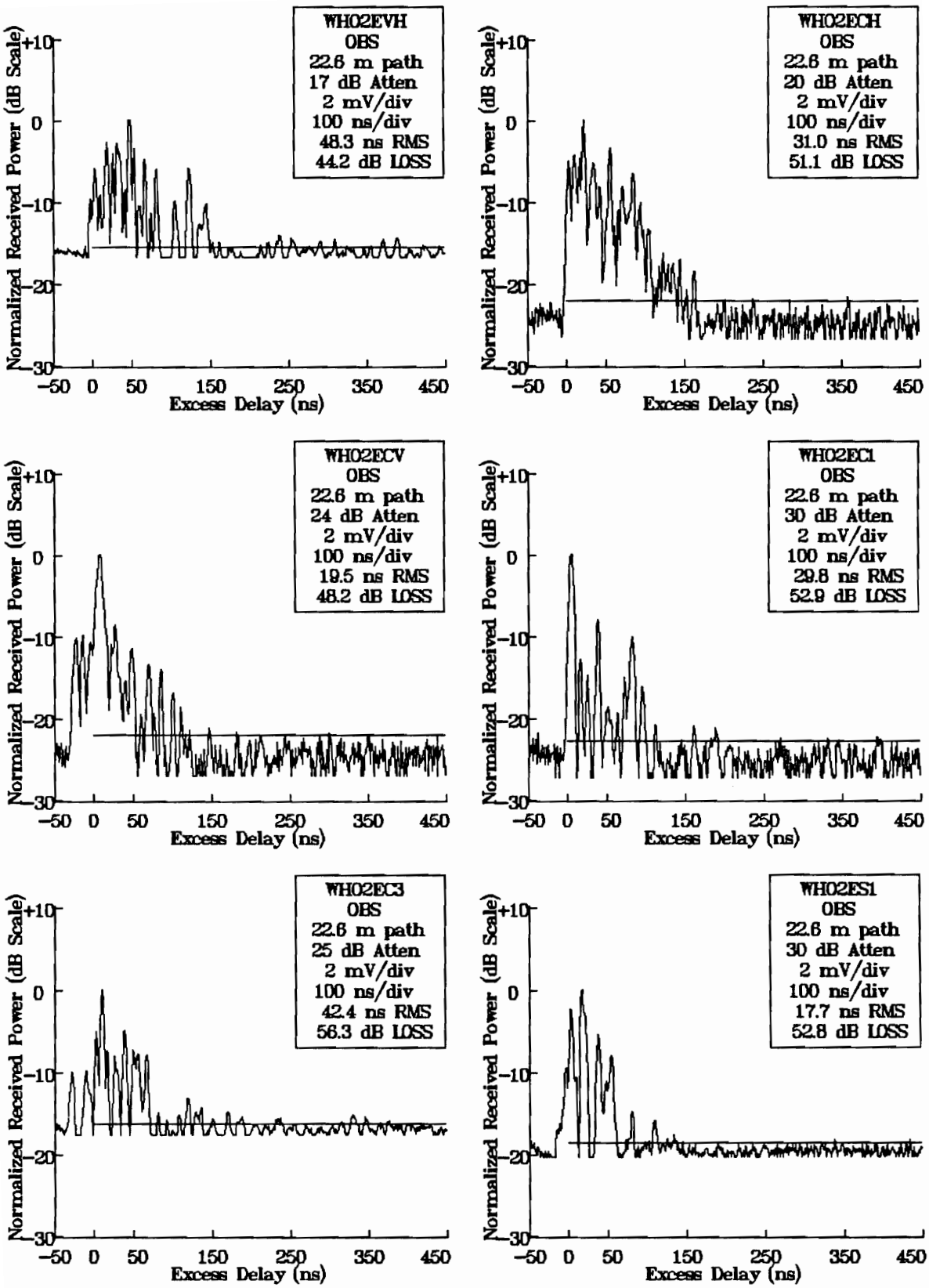
WH02EVH
OBS
22.6 m path
17 dB Atten
2 mV/div
100 ns/div
48.3 ns RMS
44.2 dB LOSS
WH02ECH
OBS
22.6 m path
20 dB Atten
2 mV/div
100 ns/div
31.0 ns RMS
51.1 dB LOSS
WH02ECV
OBS
22.6 m path
24 dB Atten
2 mV/div
100 ns/div
19.5 ns RMS
48.2 dB LOSS
WH02EC1
OBS
22.6 m path
30 dB Atten
2 mV/div
100 ns/div
29.8 ns RMS
52.9 dB LOSS
WH02EC3
OBS
22.6 m path
25 dB Atten
2 mV/div
100 ns/div
42.4 ns RMS
56.3 dB LOSS
WH02ES1
OBS
22.6 m path
30 dB Atten
2 mV/div
100 ns/div
17.7 ns RMS
52.8 dB LOSS
Normalized Received Power (dB Scale)
+10
0
-10
-20
-30
-50 0 50 150 250 350 450
Excess Delay (ns)

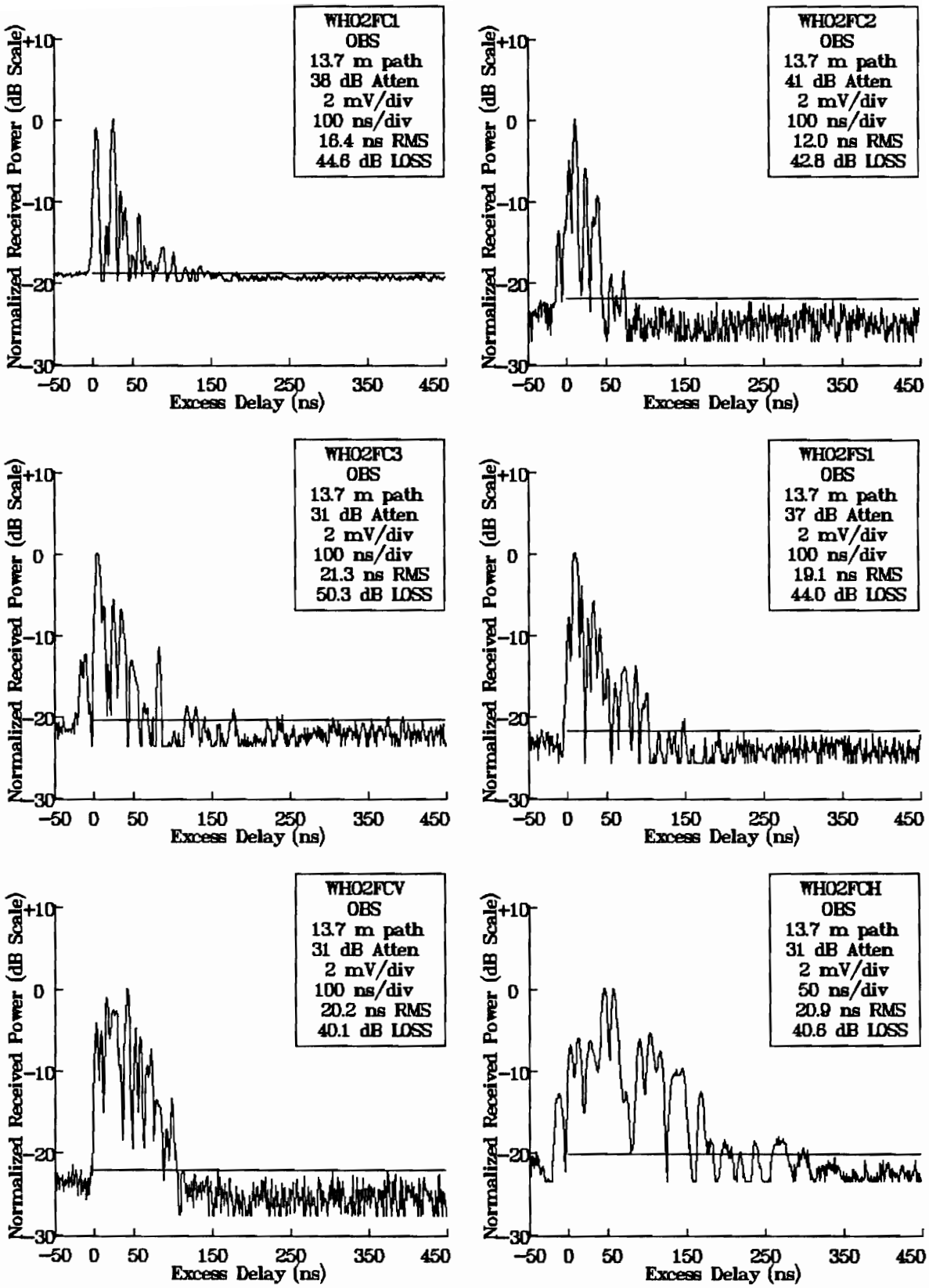
WH02FC1
OBS
13.7 m path
38 dB Atten
2 mV/div
100 ns/div
16.4 ns RMS
44.6 dB LOSS
WH02FC2
OBS
13.7 m path
41 dB Atten
2 mV/div
100 ns/div
12.0 ns RMS
42.8 dB LOSS
WH02FC3
OBS
13.7 m path
31 dB Atten
2 mV/div
100 ns/div
21.3 ns RMS
50.3 dB LOSS
WH02FS1
OBS
13.7 m path
37 dB Atten
2 mV/div
100 ns/div
19.1 ns RMS
44.0 dB LOSS
WH02FCV
OBS
13.7 m path
31 dB Atten
2 mV/div
100 ns/div
20.2 ns RMS
40.1 dB LOSS
WH02FCH
OBS
13.7 m path
31 dB Atten
2 mV/div
50 ns/div
20.9 ns RMS
40.6 dB LOSS
Normalized Received Power (dB Scale)
+10
0
-10
-20
-30
-50 0 50 150 250 350 450
Excess Delay (ns)

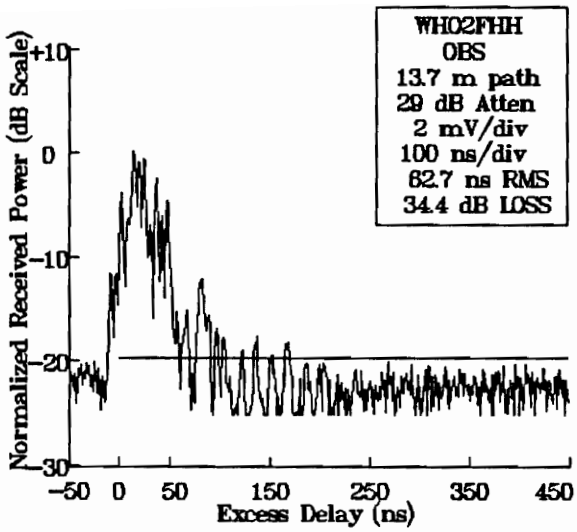
WH02FHH
OBS
13.7 m path
29 dB Atten
2 mV/div
100 ns/div
62.7 ns RMS
34.4 dB LOSS
Normalized Received Power (dB Scale)
+10
0
-10
-20
-30
-50 0 50 150 250 350 450
Excess Delay (ns)

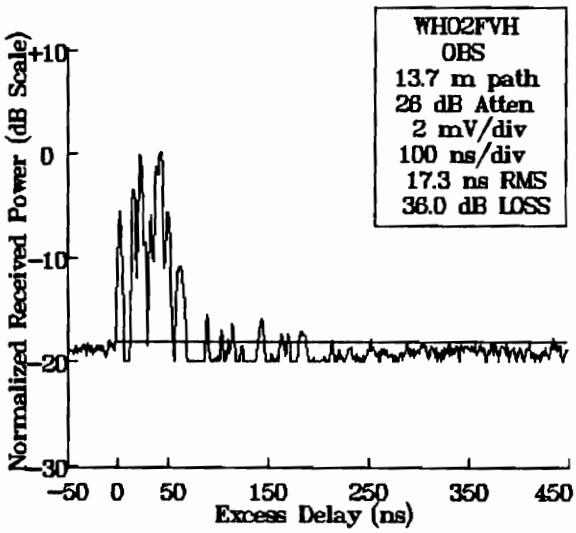
WH02FVH
OBS
13.7 m path
26 dB Atten
2 mV/div
100 ns/div
17.3 ns RMS
36.0 dB LOSS
Normalized Received Power (dB Scale)
+10
0
-10
-20
-30
-50 0 50 150 250 350 450
Excess Delay (ns)

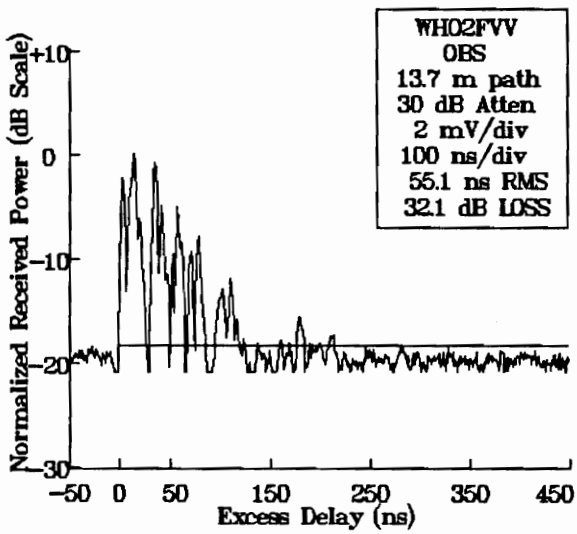
WH02FVV
OBS
13.7 m path
30 dB Atten
2 mV/div
100 ns/div
55.1 ns RMS
32.1 dB LOSS
Normalized Received Power (dB Scale)
+10
0
-10
-20
-30
-50 0 50 150 250 350 450
Excess Delay (ns)

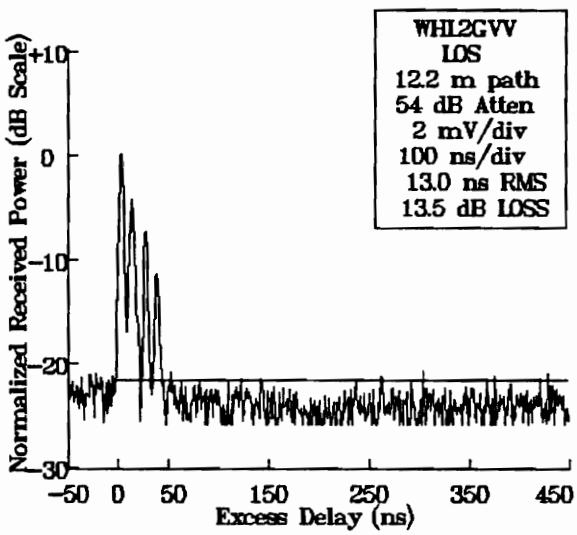
WH12GVV
LOS
12.2 m path
54 dB Atten
2 mV/div
100 ns/div
13.0 ns RMS
13.5 dB LOSS
Normalized Received Power (dB Scale)
+10
0
-10
-20
-30
-50 0 50 150 250 350 450
Excess Delay (ns)

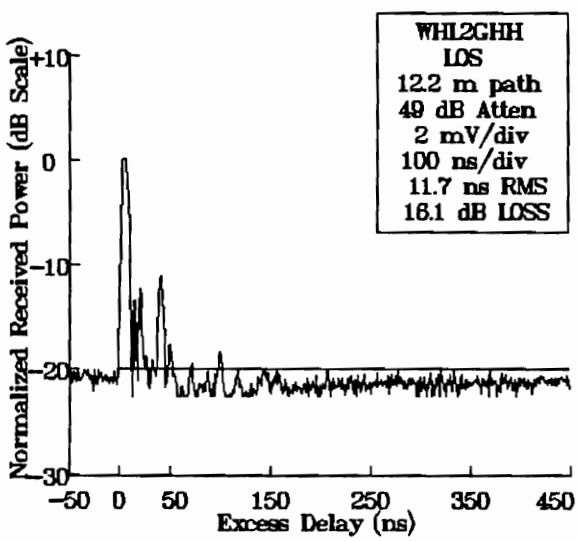
WH12GHH
LOS
12.2 m path
49 dB Atten
2 mV/div
100 ns/div
11.7 ns RMS
16.1 dB LOSS
Normalized Received Power (dB Scale)
+10
0
-10
-20
-30
-50 0 50 150 250 350 450
Excess Delay (ns)

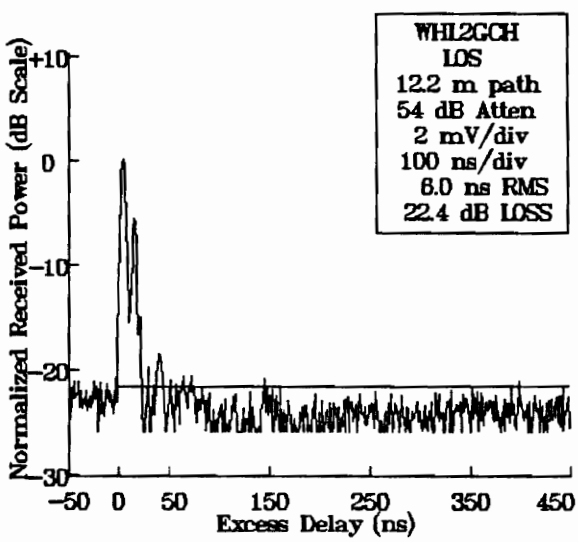
WH12GCH
LOS
12.2 m path
54 dB Atten
2 mV/div
100 ns/div
6.0 ns RMS
22.4 dB LOSS
Normalized Received Power (dB Scale)
+10
0
-10
-20
-30
-50 0 50 150 250 350 450
Excess Delay (ns)

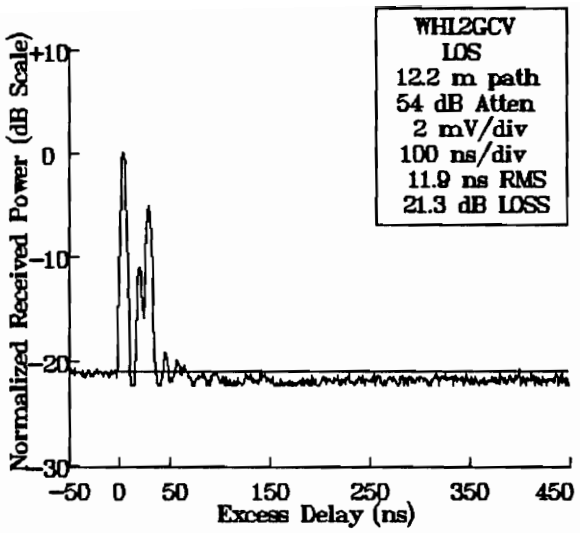
WHI2GCV
LOS
12.2 m path
54 dB Atten
2 mV/div
100 ns/div
11.9 ns RMS
21.3 dB LOSS
Normalized Received Power (dB Scale)
+10
0
-10
-20
-30
-50 0 50 150 250 350 450
Excess Delay (ns)

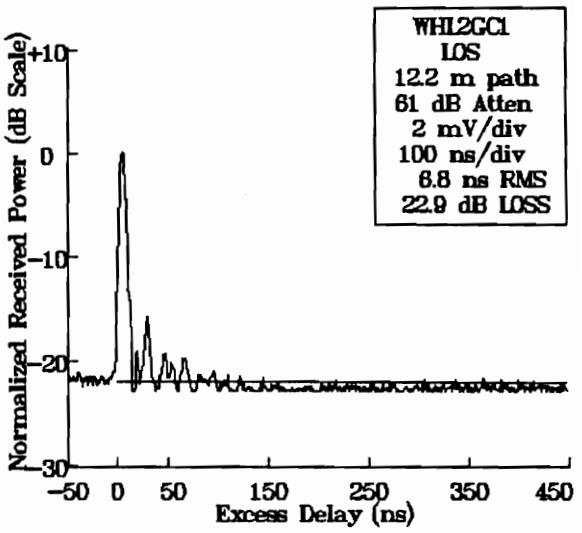
WHI2GC1
LOS
12.2 m path
61 dB Atten
2 mV/div
100 ns/div
6.8 ns RMS
22.9 dB LOSS
Normalized Received Power (dB Scale)
+10
0
-10
-20
-30
-50 0 50 150 250 350 450
Excess Delay (ns)

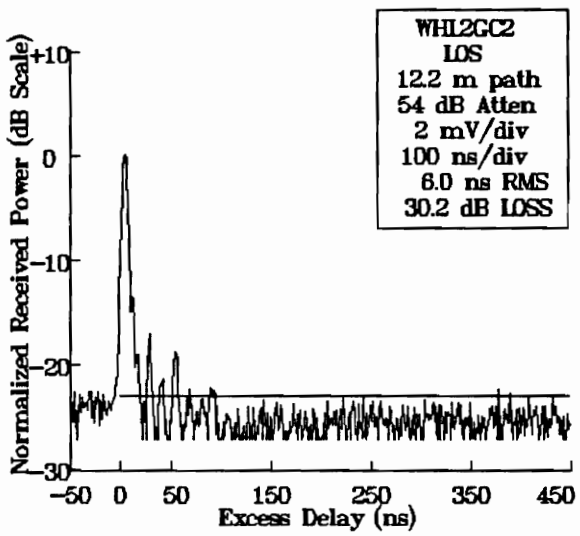
WHI2GC2
LOS
12.2 m path
54 dB Atten
2 mV/div
100 ns/div
6.0 ns RMS
30.2 dB LOSS
Normalized Received Power (dB Scale)
+10
0
-10
-20
-30
-50 0 50 150 250 350 450
Excess Delay (ns)

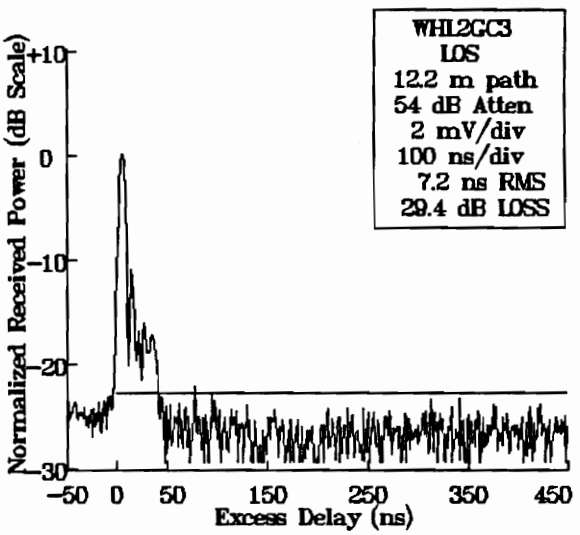
WHI2GC3
LOS
12.2 m path
54 dB Atten
2 mV/div
100 ns/div
7.2 ns RMS
29.4 dB LOSS
Normalized Received Power (dB Scale)
+10
0
-10
-20
-30
-50 0 50 150 250 350 450
Excess Delay (ns)

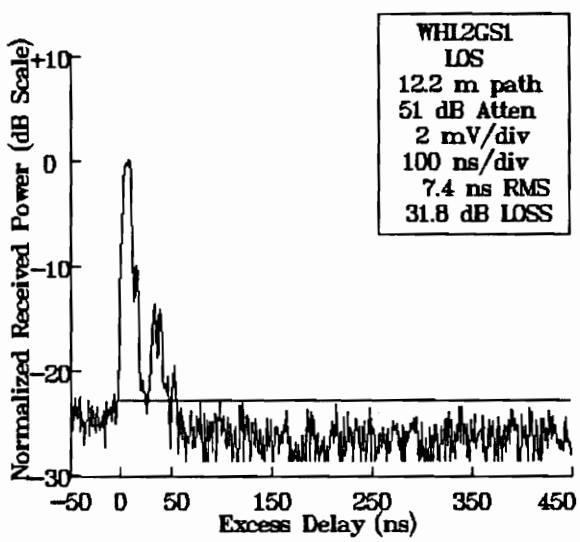
WHI2GS1
LOS
12.2 m path
51 dB Atten
2 mV/div
100 ns/div
7.4 ns RMS
31.8 dB LOSS
Normalized Received Power (dB Scale)
+10
0
-10
-20
-30
-50 0 50 150 250 350 450
Excess Delay (ns)

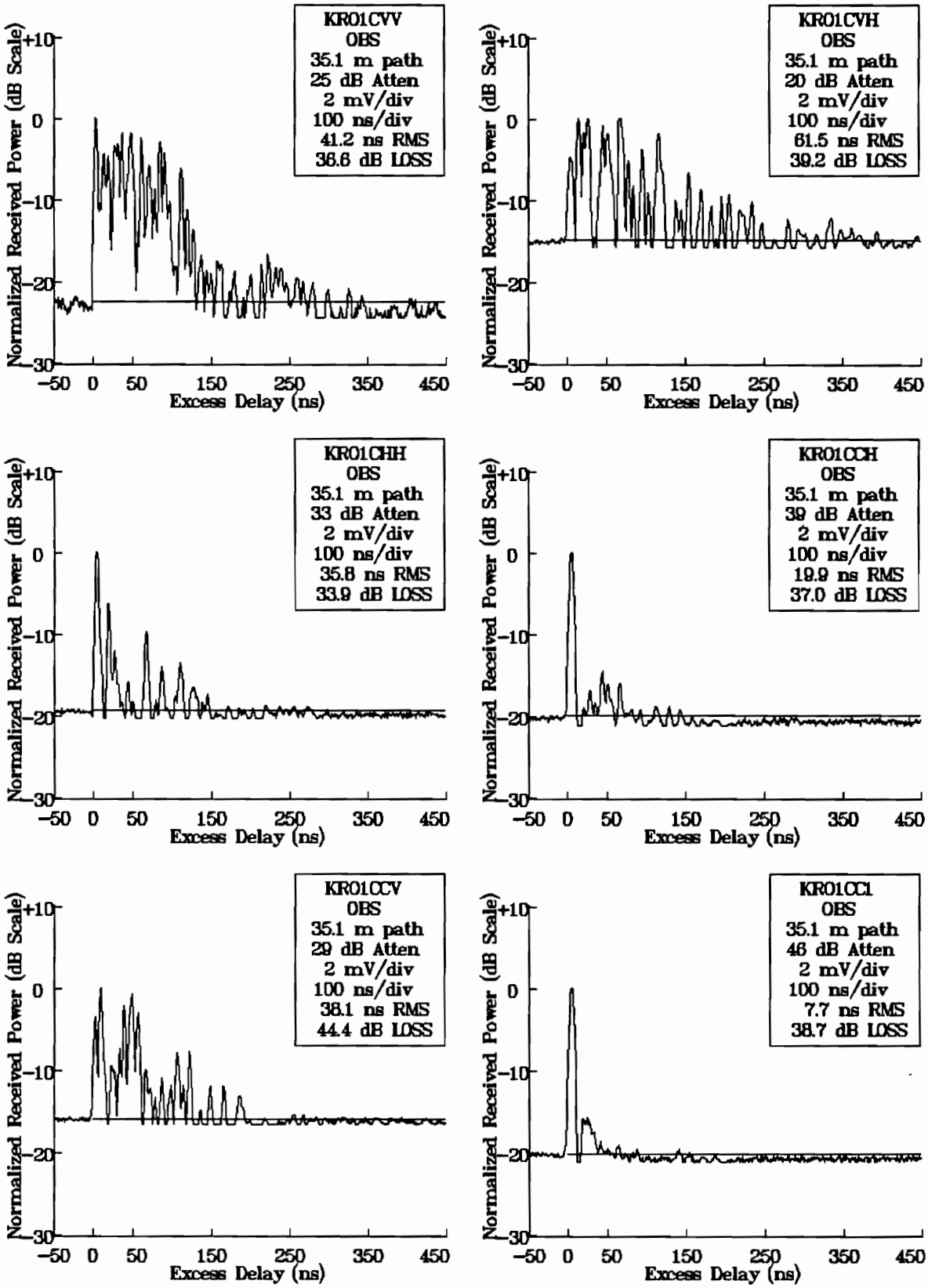
KR01CVV
OBS
35.1 m path
25 dB Atten
2 mV/div
100 ns/div
41.2 ns RMS
36.6 dB LOSS
KR01CVH
OBS
35.1 m path
20 dB Atten
2 mV/div
100 ns/div
61.5 ns RMS
39.2 dB LOSS
KR01CHH
OBS
35.1 m path
33 dB Atten
2 mV/div
100 ns/div
35.8 ns RMS
33.9 dB LOSS
KR01CCH
OBS
35.1 m path
39 dB Atten
2 mV/div
100 ns/div
19.9 ns RMS
37.0 dB LOSS
KR01CCV
OBS
35.1 m path
29 dB Atten
2 mV/div
100 ns/div
38.1 ns RMS
44.4 dB LOSS
KR01CC1
OBS
35.1 m path
46 dB Atten
2 mV/div
100 ns/div
7.7 ns RMS
38.7 dB LOSS
Normalized Received Power (dB Scale)
+10
0
-10
-20
-30
-50 0 50 150 250 350 450
Excess Delay (ns)

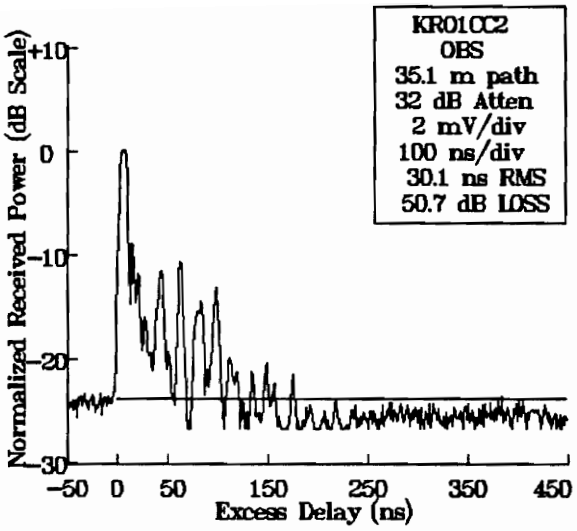
KR01CC2
OBS
35.1 m path
32 dB Atten
2 mV/div
100 ns/div
30.1 ns RMS
50.7 dB LOSS
Normalized Received Power (dB Scale)
+10
0
-10
-20
-30
-50 0 50 150 250 350 450
Excess Delay (ns)

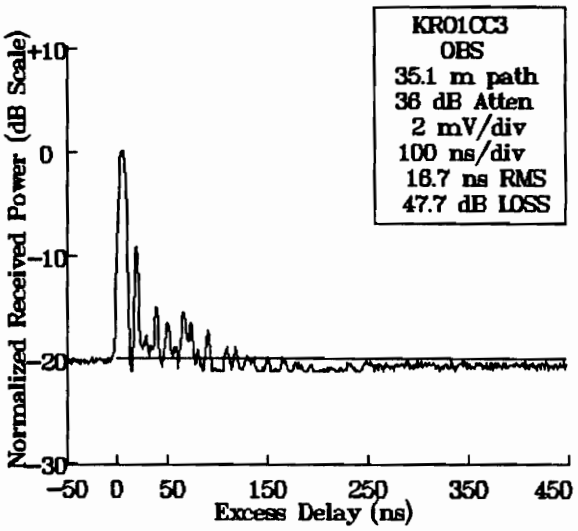
KR01CC3
OBS
35.1 m path
36 dB Atten
2 mV/div
100 ns/div
16.7 ns RMS
47.7 dB LOSS
Normalized Received Power (dB Scale)
+10
0
-10
-20
-30
-50 0 50 150 250 350 450
Excess Delay (ns)

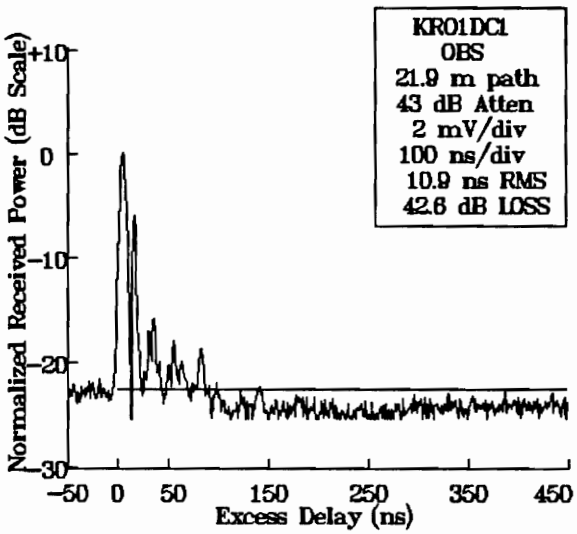
KR01DC1
OBS
21.9 m path
43 dB Atten
2 mV/div
100 ns/div
10.9 ns RMS
42.6 dB LOSS
Normalized Received Power (dB Scale)
+10
0
-10
-20
-30
-50 0 50 150 250 350 450
Excess Delay (ns)

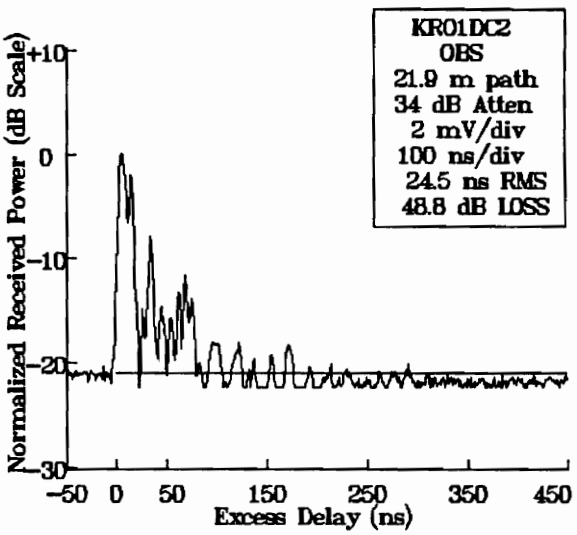
KR01DC2
OBS
21.9 m path
34 dB Atten
2 mV/div
100 ns/div
24.5 ns RMS
48.8 dB LOSS
Normalized Received Power (dB Scale)
+10
0
-10
-20
-30
-50 0 50 150 250 350 450
Excess Delay (ns)

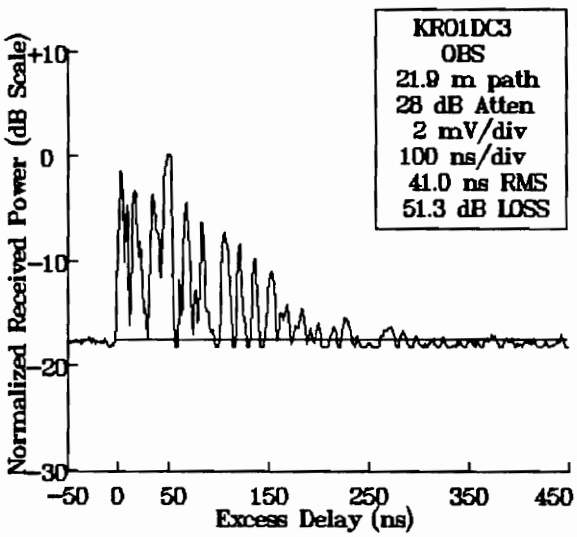
KR01DC3
OBS
21.9 m path
28 dB Atten
2 mV/div
100 ns/div
41.0 ns RMS
51.3 dB LOSS
Normalized Received Power (dB Scale)
+10
0
-10
-20
-30
-50 0 50 150 250 350 450
Excess Delay (ns)

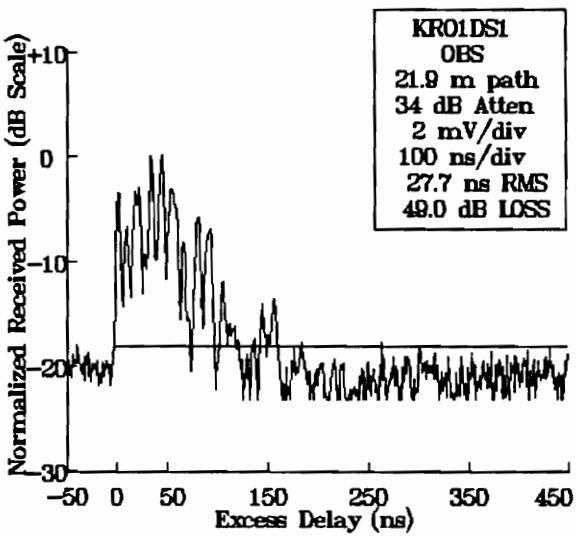
KR01DS1
OBS
21.9 m path
34 dB Atten
2 mV/div
100 ns/div
27.7 ns RMS
49.0 dB LOSS
Normalized Received Power (dB Scale)
+10
0
-10
-20
-30
-50 0 50 150 250 350 450
Excess Delay (ns)

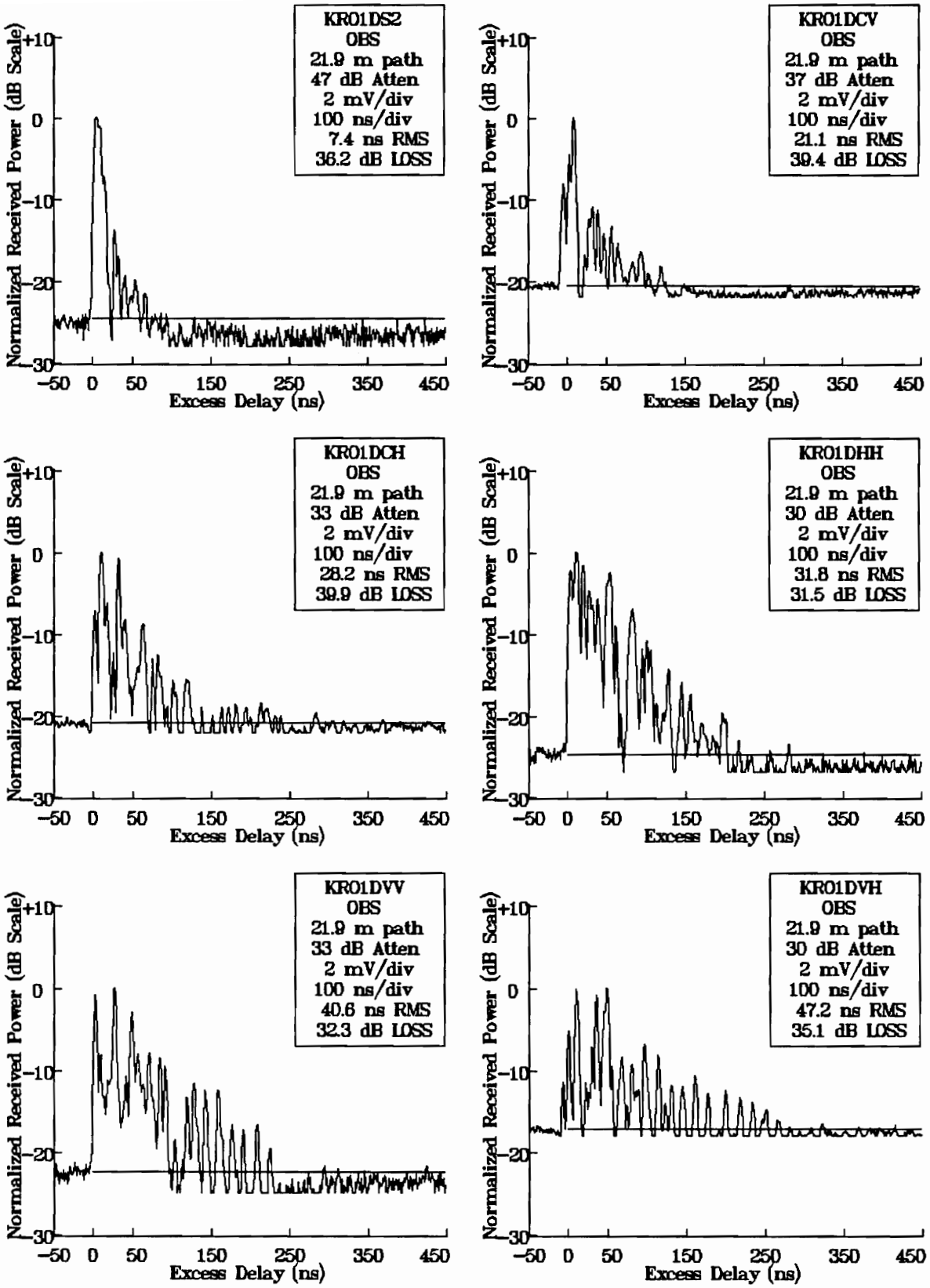
KR01DS2
OBS
21.9 m path
47 dB Atten
2 mV/div
100 ns/div
7.4 ns RMS
36.2 dB LOSS
KR01DCV
OBS
21.9 m path
37 dB Atten
2 mV/div
100 ns/div
21.1 ns RMS
39.4 dB LOSS
KR01DCH
OBS
21.9 m path
33 dB Atten
2 mV/div
100 ns/div
28.2 ns RMS
39.9 dB LOSS
KR01DHH
OBS
21.9 m path
30 dB Atten
2 mV/div
100 ns/div
31.8 ns RMS
31.5 dB LOSS
KR01DVV
OBS
21.9 m path
33 dB Atten
2 mV/div
100 ns/div
40.6 ns RMS
32.3 dB LOSS
KR01DVH
OBS
21.9 m path
30 dB Atten
2 mV/div
100 ns/div
47.2 ns RMS
35.1 dB LOSS
Normalized Received Power (dB Scale)
+10
0
-10
-20
-30
-50 0 50 150 250 350 450
Excess Delay (ns)

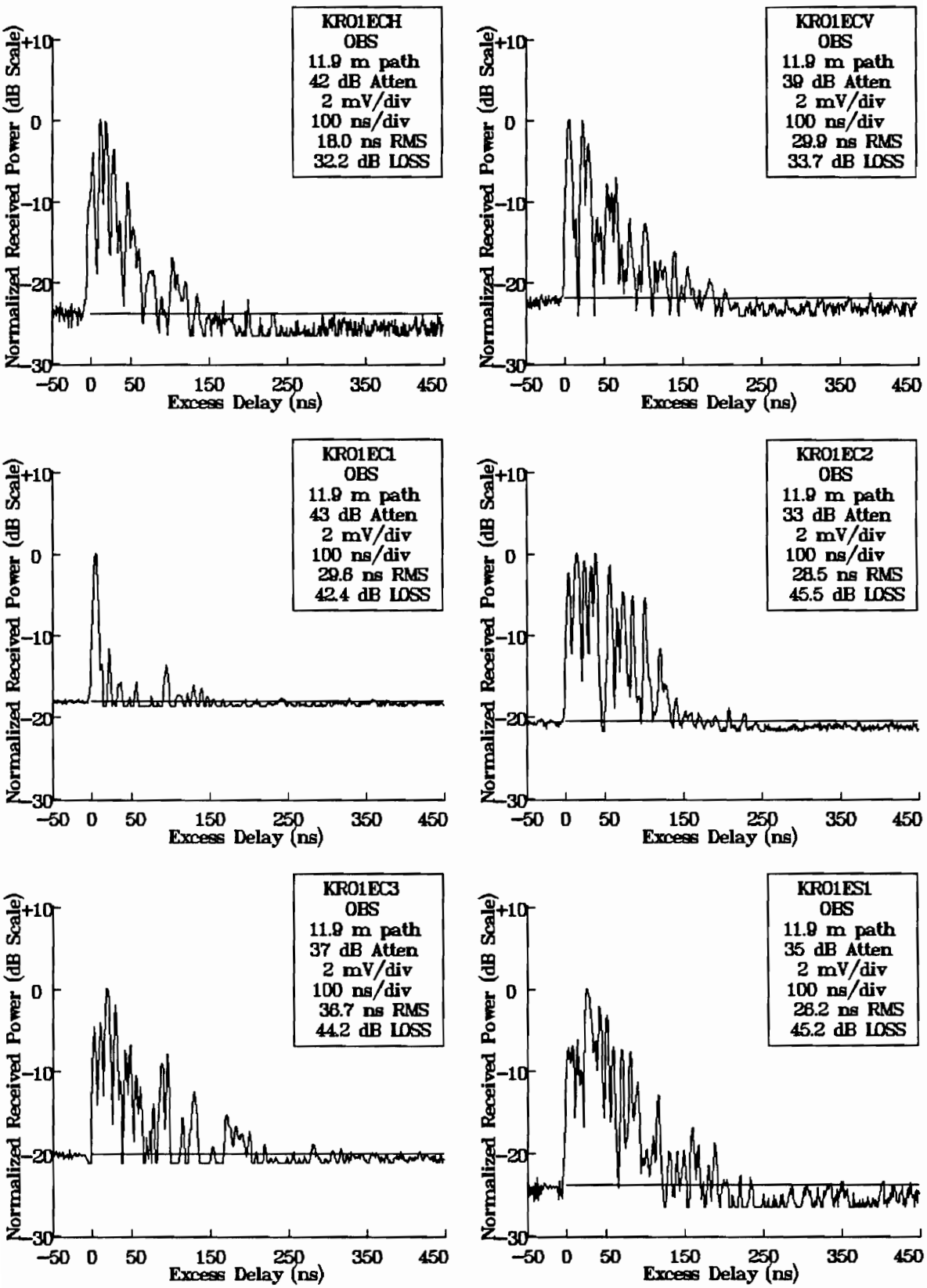
KR01ECH
OBS
11.9 m path
42 dB Atten
2 mV/div
100 ns/div
18.0 ns RMS
32.2 dB LOSS
KR01ECV
OBS
11.9 m path
39 dB Atten
2 mV/div
100 ns/div
29.9 ns RMS
33.7 dB LOSS
KR01EC1
OBS
11.9 m path
43 dB Atten
2 mV/div
100 ns/div
29.6 ns RMS
42.4 dB LOSS
KR01EC2
OBS
11.9 m path
33 dB Atten
2 mV/div
100 ns/div
28.5 ns RMS
45.5 dB LOSS
KR01EC3
OBS
11.9 m path
37 dB Atten
2 mV/div
100 ns/div
36.7 ns RMS
44.2 dB LOSS
KR01ES1
OBS
11.9 m path
35 dB Atten
2 mV/div
100 ns/div
26.2 ns RMS
45.2 dB LOSS
Normalized Received Power (dB Scale)
+10
0
-10
-20
-30
-50 0 50 150 250 350 450
Excess Delay (ns)

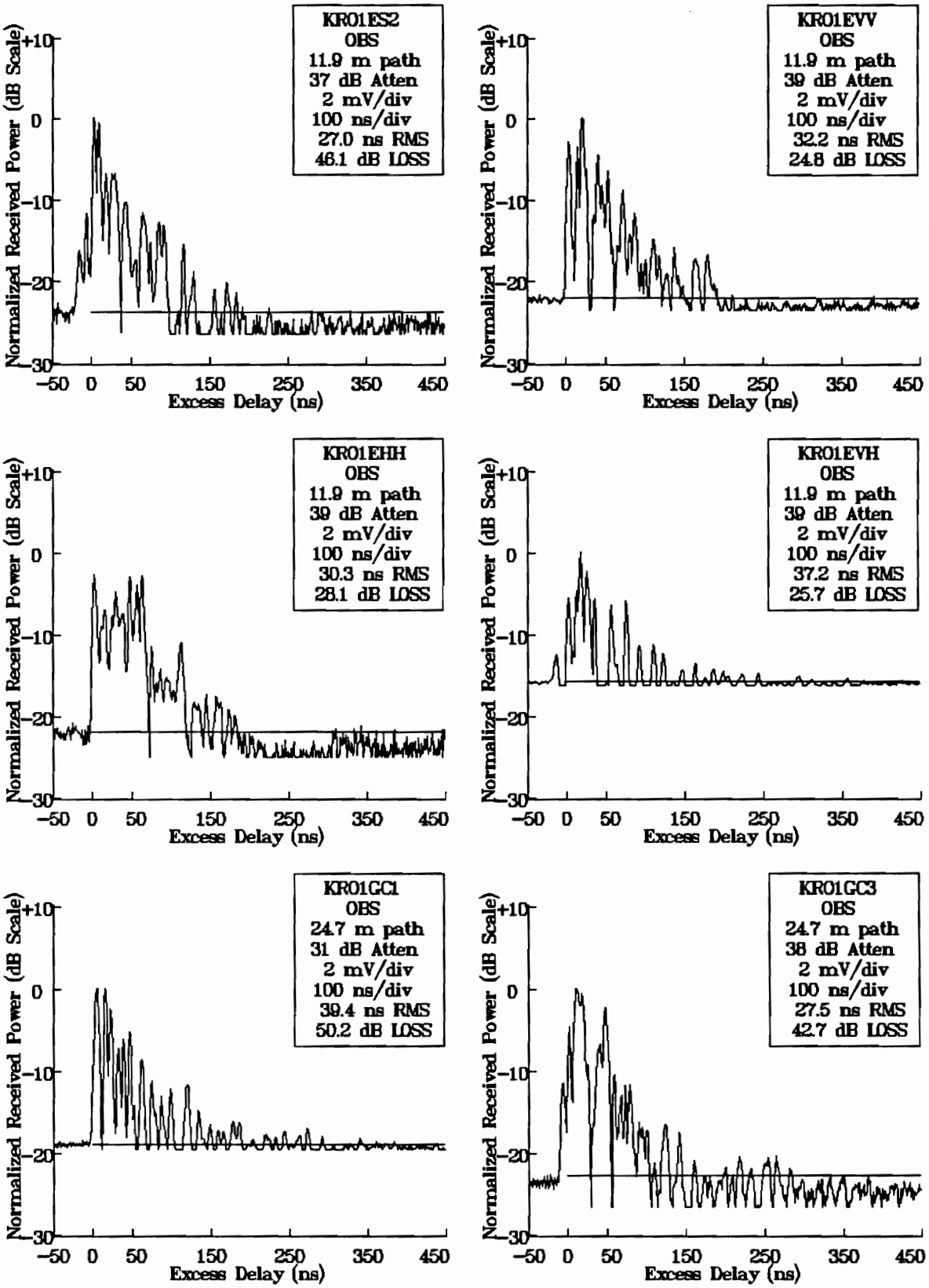
KR01ES2
OBS
11.9 m path
37 dB Atten
2 mV/div
100 ns/div
27.0 ns RMS
46.1 dB LOSS
KR01EVV
OBS
11.9 m path
39 dB Atten
2 mV/div
100 ns/div
32.2 ns RMS
24.8 dB LOSS
KR01EHH
OBS
11.9 m path
39 dB Atten
2 mV/div
100 ns/div
30.3 ns RMS
28.1 dB LOSS
KR01EVH
OBS
11.9 m path
39 dB Atten
2 mV/div
100 ns/div
37.2 ns RMS
25.7 dB LOSS
KR01GC1
OBS
24.7 m path
31 dB Atten
2 mV/div
100 ns/div
39.4 ns RMS
50.2 dB LOSS
KR01GC3
OBS
24.7 m path
38 dB Atten
2 mV/div
100 ns/div
27.5 ns RMS
42.7 dB LOSS
Normalized Received Power (dB Scale)
+10
0
-10
-20
-30
-50 0 50 150 250 350 450
Excess Delay (ns)

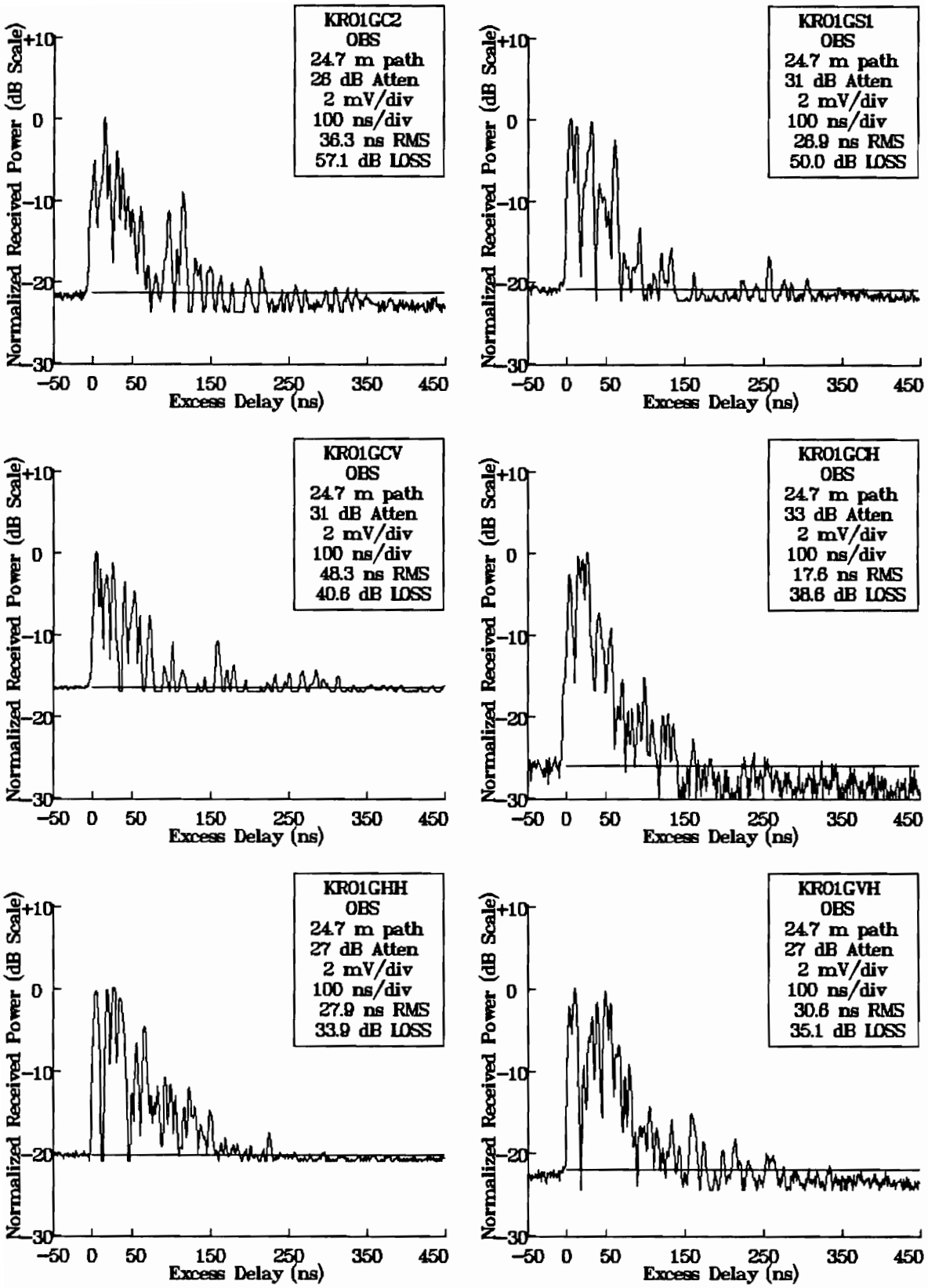
KR01GC2
OBS
24.7 m path
26 dB Atten
2 mV/div
100 ns/div
36.3 ns RMS
57.1 dB LOSS
KR01GS1
OBS
24.7 m path
31 dB Atten
2 mV/div
100 ns/div
26.9 ns RMS
50.0 dB LOSS
KR01GCV
OBS
24.7 m path
31 dB Atten
2 mV/div
100 ns/div
48.3 ns RMS
40.6 dB LOSS
KR01GCH
OBS
24.7 m path
33 dB Atten
2 mV/div
100 ns/div
17.6 ns RMS
38.6 dB LOSS
KR01GHH
OBS
24.7 m path
27 dB Atten
2 mV/div
100 ns/div
27.9 ns RMS
33.9 dB LOSS
KR01GVH
OBS
24.7 m path
27 dB Atten
2 mV/div
100 ns/div
30.6 ns RMS
35.1 dB LOSS
Normalized Received Power (dB Scale)
+10
0
-10
-20
-30
-50 0 50 150 250 350 450
Excess Delay (ns)

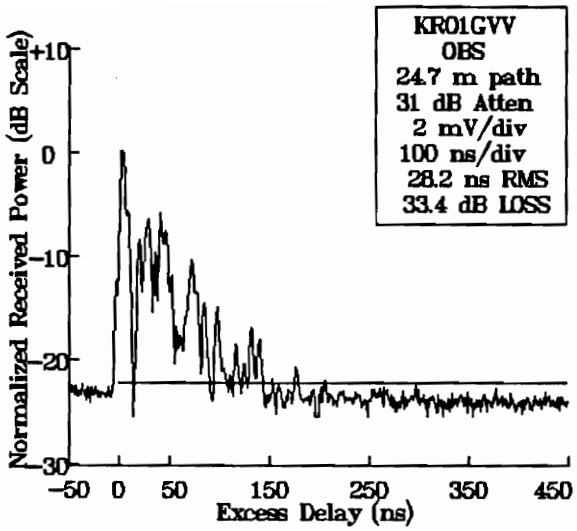
KRO1GVV
OBS
24.7 m path
31 dB Atten
2 mV/div
100 ns/div
28.2 ns RMS
33.4 dB LOSS
Normalized Received Power (dB Scale)
+10
0
-10
-20
-30
-50 0 50 150 250 350 450
Excess Delay (ns)

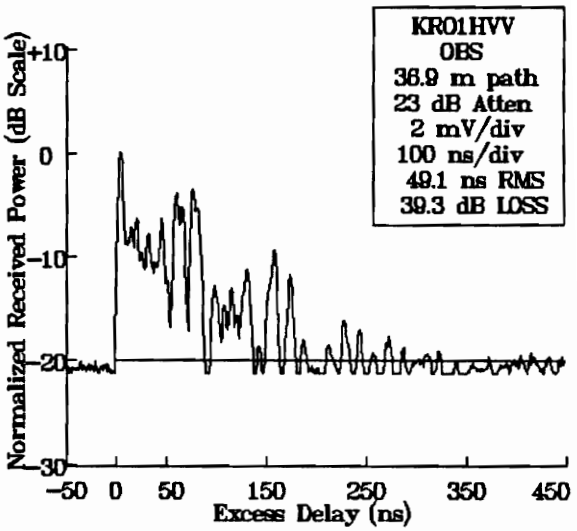
KRO1HVV
OBS
36.9 m path
23 dB Atten
2 mV/div
100 ns/div
49.1 ns RMS
39.3 dB LOSS
Normalized Received Power (dB Scale)
+10
0
-10
-20
-30
-50 0 50 150 250 350 450
Excess Delay (ns)

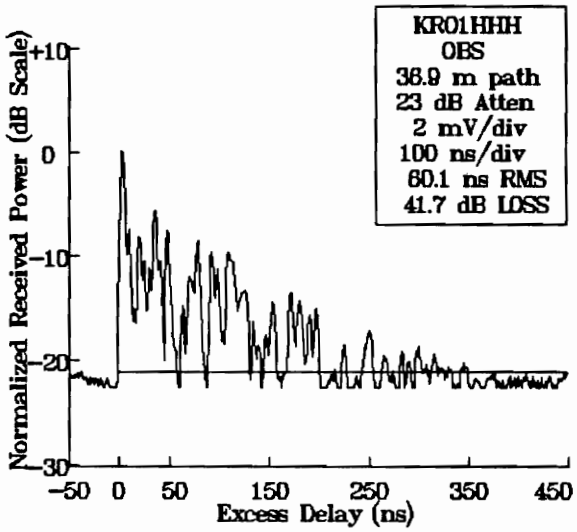
KRO1HHH
OBS
36.9 m path
23 dB Atten
2 mV/div
100 ns/div
60.1 ns RMS
41.7 dB LOSS
Normalized Received Power (dB Scale)
+10
0
-10
-20
-30
-50 0 50 150 250 350 450
Excess Delay (ns)

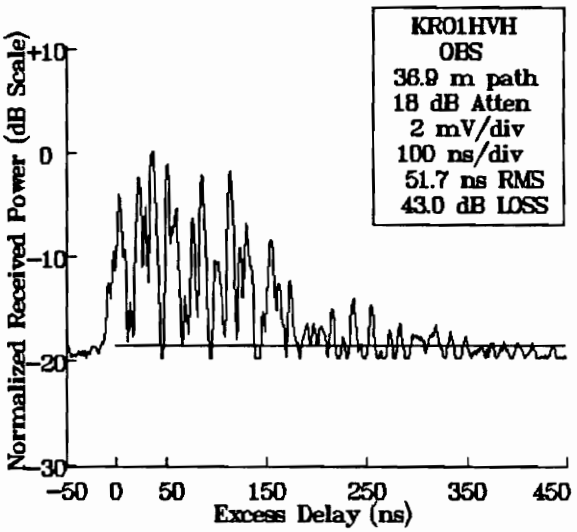
KRO1HVH
OBS
36.9 m path
18 dB Atten
2 mV/div
100 ns/div
51.7 ns RMS
43.0 dB LOSS
Normalized Received Power (dB Scale)
+10
0
-10
-20
-30
-50 0 50 150 250 350 450
Excess Delay (ns)

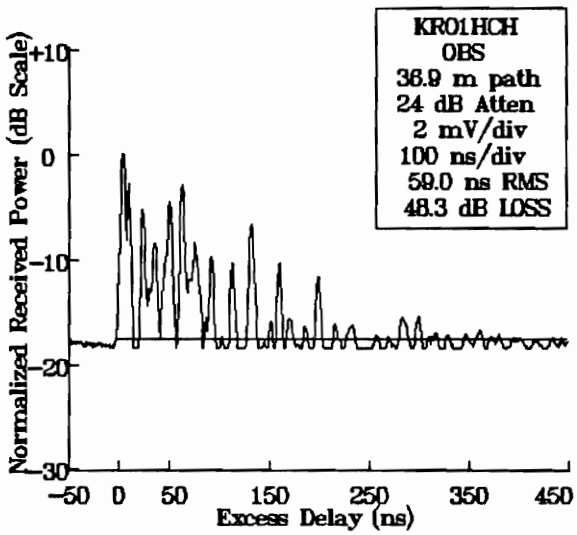
KRO1HCH
OBS
36.9 m path
24 dB Atten
2 mV/div
100 ns/div
59.0 ns RMS
48.3 dB LOSS
Normalized Received Power (dB Scale)
+10
0
-10
-20
-30
-50 0 50 150 250 350 450
Excess Delay (ns)

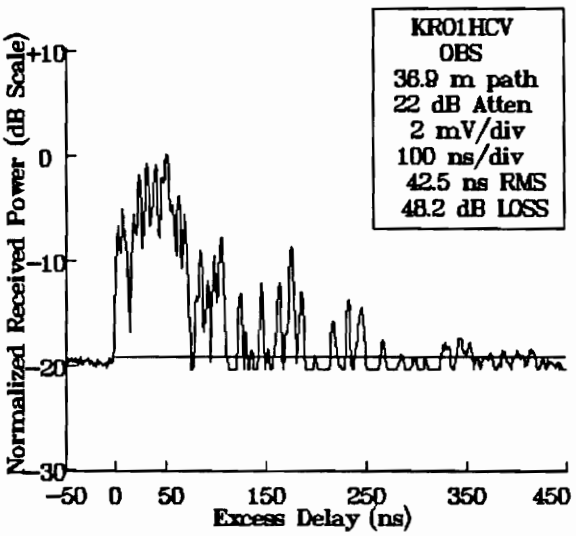
KRO1HCV
OBS
36.9 m path
22 dB Atten
2 mV/div
100 ns/div
42.5 ns RMS
48.2 dB LOSS
Normalized Received Power (dB Scale)
+10
0
-10
-20
-30
-50 0 50 150 250 350 450
Excess Delay (ns)

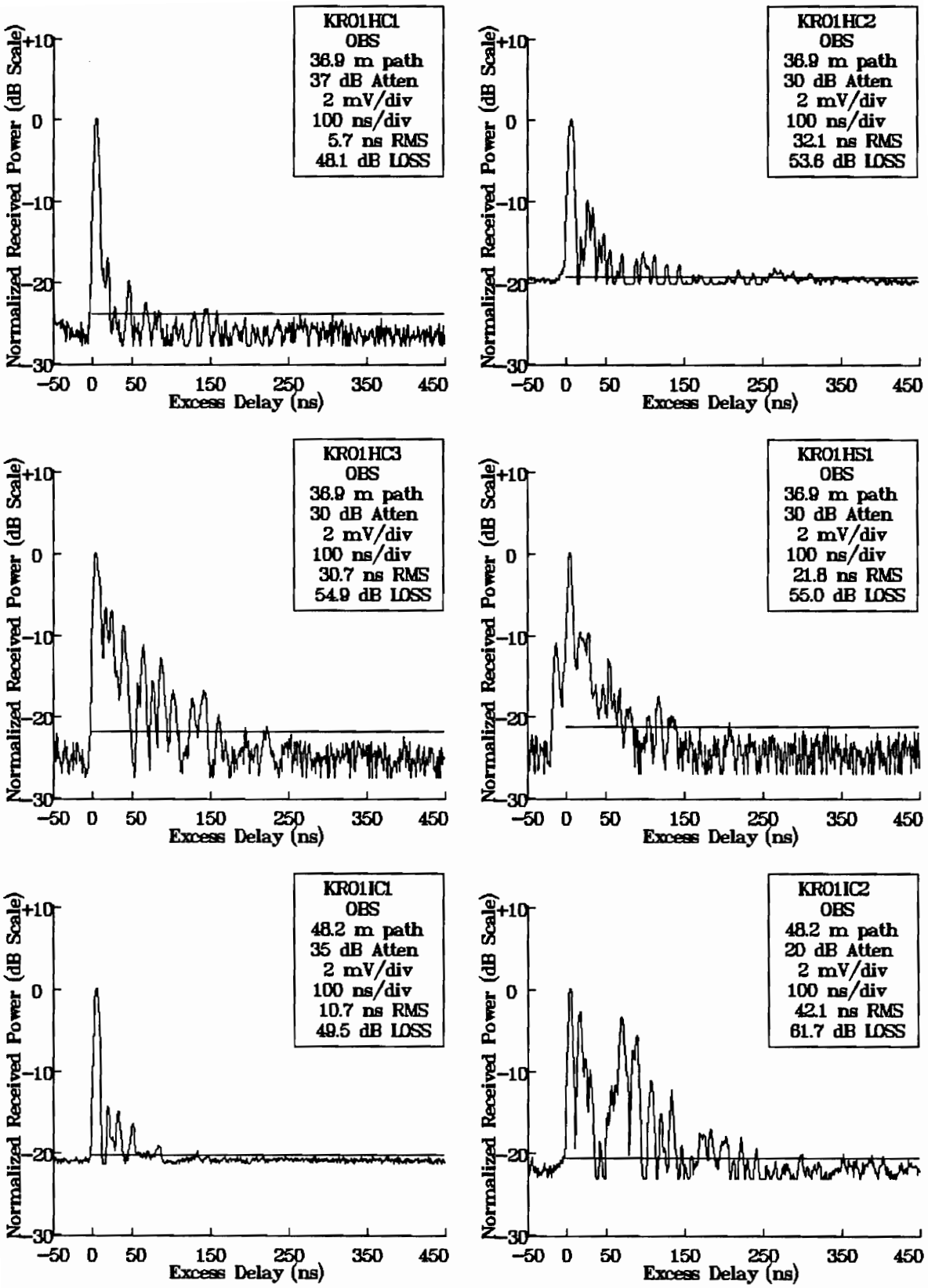
KR01HC1
OBS
36.9 m path
37 dB Atten
2 mV/div
100 ns/div
5.7 ns RMS
48.1 dB LOSS
KR01HC2
OBS
36.9 m path
30 dB Atten
2 mV/div
100 ns/div
32.1 ns RMS
53.6 dB LOSS
KR01HC3
OBS
36.9 m path
30 dB Atten
2 mV/div
100 ns/div
30.7 ns RMS
54.9 dB LOSS
KR01HS1
OBS
36.9 m path
30 dB Atten
2 mV/div
100 ns/div
21.8 ns RMS
55.0 dB LOSS
KR01IC1
OBS
48.2 m path
35 dB Atten
2 mV/div
100 ns/div
10.7 ns RMS
49.5 dB LOSS
KR01IC2
OBS
48.2 m path
20 dB Atten
2 mV/div
100 ns/div
42.1 ns RMS
61.7 dB LOSS
Normalized Received Power (dB Scale)
+10
0
-10
-20
-30
-50 0 50 150 250 350 450
Excess Delay (ns)

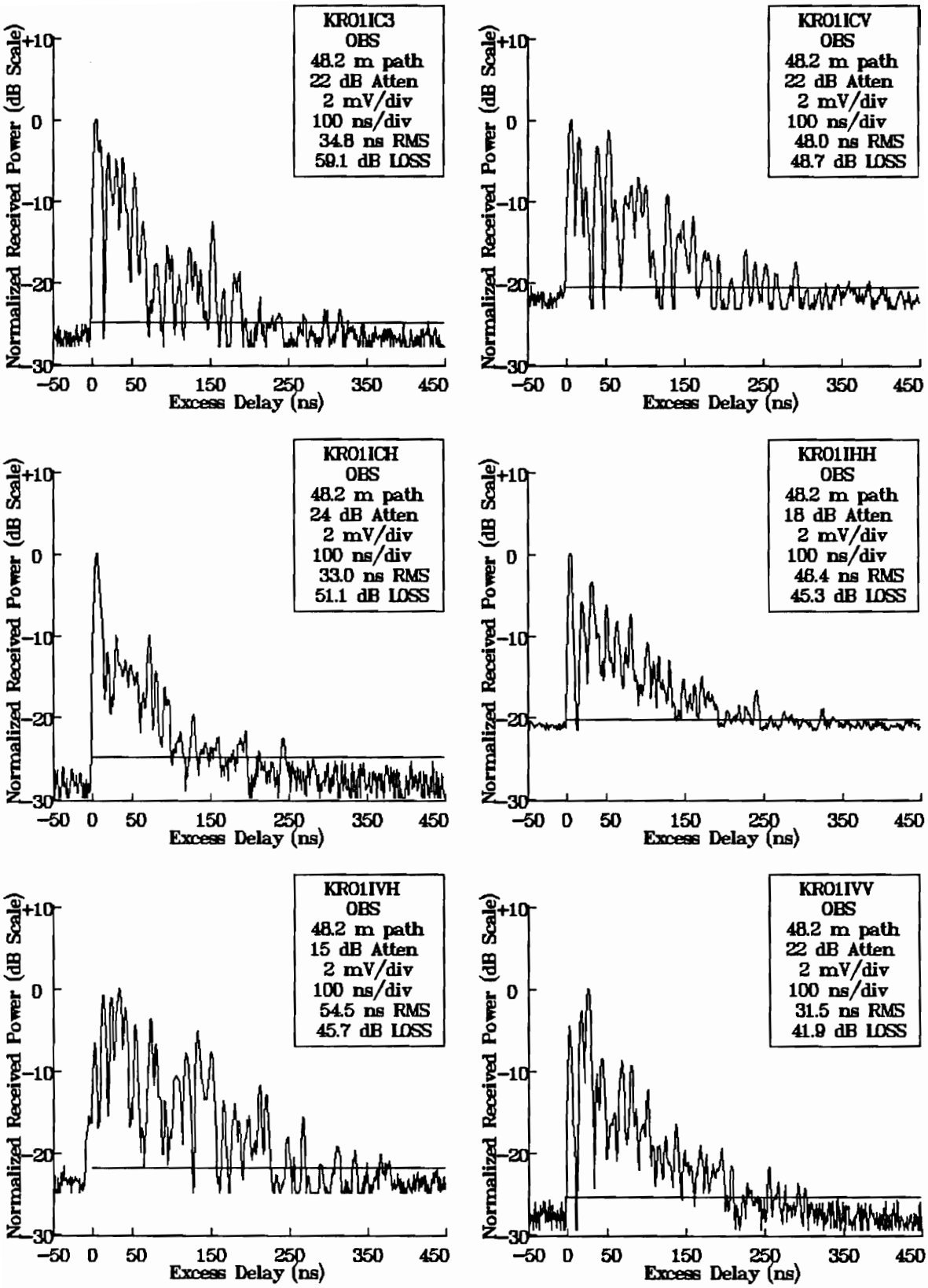
KR01IC3
OBS
48.2 m path
22 dB Atten
2 mV/div
100 ns/div
34.8 ns RMS
59.1 dB LOSS
KR01ICV
OBS
48.2 m path
22 dB Atten
2 mV/div
100 ns/div
48.0 ns RMS
48.7 dB LOSS
KR01ICH
OBS
48.2 m path
24 dB Atten
2 mV/div
100 ns/div
33.0 ns RMS
51.1 dB LOSS
KR01IHH
OBS
48.2 m path
18 dB Atten
2 mV/div
100 ns/div
46.4 ns RMS
45.3 dB LOSS
KR01IVH
OBS
48.2 m path
15 dB Atten
2 mV/div
100 ns/div
54.5 ns RMS
45.7 dB LOSS
KR01IVV
OBS
48.2 m path
22 dB Atten
2 mV/div
100 ns/div
31.5 ns RMS
41.9 dB LOSS
Normalized Received Power (dB Scale)
+10
0
-10
-20
-30
-50 0 50 150 250 350 450
Excess Delay (ns)

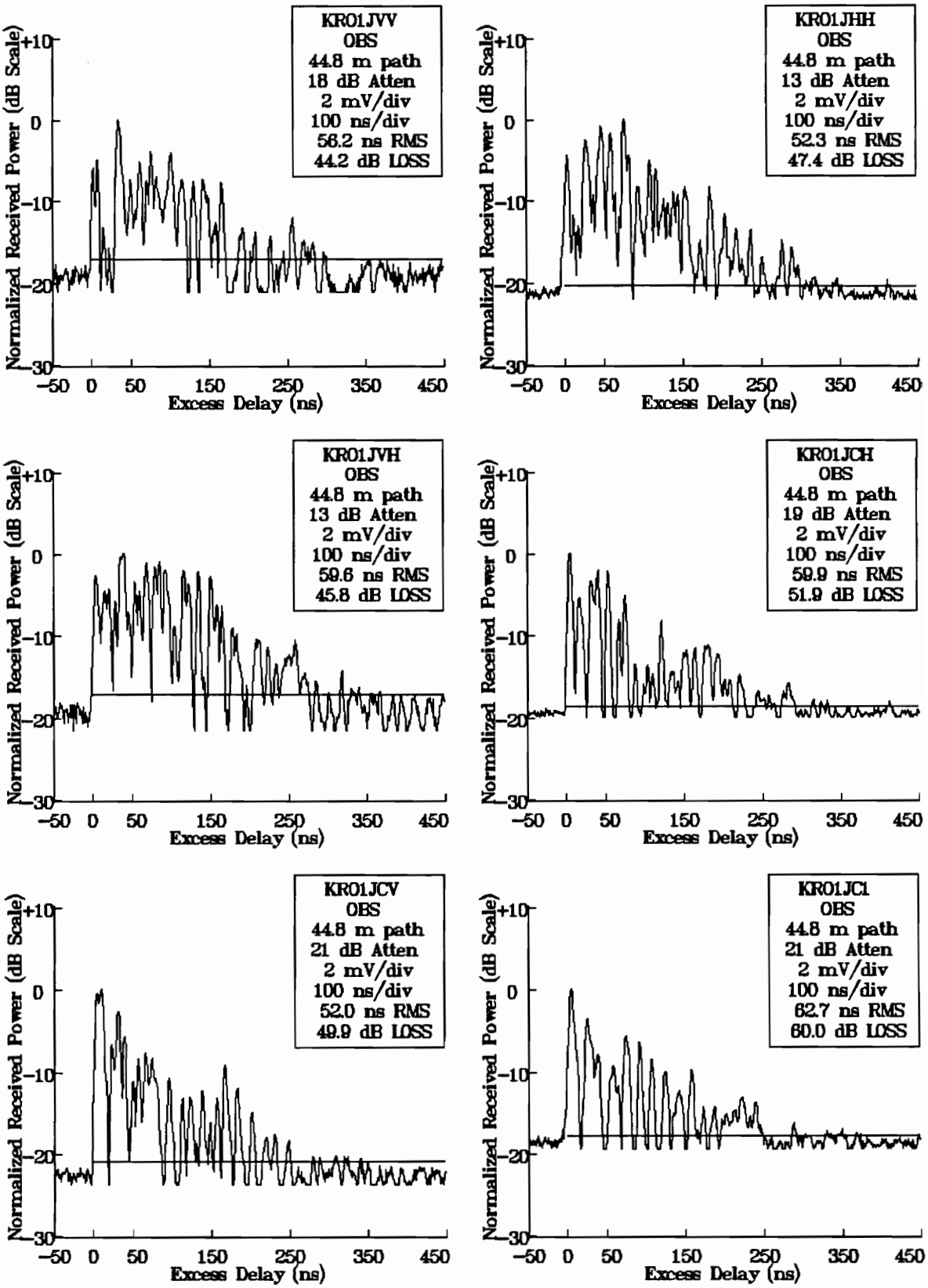
KRO1JVV
OBS
44.8 m path
18 dB Atten
2 mV/div
100 ns/div
56.2 ns RMS
44.2 dB LOSS
KRO1JHH
OBS
44.8 m path
13 dB Atten
2 mV/div
100 ns/div
52.3 ns RMS
47.4 dB LOSS
KRO1JVH
OBS
44.8 m path
13 dB Atten
2 mV/div
100 ns/div
59.6 ns RMS
45.8 dB LOSS
KRO1JCH
OBS
44.8 m path
19 dB Atten
2 mV/div
100 ns/div
59.9 ns RMS
51.9 dB LOSS
KRO1JCV
OBS
44.8 m path
21 dB Atten
2 mV/div
100 ns/div
52.0 ns RMS
49.9 dB LOSS
KRO1JC1
OBS
44.8 m path
21 dB Atten
2 mV/div
100 ns/div
62.7 ns RMS
60.0 dB LOSS
Normalized Received Power (dB Scale)
+10
0
-10
-20
-30
-50 0 50 150 250 350 450
Excess Delay (ns)

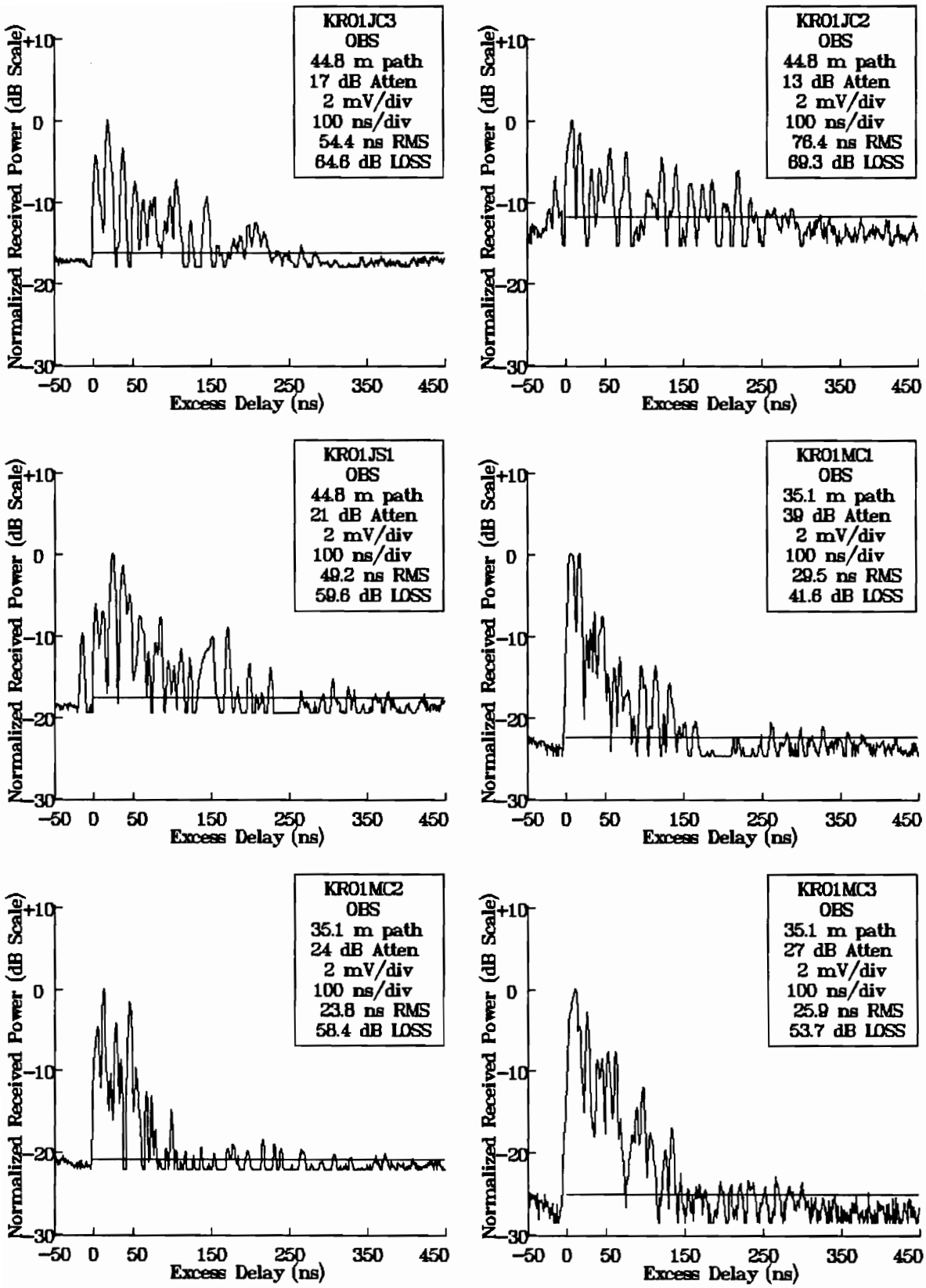
KR01JC3
OBS
44.8 m path
17 dB Atten
2 mV/div
100 ns/div
54.4 ns RMS
64.6 dB LOSS
KR01JC2
OBS
44.8 m path
13 dB Atten
2 mV/div
100 ns/div
76.4 ns RMS
69.3 dB LOSS
KR01JS1
OBS
44.8 m path
21 dB Atten
2 mV/div
100 ns/div
49.2 ns RMS
59.6 dB LOSS
KR01MC1
OBS
35.1 m path
39 dB Atten
2 mV/div
100 ns/div
29.5 ns RMS
41.6 dB LOSS
KR01MC2
OBS
35.1 m path
24 dB Atten
2 mV/div
100 ns/div
23.8 ns RMS
58.4 dB LOSS
KR01MC3
OBS
35.1 m path
27 dB Atten
2 mV/div
100 ns/div
25.9 ns RMS
53.7 dB LOSS
Normalized Received Power (dB Scale)
+10
0
-10
-20
-30
-50 0 50 150 250 350 450
Excess Delay (ns)

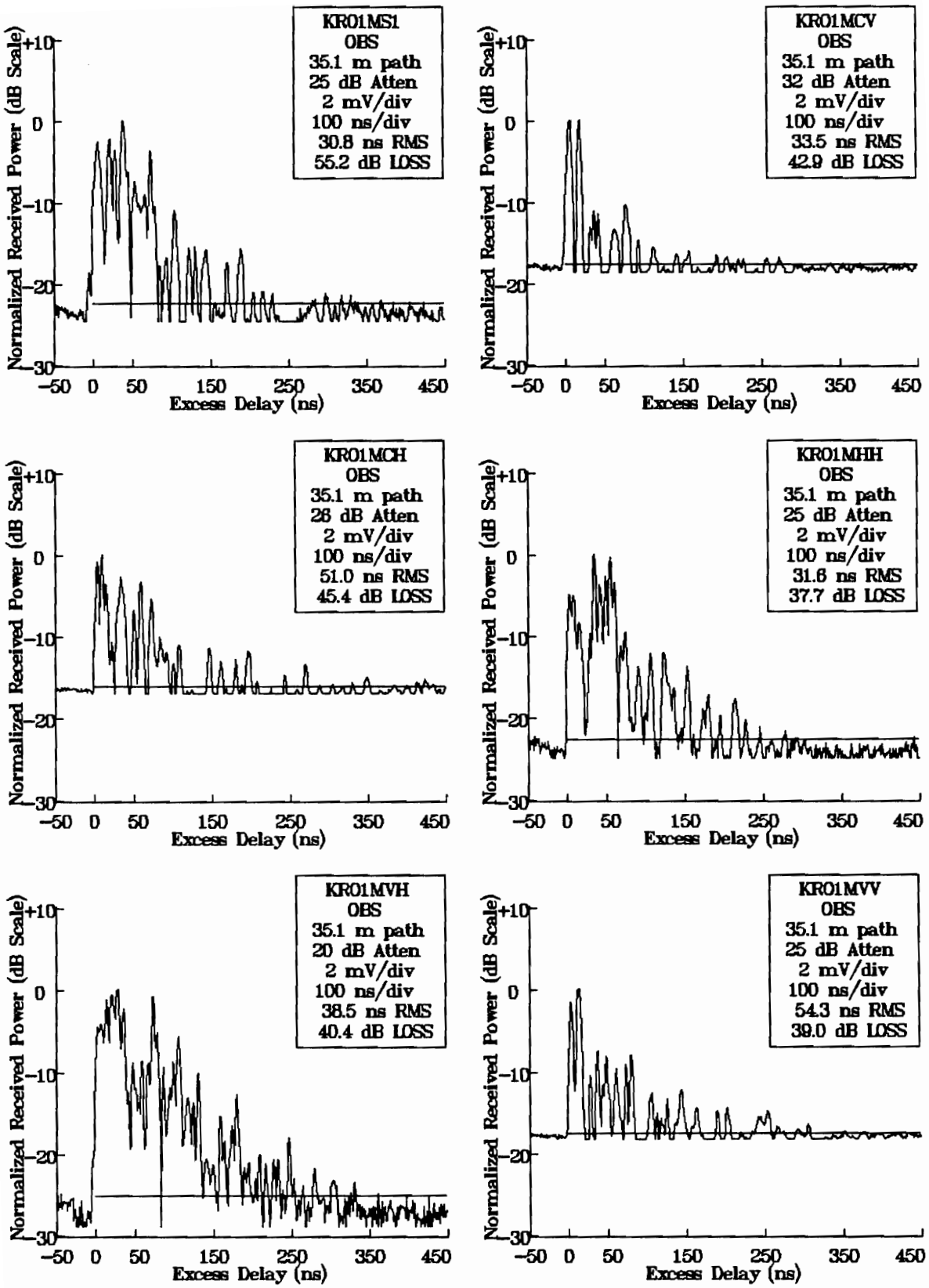
KRO1MS1
OBS
35.1 m path
25 dB Atten
2 mV/div
100 ns/div
30.8 ns RMS
55.2 dB LOSS
KRO1MCV
OBS
35.1 m path
32 dB Atten
2 mV/div
100 ns/div
33.5 ns RMS
42.9 dB LOSS
KRO1MCH
OBS
35.1 m path
26 dB Atten
2 mV/div
100 ns/div
51.0 ns RMS
45.4 dB LOSS
KRO1MHH
OBS
35.1 m path
25 dB Atten
2 mV/div
100 ns/div
31.6 ns RMS
37.7 dB LOSS
KRO1MVH
OBS
35.1 m path
20 dB Atten
2 mV/div
100 ns/div
38.5 ns RMS
40.4 dB LOSS
KRO1MVV
OBS
35.1 m path
25 dB Atten
2 mV/div
100 ns/div
54.3 ns RMS
39.0 dB LOSS
Normalized Received Power (dB Scale)
+10
0
-10
-20
-30
-50 0 50 150 250 350 450
Excess Delay (ns)

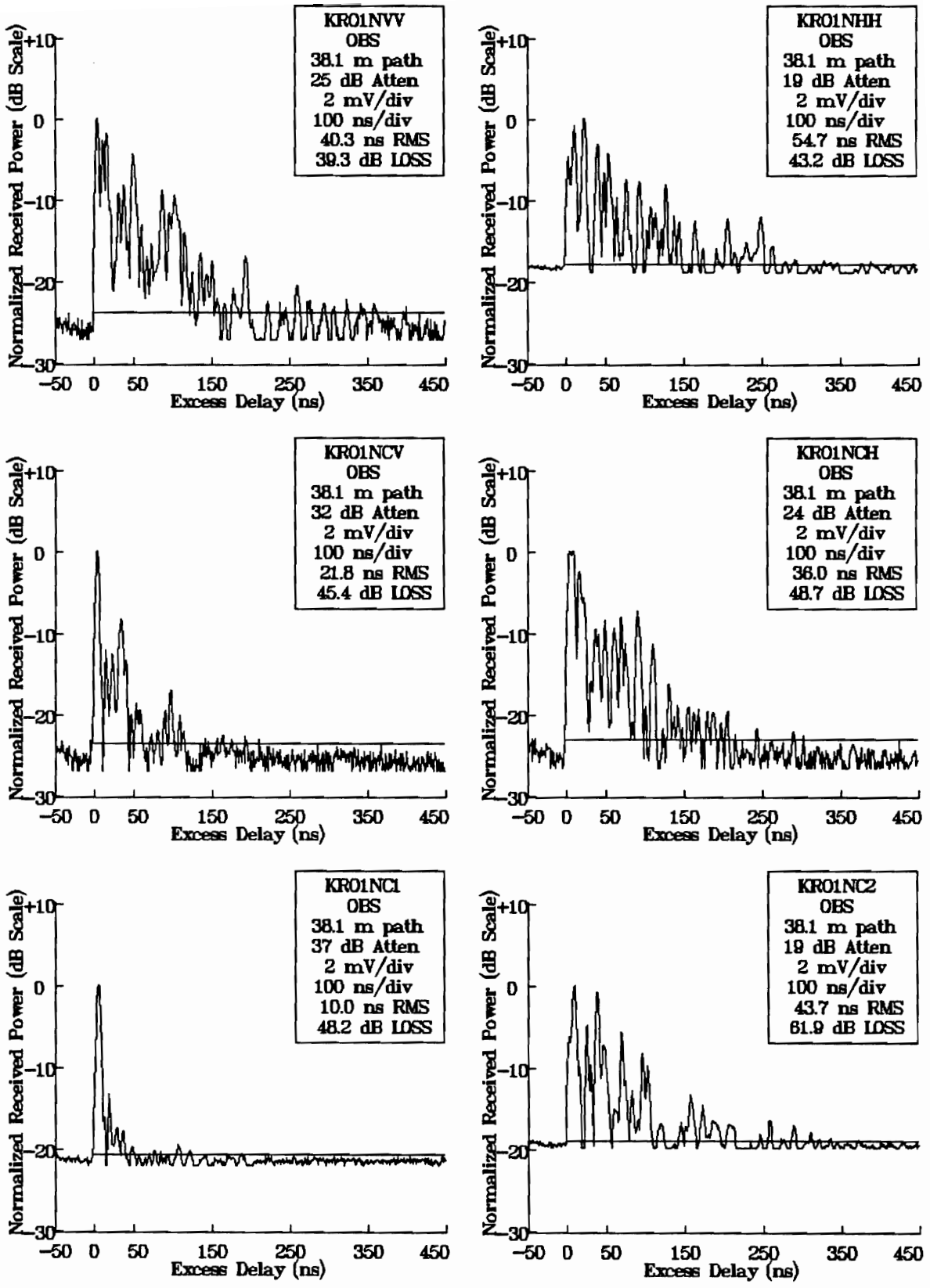
KR01NVV
OBS
38.1 m path
25 dB Atten
2 mV/div
100 ns/div
40.3 ns RMS
39.3 dB LOSS
KR01NHH
OBS
38.1 m path
19 dB Atten
2 mV/div
100 ns/div
54.7 ns RMS
43.2 dB LOSS
KR01NCV
OBS
38.1 m path
32 dB Atten
2 mV/div
100 ns/div
21.8 ns RMS
45.4 dB LOSS
KR01NCH
OBS
38.1 m path
24 dB Atten
2 mV/div
100 ns/div
36.0 ns RMS
48.7 dB LOSS
KR01NC1
OBS
38.1 m path
37 dB Atten
2 mV/div
100 ns/div
10.0 ns RMS
48.2 dB LOSS
KR01NC2
OBS
38.1 m path
19 dB Atten
2 mV/div
100 ns/div
43.7 ns RMS
61.9 dB LOSS
Normalized Received Power (dB Scale)
+10
0
−10
−20
−30
−50 0 50 150 250 350 450
Excess Delay (ns)

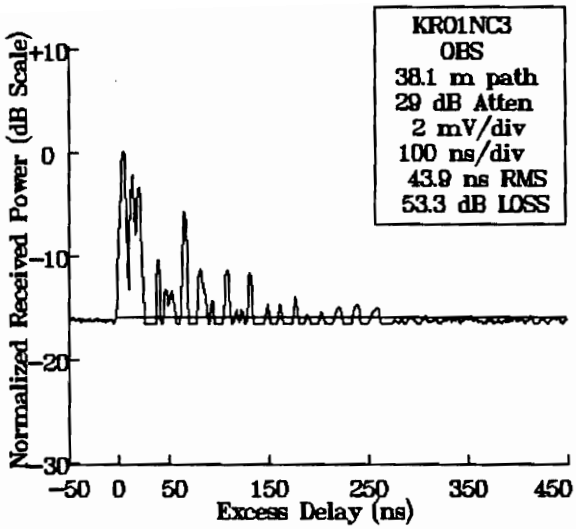
KR01NC3
OBS
38.1 m path
29 dB Atten
2 mV/div
100 ns/div
43.9 ns RMS
53.3 dB LOSS
Normalized Received Power (dB Scale)
+10
0
-10
-20
-30
-50 0 50 150 250 350 450
Excess Delay (ns)

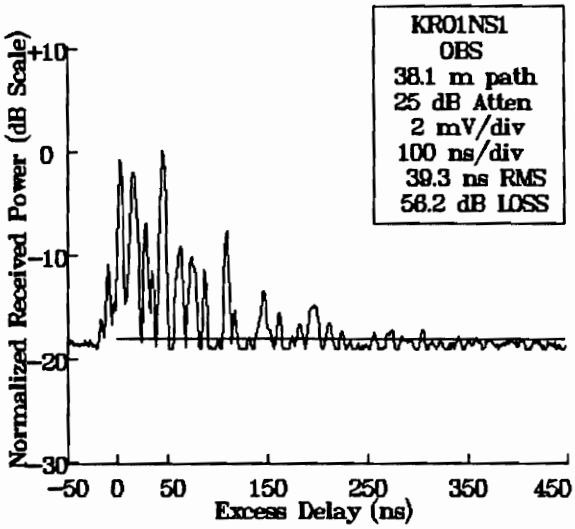
KR01NS1
OBS
38.1 m path
25 dB Atten
2 mV/div
100 ns/div
39.3 ns RMS
56.2 dB LOSS
Normalized Received Power (dB Scale)
+10
0
-10
-20
-30
-50 0 50 150 250 350 450
Excess Delay (ns)

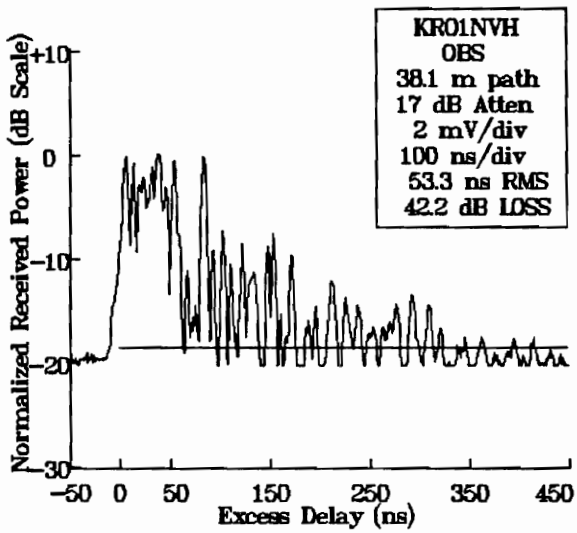
KR01NVH
OBS
38.1 m path
17 dB Atten
2 mV/div
100 ns/div
53.3 ns RMS
42.2 dB LOSS
Normalized Received Power (dB Scale)
+10
0
-10
-20
-30
-50 0 50 150 250 350 450
Excess Delay (ns)

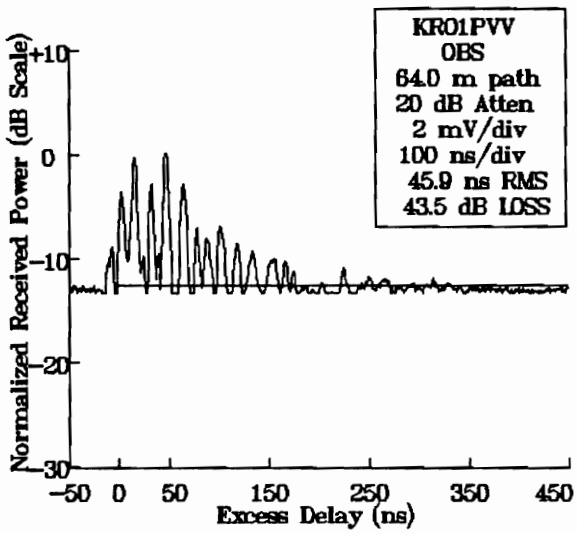
KR01PVV
OBS
64.0 m path
20 dB Atten
2 mV/div
100 ns/div
45.9 ns RMS
43.5 dB LOSS
Normalized Received Power (dB Scale)
+10
0
-10
-20
-30
-50 0 50 150 250 350 450
Excess Delay (ns)

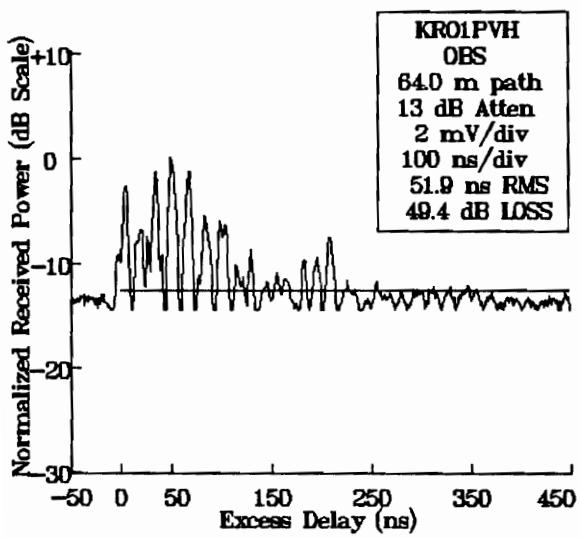
KR01PVH
OBS
64.0 m path
13 dB Atten
2 mV/div
100 ns/div
51.9 ns RMS
49.4 dB LOSS
Normalized Received Power (dB Scale)
+10
0
-10
-20
-30
-50 0 50 150 250 350 450
Excess Delay (ns)

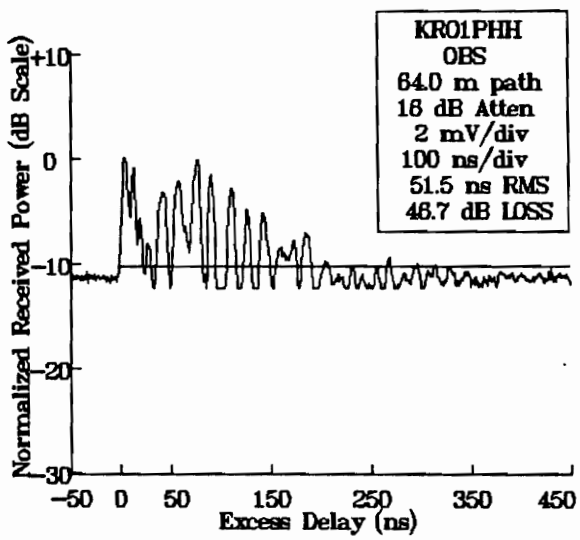
KR01PHH
OBS
64.0 m path
16 dB Atten
2 mV/div
100 ns/div
51.5 ns RMS
46.7 dB LOSS
Normalized Received Power (dB Scale)
+10
0
-10
-20
-30
-50 0 50 150 250 350 450
Excess Delay (ns)

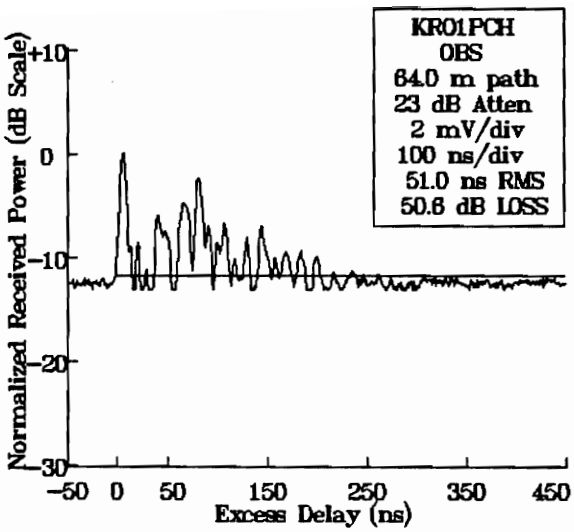
KR01PCH
OBS
64.0 m path
23 dB Atten
2 mV/div
100 ns/div
51.0 ns RMS
50.6 dB LOSS
Normalized Received Power (dB Scale)
+10
0
-10
-20
-30
-50 0 50 150 250 350 450
Excess Delay (ns)

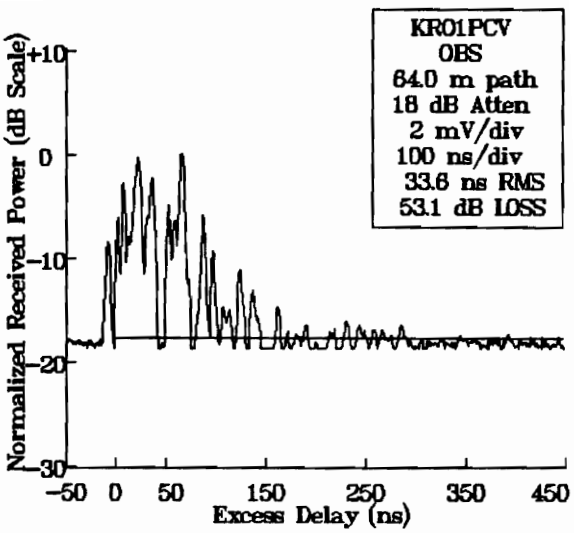
KR01PCV
OBS
64.0 m path
18 dB Atten
2 mV/div
100 ns/div
33.6 ns RMS
53.1 dB LOSS
Normalized Received Power (dB Scale)
+10
0
-10
-20
-30
-50 0 50 150 250 350 450
Excess Delay (ns)

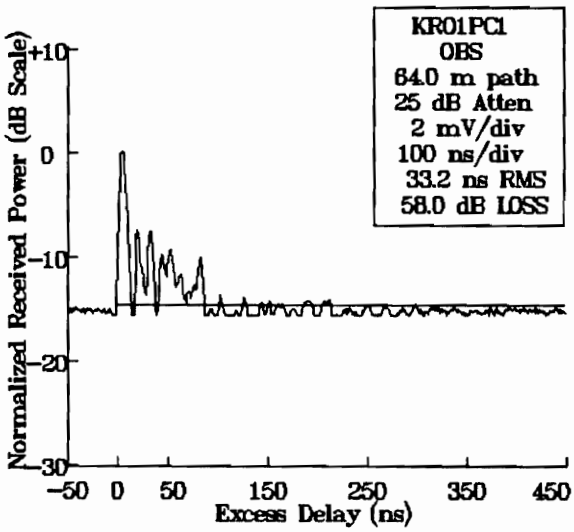
KR01PC1
OBS
64.0 m path
25 dB Atten
2 mV/div
100 ns/div
33.2 ns RMS
58.0 dB LOSS
Normalized Received Power (dB Scale)
+10
0
-10
-20
-30
-50 0 50 150 250 350 450
Excess Delay (ns)

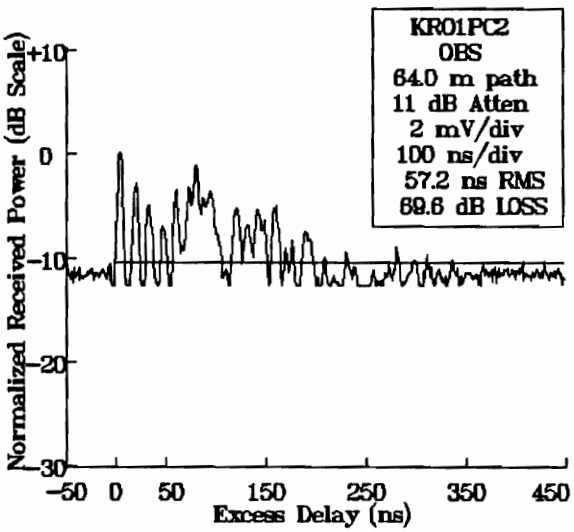
KR01PC2
OBS
64.0 m path
11 dB Atten
2 mV/div
100 ns/div
57.2 ns RMS
69.6 dB LOSS
Normalized Received Power (dB Scale)
+10
0
-10
-20
-30
-50 0 50 150 250 350 450
Excess Delay (ns)

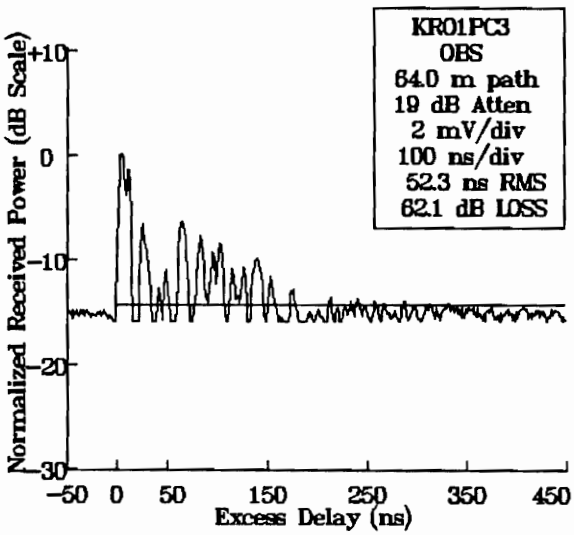
KR01PC3
OBS
64.0 m path
19 dB Atten
2 mV/div
100 ns/div
52.3 ns RMS
62.1 dB LOSS
Normalized Received Power (dB Scale)
+10
0
-10
-20
-30
-50 0 50 150 250 350 450
Excess Delay (ns)

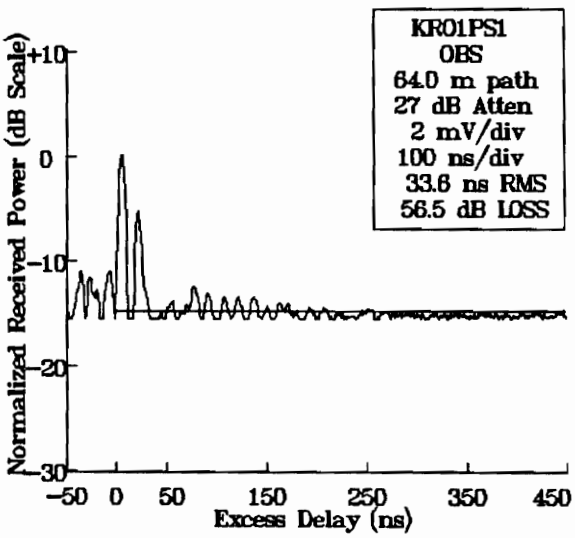
KR01PS1
OBS
64.0 m path
27 dB Atten
2 mV/div
100 ns/div
33.6 ns RMS
56.5 dB LOSS
Normalized Received Power (dB Scale)
+10
0
-10
-20
-30
-50 0 50 150 250 350 450
Excess Delay (ns)

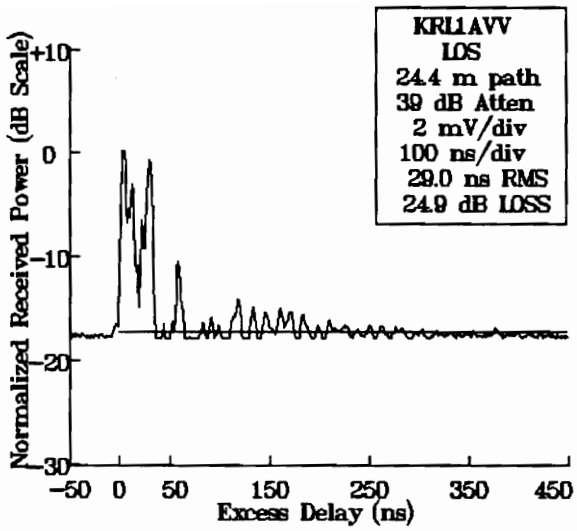
KRL1AVV
LOS
24.4 m path
39 dB Atten
2 mV/div
100 ns/div
29.0 ns RMS
24.9 dB LOSS
Normalized Received Power (dB Scale)
+10
0
-10
-20
-30
-50 0 50 150 250 350 450
Excess Delay (ns)

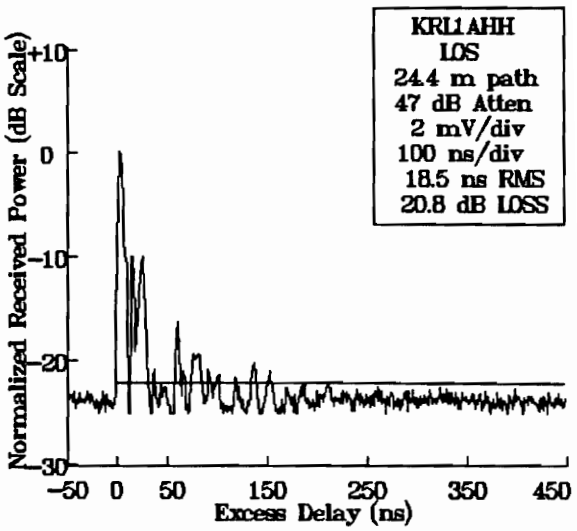
KRL1AHH
LOS
24.4 m path
47 dB Atten
2 mV/div
100 ns/div
18.5 ns RMS
20.8 dB LOSS
Normalized Received Power (dB Scale)
+10
0
-10
-20
-30
-50 0 50 150 250 350 450
Excess Delay (ns)

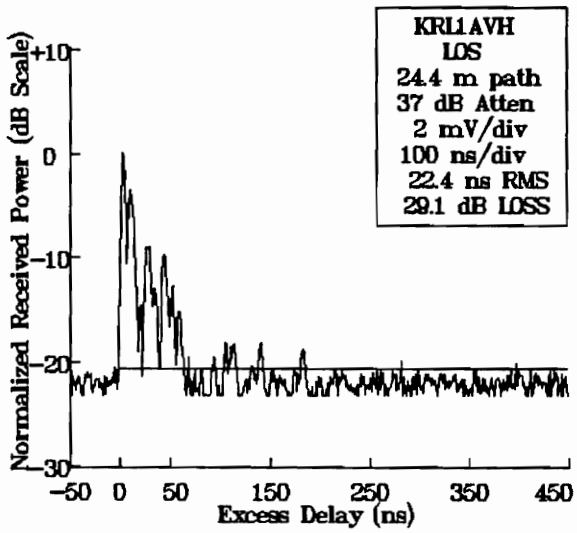
KRL1AVH
LOS
24.4 m path
37 dB Atten
2 mV/div
100 ns/div
22.4 ns RMS
29.1 dB LOSS
Normalized Received Power (dB Scale)
+10
0
-10
-20
-30
-50 0 50 150 250 350 450
Excess Delay (ns)

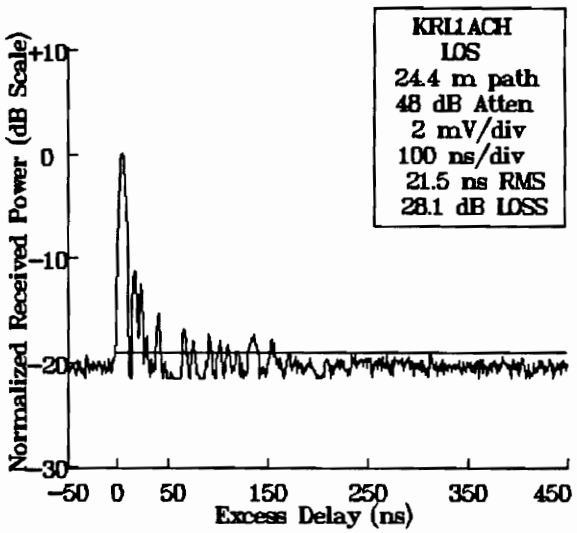
KRL1ACH
LOS
24.4 m path
48 dB Atten
2 mV/div
100 ns/div
21.5 ns RMS
28.1 dB LOSS
Normalized Received Power (dB Scale)
+10
0
-10
-20
-30
-50 0 50 150 250 350 450
Excess Delay (ns)

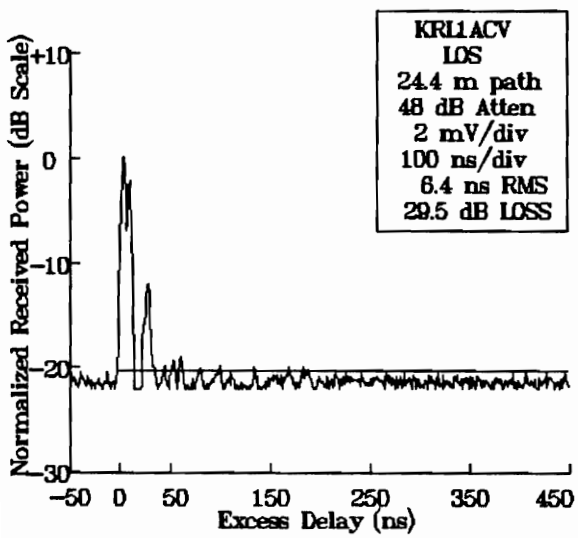
KRL1ACV
LOS
24.4 m path
48 dB Atten
2 mV/div
100 ns/div
6.4 ns RMS
29.5 dB LOSS
Normalized Received Power (dB Scale)
+10
0
-10
-20
-30
-50 0 50 150 250 350 450
Excess Delay (ns)

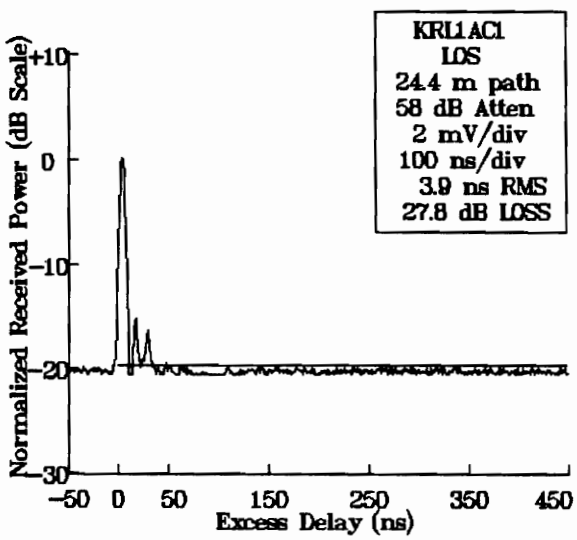
KRL1AC1
LOS
24.4 m path
58 dB Atten
2 mV/div
100 ns/div
3.9 ns RMS
27.8 dB LOSS
Normalized Received Power (dB Scale)
+10
0
-10
-20
-30
-50 0 50 150 250 350 450
Excess Delay (ns)

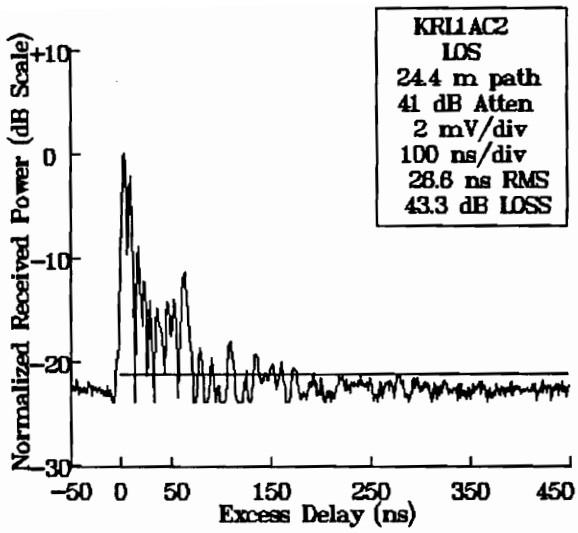
KRL1AC2
LOS
24.4 m path
41 dB Atten
2 mV/div
100 ns/div
28.6 ns RMS
43.3 dB LOSS
Normalized Received Power (dB Scale)
+10
0
-10
-20
-30
-50 0 50 150 250 350 450
Excess Delay (ns)

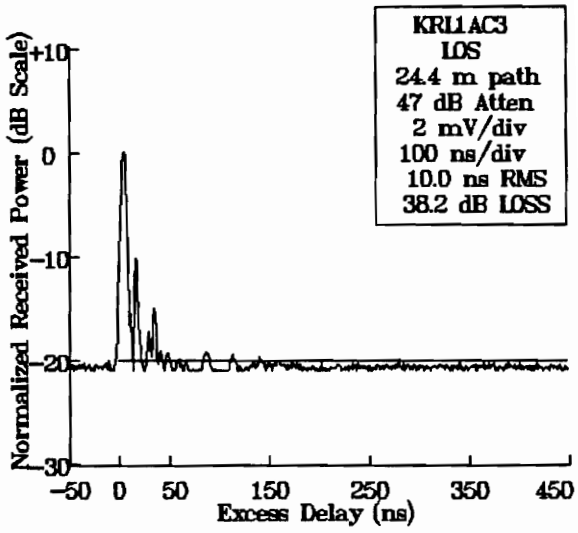
KRL1AC3
LOS
24.4 m path
47 dB Atten
2 mV/div
100 ns/div
10.0 ns RMS
38.2 dB LOSS
Normalized Received Power (dB Scale)
+10
0
-10
-20
-30
-50 0 50 150 250 350 450
Excess Delay (ns)

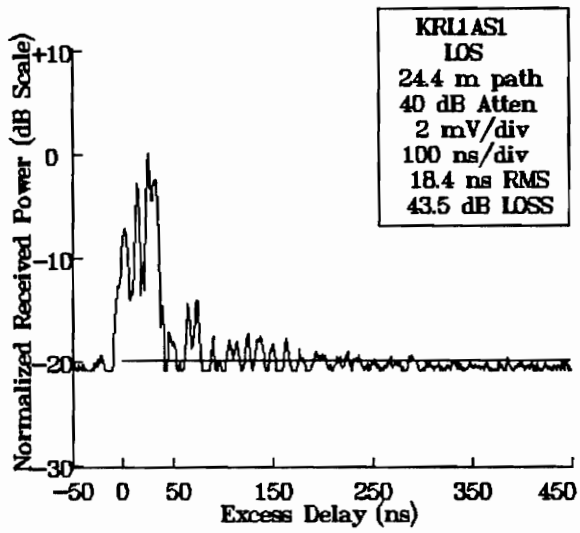
KRL1AS1
LOS
24.4 m path
40 dB Atten
2 mV/div
100 ns/div
18.4 ns RMS
43.5 dB LOSS
Normalized Received Power (dB Scale)
+10
0
-10
-20
-30
-50 0 50 150 250 350 450
Excess Delay (ns)

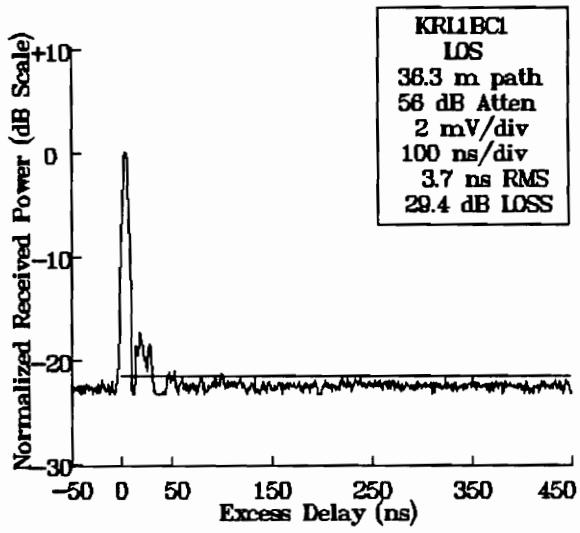
KRL1BC1
LOS
36.3 m path
56 dB Atten
2 mV/div
100 ns/div
3.7 ns RMS
29.4 dB LOSS
Normalized Received Power (dB Scale)
+10
0
-10
-20
-30
-50 0 50 150 250 350 450
Excess Delay (ns)

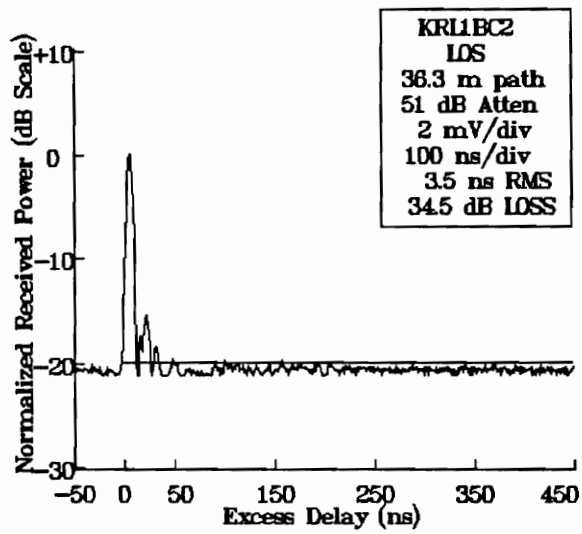
KRL1BC2
LOS
36.3 m path
51 dB Atten
2 mV/div
100 ns/div
3.5 ns RMS
34.5 dB LOSS
Normalized Received Power (dB Scale)
+10
0
-10
-20
-30
-50 0 50 150 250 350 450
Excess Delay (ns)

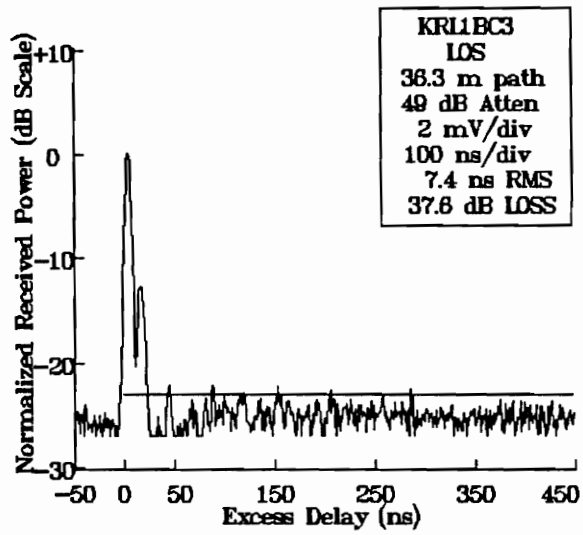
KRL1BC3
LOS
36.3 m path
49 dB Atten
2 mV/div
100 ns/div
7.4 ns RMS
37.6 dB LOSS
Normalized Received Power (dB Scale)
+10
0
-10
-20
-30
-50 0 50 150 250 350 450
Excess Delay (ns)

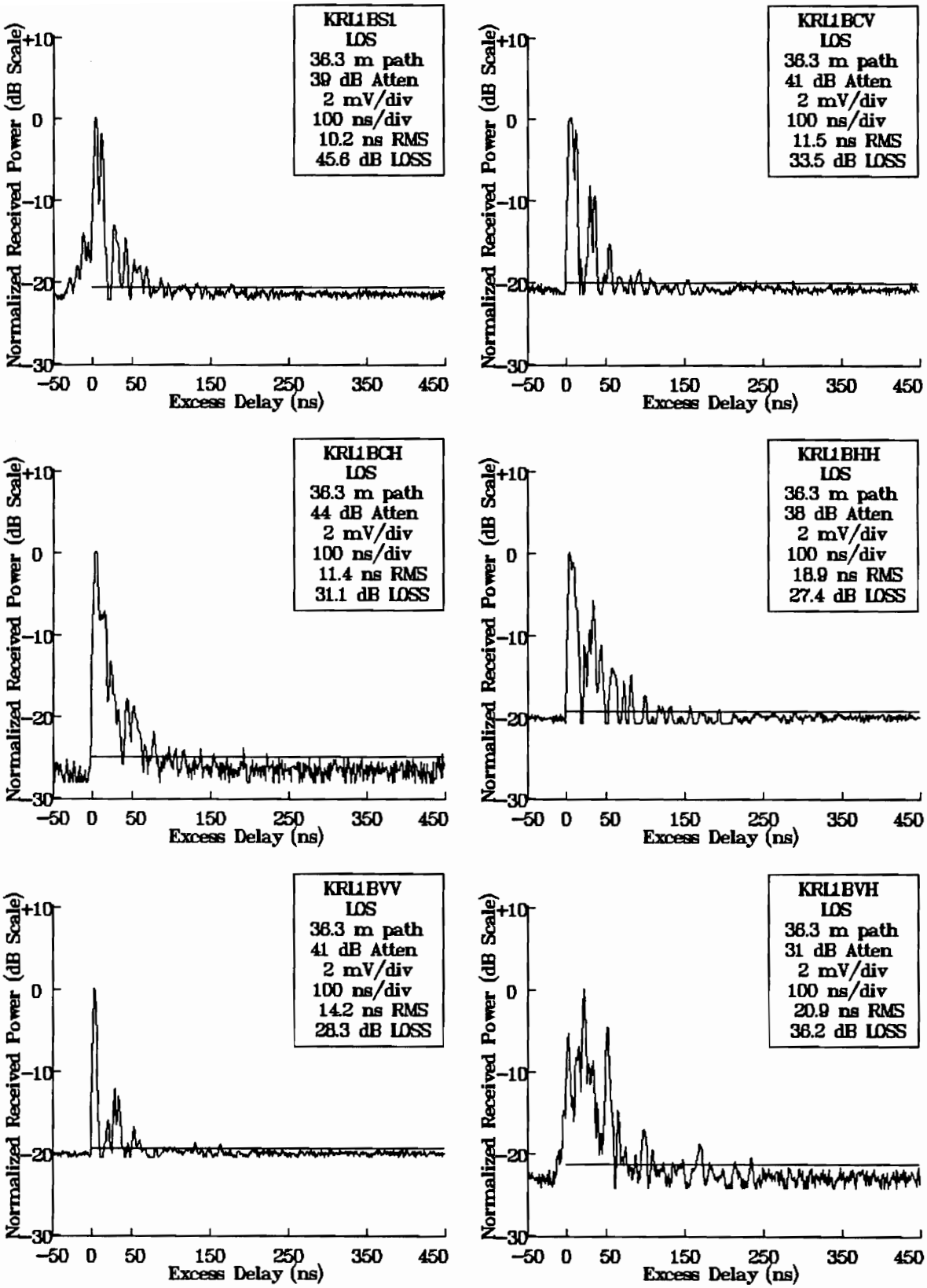
KRL1BS1
LOS
36.3 m path
39 dB Atten
2 mV/div
100 ns/div
10.2 ns RMS
45.6 dB LOSS
KRL1BCV
LOS
36.3 m path
41 dB Atten
2 mV/div
100 ns/div
11.5 ns RMS
33.5 dB LOSS
KRL1BCH
LOS
36.3 m path
44 dB Atten
2 mV/div
100 ns/div
11.4 ns RMS
31.1 dB LOSS
KRL1BHH
LOS
36.3 m path
38 dB Atten
2 mV/div
100 ns/div
18.9 ns RMS
27.4 dB LOSS
KRL1BVV
LOS
36.3 m path
41 dB Atten
2 mV/div
100 ns/div
14.2 ns RMS
28.3 dB LOSS
KRL1BVH
LOS
36.3 m path
31 dB Atten
2 mV/div
100 ns/div
20.9 ns RMS
36.2 dB LOSS
Normalized Received Power (dB Scale)
+10
0
-10
-20
-30
-50 0 50 150 250 350 450
Excess Delay (ns)

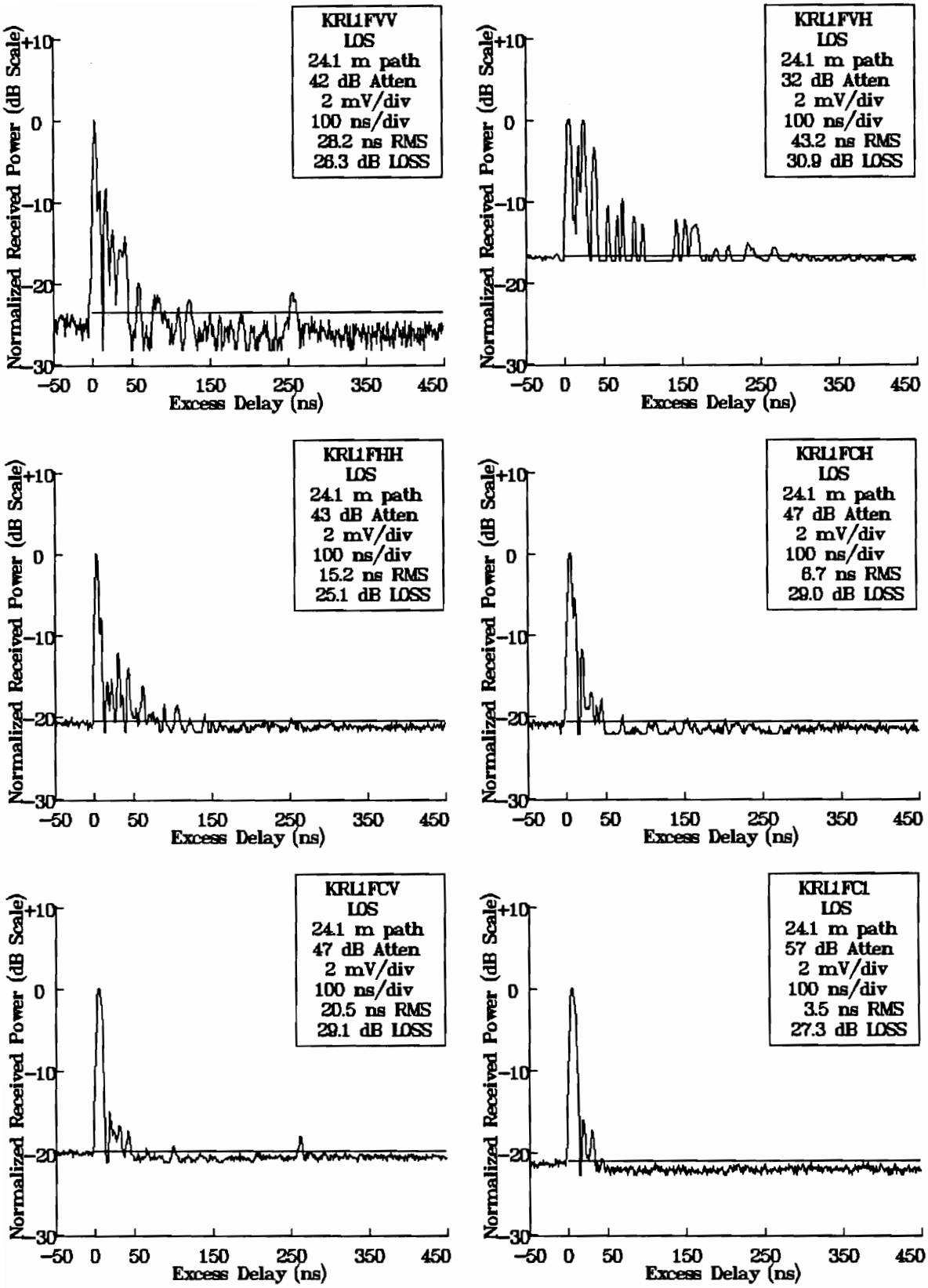
KRL1FVV
LOS
24.1 m path
42 dB Atten
2 mV/div
100 ns/div
28.2 ns RMS
26.3 dB LOSS
KRL1FVH
LOS
24.1 m path
32 dB Atten
2 mV/div
100 ns/div
43.2 ns RMS
30.9 dB LOSS
KRL1FHH
LOS
24.1 m path
43 dB Atten
2 mV/div
100 ns/div
15.2 ns RMS
25.1 dB LOSS
KRL1FCH
LOS
24.1 m path
47 dB Atten
2 mV/div
100 ns/div
6.7 ns RMS
29.0 dB LOSS
KRL1FCV
LOS
24.1 m path
47 dB Atten
2 mV/div
100 ns/div
20.5 ns RMS
29.1 dB LOSS
KRL1FC1
LOS
24.1 m path
57 dB Atten
2 mV/div
100 ns/div
3.5 ns RMS
27.3 dB LOSS
Normalized Received Power (dB Scale)
+10
0
-10
-20
-30
-50 0 50 150 250 350 450
Excess Delay (ns)

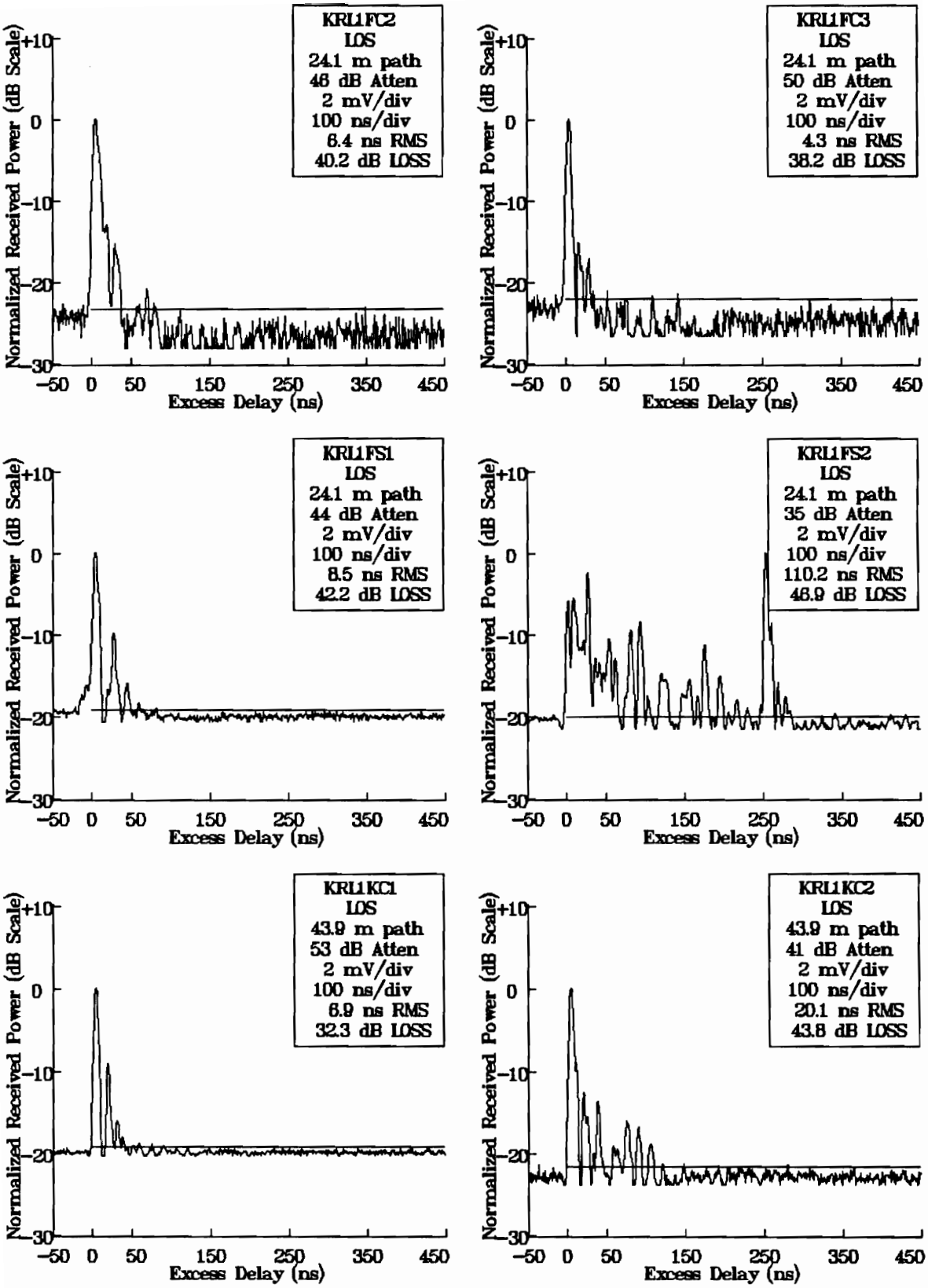
KRL1FC2
LOS
24.1 m path
46 dB Atten
2 mV/div
100 ns/div
6.4 ns RMS
40.2 dB LOSS
KRL1FC3
LOS
24.1 m path
50 dB Atten
2 mV/div
100 ns/div
4.3 ns RMS
38.2 dB LOSS
KRL1FS1
LOS
24.1 m path
44 dB Atten
2 mV/div
100 ns/div
8.5 ns RMS
42.2 dB LOSS
KRL1FS2
LOS
24.1 m path
35 dB Atten
2 mV/div
100 ns/div
110.2 ns RMS
46.9 dB LOSS
KRL1KC1
LOS
43.9 m path
53 dB Atten
2 mV/div
100 ns/div
6.9 ns RMS
32.3 dB LOSS
KRL1KC2
LOS
43.9 m path
41 dB Atten
2 mV/div
100 ns/div
20.1 ns RMS
43.8 dB LOSS
Normalized Received Power (dB Scale)
+10
0
-10
-20
-30
-50 0 50 150 250 350 450
Excess Delay (ns)

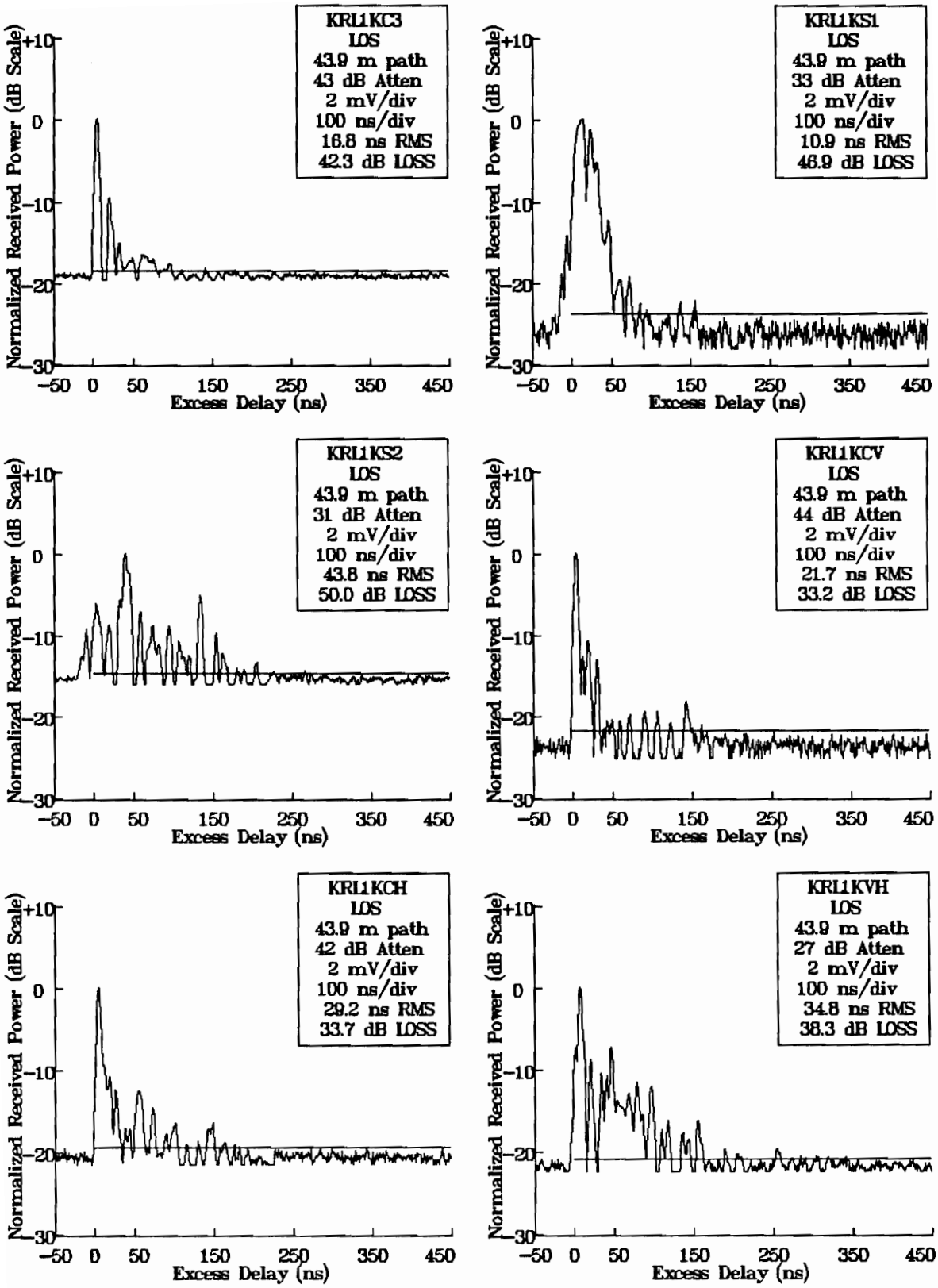
KRL1KC3
LOS
43.9 m path
43 dB Atten
2 mV/div
100 ns/div
16.8 ns RMS
42.3 dB LOSS
KRL1KS1
LOS
43.9 m path
33 dB Atten
2 mV/div
100 ns/div
10.9 ns RMS
46.9 dB LOSS
KRL1KS2
LOS
43.9 m path
31 dB Atten
2 mV/div
100 ns/div
43.8 ns RMS
50.0 dB LOSS
KRL1KCV
LOS
43.9 m path
44 dB Atten
2 mV/div
100 ns/div
21.7 ns RMS
33.2 dB LOSS
KRL1KCH
LOS
43.9 m path
42 dB Atten
2 mV/div
100 ns/div
29.2 ns RMS
33.7 dB LOSS
KRL1KVH
LOS
43.9 m path
27 dB Atten
2 mV/div
100 ns/div
34.8 ns RMS
38.3 dB LOSS
Normalized Received Power (dB Scale)
+10
0
-10
-20
-30
-50 0 50 150 250 350 450
Excess Delay (ns)

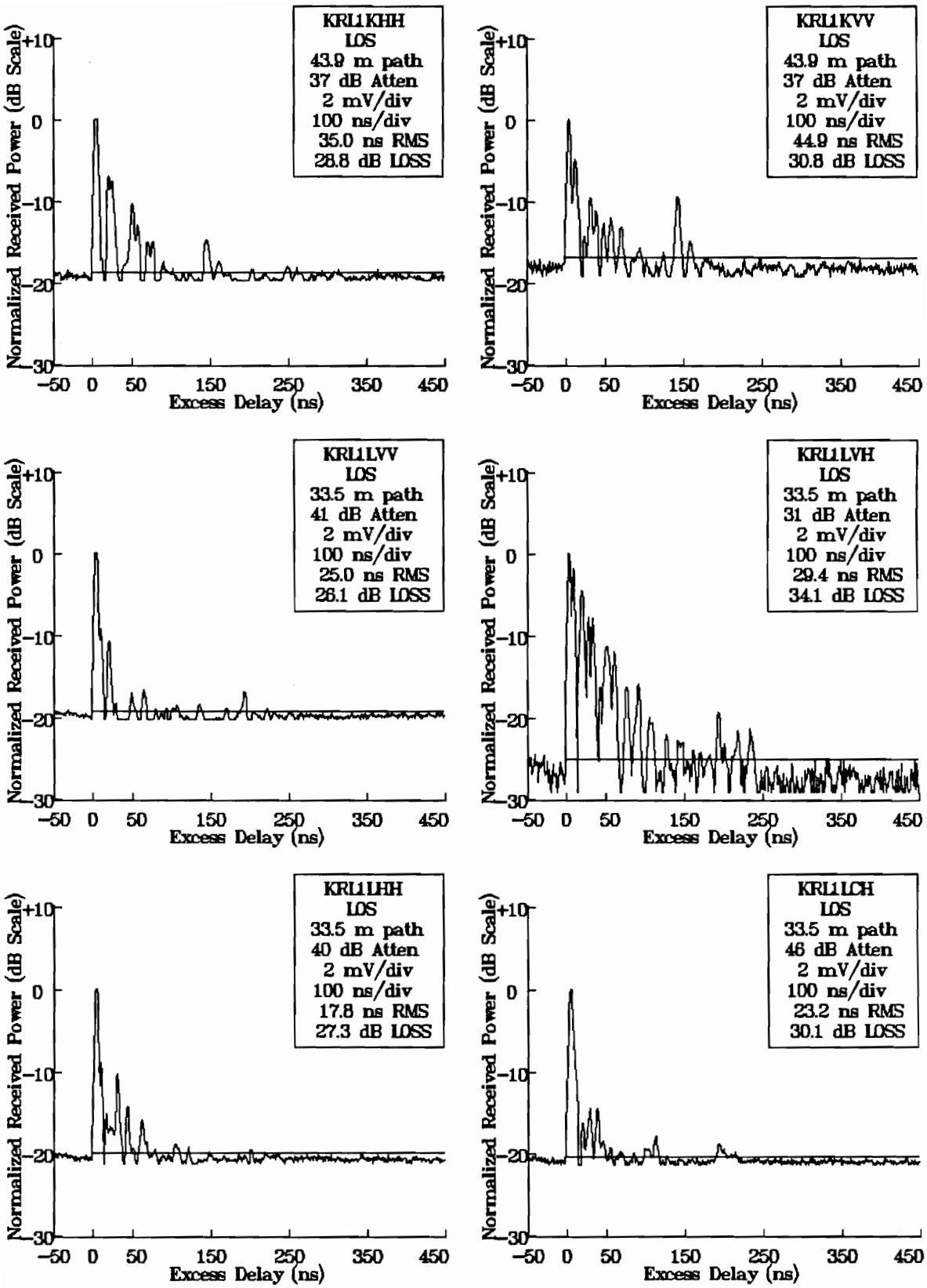
KRL1KHH
LOS
43.9 m path
37 dB Atten
2 mV/div
100 ns/div
35.0 ns RMS
28.8 dB LOSS
KRL1KVV
LOS
43.9 m path
37 dB Atten
2 mV/div
100 ns/div
44.9 ns RMS
30.8 dB LOSS
KRL1LVV
LOS
33.5 m path
41 dB Atten
2 mV/div
100 ns/div
25.0 ns RMS
26.1 dB LOSS
KRL1LVH
LOS
33.5 m path
31 dB Atten
2 mV/div
100 ns/div
29.4 ns RMS
34.1 dB LOSS
KRL1LHH
LOS
33.5 m path
40 dB Atten
2 mV/div
100 ns/div
17.8 ns RMS
27.3 dB LOSS
KRL1LCH
LOS
33.5 m path
46 dB Atten
2 mV/div
100 ns/div
23.2 ns RMS
30.1 dB LOSS
Normalized Received Power (dB Scale)
+10
0
-10
-20
-30
-50 0 50 150 250 350 450
Excess Delay (ns)

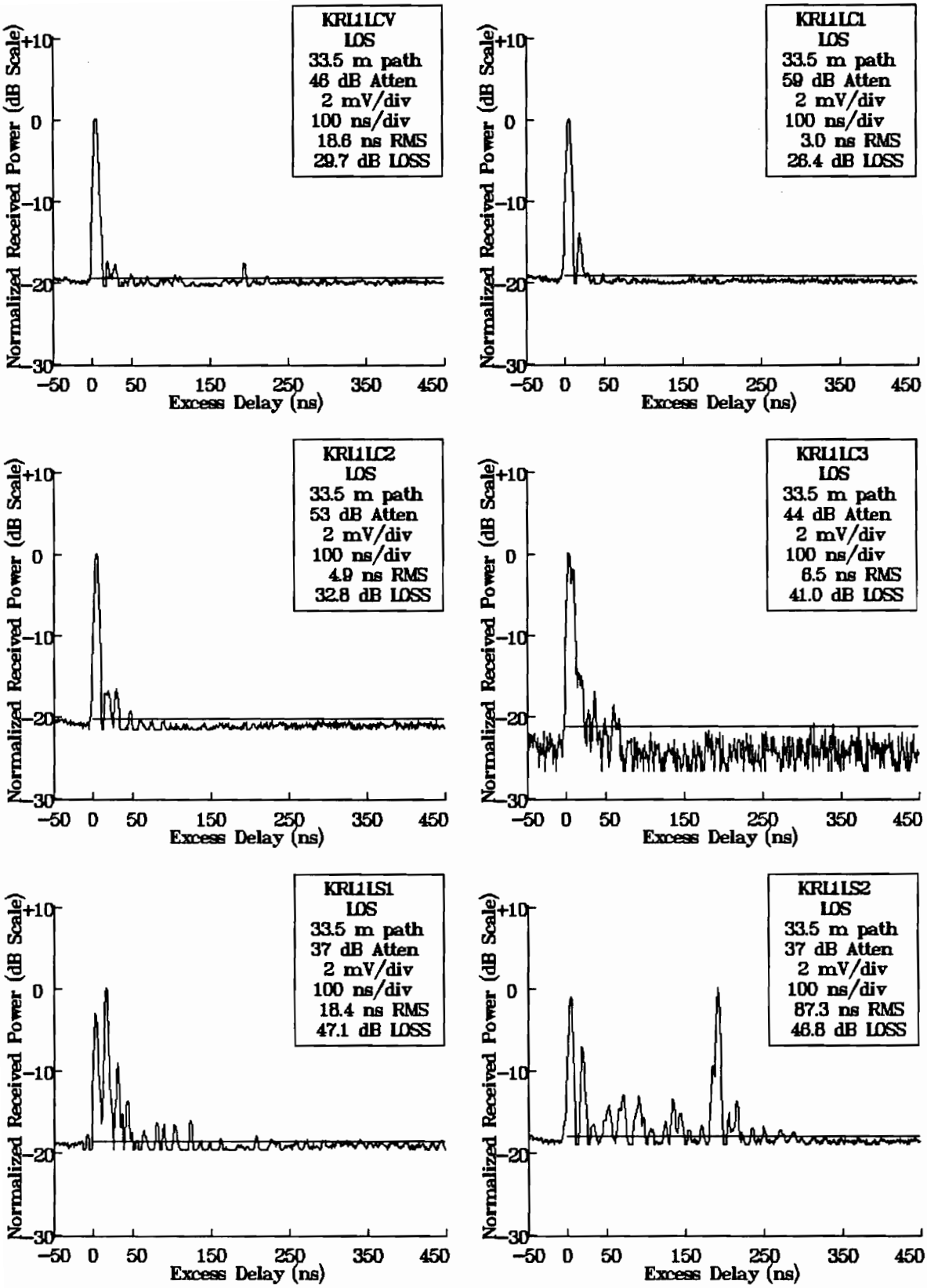
KRL1LCV
LOS
33.5 m path
46 dB Atten
2 mV/div
100 ns/div
18.6 ns RMS
29.7 dB LOSS
KRL1LC1
LOS
33.5 m path
59 dB Atten
2 mV/div
100 ns/div
3.0 ns RMS
26.4 dB LOSS
KRL1LC2
LOS
33.5 m path
53 dB Atten
2 mV/div
100 ns/div
4.9 ns RMS
32.8 dB LOSS
KRL1LC3
LOS
33.5 m path
44 dB Atten
2 mV/div
100 ns/div
6.5 ns RMS
41.0 dB LOSS
KRL1LS1
LOS
33.5 m path
37 dB Atten
2 mV/div
100 ns/div
18.4 ns RMS
47.1 dB LOSS
KRL1LS2
LOS
33.5 m path
37 dB Atten
2 mV/div
100 ns/div
87.3 ns RMS
46.8 dB LOSS
Normalized Received Power (dB Scale)
+10
0
−10
−20
−30
−50 0 50 150 250 350 450
Excess Delay (ns)

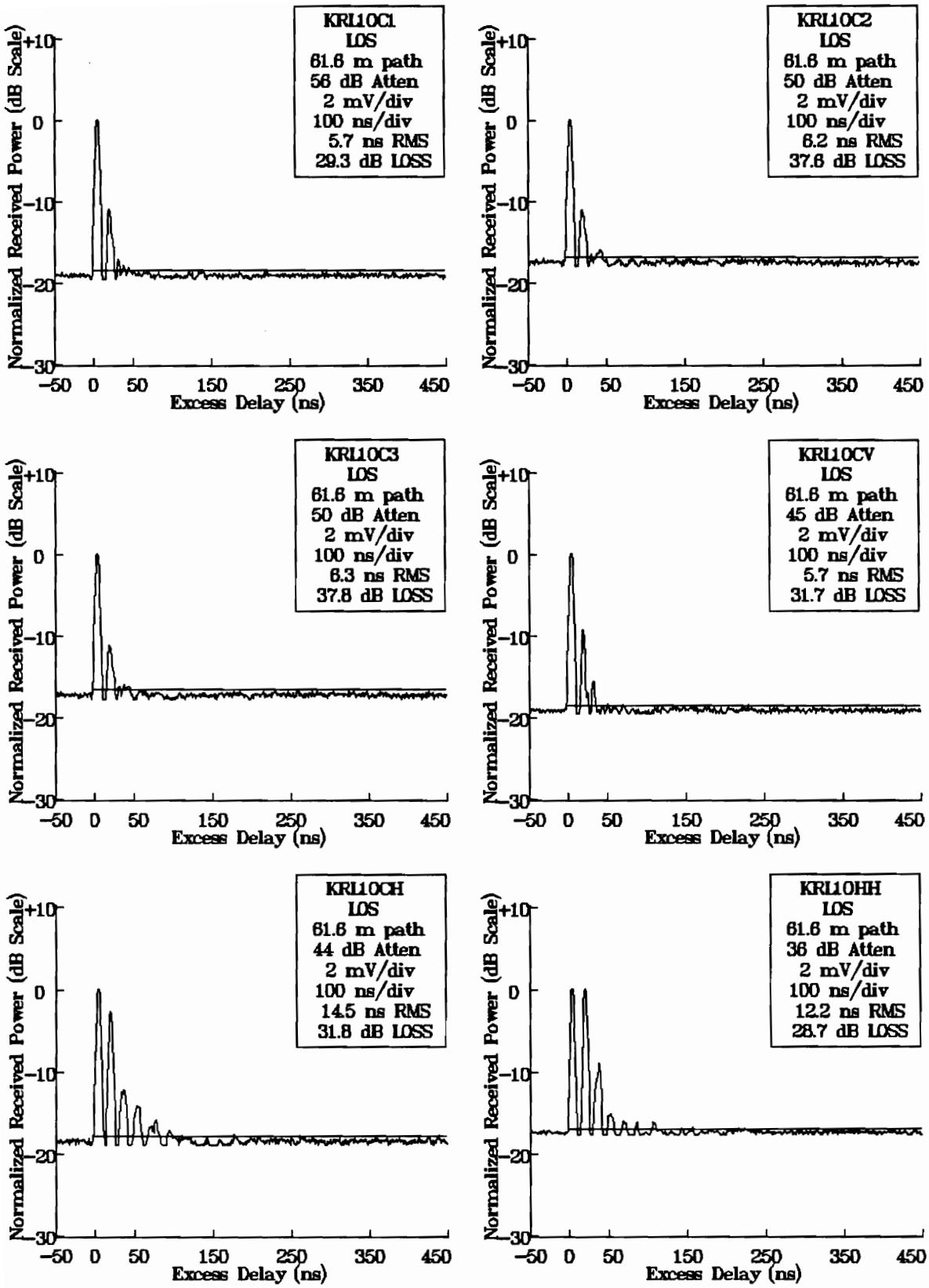
KRL10C1
LOS
61.6 m path
56 dB Atten
2 mV/div
100 ns/div
5.7 ns RMS
29.3 dB LOSS
KRL10C2
LOS
61.6 m path
50 dB Atten
2 mV/div
100 ns/div
6.2 ns RMS
37.6 dB LOSS
KRL10C3
LOS
61.6 m path
50 dB Atten
2 mV/div
100 ns/div
6.3 ns RMS
37.8 dB LOSS
KRL10CV
LOS
61.6 m path
45 dB Atten
2 mV/div
100 ns/div
5.7 ns RMS
31.7 dB LOSS
KRL10CH
LOS
61.6 m path
44 dB Atten
2 mV/div
100 ns/div
14.5 ns RMS
31.8 dB LOSS
KRL10HH
LOS
61.6 m path
36 dB Atten
2 mV/div
100 ns/div
12.2 ns RMS
28.7 dB LOSS
Normalized Received Power (dB Scale)
+10
0
-10
-20
-30
-50 0 50 150 250 350 450
Excess Delay (ns)

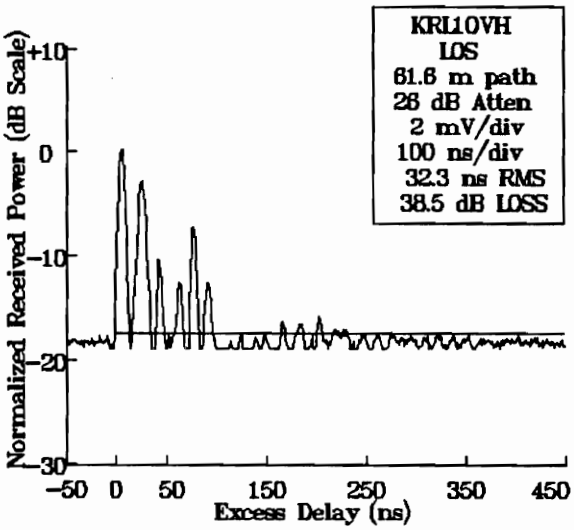
KRL10VH
LOS
61.6 m path
26 dB Atten
2 mV/div
100 ns/div
32.3 ns RMS
38.5 dB LOSS
Normalized Received Power (dB Scale)
+10
0
-10
-20
-30
-50
0
50
150
250
350
450
Excess Delay (ns)

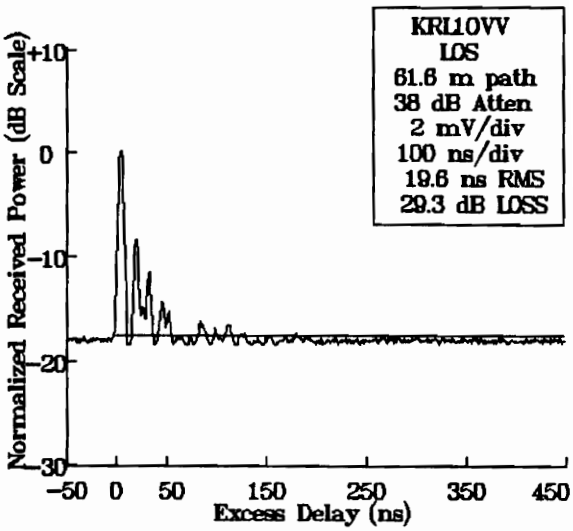
KRL10VV
LOS
61.6 m path
38 dB Atten
2 mV/div
100 ns/div
19.6 ns RMS
29.3 dB LOSS
Normalized Received Power (dB Scale)
+10
0
-10
-20
-30
-50
0
50
150
250
350
450
Excess Delay (ns)

Appendix B. Computer Programs

```
    /*  CAPTURE.C  */

/* ---------------------------------------------------------------

This is the is the raw data acquisition program CAPTURE.C, written in
Turbo C 1.0.  The program is responsible for interfacing with the
digitizing oscilloscope during the collection of wide band propagation
data.  During one measurement run, the program captures 128 power delay
profiles as measured by the scope.  The following 3 data files are stored
on the computer's hard drive as directed by this program.

     filename.DAT -- 256 data points for each of the 128 profiles.
     filename.HDR -- oscilloscope preamble parameters.
     filename.DES -- user-defined measurement location description file.

Last Revised -- May 14, 1990 (DAH).

---------------------------------------------------------------------*/

#include "STDIO.H"
#include "STRING.H"
#include "CHPIB.H"
#include "CFUNC.H"
#include "CONIO.H"

/*--------------------------------------------------------------------*/

error_handler(error,routine)
int error;
char *routine;
{
char ch;
if (error != NOERR)
          {
          printf("Error in call to %s \n",routine);
          printf("%d %s \n",error,errstr(error));
          printf("Press Enter to continue: ");
          scanf("%c",&ch);
          }
}

/*--------------------------------------------------------------------*/

initialize(isc)
{
int error;

error = IORESET(isc);
error_handler(error,"IORESET");
error = IOTIMEOUT(isc,5.0);
error_handler(error,"IOTIMEOUT");
error=IOCLEAR(isc);
error_handler(error,"IOCLEAR");
}

/*--------------------------------------------------------------------*/

send_command(char *cmd,int scope)
{
int length;
length=strlen(cmd);
error_handler(IOOUTPUTS(scope,cmd,length),"IOOUTPUTS");
}
```

```
/*-----------------------------------------------------------------*/

main()
{
FILE    *fnout ;
FILE    *fnhdr ;
FILE    *fndes ;
FILE    *fnout2 ;

char    fnm[20],fnm2[20],fnm3[20],fnm4[20] ;
char    topo_descr[300] ;
char    direction[300] ;
char    trig_test,los_path,strt_data ;

int     isc,scope,speednum,count ;
int     length,i,j,k,freq ;
int     waveform[256] ;
int     elements,swapsize ;
int     error, ss ;

float   preamble[10] ;
float   xinc,xref,yinc,yorg,yref ;
float   tdel = -708.6e-09 ;

int     dec ;
int     sign ;
float   speed ;
float   atten,rx_ant_ht,tr_sep ;
float   tr_sep_time,tdel_set20,tdel_set50,tdel_set100,tdel_set1000 ;
float   tx_ant_ht = 68.0 ;
float   sol = 0.98425e+09 ;
float   cable_delay ;

isc=7;
scope=isc*100+7;
initialize(isc);

send_command(":SYSTEM:HEADER OFF;:EOI ON",scope);

printf("Enter desired filename: ");
scanf ("%s",fnm);
strcpy(fnm2,fnm) ;
strcpy(fnm3,fnm) ;
strcpy(fnm4,fnm) ;
strcat(fnm,".dat") ;
strcat(fnm2,".hdr") ;
strcat(fnm3,".des") ;
strcat(fnm4,".vw") ;
fnout=fopen(fnm,"wb");
fnout2=fopen(fnm4,"w") ;
fnhdr=fopen(fnm2,"wb");
fndes=fopen(fnm3,"w");

printf("Enter frequency of operation (1 or 4):");
scanf("%d",&freq) ;
printf("Enter T-R separation (in feet) :");
scanf("%f",&tr_sep) ;
printf("Enter amount of pre-LNA cable (in feet) :") ;
scanf("%f",&cable_delay) ;

tdel = tdel + (1.5e-09 * cable_delay) ;
tr_sep_time = tr_sep/sol ;
tdel_set20  = tdel + tr_sep_time - 20.0e-09 ;
tdel_set50  = tdel + tr_sep_time - 50.0e-09 ;
tdel_set100 = tdel + tr_sep_time - 100.e-09 ;
```

```
tdel_set1000 = tdel + tr_sep_time - 1000.e-09 ;

printf("Is the triggering cable being used (y or n) ? \n\n");
trig_test = getch() ;
if (trig_test != 'n')
   {
   send_command(":CHAN4:RANG 0.4;OFFS 0.0",scope) ;
   send_command(":TRIG:PATH CHAN4;MODE EDGE",scope) ;
   send_command(":TRIG:LEV -0.50;POL NEG",scope) ;

printf("For the given T-R separation, SET TIME DELAY\n") ;
printf("as follows to place the LOS component 1 block from\n") ;
printf("the left side of the screen:\n\n") ;

printf("       For     20ns/div : %e\n ",tdel_set20) ;
printf("      For     50ns/div : %e\n ",tdel_set50) ;
printf("      For    100ns/div : %e\n ",tdel_set100) ;
printf("      For      1us/div : %e\n\n ",tdel_set1000) ;
   }

printf("Set the receiver to accept the desired CARRIER FREQUENCY.\n");
printf("Double check the transmitter to be sure that the correct\n");
printf("CARRIER FREQUENCY is being transmitted.\n\n");
printf("Set the scope display as desired.\n\n") ;


printf("Enter the receiver antenna height (in inches) :");
scanf("%f",&rx_ant_ht) ;


printf("Does a LOS path exist (y or n) :\n\n");
los_path = getch();

printf("Describe the transmitter motion with respect to the receiver.\n\n") ;
scanf("%s",direction) ;

printf("\n") ;

printf("Enter the conditions for vehicle speed :\n\n") ;
printf("1.) 1.3 GHz  20 ns per division\n") ;
printf("2.) 1.3 GHz  50 ns per division\n") ;
printf("3.) 1.3 GHz 100 ns per division\n") ;
printf("4.) 4.0 GHz  20 ns per division\n") ;
printf("5.) 4.0 GHz  50 ns per division\n") ;
printf("6.) 4.0 GHz 100 ns per division\n") ;
scanf("%d",&speednum) ;
switch(speednum)
  {
    case 1 : speed = 1.27 ;
             break ;
    case 2 : speed = 2.02 ;
             break ;
    case 3 : speed = 2.56 ;
             break ;
    case 4 : speed = 0.42 ;
             break ;
    case 5 : speed = 0.67 ;
             break ;
    case 6 : speed = 0.85 ;
             break ;
    default  : speed = 1.0 ;
  }
printf("\n") ;

printf("Briefly describe the topography.\n\n");
```

```
scanf("%s",topo_descr) ;
printf("\n") ;

printf("\nEnter the attenuation value:") ;
scanf("%f",&atten) ;
printf("\n") ;

printf("\nEnter the number of snapshots: ") ;
scanf("%d",&ss) ;
ss = ss - 1 ;

fprintf(fndes,"Number of snapshots: %d\n ",ss+1) ;
fprintf(fndes,"Frequency of operation: %d\n ",freq) ;
fprintf(fndes,"Pre-LNA cable (in feet): %f\n ",cable_delay) ;
fprintf(fndes,"T-R separation (in feet): %f\n ",tr_sep) ;
fprintf(fndes,"LOS present? %c\n ",los_path) ;
fprintf(fndes,"Triggering cable used? %c\n ",trig_test) ;
fprintf(fndes,"Receiver attenuation value: %f\n  ",atten) ;
fprintf(fndes,"Transmitter antenna height: %f\n ",tx_ant_ht) ;
fprintf(fndes,"Receiver antenna height: %f\n ",rx_ant_ht) ;
fprintf(fndes,"Description of topography:\n ") ;
fprintf(fndes,"%s\n",topo_descr);
fprintf(fndes,"Direction of Vehicle: %s\n",direction) ;
fprintf(fndes,"Vehicle Speed %f\n",speed) ;

printf("\nNumber of snapshots: %d\n ",ss+1) ;
printf("Frequency of operation: %d\n ",freq) ;
printf("Pre-LNA cable (in feet): %f\n ",cable_delay) ;
printf("T-R separation (in feet): %f\n ",tr_sep) ;
printf("LOS present? %c\n ",los_path) ;
printf("Triggering cable used? %c\n ",trig_test) ;
printf("Receiver attenuation value: %f\n  ",atten) ;
printf("Transmitter antenna height: %f\n ",tx_ant_ht) ;
printf("Receiver antenna height: %f\n ",rx_ant_ht) ;
printf("Description of topography:\n ") ;
printf("%s\n",topo_descr);
printf("\nDirection of Vehicle:%s\n",direction) ;
printf("\nVehicle Speed %f\n\n",speed) ;
if (trig_test != 'n')

   {
printf("Reminder:\n") ;

printf("       For     20ns/div : %e\n ",tdel_set20) ;
printf("      For     50ns/div : %e\n ",tdel_set50) ;
printf("      For    100ns/div : %e\n ",tdel_set100) ;
printf("      For      1us/div : %e\n\n ",tdel_set1000) ;
   }

printf("Press any key to begin data acquisition in five seconds. \n");
strt_data = getche();

send_command(":ACQUIRE:TYPE AVERAGE;COUNT 16;POINTS 256",scope);
send_command(":DIGITIZE CHANNEL1",scope) ;
send_command(":WAV:SOURCE CHANNEL1",scope);
send_command(":WAV:FORMAT WORD",scope);
send_command(":WAV:PREAMBLE?",scope);
elements=10;
error_handler(IOENTERA(scope,preamble,&elements),"IOENTERA");
fprintf(fnhdr,"%d\n",ss) ;
fwrite(preamble,1,sizeof(preamble),fnhdr) ;

error=IOCLEAR(isc);
error_handler(error,"IOCLEAR");
```

```
for (j=0;j<=ss;j++)
  {
    send_command(":DIGITIZE CHANNEL1",scope) ;
    send_command(":WAV:DATA?",scope);

    elements=512;
    swapsize=2;
    error_handler(IOENTERAB(scope,waveform,&elements,swapsize),"IOENTERA");

    fwrite(waveform,1,sizeof(waveform),fnout) ;

    error=IOCLEAR(isc);
    error_handler(error,"IOCLEAR");

    printf("Snapshot number - %d\n",j+1) ;

  }

  error_handler(IOLOCAL(scope),"IOLOCAL");

        for (k=0;k<=255;k++)
          {
            fprintf(fnout2,"%d\n",waveform[k]) ;
          }


  fclose(fnhdr);
  fclose(fnout);
  fclose(fnout2) ;
  fclose(fndes);

}
```

```
{  BINDATA.PAS  }

{  ---------------------------------------------------------------

This program accepts the raw data profiles from filename.DAT and
preamble information from filename.HED (filename.HED is simply the 'text'
format of the preamble parameters originally stored in binary format
as filename.HDR).  From these files, the spatially averaged profile for
a measurement run is computed and stored on the F: directory as
F:\ ... \AVG\DAT\filename.DAT.
The program also computes the quantized power delay profiles for all
recorded snapshots and stores the resulting files as filename.BIN.

Last Revised -- July 5, 1990 (DAH).

--------------------------------------------------------------------  }

program bindata ;
{$N+}
uses Graph, Crt, Dos, Printjet ;

const
  laby :    array[0..4] of string[4] = ('0.00','0.25','0.50','0.75','1.00') ;
  labydb :  array[0..4] of string[4] = ('-30.0','-20.0','-10.0','0.0','+10.0');
  labx20  : array[0..5] of string[3] = ('-20','20 ','60 ','100','140','180') ;
  labx50  : array[0..5] of string[3] = ('-50','50 ','150','250','350','450') ;
  labx100 : array[0..5] of string[4] = ('-100 ','100 ','300'
                                       ,'500 ','700','900 ') ;


type
  atype                    =      array[1..128,1..255] of integer ;
  btype                    =      array[1..128,1..255] of integer ;
  ctype                    =      array[1..128,1..255] of integer ;

var
  i,j,k,l,m,shots,choice1   :     integer                    ;
  tempor1,tempor2,bintotal  :     integer                    ;
  check2,endloop            :     integer                    ;
  sumpower                  :     longint                    ;
  lgth                      :     word                       ;
  grdriver,grmode           :     integer                    ;
  filename,filename1        :     string[50]                 ;
  path,pathdat              :     string[50]                 ;
  filetext                  :     text                       ;
  filevar                   :     file                       ;
  fileout                   :     file                       ;
  filehdr                   :     file                       ;
  waveform                  :     array[1..256] of integer   ;
  waveform1                 :     array[1..255] of integer   ;
  average                   :     array[1..255] of integer   ;
  preamble                  :     array[0..9] of real        ;
  labx                      :     array[0..5] of string[4]   ;
  rdata                     :     ^atype                     ;
  zdata                     :     ^btype                     ;
  bdata                     :     ^ctype                     ;
  Dirinfo                   :     Searchrec                  ;
  keyword                   :     array[1..6] of string[80]  ;
  pathnum,keynumber         :     integer                    ;
  sum,sumbin                :     longint                    ;
  avgint                    :     array[1..128] of longint   ;
  maxvalue                  :     array[1..128] of integer   ;
  avg,snr,window            :     real                       ;
  nextbin,time              :     real                       ;
  xinc,xstart               :     real                       ;
```

```
  dataplot,binplot          :      array[1..255] of real       ;
  dataplotdb,binplotdb      :      array[1..255] of real       ;
  char1,ch                  :      char                        ;
  ss                        :      string                      ;

{ ---------------------------------------------------------------- }

Function log(x:double) : double ;
begin
  if x > 0.0 then log := ln(x)/ln(10.0) else log := -100.0 ;
end ;


{ ---------------------------------------------------------------- }


Procedure Read_Data ;
begin
   if pathnum = 10 then shots := 1 ;
   if pathnum < 10 then
   begin
      assign(filetext,path+'hed\'+filename1+'.hed') ;
      reset(filetext) ;
      readln(filetext,shots) ;
      shots := shots + 1 ;
   end ;
   if pathnum > 10 then shots := 128 ;
   if (pathnum < 11)  then
   begin
      for i := 0 to 9 do readln(filetext,preamble[i]) ;
      close(filetext) ;
      window := preamble[4] * 2.56e+11 ;
   end ;
   if (pathnum = 11) then window := 200.0 ;
   if (pathnum = 12) then window := 500.0 ;
   if (pathnum = 13) then window := 1000.0 ;
   window := round(window) ;
   assign(filevar,pathdat+'dat\'+filename1+'.dat') ;
   reset(filevar,1) ;
   for i := 1 to shots do
   begin
      blockread(filevar,waveform,sizeof(waveform)) ;
      for j := 1 to 255 do rdata^[i,j] := waveform[j] ;
   end ;
   close(filevar) ;
end ;


{ ---------------------------------------------------------------- }


Procedure Zero_Data ;
begin
   for i := 1 to shots do
   begin
      sum := 0 ;
      for j := 216 to 255 do
      begin
         sum := sum + rdata^[i,j] ;
      end ;
      avg := sum/40. ;
      avgint[i] := round(avg) ;
   end ;

   for i := 1 to shots do
```

```
   begin
      for j := 1 to 255 do
      begin
         if rdata^[i,j] >= avgint[i] then zdata^[i,j] := 32767
         else zdata^[i,j] := rdata^[i,j] + (32767 - avgint[i]) ;
         if avgint[i] < 20480 then zdata^[i,j] := 32766 ;
      end ;
   end ;
end ;

{ ---------------------------------------------------------------- }

Procedure Compute_Average_Profile ;
begin
   for j := 1 to 255 do
   begin
      sumpower := 0 ;
      l := 0 ;
      for i := 1 to shots do
      begin
         if avgint[i] > 20479 then
         begin
            l := l + 1 ;
            sumpower := sumpower + zdata^[i,j] ;
         end ;
      end ;
      average[j] := round(sumpower/l) ;

   end ;
   assign(fileout,path+'avg\dat\'+filename1+'.dat') ;
   rewrite(fileout,1) ;
   blockwrite(fileout,average,sizeof(average)) ;
   close(fileout) ;
end ;

{ ---------------------------------------------------------------- }

Procedure Quantize ;
begin
   for i := 1 to shots do
   begin
      l := 0 ;
      k := 0 ;
      nextbin := window/512.0 ;
      sumbin := 0 ;
      if ((nextbin < 0.5) or (nextbin > 1.5)) then endloop := 256 ;
      if ((nextbin > 0.5) and (nextbin <1.5)) then endloop := 255 ;
      for j := 1 to endloop do
      begin
         time := j * (window/256.0) ;
         if time >= nextbin + 3.90625 then
         begin
            nextbin := nextbin + 3.90625 ;
            l := l + 1 ;
            bdata^[i,l] := round(sumbin/k) ;
            sumbin := 0 ;
            k := 0 ;
         end ;
         sumbin := sumbin + zdata^[i,j] ;
         k := k +1 ;
      end ;
```

```
   end ;
end ;

{ ------------------------------------------------------------------ }

Procedure Graph_Bins ;
var
   maxx,maxy,minx,miny          :    integer                    ;
   min1                         :    array[1..128] of real      ;
   min2                         :    array[1..128] of real      ;

begin
   grDriver := Detect ;
   InitGraph(grDriver,grMode,'d:\tpascal5\') ;
   if graphresult = grOk then
   begin
      maxx := round(0.80 * getmaxx) ;
      minx := round(0.10 * getmaxx) ;
      maxy := round(0.85 * getmaxy) ;
      miny := round(0.15 * getmaxx) ;
      for i := 1 to check2 do
      begin
         min1[i] := 32767.0 ;
         min2[i] := 32767.0 ;
         for j := 1 to 255 do
            if zdata^[i,j] < min1[i] then min1[i] := zdata^[i,j] ;
         for l := 1 to bintotal do
            if bdata^[i,l] < min2[i] then min2[i] := bdata^[i,l] ;
         for j := 1 to 255 do
         begin
            dataplot[j] := (32767.0 - zdata^[i,j])/(32767.0 - min1[i]) ;
            dataplotdb[j] := 10.0 * log(dataplot[j]) ;
            if dataplotdb[j] < -30.00 then dataplotdb[j] := -30.00 ;
         end ;
         for l := 1 to bintotal do
         begin
            binplot[l]  := (32767.0 - bdata^[i,l])/(32767.0 - min1[i]) ;
            binplotdb[l] := 10.0 * log(binplot[l]) ;
            if binplotdb[l] < -30.00 then binplotdb[l] := -30.00 ;
         end ;

         clearviewport ;
         setcolor(4) ;
         settextstyle(2,0,5) ;
         line(minx,maxy+1,minx,round(maxy*0.2)) ;
         line(minx,maxy+1,minx+maxx,maxy+1) ;
         for j := 0 to 4 do
                  line(minx,maxy-(j*round(maxy*0.2)),
                  minx+7,maxy-(j *  round(maxy*0.2))) ;
         for j := 0 to 4 do
            outtextxy(minx-40,maxy-3-(j*round(maxy*0.2)),laby[j]) ;

         for j := 0 to 5 do
           line(minx+(j*round(maxx*0.20)),maxy+1,
                minx+(j*round(maxx*0.20)),maxy-6) ;

         line(minx+round(0.5*(maxx*0.20)),maxy+3,
              minx+round(0.5*(maxx*0.20)),maxy-7) ;
         outtextxy((minx+round(0.5*(maxx*0.20))-3),maxy+12,'0') ;

         for j := 0 to 5 do
         begin
            if (window = 200) then labx[j] := labx20[j] ;
```

```
   if (window = 500) then labx[j] := labx50[j] ;
   if (window = 1000) then labx[j] := labx100[j] ;
end ;
for j := 0 to 5 do
   outtextxy(minx-10+(j*round(maxx*0.20)),maxy+12,labx[j]) ;

outtextxy(round((minx+maxx)/2.0)-33,maxy+35,'Excess Delay (ns)') ;

settextstyle(2,1,5) ;
outtextxy(minx-60,round(maxy*0.20),
          'Normalized Receiver Power (Linear Scale)') ;

setcolor(5) ;
moveto(minx,maxy) ;
for j := 1 to 255 do
         lineto(minx + round(j*(maxx/256.0)),
                round(maxy*(1.0-(0.8 * dataplot[j])))) ;
setcolor(4) ;
xstart := minx +
(((window/512.0)/((window/512.0)+(bintotal*3.90625)))*maxx) ;
xinc   := (xstart - minx) *  (2000.0 / window) ;
moveto(round(xstart),maxy) ;
for l := 1 to bintotal-1 do
begin
   lineto(round(((l-1)*xinc)+xstart),
          round(maxy*(1.0-(0.8 * binplot[l])))) ;
   lineto(round((l*xinc)+xstart),
          round(maxy*(1.0-(0.8 * binplot[l])))) ;
end ;
repeat until keypressed ;
ch := readkey ;
if upcase(ch) = 'P' then Screen_Dump(VGA) ;
clearviewport ;
setcolor(4) ;
settextstyle(2,0,5) ;
line(minx,maxy+1,minx,round(maxy*0.2)) ;
line(minx,maxy+1,minx+maxx,maxy+1) ;
for j := 0 to 4 do
         line(minx,maxy-(j*round(maxy*0.2)),
         minx+7,maxy-(j *  round(maxy*0.2))) ;
for j := 0 to 4 do
   outtextxy(minx-40,maxy-3-(j*round(maxy*0.2)),labydb[j]) ;

for j := 0 to 5 do
  line(minx+(j*round(maxx*0.20)),maxy+1,
       minx+(j*round(maxx*0.20)),maxy-6) ;

line(minx+round(0.5*(maxx*0.20)),maxy+3,
     minx+round(0.5*(maxx*0.20)),maxy-7) ;
outtextxy((minx+round(0.5*(maxx*0.20))-3),maxy+12,'0') ;

for j := 0 to 5 do
begin
   if (window = 200) then labx[j] := labx20[j] ;
   if (window = 500) then labx[j] := labx50[j] ;
   if (window = 1000) then labx[j] := labx100[j] ;
end ;
for j := 0 to 5 do
   outtextxy(minx-10+(j*round(maxx*0.20)),maxy+12,labx[j]) ;

outtextxy(round((minx+maxx)/2.0)-33,maxy+35,'Excess Delay (ns)') ;

settextstyle(2,1,5) ;
outtextxy(minx-60,round(maxy*0.20),
          'Normalized Receiver Power (dB Scale)') ;
```

```
        setcolor(5) ;
        moveto(minx,maxy) ;
        for j := 1 to 255 do
                lineto(minx + round(j*(maxx/256.0)),
                      round(maxy-((dataplotdb[j]/50.0) + 0.6) * maxy)) ;
        setcolor(1) ;
        xstart := minx +
        (((window/512.0)/((window/512.0)+(bintotal*3.90625)))*maxx) ;
        xinc   := (xstart - minx) *  (2000.0 / window) ;
        moveto(round(xstart),maxy) ;
        for l := 1 to bintotal-1 do
        begin
           lineto(round(((l-1)*xinc)+xstart),
                  round(maxy-((binplotdb[l]/50.0) + 0.6) * maxy)) ;
           lineto(round((l*xinc)+xstart),
                  round(maxy-((binplotdb[l]/50.0) + 0.6) * maxy)) ;
        end ;
        repeat until keypressed ;
        ch := readkey ;
        if upcase(ch) = 'P' then Screen_Dump(VGA) ;
      end ;
   end;
   closeGraph ;
end ;


{  ------------------------------------------------------------------  }


Procedure File_Output ;
begin
   assign(fileout,pathdat+'bin\'+filename1+'.bin') ;
   rewrite(fileout,1) ;
   for i := 1 to shots do
   begin
      for j := 1 to bintotal do waveform1[j] := bdata^[i,j] ;
      lgth := bintotal * 2 ;
      blockwrite(fileout,waveform1,lgth) ;
   end ;
   close(fileout) ;
end ;


{  ------------------------------------------------------------------  }


Procedure Main_Module ;
begin
   case pathnum of
      1 : path :='f:\rdata\los\trlow\' ;
      2 : path :='f:\rdata\los\trmed\' ;
      3 : path :='f:\rdata\los\trhigh\' ;
      4 : path :='f:\rdata\par\trlow\' ;
      5 : path :='f:\rdata\par\trmed\' ;
      6 : path :='f:\rdata\par\trhigh\' ;
      7 : path :='f:\rdata\obs\trlow\' ;
      8 : path :='f:\rdata\obs\trmed\' ;
      9 : path :='f:\rdata\obs\trhigh\' ;
      10: path :='f:\gendat\' ;
      11: path :='f:\rdata\chkthd20\' ;
      12: path :='f:\rdata\chkthd50\' ;
      13: path :='f:\rdata\chktd100\' ;
   end ;
   case pathnum of
```

```
      1 : pathdat :='g:\rdata\los\trlow\' ;
      2 : pathdat :='g:\rdata\los\trmed\' ;
      3 : pathdat :='g:\rdata\los\trhigh\' ;
      4 : pathdat :='g:\rdata\par\trlow\' ;
      5 : pathdat :='g:\rdata\par\trmed\' ;
      6 : pathdat :='g:\rdata\par\trhigh\' ;
      7 : pathdat :='g:\rdata\obs\trlow\' ;
      8 : pathdat :='g:\rdata\obs\trmed\' ;
      9 : pathdat :='g:\rdata\obs\trhigh\' ;
      10: pathdat :='f:\gendat\' ;
      11: pathdat :='g:\rdata\chkthd20\' ;
      12: pathdat :='g:\rdata\chkthd50\' ;
      13: pathdat :='g:\rdata\chktd100\' ;
   end ;

   if choice1 = 1 then Keyword[keynumber] := '*' ;
   if choice1 = 2 then
   begin
      write('Number of filenames : ') ;
      readln(keynumber) ;
      for i := 1 to keynumber do
      begin
         write('filename[',i:1,'] : ') ;
         readln(Keyword[i]) ;
         Keyword[i] := pathdat+'dat\'+keyword[i]+'.dat' ;
      end ;
   end
   else Keyword[keynumber] := pathdat+'dat\'+keyword[keynumber]+'.dat' ;
   writeln(Keyword[keynumber]) ;
   writeln(path) ;
   for k := 1 to keynumber do
   begin
      FindFirst(keyword[k],archive,dirinfo) ;
      while DosERROR = 0 do
      begin
         filename1 := copy(dirinfo.name,1,length(dirinfo.name)-4) ;
         writeln(filename1) ;
         Read_Data ;
         Zero_Data ;
         Compute_Average_Profile ;
         Quantize  ;
         bintotal := l ;
         writeln(bintotal:10) ;
         if char1 = 'y' then Graph_Bins ;
         File_Output ;
         FindNext(dirinfo) ;
      end ;
   end ;
end ;


{  ------------------------------------------------------------------  }


begin
   new(rdata) ;
   new(zdata) ;
   new(bdata) ;

   writeln ;
   write('Enter (1) to compute for all paths, (2) to choose specifics : ') ;
   readln(choice1) ;
   write('Would you like to view bindata comparison (y or n) ? ') ;
   readln(char1) ;
   if char1 = 'y' then
```

```
    begin
       write('How many snapshots do you wish to view? ') ;
       readln(check2) ;
    end ;
    if choice1 = 2 then
    begin
       write('Enter Path Number : ') ;
       readln(pathnum) ;
       Main_Module ;
    end
    else
    begin
       keynumber := 1 ;
       for pathnum := 1 to 9 do Main_Module ;
    end ;
    dispose(rdata) ;
    dispose(zdata) ;
    dispose(bdata) ;
end.
```

```
{  THRSHOLD.PAS  }

{  ---------------------------------------------------------------

This program accepts the quantized power delay profile data as filename.BIN
and determines the noise threshold level for each individual profile and the
spatially averaged profile based on the mean and standard
deviation of the noise floor obtained from the last 15% of the profiles.
After the level is determined, all bin amplitudes which fall below the level
are set to 0, and usable thresholded data is obtained from this program.
The thresholded data are stored as filename.THR.
All data processing files access the .THR files to determine the wide band
channel parameters.

Last Revised --  July 6, 1990.

---------------------------------------------------------------  }

program thrshold ;
{$M 65520,0,655360 }
{$N+}
uses dos ;

type
  atype                    =     array[1..128,1..255] of integer ;
  btype                    =     array[1..128,1..255] of integer ;

var
  i,j,k,l,m,shots          :     integer                    ;
  choice1,check3           :     integer                    ;
  tempor1,tempor2,meanoise :     longint                    ;
  bintotal,lgth,avglevel   :     integer                    ;
  kk,kkk                   :     longint                    ;
  cutoff1,cutoff2,cutoff3  :     integer                    ;
  filename,filename1       :     string[50]                 ;
  path,pathdat             :     string[50]                 ;
  filetext                 :     text                       ;
  filess                   :     text                       ;
  filevar                  :     file                       ;
  filevar1                 :     file                       ;
  fileout                  :     file                       ;
  filehdr                  :     file                       ;
  waveform,waveraw         :     array[1..256] of integer   ;
  average                  :     array[1..255] of integer   ;
  avgtdata                 :     array[1..255] of integer   ;
  preamble                 :     array[0..9] of real        ;
  bdata                    :     ^atype                     ;
  tdata                    :     ^btype                     ;
  Dirinfo                  :     Searchrec                  ;
  keyword                  :     array[1..6] of string[80]  ;
  pathnum,keynumber        :     integer                    ;
  sum,sum1,sum2            :     longint                    ;
  sumnoise,sumtemp         :     longint                    ;
  avgint                   :     array[1..128] of longint   ;
  minvalue3                :     array[1..128] of longint   ;
  maxvalue                 :     array[1..128] of integer   ;
  avg,snr,window           :     real                       ;
  factr,factor,factor2     :     real                       ;
  ber1,ber2,ber3,stdevnse  :     real                       ;
  devavg,meanavg,devratio  :     real                       ;
  sumstand,summean         :     real                       ;
  nextbin,time             :     real                       ;
  deltatime,sumth          :     real                       ;
```

```
{ ------------------------------------------------------------ }

Procedure Read_Data ;
begin
   assign(filevar,path+'avg\dat\'+filename1+'.dat') ;
   reset(filevar,1) ;
      blockread(filevar,average,sizeof(average)) ;
   close(filevar) ;

   if pathnum = 10 then shots := 1 ;
   if pathnum < 10 then
   begin
      assign(filetext,path+'hed\'+filename1+'.hed') ;
      reset(filetext) ;
      readln(filetext,shots) ;
      shots := shots + 1 ;
   end ;
   if pathnum > 10 then shots := 128 ;
   if (pathnum < 11)  then
   begin
      for i := 0 to 9 do readln(filetext,preamble[i]) ;
      close(filetext) ;
      window := preamble[4] * 2.56e+11 ;
   end ;
   if (window > 300) then bintotal := round((window/3.90625)-1) ;
   if (window < 300) then bintotal := 51 ;
   lgth := bintotal * 2 ;

   assign(filevar,pathdat+'bin\'+filename1+'.bin') ;
   reset(filevar,1) ;
   for i := 1 to shots do
   begin
      blockread(filevar,waveform,lgth) ;
      for j := 1 to bintotal do bdata^[i,j] := waveform[j] ;
   end ;
   close(filevar) ;

end ;

{ ------------------------------------------------------------ }

Procedure Thold_Data ;
begin
   l := 0 ;
   summean := 0 ;
   sumstand := 0 ;
   for i := 1 to shots do
   begin
      tempor1 := 32767 ;
      tempor2 := 32767 ;
      cutoff1  := round(bintotal * 0.85) ;
      for j := 1 to cutoff1 do
         if bdata^[i,j] < tempor2 then tempor2 := bdata^[i,j] ;
      for j := cutoff1+1 to bintotal do
         if bdata^[i,j] < tempor1 then tempor1 := bdata^[i,j] ;
      if (tempor1 = 32767) then tempor1 := 32766 ;
      if (tempor2 > 31500) or (tempor1 < tempor2) then snr := 1.0
         else snr := (32767. - tempor2)/(32767. - tempor1) ;
      if pathnum > 10 then snr := 100 ;
      if snr < 5.0 then
      begin
         for m := 1 to bintotal do bdata^[i,m] := 32767 ;
```

```
            l := l + 1 ;
         end ;
         if (pathnum < 11) then cutoff3 := cutoff1 ;
         sumnoise := 0 ;
         for j := cutoff3 to bintotal do sumnoise := sumnoise + bdata^[i,j] ;
         meanoise := round(sumnoise / (bintotal + 1 - cutoff3)) ;
         sumtemp := 0 ;
         for j := cutoff3 to bintotal do
                  sumtemp := sumtemp + sqr(bdata^[i,j] - meanoise) ;
         stdevnse := sqrt(sumtemp / (bintotal - cutoff3)) ;
         if (meanoise = 32767) then devratio := 0.0
                               else devratio := stdevnse/(32767 - meanoise) ;

         if (devratio < 1.3) then factor2 := 3.5 else factor2 := 4.0 ;
         minvalue3[i] := round(meanoise - (factor2 * stdevnse)) ;
         sumstand := sumstand + stdevnse ;
         summean := summean + meanoise ;
      end ;
      devavg := sumstand/shots ;
      meanavg := summean/shots ;

      assign(filess,path+'gss\'+filename1+'.gss') ;
      rewrite(filess) ;
      writeln(filess,shots-l) ;
      writeln((shots-l):10) ;
      close(filess) ;

      cutoff2 := round(bintotal*0.10) ;
      for i := 1 to shots do
      begin
         for j := 1 to cutoff2 do
         begin
            if bdata^[i,j] >= (minvalue3[i]-3000) then tdata^[i,j] := 32767
            else tdata^[i,j] := bdata^[i,j] ;
         end ;
         for j := cutoff2+1 to bintotal do
         begin
            if (bdata^[i,j] < minvalue3[i]) then
            begin
               tdata^[i,j] := bdata^[i,j] ;
            end else
               tdata^[i,j] := 32767 ;
         end ;
      end ;
   end ;

   { ------------------------------------------------------------- }


   Procedure File_Output ;
   begin
      assign(fileout,path+'thr\'+filename1+'.thr') ;
      rewrite(fileout,1) ;
      for i := 1 to shots do
      begin
         for j := 1 to bintotal do waveform[j] := tdata^[i,j] ;
         blockwrite(fileout,waveform,lgth) ;
      end ;
      close(fileout) ;
   end ;


   { ------------------------------------------------------------- }
```

```
Procedure Thold_Average_Data ;
begin
   l := 0 ;
   summean := 0 ;
   sumstand := 0 ;
   tempor1 := 32767 ;
   tempor2 := 32767 ;
   cutoff1  := round(255 * 0.85) ;
   for j := 1 to cutoff1 do
      if average[j] < tempor2 then tempor2 := average[j] ;
   for j := cutoff1+1 to 255 do
      if average[j] < tempor1 then tempor1 := average[j] ;
   if (tempor1 = 32767) then tempor1 := 32766 ;
   if (tempor2 > 31500) or (tempor1 < tempor2) then snr := 1.0
      else snr := (32767. - tempor2)/(32767. - tempor1) ;
   if pathnum > 10 then snr := 100 ;
   if snr < 5.0 then for m := 1 to 255 do average[m] := 32767 ;
   if (pathnum < 11) then cutoff3 := cutoff1 ;
   sumnoise := 0 ;
   for j := cutoff3 to 255 do sumnoise := sumnoise + average[j] ;
   meanoise := round(sumnoise / (256 - cutoff3)) ;
   sumtemp := 0 ;
   for j := cutoff3 to 255 do
            sumtemp := sumtemp + sqr(average[j] - meanoise) ;
   stdevnse := sqrt(sumtemp / (255 - cutoff3)) ;
   if (meanoise = 32767) then devratio := 0.0
                         else devratio := stdevnse/(32767 - meanoise) ;

   if (devratio < 1.3) then factor2 := 3.5 else factor2 := 4.0 ;
   avglevel := round(meanoise - (factor2 * stdevnse)) ;
   writeln(avglevel:10) ;
   cutoff2 := round(255.0*0.10) ;
   for j := 1 to cutoff2 do
   begin
      if average[j] >= (avglevel-2000) then avgtdata[j] := 32767
      else avgtdata[j] := average[j] ;
   end ;
   for j := cutoff2+1 to 255 do
   begin
      if (average[j] < avglevel) then
      begin
         avgtdata[j] := average[j] ;
      end else
         avgtdata[j] := 32767 ;
   end ;
end ;


{  ------------------------------------------------------------  }


Procedure File_Output_Average_Data ;
begin
   assign(fileout,path+'avg\thr\'+filename1+'.thr') ;
   rewrite(fileout,1) ;
      blockwrite(fileout,avgtdata,sizeof(avgtdata)) ;
   close(fileout) ;

   assign(filetext,path+'avg\lev\'+filename1+'.lev') ;
   rewrite(filetext) ;
      writeln(filetext,avglevel) ;
   close(filetext) ;
end ;
```

```
{ ------------------------------------------------------------ }

Procedure Main_Module ;
begin
   case pathnum of
      1 : path :='f:\rdata\los\trlow\' ;
      2 : path :='f:\rdata\los\trmed\' ;
      3 : path :='f:\rdata\los\trhigh\' ;
      4 : path :='f:\rdata\par\trlow\' ;
      5 : path :='f:\rdata\par\trmed\' ;
      6 : path :='f:\rdata\par\trhigh\' ;
      7 : path :='f:\rdata\obs\trlow\' ;
      8 : path :='f:\rdata\obs\trmed\' ;
      9 : path :='f:\rdata\obs\trhigh\' ;
      10: path :='f:\gendat\' ;
      11: path :='f:\rdata\chkthd20\' ;
      12: path :='f:\rdata\chkthd50\' ;
      13: path :='f:\rdata\chktd100\' ;
   end ;
   case pathnum of
      1 : pathdat :='g:\rdata\los\trlow\' ;
      2 : pathdat :='g:\rdata\los\trmed\' ;
      3 : pathdat :='g:\rdata\los\trhigh\' ;
      4 : pathdat :='g:\rdata\par\trlow\' ;
      5 : pathdat :='g:\rdata\par\trmed\' ;
      6 : pathdat :='g:\rdata\par\trhigh\' ;
      7 : pathdat :='g:\rdata\obs\trlow\' ;
      8 : pathdat :='g:\rdata\obs\trmed\' ;
      9 : pathdat :='g:\rdata\obs\trhigh\' ;
      10: pathdat :='f:\gendat\' ;
      11: pathdat :='g:\rdata\chkthd20\' ;
      12: pathdat :='g:\rdata\chkthd50\' ;
      13: pathdat :='g:\rdata\chktd100\' ;
   end ;

   if choice1 = 1 then Keyword[keynumber] := '*' ;
   if choice1 = 2 then
   begin
      write('Number of filenames : ') ;
      readln(keynumber) ;

      for i := 1 to keynumber do
      begin
         write('filename[',i:1,'] : ') ;
         readln(Keyword[i]) ;
         Keyword[i] := pathdat+'dat\'+keyword[i]+'.dat' ;
      end ;
   end
   else Keyword[keynumber] := pathdat+'dat\'+keyword[keynumber]+'.dat' ;
   writeln(Keyword[keynumber]) ;
   writeln(path) ;
   for k := 1 to keynumber do
   begin
      FindFirst(keyword[k],archive,dirinfo) ;
      while DosERROR = 0 do
      begin
         filename1 := copy(dirinfo.name,1,length(dirinfo.name)-4) ;
         write(filename1) ;
         Read_Data ;
         if check3 = 1 then
         begin
            Thold_Data ;
            File_Output ;
```

```
            end ;
            if check3 = 2 then
            begin
               Thold_Average_Data ;
               File_Output_Average_Data ;
            end ;
            FindNext(dirinfo) ;
         end ;
      end ;
   end ;

{ ------------------------------------------------------------ }


begin
   new(bdata) ;
   new(tdata) ;

   write('Enter (1) for all local profiles, (2) for average local profile :');
   readln(check3) ;
   write('Enter (1) to compute for all paths, (2) to choose specifics : ') ;
   readln(choice1) ;
   if choice1 = 2 then
   begin
      write('Enter path number :') ;
      readln(pathnum) ;
      Main_Module ;
   end else begin
      keynumber := 1 ;
      for pathnum := 1 to 9 do Main_Module ;
   end;

   dispose(bdata) ;
   dispose(tdata) ;
end.
```

```
{  RMS.PAS  }

{  ------------------------------------------------------------

This program uses the filename.THR data files for each measurement
run to compute:

1.  The mean excess delay of all individual profiles.
2.  The mean excess delay of all spatially averaged profiles.
3.  The rms delay spread of all individual profiles.
4.  The rms delay spread of all spatially averaged profiles.
5.  The maximum excess delay < 10 dB for each measurement run.

6.  The parameter averaged values of rms delay spread and mean excess
    delay for each measurement location.

Last Revised --  July 31, 1990 (DAH).

------------------------------------------------------------  }

program rms ;
{$N+}
uses dos ;

type
  atype                    =     array[1..128,1..255] of integer ;

var
  shots,choice1,minvalue,lll:    longint                    ;
  i,j,k,l,m,n,ksa          :     longint                    ;
  avgtimeref,check3        :     integer                    ;
  filename,filename1,path  :     string[50]                 ;
  filetext                 :     text                       ;
  filevar                  :     file                       ;
  fileout1                 :     file                       ;
  fileout2                 :     file                       ;
  fileout3                 :     text                       ;
  filetemp                 :     text                       ;
  preamble                 :     array[0..9] of single      ;
  waveform                 :     array[1..256] of integer   ;
  max,timeref              :     array[1..128] of longint   ;
  min,yy                   :     array[1..128] of longint   ;
  tdata                    :     ^atype                     ;
  Dirinfo                  :     Searchrec                  ;
  keyword                  :     array[1..6] of string[80]  ;
  pathnum,keynumber        :     integer                    ;
  excdel,excdel1           :     array[1..256] of real      ;
  rmsdelay,rmsdelay1       :     array[1..256] of real      ;
  all                      :     array[1..8] of real        ;
  tdp                      :     array[1..5] of real        ;
  avgtdata                 :     array[1..255] of integer   ;
  bintotal,lgth,tempor1    :     integer                    ;
  avg,window,rmstest,medtest:    real                       ;
  trsep,atten              :     real                       ;
  avgt1,avgt2,denom,exctemp :    real                       ;
  time,alphaksq            :     real                       ;
  sum1,sum2,sum3,nn        :     real                       ;
  rmsavg,medavg            :     real                       ;
  maxrms,maxmed            :     real                       ;
  stddevmed,stddevrms      :     real                       ;
  maxvalue,maxtime         :     real                       ;
  avgexcdel,avgrmsdelay    :     real                       ;
  mvoltmax,mvolts,dbref    :     real                       ;
  dbreal,realmvolts        :     real                       ;
```

```
{ ------------------------------------------------------------ }

Function Log(x:double): double ;
begin
   if x <= 0.00000 then log := -200.00
   else log := ln(x)/ln(10.0) ;
end ;

{ ------------------------------------------------------------ }

Function Power (number,exponent : double ) : double ;
begin
   if exponent < -15.0 then power := 0.0 else
   begin
      if exponent = 0.0 then
         power := 1.0
      else if number < 0.0 then
         power := 0.0
      else
         power := exp(exponent * ln(number)) ;
   end ;
end ;

{ ------------------------------------------------------------ }

Procedure Read_Data ;
begin
   assign(filetext,path+'hed\'+filename1+'.hed') ;
   reset(filetext) ;
   readln(filetext,shots) ;
   shots := shots + 1 ;

   for i:=0 to 9 do readln(filetext,preamble[i]) ;
   close(filetext) ;

   mvoltmax := preamble[7] * preamble[9] * 2000.0 ;
   window := preamble[4] * 2.56e+11 ;
   if (window > 300) then bintotal := round((window/3.90625) - 1) ;
   if (window < 300) then bintotal := 51 ;
   lgth := bintotal * 2 ;
   window := preamble[4] * 2.56e+11 ;
   if (window > 300) then bintotal := round((window/3.90625)-1) ;
   if (window < 300) then bintotal := 51 ;
   lgth := bintotal * 2 ;

   assign(filevar,path+'thr\'+filename1+'.thr') ;
   reset(filevar,1) ;
   for i := 1 to shots do
      begin
        blockread(filevar,waveform,lgth) ;
        for j := 1 to bintotal do tdata^[i,j] := waveform[j] ;
      end ;
   close(filevar) ;

   assign(filevar,path+'avg\thr\'+filename1+'.thr') ;
   reset(filevar,1) ;
   blockread(filevar,avgtdata,sizeof(avgtdata)) ;
   close(filevar) ;
end ;
```

```
{ ---------------------------------------------------------- }

Procedure Calc_RMS_Delay ;
begin
   ksa := 0 ;

   for i := 1 to shots do
   begin
      avgt1 := 0 ;
      avgt2 := 0 ;
      denom := 0 ;
      tempor1 := 32767 ;
      for j := 1 to bintotal do
      begin
         if (tdata^[i,j] < tempor1) then tempor1 := tdata^[i,j] ;
      end ;
      if tempor1 > 28670 then
      begin
         tempor1 := 32767 ;
         for j := 1 to bintotal do tdata^[i,j] := 32767 ;
      end ;

      for j := 1 to bintotal do
      begin
         mvolts := ((32767 - tdata^[i,j])/32767.0) * (mvoltmax/40.0) ;
         dbref := 10 * log(mvolts) ;
         if (dbref > -16) then dbreal := dbref*1.1 else dbreal := dbref*1.2 ;
         realmvolts := 40.0 * power(10.0,dbreal/10.0) ;
         tdata^[i,j] := round(32767.0 - ((realmvolts * 32767.0)/mvoltmax)) ;
      end ;

      if tempor1 = 32767 then l := 1 ;
      if tempor1 < 28669 then
      begin
         m := 1 ;
         repeat
            m := m + 1 ;
         until tdata^[i,m] > tdata^[i,m-1] ;
         l := m - 1 ;
      end ;
      timeref[i] := l ;
      m := 0 ;
      minvalue := 32767 ;
      for j := l to bintotal do
      begin
         if tdata^[i,j] < minvalue then
         begin
            minvalue := tdata^[i,j] ;
            yy[i] := j ;
         end ;
         time     := ((j-timeref[i]) * 3.90625) - 1.953125 ;
         time     := time * 1e-09 ;
         alphaksq := 32767.0 - tdata^[i,j] ;
         avgt1    := avgt1 + alphaksq * time ;
         avgt2    := avgt2 + alphaksq * sqr(time) ;
         denom    := denom + alphaksq ;
      end ;
      min[i] := minvalue ;
      if denom = 0.0 then excdel[i] := 0.0 ;
      if denom = 0.0 then rmsdelay[i] := 0.0
      else begin
         exctemp     :=  avgt1 / denom ;
```

```
         excdel[i]   :=  exctemp * 1e09 ;
         avgt2       :=  avgt2 / denom ;
         rmsdelay[i] :=  (sqrt(abs(avgt2 - sqr(exctemp)))) * 1e09 ;
      end ;
      if rmsdelay[i] < 3.5 then
      begin
         rmsdelay[i] := 0.0 ;
         ksa := ksa + 1 ;
      end ;
   end ;
end ;


{ ------------------------------------------------------------ }


Procedure Calc_RMS_Delay_Average_Profile ;
begin
   avgt1 := 0 ;
   avgt2 := 0 ;
   denom := 0 ;
   tempor1 := 32767 ;
   for j := 1 to 255 do
   begin
      if (avgtdata[j] < tempor1) then tempor1 := avgtdata[j] ;
   end ;
   if tempor1 > 31100 then
   begin
      tempor1 := 32767 ;
      for j := 1 to 255 do avgtdata[j] := 32767 ;
   end ;

   for j := 1 to 255 do
      begin
         mvolts := ((32767 - avgtdata[j])/32767.0) * (mvoltmax/40.0) ;
         dbref := 10 * log(mvolts) ;
         if (dbref > -16) then dbreal := dbref*1.1 else dbreal := dbref*1.2 ;
         realmvolts := 40.0 * power(10.0,dbreal/10.0) ;
         avgtdata[j] := round(32767.0 - ((realmvolts * 32767.0)/mvoltmax)) ;
      end ;

   if tempor1 = 32767 then l := 1 ;
   if tempor1 < 31101 then
   begin
      m := 1 ;
      repeat
         m := m + 1 ;
      until avgtdata[m] < avgtdata[m-1] ;
      l := m - 1 ;
   end ;
   avgtimeref := l ;
   m := 0 ;
   minvalue := 32767 ;
   for j := l to 255 do
   begin
      if avgtdata[j] < minvalue then minvalue := avgtdata[j] ;
      time     := ((j-avgtimeref) * (window/255.0)) ;
      time     := time * 1e-09 ;
      alphaksq := 32767.0 - avgtdata[j] ;
      avgt1    := avgt1 + alphaksq * time ;
      avgt2    := avgt2 + alphaksq * sqr(time) ;
      denom    := denom + alphaksq ;
   end ;
   if denom = 0.0 then avgexcdel := 0.0 ;
   if denom = 0.0 then avgrmsdelay := 0.0
```

```
   else begin
      exctemp     :=  avgt1 / denom ;
      avgexcdel   :=  exctemp * 1e09 ;
      avgt2       :=  avgt2 / denom ;
      avgrmsdelay :=  (sqrt(abs(avgt2 - sqr(exctemp)))) * 1e09 ;
   end ;
   writeln(avgexcdel:10:4,avgrmsdelay:20:4) ;

   assign(filetext,path+'avg\rms\'+filename1+'.rms') ;
   rewrite(filetext) ;
   writeln(filetext,avgrmsdelay) ;
   close(filetext) ;

   assign(filetext,path+'avg\med\'+filename1+'.med') ;
   rewrite(filetext) ;
   writeln(filetext,avgexcdel) ;
   close(filetext) ;
end ;


{  ------------------------------------------------------------  }


Procedure Statistics ;
begin
   nn := shots - ksa ;
   sum1 := 0.0 ;
   sum3 := 0.0 ;

   for i := 1 to shots do
   begin
      sum1 := sum1 + rmsdelay[i] ;
      sum3 := sum3  +  excdel[i] ;
   end;

   rmsavg := sum1/nn ;
   medavg := sum3/nn ;

   sum2 := 0 ;
   for i := 1 to shots do
   begin
      if rmsdelay[i] < 1.0 then rmstest := 0 else rmstest := rmsavg ;
      sum2 := sum2 + sqr(rmsdelay[i] - rmstest) ;
   end ;
   stddevrms := sqrt((sum2)/(nn-1)) ;

   sum3 := 0 ;
   for i := 1 to shots do
   begin
      if excdel[i] < 1.0 then medtest := 0 else medtest := rmsavg ;
      sum3 := sum3 + sqr(excdel[i] - medtest) ;
   end ;
   stddevmed := sqrt((sum3)/(nn-1)) ;
   maxrms := 0.0 ;
   maxmed := 0.0 ;
   for i := 1 to shots do
   begin
      if (rmsdelay[i] > maxrms) then maxrms := rmsdelay[i] ;
      if (excdel[i] > maxmed) then maxmed := excdel[i] ;
   end ;
   writeln(maxrms:10:4,maxmed:10:4) ;
end ;


{  ------------------------------------------------------------  }
```

```
Procedure Max_Excess_Delay ;
begin
   for i := 1 to shots do
   begin
      m := 0 ;
      maxvalue := 32767 - min[i] ;
      for j := 1 to bintotal do
      begin
         alphaksq := 32767 - tdata^[i,j] ;
         if (alphaksq > (maxvalue/10.0)) and
            (j > (yy[i]+(round((bintotal/255.0) * 5.0)))) then m:=j ;
      end ;

      max[i] := m ;
      if rmsdelay[i] < 3.5 then max[i] := 1 ;
   end ;
   maxvalue := -100.0 ;
   for i := 1 to shots do
   begin
      if max[i] > maxvalue then
      begin
         maxvalue := max[i] ;
         lll := timeref[i] ;
      end ;
   end ;
   maxtime := ((maxvalue-lll) * 3.90625) - 1.953125 ;
   writeln(nn:10:2,rmsavg:10:4,medavg:10:4,stddevrms:10:4,maxtime:10:4) ;
end ;


{ ------------------------------------------------------------ }


Procedure File_Output ;
begin
   assign(fileout1,path+'med\'+filename1+'.med') ;
   assign(fileout2,path+'rms\'+filename1+'.rms') ;
   rewrite(fileout1,1) ;
   rewrite(fileout2,1) ;
   blockwrite(fileout1,excdel,sizeof(excdel)) ;
   blockwrite(fileout2,rmsdelay,sizeof(rmsdelay)) ;
   close(fileout1) ;
   close(fileout2) ;

   assign(filetemp,path+'all\'+filename1+'.all') ;
   reset(filetemp) ;
   for i := 1 to 8 do readln(filetemp,all[i]) ;
   close(filetemp) ;

   trsep := all[3] ;
   atten := all[4] ;
   tdp[1] := medavg ;
   tdp[2] := stddevmed ;
   tdp[3] := rmsavg ;
   tdp[4] := stddevrms ;
   tdp[5] := maxtime ;

   assign(filetemp,path+'tdp\'+filename1+'.tdp') ;
   rewrite(filetemp) ;
   for i := 1 to 5 do writeln(filetemp,tdp[i]) ;
   close(filetemp) ;

   assign(filetemp,path+'trs\'+filename1+'.trs') ;
```

```
   rewrite(filetemp) ;
   writeln(filetemp,trsep) ;
   close(filetemp) ;

   assign(filetemp,path+'att\'+filename1+'.att') ;
   rewrite(filetemp) ;
   writeln(filetemp,atten) ;
   close(filetemp) ;
end ;


{ ------------------------------------------------------------ }


Procedure Main_Module ;
begin
   case pathnum of
      1 : path :='f:\rdata\los\trlow\' ;
      2 : path :='f:\rdata\los\trmed\' ;
      3 : path :='f:\rdata\los\trhigh\' ;
      4 : path :='f:\rdata\par\trlow\' ;
      5 : path :='f:\rdata\par\trmed\' ;
      6 : path :='f:\rdata\par\trhigh\' ;
      7 : path :='f:\rdata\obs\trlow\' ;
      8 : path :='f:\rdata\obs\trmed\' ;
      9 : path :='f:\rdata\obs\trhigh\' ;
   end ;
   if choice1 = 1 then Keyword[keynumber] := '*' ;
   if choice1 = 2 then
   begin
      write('Number of filenames : ') ;
      readln(keynumber) ;

      for i := 1 to keynumber do
      begin
         write('filename[',i:1,'] : ') ;
         readln(Keyword[i]) ;
         Keyword[i] := path+'thr\'+keyword[i]+'.thr' ;
      end ;
   end
   else Keyword[keynumber] := path+'thr\'+Keyword[keynumber]+'.thr' ;
   writeln(pathnum) ;
   writeln(Keyword[keynumber]) ;
   writeln(path) ;
   for k := 1 to keynumber do
   begin
      FindFirst(keyword[k],archive,dirinfo) ;
      while DosERROR = 0 do
      begin
         filename1 := copy(dirinfo.name,1,length(dirinfo.name)-4) ;
         write(filename1) ;
         Read_Data ;
         if (check3 = 2) then Calc_RMS_Delay_Average_Profile
         else begin
            Calc_RMS_Delay ;
            Statistics ;
            Max_Excess_Delay ;
            File_Output ;
         end ;
         FindNext(dirinfo) ;
      end ;
   end ;
end ;
```

```
{ ------------------------------------------------------------ }

begin
   new(tdata) ;

   write('Enter (1) for all local profiles, (2) for average local profile : ');
   readln(check3) ;
   write('Enter (1) to compute for all paths, (2) to choose specifics : ') ;
   readln(choice1) ;
   if choice1 = 2 then
   begin
      write('Enter Path Number : ') ;
      readln(pathnum) ;
      Main_Module ;
   end
   else
   begin
      keynumber := 1 ;
      for pathnum := 1 to 9 do Main_Module ;
   end ;

   dispose(tdata) ;
end.
```

```
{  JITTER.PAS  }

{  ------------------------------------------------------------

This program computes the time delay jitter and differential delay jitter
for each profile and each set of 2 consecutive profiles, respectively.
The program stores the raw delay jitter files as filename.JIT and the raw
differential delay jitter files as filename.DDJ.
The program also computes the peak-to-peak values (with other less meaningful
values) as filename.JTS and filename.DJS for time delay jitter and
differential delay jitter, respectively.

Last Revised --  July 1, 1990 (DAH).

------------------------------------------------------------------  }



program jitter ;
{$N+}
uses Graph, Crt, Dos, PrintJet ;

var
  i,k,l,ll,shots,choice1    :     integer                    ;
  check2,endloop,atten      :     integer                    ;
  grdriver,grmode           :     integer                    ;
  pathnum,keynumber         :     integer                    ;
  filename,filename1        :     string[50]                 ;
  path,pathdat              :     string[50]                 ;
  all                       :     array[1..8] of real        ;
  meanexc,rmsdelay          :     array[1..128] of real      ;
  jitter_use_avgmed         :     array[1..128] of real      ;
  jitter_use_medavg         :     array[1..128] of real      ;
  diff_jitter               :     array[1..127] of real      ;
  dummy                     :     real                       ;
  avgrms,rmsavg             :     real                       ;
  avgmed,medavg             :     real                       ;
  jitter1min,jitter2min     :     real                       ;
  jitter1max,jitter2max     :     real                       ;
  sumjit1raw,sumjit2raw     :     real                       ;
  sumjit1abs,sumjit2abs     :     real                       ;
  rawavgjit1,rawavgjit2     :     real                       ;
  absavgjit1,absavgjit2     :     real                       ;
  peakpeakjit1,peakpeakjit2 :     real                       ;
  maxdevjit1,maxdevjit2     :     real                       ;
  difjitmin,difjitmax       :     real                       ;
  sumddjraw,sumddjabs       :     real                       ;
  rawavgddj,absavgddj       :     real                       ;
  peakpeakdifjit            :     real                       ;
  maxdevdifjit              :     real                       ;
  filetext                  :     text                       ;
  filevar                   :     file                       ;
  fileout                   :     file                       ;
  Dirinfo                   :     Searchrec                  ;
  keyword                   :     array[1..6] of string[80]  ;

{  ------------------------------------------------------------  }


Procedure Read_Data ;
begin
   assign(filetext,path+'hed\'+filename1+'.hed') ;
   reset(filetext) ;
```

```
   readln(filetext,shots) ;
   shots := shots + 1 ;
   close(filetext) ;

   assign(filetext,path+'tdp\'+filename1+'.tdp') ;
   reset(filetext) ;
   readln(filetext,avgmed) ;
   readln(filetext,dummy) ;
   readln(filetext,avgrms) ;
   close(filetext) ;

   assign(filetext,path+'avg\rms\'+filename1+'.rms') ;
   reset(filetext) ;
   readln(filetext,rmsavg) ;
   close(filetext) ;

   assign(filetext,path+'avg\med\'+filename1+'.med') ;
   reset(filetext) ;
   readln(filetext,medavg) ;
   close(filetext) ;

   assign(filevar,path+'rms\'+filename1+'.rms') ;
   reset(filevar,1) ;
   blockread(filevar,rmsdelay,sizeof(rmsdelay)) ;
   close(filevar) ;

   assign(filevar,path+'med\'+filename1+'.med') ;
   reset(filevar,1) ;
   blockread(filevar,meanexc,sizeof(meanexc)) ;
   for i := 1 to 128 do writeln(i:10,meanexc[i]:10:2) ;
   close(filevar) ;
end ;


{  ------------------------------------------------------------  }


Procedure Compute_Jitter ;
begin
   assign(filetext,path+'jit\'+filename1+'.jit') ;
   rewrite(filetext) ;

   jitter1max := -100.0 ;
   jitter2max := -100.0 ;
   jitter1min := +100.0 ;
   jitter2min := +100.0 ;
   sumjit1raw := 0.0 ;
   sumjit1abs := 0.0 ;
   sumjit2raw := 0.0 ;
   sumjit2abs := 0.0 ;
   l := 0 ;
   for i := 1 to shots do
   begin
      if (meanexc[i] > 1.0) then
      begin
         jitter_use_avgmed[i] := meanexc[i] - avgmed ;
         if jitter_use_avgmed[i] > jitter1max then
                                   jitter1max := jitter_use_avgmed[i] ;
         if jitter_use_avgmed[i] < jitter1min then
                                   jitter1min := jitter_use_avgmed[i] ;
         sumjit1raw := sumjit1raw + jitter_use_avgmed[i] ;
         sumjit1abs := sumjit1abs + abs(jitter_use_avgmed[i]) ;

         jitter_use_medavg[i] := meanexc[i] - medavg ;
         if jitter_use_medavg[i] > jitter2max then
```

```
                                    jitter2max := jitter_use_medavg[i] ;
          if jitter_use_medavg[i] < jitter2min then
                                    jitter2min := jitter_use_medavg[i] ;
          sumjit2raw := sumjit2raw + jitter_use_medavg[i] ;
          sumjit2abs := sumjit2abs + abs(jitter_use_medavg[i]) ;

          l := l + 1 ;
          writeln(filetext,i:3,jitter_use_avgmed[i]:8:2,
                               jitter_use_medavg[i]:8:2) ;
       end ;
    end ;
    close(filetext) ;
    write(l:6) ;
    rawavgjit1 := sumjit1raw/l ;
    absavgjit1 := sumjit1abs/l ;
    rawavgjit2 := sumjit2raw/l ;
    absavgjit2 := sumjit2abs/l ;
    peakpeakjit1 := jitter1max-jitter1min ;
    peakpeakjit2 := jitter2max-jitter2min ;

    if (abs(jitter1max) > abs(jitter1min)) then maxdevjit1 := abs(jitter1max) ;
    if (abs(jitter2max) > abs(jitter2min)) then maxdevjit2 := abs(jitter2max) ;
    if (abs(jitter1max) < abs(jitter1min)) then maxdevjit1 := abs(jitter1min) ;
    if (abs(jitter2max) < abs(jitter2min)) then maxdevjit2 := abs(jitter2min) ;

    assign(filetext,path+'jts\'+filename1+'.jts') ;
    rewrite(filetext) ;
    writeln(filetext,jitter1max:8:2,jitter2max:8:2) ;
    writeln(filetext,jitter1min:8:2,jitter2min:8:2) ;
    writeln(filetext,peakpeakjit1:8:2,peakpeakjit2:8:2) ;
    writeln(filetext,maxdevjit1:8:2,maxdevjit2:8:2) ;
    writeln(filetext,rawavgjit1:8:2,rawavgjit2:8:2) ;
    writeln(filetext,absavgjit1:8:2,absavgjit2:8:2) ;
    close(filetext) ;
end ;


{ ------------------------------------------------------------ }


Procedure Compute_Diff_Jitter ;
begin
    assign(filetext,path+'ddj\'+filename1+'.ddj') ;
    rewrite(filetext) ;
    ll := 0 ;
    difjitmax := -500.0 ;
    difjitmin := +500.0 ;
    sumddjraw := 0.0 ;
    sumddjabs := 0.0 ;
    for i := 1 to shots-1 do
    begin
       if (meanexc[i] > 1.0) and (meanexc[i+1] > 1.0) then
       begin
          diff_jitter[i] := meanexc[i+1] - meanexc[i] ;
          if diff_jitter[i] > difjitmax then
                                    difjitmax := diff_jitter[i] ;
          if diff_jitter[i] < difjitmin then
                                    difjitmin := diff_jitter[i] ;
          sumddjraw := sumddjraw + diff_jitter[i] ;
          sumddjabs := sumddjabs + abs(diff_jitter[i]) ;
          ll := ll + 1 ;
          writeln(filetext,i:3,diff_jitter[i]:8:2) ;
       end ;
    end ;
    close(filetext) ;
```

```
    writeln(ll:6,difjitmax:10:2,difjitmin:10:2,(difjitmax - difjitmin):10:2) ;
    rawavgddj := sumddjraw/l ;
    absavgddj := sumddjabs/l ;
    peakpeakdifjit := difjitmax - difjitmin ;
    if (abs(difjitmax) > abs(difjitmin)) then maxdevdifjit := abs(difjitmax) ;
    if (abs(difjitmax) < abs(difjitmin)) then maxdevdifjit := abs(difjitmin) ;

    assign(filetext,path+'djs\'+filename1+'.djs') ;
    rewrite(filetext) ;
    writeln(filetext,difjitmax:8:2) ;
    writeln(filetext,difjitmin:8:2) ;
    writeln(filetext,peakpeakdifjit:8:2) ;
    writeln(filetext,maxdevdifjit:8:2) ;
    writeln(filetext,rawavgddj:8:2) ;
    writeln(filetext,absavgddj:8:2) ;
    close(filetext) ;
end ;


{  ------------------------------------------------------------  }


Procedure Main_Module ;
begin
    case pathnum of
       1 : path :='f:\rdata\los\trlow\' ;
       2 : path :='f:\rdata\los\trmed\' ;
       3 : path :='f:\rdata\los\trhigh\' ;
       4 : path :='f:\rdata\par\trlow\' ;
       5 : path :='f:\rdata\par\trmed\' ;
       6 : path :='f:\rdata\par\trhigh\' ;
       7 : path :='f:\rdata\obs\trlow\' ;
       8 : path :='f:\rdata\obs\trmed\' ;
       9 : path :='f:\rdata\obs\trhigh\' ;
    end ;
    case pathnum of
       1 : pathdat :='g:\rdata\los\trlow\' ;
       2 : pathdat :='g:\rdata\los\trmed\' ;
       3 : pathdat :='g:\rdata\los\trhigh\' ;
       4 : pathdat :='g:\rdata\par\trlow\' ;
       5 : pathdat :='g:\rdata\par\trmed\' ;
       6 : pathdat :='g:\rdata\par\trhigh\' ;
       7 : pathdat :='g:\rdata\obs\trlow\' ;
       8 : pathdat :='g:\rdata\obs\trmed\' ;
       9 : pathdat :='g:\rdata\obs\trhigh\' ;
    end ;

    if choice1 = 1 then Keyword[keynumber] := '*' ;
    if choice1 = 2 then
    begin
       write('Number of filenames : ') ;
       readln(keynumber) ;

       for i := 1 to keynumber do
       begin
          write('filename[',i:1,'] : ') ;
          readln(Keyword[i]) ;
          Keyword[i] := pathdat+'dat\'+keyword[i]+'.dat' ;
       end ;
    end
    else Keyword[keynumber] := pathdat+'dat\'+keyword[keynumber]+'.dat' ;
    writeln(Keyword[keynumber]) ;
    writeln(path) ;
    for k := 1 to keynumber do
    begin
```

```
      FindFirst(keyword[k],archive,dirinfo) ;
      while DosERROR = 0 do
      begin
         filename1 := copy(dirinfo.name,1,length(dirinfo.name)-4) ;
         write(filename1) ;

         Read_Data ;
         Compute_Jitter ;
         Compute_Diff_Jitter ;
         FindNext(dirinfo) ;
      end ;
   end ;
end ;


{  ------------------------------------------------------------  }


begin
   write('Enter (1) to compute for all paths, (2) to choose specifics : ') ;
   readln(choice1) ;
   if choice1 = 2 then
   begin
      write('Enter Path Number : ') ;
      readln(pathnum) ;
      Main_Module ;
   end
   else
   begin
      keynumber := 1 ;
      for pathnum := 1 to 9 do Main_Module ;
   end ;
end.
```

```
{  PATHLOSS.PAS  }

{  ---------------------------------------------------------------

This program computes path loss values with reference to 1 meter for
each individual profile.  The program also computes the parameter average,
minimum and maximum path loss values for each measurement run and stores
these 3 parameters as filename.PS1 parameters.
This program can be easily modified to determine values reference to
10 wavelengths, and at one point computed these values and stored the
same 3 parameters for a 10 wavelength reference as filename.PLS.

Last Revised -- October 10, 1990 (DAH).

--------------------------------------------------------------------  }


{$N+}
uses dos ;

type
  atype                    =     array[1..128,1..255] of integer ;
  datatype1                =     array[1..29] of double          ;

var
  i,j,k,l,m,check3         :     integer                     ;
  shots,choice1,lgth       :     integer                     ;
  tempor1,tempor2,bintotal :     integer                     ;
  filename,filename1,path  :     string[50]                  ;
  filebb,freq,site,anth    :     string[50]                  ;
  bsl,numb,filecc          :     string[50]                  ;
  splntext                 :     text                        ;
  filetext                 :     text                        ;
  fileall                  :     text                        ;
  bbstat                   :     text                        ;
  plstats                  :     text                        ;
  plrawdat                 :     file                        ;
  filevar                  :     file                        ;
  bbdat                    :     file                        ;
  bbhdr                    :     file                        ;
  preamble                 :     array[0..9] of single       ;
  waveform                 :     array[1..256] of integer    ;
  bbpre                    :     array[0..9] of single       ;
  bbwfm                    :     array[1..256] of integer    ;
  bbmvdata                 :     array[1..256] of real       ;
  prmvdata                 :     array[1..256] of real       ;
  prpower                  :     array[1..128] of real       ;
  ploss                    :     array[1..128] of real       ;
  maxvolt                  :     array[1..128] of real       ;
  avgtdata                 :     array[1..255] of integer    ;
  avgprmvdata              :     array[1..255] of real       ;
  tdata                    :     ^atype                      ;
  mv,dbm,y1                :     datatype1                   ;
  Dirinfo                  :     Searchrec                   ;
  keyword                  :     array[1..6] of string[80]   ;
  pathnum,keynumber        :     integer                     ;
  sum                      :     longint                     ;
  avgint                   :     array[1..128] of longint    ;
  minvalue                 :     array[1..128] of integer    ;
  maxvalue                 :     array[1..128] of integer    ;
  avg,taubb,sumbb,refpower :     real                        ;
  atten,bbatten,taupr,sumpr :    real                        ;
  bbvolts,bbmvolts         :     real                        ;
  volts,mvolts,gss,ratio   :     real                        ;
  trsep,value,valuedb      :     real                        ;
```

```
  ref1,ref2,logger          :      real                        ;
  cblefact,errfact,ratio1   :      real                        ;
  sumloss,minloss,antfact   :      real                        ;
  avgloss,maxloss,detfact   :      real                        ;
  window,sumtemp,realloss   :      real                        ;
  maxavvolt,avgprpower      :      real                        ;
  avgpathloss               :      real                        ;

{  ------------------------------------------------------------  }

Function Log(x:double): double ;
begin
   if x <= 0.00000 then log := -200.00
   else log := ln(x)/ln(10.0) ;
end ;

{  ------------------------------------------------------------  }

Function Power (number,exponent : double ) : double ;
begin
   if exponent = 0.0 then
      power := 1.0
   else if number < 0.0 then
      power := 0.0
   else
      power := exp(exponent * ln(number)) ;
end ;

{  ------------------------------------------------------------  }

Procedure Read_Data ;
begin
   assign(filevar,path+'avg\dat\'+filename1+'.dat') ;
   reset(filevar,1) ;
   blockread(filevar,avgtdata,sizeof(avgtdata)) ;
   close(filevar) ;

   assign(filetext,path+'hed\'+filename1+'.hed') ;
   reset(filetext) ;
   readln(filetext,shots) ;
   shots := shots + 1 ;
   for i:=0 to 9 do readln(filetext,preamble[i]) ;
   close(filetext) ;

   mvolts := preamble[7] * preamble[9] * 2000.0 ;
   window := preamble[4] * 2.56e+11 ;
   if (window > 300) then bintotal := round((window/3.90625) - 1) ;
   if (window < 300) then bintotal := 51 ;
   lgth := bintotal * 2 ;

   assign(filevar,path+'thr\'+filename1+'.thr') ;
   reset(filevar,1) ;
   for i := 1 to shots do
   begin
      blockread(filevar,waveform,lgth) ;
      for j := 1 to 255 do tdata^[i,j] := waveform[j] ;
   end ;
   close(filevar) ;
```

```
   assign(fileall,path+'trs\'+filename1+'.trs') ;
   reset(fileall) ;
   readln(fileall,trsep) ;
   close(fileall) ;

   assign(fileall,path+'att\'+filename1+'.att') ;
   reset(fileall) ;
   readln(fileall,atten) ;
   close(fileall) ;

   assign(bbhdr,filecc+'.hdr') ;
   reset(bbhdr,1) ;
   blockread(bbhdr,bbpre,sizeof(bbpre)) ;
   bbmvolts := bbpre[7]*bbpre[9]*2000.0 ;
   close(bbhdr) ;

   assign(bbdat,filecc+'.dat') ;
   reset(bbdat,1) ;
   blockread(bbdat,bbwfm,sizeof(bbwfm)) ;
   close(bbdat) ;

   assign(bbstat,filecc+'.bbd') ;
   reset(bbstat) ;
   readln(bbstat,bbvolts) ;
   readln(bbstat,bbatten) ;
   close(bbstat) ;

end ;


{ ------------------------------------------------------------ }


Procedure Reference_Power ;
begin
   taubb := 3.90625e-10 ;
   sumbb := 0.0 ;
   for i := 1 to 255 do
   begin
      bbwfm[i] := 32767 - bbwfm[i] ;
      bbmvdata[i] := (bbwfm[i]/32767.0) * bbmvolts ;
      if bbmvdata[i] < 3.0 then bbmvdata[i] := 0.01 ;
      sumbb := sumbb + bbmvdata[i] ;
   end ;
   refpower := sumbb * taubb ;
end ;


{ ------------------------------------------------------------ }


Procedure Profile_Power ;
begin
   taupr := (1000.0/255.0) * 1e-09 ;
   for i := 1 to shots do
   begin
      sumpr := 0.0 ;
      maxvolt[i] := 0.0 ;
      for j := 1 to bintotal do
      begin
         tdata^[i,j] := 32767 - tdata^[i,j] ;
         prmvdata[j] := (tdata^[i,j]/32767.0) * mvolts ;
         if prmvdata[j] > maxvolt[i] then maxvolt[i] := prmvdata[j] ;
         sumpr := sumpr + prmvdata[j] ;
      end ;
```

```
      prpower[i] := sumpr * taupr ;
      logger := 10.0 * log(prpower[i]/refpower) ;
      if freq = '1' then antfact := 0.173 ;
      if freq = '4' then antfact := 7.447 ;

      if maxvolt[i] < 41.0 then detfact := 0.40 ;
      if maxvolt[i] < 20.0 then detfact := 0.75 ;
      if maxvolt[i] < 10.0 then detfact := 1.35 ;
      if maxvolt[i] < 5.00 then detfact := 2.10 ;
      if maxvolt[i] < 2.50 then detfact := 2.80 ;
      if maxvolt[i] < 1.25 then detfact := 3.30 ;
      if maxvolt[i] < 0.001 then detfact := 0.00 ;

      ploss[i] := (bbatten-atten) + detfact - logger ;

      if (freq = '4') then ploss[i] := ploss[i] - 49.506 ;
      if (freq = '1') then ploss[i] := ploss[i] - 42.126 ;

      if (anth = 'H') and (freq = '4') then cblefact := 2.5 ;
      if (anth = 'H') and (freq = '1') then cblefact := 1.2 ;
      if (anth = 'L')                  then cblefact := 0.0 ;

      if ((site='1') and (bsl='A') and ((numb='5') or (numb='6'))) then
      errfact := 10.0
      else errfact := 0.0 ;

      if (freq = '1') then ploss[i] := ploss[i] + 7.26 ;
      if (freq = '4') then ploss[i] := ploss[i] - 2.50 ;

      ploss[i] := ploss[i] - cblefact + errfact ;
   end ;
end ;


{ ------------------------------------------------------------ }


Procedure Profile_Power_Average_Profile ;
begin
   taupr := (window/255.0) * 1e-09 ;
   sumpr := 0.0 ;
   maxavvolt := 0.0 ;
   for j := 1 to 255 do
   begin
      avgtdata[j] := 32767 - avgtdata[j] ;
      avgprmvdata[j] := (avgtdata[j]/32767.0) * mvolts ;
      if avgprmvdata[j] > maxavvolt then maxavvolt := avgprmvdata[j] ;
      sumpr := sumpr + avgprmvdata[j] ;
   end ;
   avgprpower := sumpr * taupr ;
   logger := 10.0 * log(avgprpower/refpower) ;
   if freq = '1' then antfact := 0.173 ;
   if freq = '4' then antfact := 7.447 ;

   if maxavvolt < 41.0 then detfact := 0.40 ;
   if maxavvolt < 20.0 then detfact := 0.75 ;
   if maxavvolt < 10.0 then detfact := 1.35 ;
   if maxavvolt < 5.00 then detfact := 2.10 ;
   if maxavvolt < 2.50 then detfact := 2.80 ;
   if maxavvolt < 1.25 then detfact := 3.30 ;
   if maxavvolt < 0.001 then detfact := 0.00 ;

   avgpathloss := (bbatten-atten) + detfact - logger ;
   if (freq = '4') then avgpathloss := avgpathloss - 49.506 ;
   if (freq = '1') then avgpathloss := avgpathloss - 42.126 ;
```

```
   if (anth = 'H') and (freq = '4') then cblefact := 2.5 ;
   if (anth = 'H') and (freq = '1') then cblefact := 1.2 ;
   if (anth = 'L')                  then cblefact := 0.0 ;

   if ((site='1') and (bsl='A') and ((numb='5') or (numb='6'))) then
   errfact := 10.0
   else errfact := 0.0 ;

   if (freq = '1') then avgpathloss := avgpathloss + 7.26 ;
   if (freq = '4') then avgpathloss := avgpathloss - 2.50 ;

   avgpathloss := avgpathloss - cblefact + errfact ;
   writeln(avgpathloss:12:4,avgloss:12:4,(avgpathloss-avgloss):12:7) ;

   assign(filetext,path+'avg\ps1\'+filename1+'.ps1') ;
   rewrite(filetext) ;
   writeln(filetext,avgpathloss) ;
   close(filetext) ;
end ;


{ ------------------------------------------------------------ }


Procedure Path_Loss_Statistics ;
begin
j := 0 ;
sumtemp := 0.0 ;
sumloss := 0.0 ;
maxloss := 0.0 ;
minloss := 150.0 ;
   for i := 1 to shots do
   begin
      if abs(ploss[i]) < 200.0 then
      begin
         ratio1 := 1.0 / Power(10.0,(ploss[i]/10.0)) ;
         j := j + 1 ;
         sumloss := sumloss + ploss[i] ;
         sumtemp := sumtemp + ratio1 ;
         if ploss[i] > maxloss then maxloss := ploss[i] ;
         if ploss[i] < minloss then minloss := ploss[i] ;
      end ;
   end ;
      avgloss := sumloss/j ;
      realloss := sumtemp/j ;
      realloss := abs(10.0 * log(realloss)) ;
end ;


{ ------------------------------------------------------------ }


Procedure File_Out ;
begin
   assign(plstats,path+'pls\'+filename1+'.pls') ;
   rewrite(plstats) ;
   writeln(plstats,trsep:12:4,realloss:12:4) ;
   writeln(trsep:12:4,realloss:12:4) ;
   close(plstats) ;

   assign(filevar,path+'pld\'+filename1+'.pld') ;
   rewrite(filevar,1) ;
   blockwrite(filevar,ploss,sizeof(ploss)) ;
   close(filevar) ;
```

```
end ;

{ ------------------------------------------------------------ }

Procedure Main_Module ;
begin
   case pathnum of
      1 : path :='f:\rdata\los\trlow\' ;
      2 : path :='f:\rdata\los\trmed\' ;
      3 : path :='f:\rdata\los\trhigh\' ;
      4 : path :='f:\rdata\par\trlow\' ;
      5 : path :='f:\rdata\par\trmed\' ;
      6 : path :='f:\rdata\par\trhigh\' ;
      7 : path :='f:\rdata\obs\trlow\' ;
      8 : path :='f:\rdata\obs\trmed\' ;
      9 : path :='f:\rdata\obs\trhigh\' ;
   end ;
   if choice1 = 1 then Keyword[keynumber] := '*' ;

   if choice1 = 2 then
   begin
      write('Number of filenames : ') ;
      readln(keynumber) ;

      for i := 1 to keynumber do
      begin
         write('filename[',i:1,'] : ') ;
         readln(Keyword[i]) ;
         Keyword[i] := path+'thr\'+keyword[i]+'.thr' ;
      end ;
   end
   else Keyword[keynumber] := path+'thr\'+keyword[keynumber]+'.thr' ;
   writeln(pathnum) ;
   writeln(path) ;
   for k := 1 to keynumber do
   begin
      FindFirst(keyword[k],archive,dirinfo) ;
      while DosERROR = 0 do
      begin
         filename1 := copy(dirinfo.name,1,length(dirinfo.name)-4) ;
         freq := copy(filename1,2,1) ;
         site := copy(filename1,4,1) ;
         bsl  := copy(filename1,5,1) ;
         numb := copy(filename1,7,1) ;
         anth := copy(filename1,8,1) ;

         if (freq='1') then
         begin
            if (site='1') then filebb := 'f1bb309' ;
            if (site='2') then filebb := 'f1bb311' ;
            if (site='3') then
            begin
               if ((bsl='A') and ((numb='1') or (numb='2')))
               then filebb := 'f1bb323' ;
               if (bsl='A') and ((numb='3') or (numb='4'))
               then filebb := 'f1bb3232' ;
               if (bsl='B') and (numb='1') then filebb := 'f1bb324' ;
               if (bsl='B') and ((numb='2') or (numb='3'))
               then filebb := 'f1bb3242' ;
               if (bsl='B') and (numb='4') then filebb := 'f1bb3243' ;
               if (bsl='C') and ((numb='1') or (numb='2'))
               then filebb := 'f1bb3244' ;
               if (bsl='C') and ((numb='3') or (numb='4'))
```

```
            then filebb := 'f1bb3245' ;
            if (bsl='D') then filebb := 'f1bb3245' ;
         end ;
         if (site='4') then filebb := 'f1bb401' ;
      end ;

      if (freq='4') then
      begin
         if (site='1') then filebb := 'f4bb309' ;
         if (site='2') then filebb := 'f4bb311' ;
         if (site='3') then
         begin
            if ((bsl='A') and ((numb='1') or (numb='2')))
            then filebb := 'f4bb323' ;
            if (bsl='A') and ((numb='3') or (numb='4'))
            then filebb := 'f4bb3232' ;
            if (bsl='B') and (numb='1') then filebb := 'f4bb324' ;
            if (bsl='B') and ((numb='2') or (numb='3'))
            then filebb := 'f4bb3242' ;
            if (bsl='B') and (numb='4') then filebb := 'f4bb3243' ;
            if (bsl='C') and ((numb='1') or (numb='2'))
            then filebb := 'f4bb3244' ;
            if (bsl='C') and ((numb='3') or (numb='4'))
            then filebb := 'f4bb3245' ;
            if (bsl='D') then filebb := 'f4bb3245' ;
         end ;
         if (site='4') then filebb := 'f4bb401' ;
      end ;
      filecc := 'f:\gendat\'+filebb ;
      write(filename1,'   ') ;
      Read_Data ;
      Reference_Power ;
      if check3 = 2 then Profile_Power_Average_Profile
      else begin
         Profile_Power ;
         Path_Loss_Statistics ;
         File_Out ;
      end ;
      FindNext(dirinfo) ;
   end ;
end ;
end ;


{ ------------------------------------------------------------ }


begin
   new(tdata) ;
   writeln ;
   write('Enter (1) for all local profiles, (2) for average local profile : ');
   readln(check3) ;
   write('Enter (1) to compute for all paths, (2) to choose specifics : ') ;
   readln(choice1) ;
   if choice1 = 2 then
   begin
      write('Enter Path Number : ') ;
      readln(pathnum) ;
      Main_Module ;
   end
   else
   begin
      keynumber := 1 ;
      for pathnum := 1 to 9 do Main_Module ;
   end ;
```

```
    dispose(tdata) ;
end.
```

```
{  OUTAGE.PAS  }

{  ---------------------------------------------------------------------

This program computes the distribution function of the probability of
outage due to path loss for a proposed circular coverage region with
user-specified maximum radius.  The user also specifies a number for the
minimum radius of the cell, however this is only for integration limit
purposes and can be set to a constant small value, i.e. 1 meter.
The user also specifies values for the power law exponent n and the
standard deviation of path loss values about the best-fit power law
model.

Last Revised -- July 27, 1990.

--------------------------------------------------------------------- }


program outage ;
{$N+}
uses dos,crt ;


var
   fileout                                  :  text                    ;
   filename                                 :  string[50]              ;
   powerlaw,sigma,c,A,Abar,expon,pdfrad     :  double                  ;
   summer,sumint,h,integral,rad             :  double                  ;
   rmin,rmax,i,j                            :  integer                 ;
   argument                                 :  array[1..500] of double ;
   pdf,cdf                                  :  array[-40..300] of double ;


{  ------------------------------------------------------------------ }


Function Log(x:double): double ;
begin
   if x <= 0.00000 then log := -200.00
   else log := ln(x)/ln(10.0) ;
end ;


{  ------------------------------------------------------------------ }


Function Power (number,exponent : double ) : double ;
begin
   if exponent = 0.0 then
      power := 1.0
   else if number < 0.0 then
      power := 0.0
   else
      power := exp(exponent * ln(number)) ;
end ;


{  ------------------------------------------------------------------ }


Procedure Numerical_Integrate ;
begin
   argument[rmin*4] := argument[rmin*4]/2.0 ;
   argument[rmax*4] := argument[rmax*4]/2.0 ;
   h := (rmax - rmin)/(4.0 * (rmax-rmin)) ;
```

```
   sumint := 0.0 ;
   for j := (rmin * 4) to (rmax * 4) do sumint := sumint + argument[j] ;
   integral := h * sumint ;
end ;


{ ------------------------------------------------------------- }


begin
   writeln;
   write('Enter the filename of outage CDF (no ext.)') ;
   readln(filename) ;
   write('Enter the value for power law exponent (n) > ') ;
   readln(powerlaw) ;
   write('Enter the standard deviation from model (sigma) > ') ;
   readln(sigma) ;
   write('Enter minimum range value for cell (integer) > ') ;
   readln(rmin) ;
   write('Enter maximum range value for cell (integer) > ') ;
   readln(rmax) ;

   c := 1/(sqrt(2.0 * pi) * sigma) ;
   summer := 0.0 ;

   assign(fileout,'f:\datastat\cdf\out\'+filename+'.out') ;
   rewrite(fileout) ;

   for i := -20 to 220 do
   begin
      A := i/2.0 ;
      for j := (rmin * 4) to (rmax * 4) do
      begin
         rad := j/4.0 ;
         Abar := 10.0 * powerlaw * log(rad) ;
         expon := -0.5 * sqr((A - Abar)/sigma) ;
         pdfrad := (2.0 * rad)/sqr(rmax) ;
         argument[j] := c * pdfrad * exp(expon) ;
      end ;

      Numerical_Integrate ;

      pdf[i] := 0.5 * integral ;
      summer := summer + pdf[i] ;
      CDF[i] := 100.0 * (1.0 - summer) ;

      writeln(A:8:2,pdf[i]:8:4,CDF[i]:8:4) ;
      writeln(fileout,a:8:2,pdf[i]:8:4,CDF[i]:10:4) ;
   end ;
   close(fileout) ;
end.
```

Vita

Dwayne Allen Hawbaker was born in Hagerstown, Maryland on May 16, 1966. He graduated with the Bachelor of Science degree in Electrical Engineering from Virginia Tech in 1989. For seven academic terms between 1985 and 1988, he served as a Cooperative Education (Co-Op) student in the Earth Terminal Antenna Department at Comsat Laboratories, Clarksburg, Maryland, where he developed and tested various microwave antennas, and performed antenna system analyses. In 1989, he joined the Mobile and Portable Radio Research Group at Virginia Tech, where his graduate research has focused on characterizing radio frequency multipath propagation in various indoor environments. His primary areas of interest include communication system design, RF propagation, radar, and antennas.

Mr Hawbaker is a member of Eta Kappa Nu honor society and the IEEE. His graduate work has been supported by a Harry Lynde Bradley fellowship award, which he received from Virginia Tech's Bradley Department of Electrical Engineering in 1989.